

**IMAGING SERVICES NORTH**

Boston Spa, Wetherby

West Yorkshire, LS23 7BQ

[www.bl.uk](http://www.bl.uk)

**This PDF was created from the British Library's microfilm copy of the original thesis. As such the images are greyscale and no colour was captured.**

**Due to the scanning process, an area greater than the page area is recorded and extraneous details can be captured.**

**This is the best available copy**

**DX**

**172231**

**THE BRITISH LIBRARY**  
**BRITISH THESIS SERVICE**

METAL COMPLEXES OF OXYGEN-, NITROGEN-, AND SULPHUR-CONTAINING

**TITLE .....** MACROCYCLIC LIGANDS; SYNTHETIC AND STRUCTURAL STUDIES.

**AUTHOR .....** SMRUTI WAIKAR .....

**DEGREE .....**

**AWARDING BODY** (C.N.A.A)  
**DATE .....** University of North London.  
(1992)

**THESIS  
NUMBER .....**

**THIS THESIS HAS BEEN MICROFILMED EXACTLY AS RECEIVED**

The quality of this reproduction is dependent upon the quality of the original thesis submitted for microfilming. Every effort has been made to ensure the highest quality of reproduction.

Some pages may have indistinct print, especially if the original papers were poorly produced or if the awarding body sent an inferior copy.

If pages are missing, please contact the awarding body which granted the degree.

Previously copyrighted materials (journal articles, published texts, etc.) are not filmed.

This copy of the thesis has been supplied on condition that anyone who consults it is understood to recognise that its copyright rests with its author and that no information derived from it may be published without the author's prior written consent.

Reproduction of this thesis, other than as permitted under the United Kingdom Copyright Designs and Patents Act 1988, or under specific agreement with the copyright holder, is prohibited.

1	2	3	4	5	6	REDUCTION X <b>20</b>
						CAMERA <b>5</b>
						No. of pages

METAL COMPLEXES OF OXYGEN-, NITROGEN-, AND SULPHUR-CONTAINING  
MACROCYCLIC LIGANDS; SYNTHETIC AND STRUCTURAL STUDIES.

By

SNRUTI WAIKAR

A thesis submitted in partial fulfillment of the requirements of the  
Council for National Academic Awards for the degree of Doctor of  
Philosophy.

University of North London.

July 1992.

*For my Parents,*

*Shweta and Ketan.*

#### ACKNOWLEDGEMENTS

I would like to thank my academic supervisors Dr. Brian Murphy and Professor Mary McPartlin for their guidance, support and patience throughout the highlights, and also the often subdued moments encountered during the course of my studies.

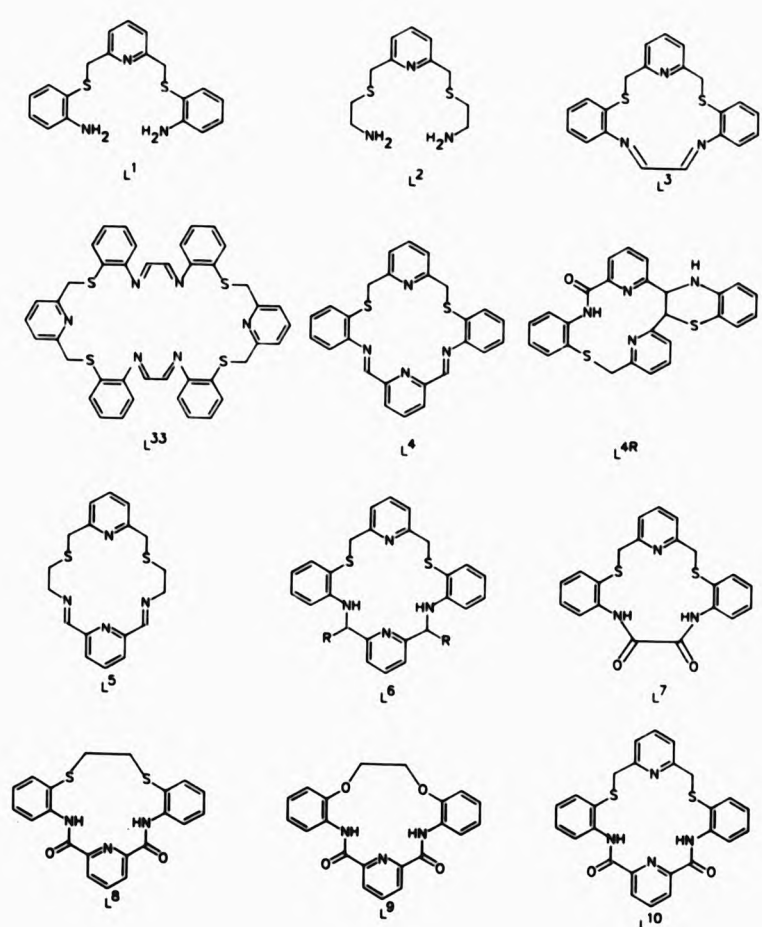
I am also indebted to Dr Peter A. Tasker and Dr Jeremy Holmes at ICI - Fine Chemicals Research Centre, for spending some of their valuable time engaged in helpful discussions and for their constant encouragement and kindness.

Many thanks also to Dr. Charles Harding at The Open University for obtaining and interpreting e.s.r. spectra and measurements for some of the magnetic susceptibilities. The 'Crystallography Team' at the University of North London - Professor Mary McPartlin, Dr. Harry Powell, Alan Bashall, Nick Choi and Wan-Sheung Li for solving the structures presented in Chapters Two, Four and Five.

I would also like to thank Dr. Ray Matthews for his informative discussions on n.m.r. and consistent interest in my project, and Dr. Dominic Spillane for his useful hints on electronic and infrared spectroscopy.

Finally, I would like to thank all the academic, research and technical staff in the Chemistry department for making life easier and more enjoyable, in particular I would like to thank Ian J. Scowen, Dr. Gráinne Conole, Soraya Chaudhary and Maria Constantinou for their individual expertise, moral support and friendship.

Last, but by no means least many thanks to the S. E. R. C. for funding this project and for providing an educationally stimulating conference/holiday in Australia.



LIST OF ABBREVIATIONS

$\text{\AA}$	Angstrom, $10^{-10}$ metre.
$A_J$	Hyperfine coupling constant, in G.
bz	benzyl.
bipy	2,2-bipyridine.
B.M.	Bohr Magneton ( $1 \text{ B.M.} = 9.274 \times 10^{-24} \text{ A m}^2$ ).
CFSE	Crystal Field Stabilisation Energy.
COSY	Correlation Spectroscopy.
$\delta$	Chemical shift.
DEPT	Distortion Enhancement Polarisation Transfer.
DMSO	Dimethyl sulphoxide.
DMA	Dimethylacetamide.
DMP	<i>N,N</i> -Dimethylformamide.
$\epsilon$	Molar decadic absorptivity.
e.s.r.	Electron spin resonance.
en	1,2-Diaminoethane.
F.a.b.	Fast atom bombardment.
G	Gauss.
$g_{\parallel}$	$g$ factor in unique direction.
$g_{\perp}$	$g$ factor in any direction in the plane perpendicular to $g_{\parallel}$
g	Grams.
Hz	Hertz.
HSAB	Hard-Soft Acid-Base.
I.R.	Infrared;
	$s = \text{strong}, m = \text{medium}, w = \text{weak}, sh = \text{shoulder}, br = \text{broad}.$
J	Coupling constant, in Hz.
K	Kelvin.
$\lambda$	Wavelength.
$\mu_{\text{eff}}$	Effective magnetic moment.

mmol Millimole.  
ν Frequency.  
nm Nanometre.  
N.m.r. Nuclear magnetic resonance;  
s = singlet, d = doublet, t = triplet, dd = doublet of  
doublets, td = triplet of doublets,ddd = doublet of doublet  
of doublets, m = multiplet.  
NOBA 3-nitrobenzyl alcohol.  
ph Phenylene.  
p.p.m. Parts per million.  
py pyridyl.

Throughout this thesis all ionic radii have been obtained from:

R. D. Shannon, *Acta Crystallogr., Sect. A.*, 1976, 32, 751.

Numbers in curly brackets ( ) refer to ligands from reference work.  
Each chapter starts with model ligand (1) and references appear at the  
end of each chapter.

CONTENTS

CHAPTER 1 - INTRODUCTION TO MACROCYCLIC CHEMISTRY.

1.1	General Introduction.	1
1.2	Definition of a macrocyclic ligand.	2
1.3	Historical Background.	2
1.3.1	Naturally Occurring Macrocycles.	3
1.3.2	Synthetic Macrocycles.	5
1.4	Metal - Ligand Interactions.	10
1.4.1	Stability of Metal Complexes.	10
1.4.2	The Chelate Effect.	12
1.4.3	The Macrocyclic Effect.	13
1.4.4	The Cryptate Effect.	16
1.5	Metal-ion Recognition.	18
1.5.1	Metal-ion Preferences.	18
1.5.2	Ligand Framework.	19
1.5.3	Ligand Hole Size.	22
1.5.4	Structural Dislocation.	26
1.6	Synthetic Strategies.	29
1.6.1	Direct Syntheses.	29
1.6.2	Metal Template Syntheses.	30
1.7	Toxic Heavy Metals.	36
1.7.1	Toxicity.	36
1.7.2	Extraction and Recovery of Heavy Metals.	40
1.8	Proposed Program for Ligand Design.	41
	References.	43

CHAPTER 2 - SYNTHESES, CHARACTERISATION AND CO-ORDINATION  
STUDIES OF TWO QUINQUEDENTATE NITROGEN-SULPHUR ACYCLIC PRECURSOR  
LIGANDS L<sup>1</sup> AND L<sup>2</sup>.

2.1 General Introduction.	50
2.2 Synthesis of L <sup>1</sup> .	50
2.3 Characterisation of L <sup>1</sup> .	53
2.4 Co-ordination Studies of [ML <sup>1</sup> ] <sup>n+</sup> .	60
2.4.1 Spectroscopic Studies of [ML <sup>1</sup> ] <sup>n+</sup> .	62
2.4.2 Single-Crystal X-ray Structure of [HgL <sup>1</sup> (Cl) <sub>2</sub> ].	80
2.4.3 Single-Crystal X-ray Structure of [NiL <sup>1</sup> (Cl)]Cl.MeOH.	87
2.4.4 Stability Constant Measurements for [CuL <sup>1</sup> ](ClO <sub>4</sub> ) <sub>2</sub> .	91
2.5 Synthesis of L <sup>2</sup> .	95
2.6 Characterisation and Co-ordination Studies of [ML <sup>2</sup> ] <sup>n+</sup> .	97
References.	99

CHAPTER 3 - SYNTHESES, CHARACTERISATION AND CO-ORDINATION  
STUDIES OF [1+1] AND [2+2] NITROGEN-SULPHUR SCHIFF-BASE  
MACROCYCLIC LIGANDS L<sup>3</sup> AND L<sup>33</sup>.

3.1 General Introduction.	
3.2 Introduction to L <sup>3</sup> .	102
3.3 Template Synthesis of L <sup>3</sup> .	102
3.4 Co-ordination Studies of [AgL <sup>3</sup> ]ClO <sub>4</sub> and [Cu <sub>2</sub> L <sup>33</sup> ](ClO <sub>4</sub> ) <sub>2</sub> .	102
3.4.1 Spectroscopic Studies of [AgL <sup>3</sup> ]ClO <sub>4</sub> and [Cu <sub>2</sub> L <sup>33</sup> ](ClO <sub>4</sub> ) <sub>2</sub> .	102
3.5 Transmetallation Reactions of [AgL <sup>3</sup> ]ClO <sub>4</sub> .	123
References.	125

CHAPTER 4 - SYNTESSES, CHARACTERISATION AND CO-ORDINATION STUDIES  
OF TWO SEXIDENTATE NITROGEN-SULPHUR SCHIFF-BASE MACROCYCLIC  
LIGANDS L<sup>4</sup> AND L<sup>5</sup>.

4.1	Introduction to L <sup>4</sup> .	127
4.2	Non-template and Template Syntheses of L <sup>4</sup> .	128
4.3	Co-ordination Studies of [PbL <sup>4</sup> ] <sup>2+</sup> , [AgL <sup>4</sup> ] <sup>+</sup> and [HgL <sup>4</sup> ] <sup>2+</sup> .	128
4.3.1	Spectroscopic Studies of [PbL <sup>4</sup> ] <sup>2+</sup> , [AgL <sup>4</sup> ] <sup>+</sup> and [HgL <sup>4</sup> ] <sup>2+</sup> .	129
4.3.2	Single-Crystal X-ray Structure of [PbL <sup>4</sup> (H <sub>2</sub> O)(MeOH)][ClO <sub>4</sub> ] <sub>2</sub> .	144
4.3.3	Single-Crystal X-ray Structure of [HgL <sup>4</sup> (SCN) <sub>2</sub> ].MeOH.	152
4.4	Co-ordination Studies of [CdL <sup>4</sup> ] <sup>2+</sup> and [ZnL <sup>4</sup> ] <sup>2+</sup> .	157
4.4.1	Spectroscopic Studies of [CdL <sup>4</sup> ] <sup>2+</sup> and [ZnL <sup>4</sup> ] <sup>2+</sup> .	157
4.4.2	Single-Crystal X-ray Structure of L <sup>4B</sup> .	175
4.5	Co-ordination Studies of [PbL <sup>5</sup> ] <sup>2+</sup> .	180
4.5.1	Spectroscopic Studies of [PbL <sup>5</sup> ] <sup>2+</sup> .	180
	References.	190

CHAPTER 5 - SYNTESSES, CHARACTERISATION AND CO-ORDINATION STUDIES  
OF A SEXIDENTATE NITROGEN-SULPHUR MACROCYCLIC LIGAND L<sup>6</sup> AND ITS  
DERIVATIVES L<sup>6A-D</sup>.

5.1	General Introduction.	193
5.2	Synthesis and Characterisation of L <sup>6</sup> .	193
5.3	Co-ordination Studies of [CuL <sup>6</sup> ] <sup>2+</sup> and [NiL <sup>6</sup> ] <sup>2+</sup> .	201
5.3.1	Spectroscopic Studies of [CuL <sup>6</sup> ] <sup>2+</sup> and [NiL <sup>6</sup> ] <sup>2+</sup> .	201
5.3.2	Single-Crystal X-ray Structure of [NiL <sup>6</sup> ][ClO <sub>4</sub> ] <sub>2</sub> .	204
5.4	Co-ordination Studies of [ML <sup>6A-D</sup> ] <sup>2+</sup> .	211
5.4.1	Spectroscopic Studies of [ML <sup>6A-D</sup> ] <sup>2+</sup> .	211
5.4.2	Single-Crystal X-ray Structure of [CuL <sup>6B</sup> ][ClO <sub>4</sub> ] <sub>2</sub> .	216
	References.	221

**CHAPTER 6 - SYNTHESES, CHARACTERISATION AND CO-ORDINATION STUDIES  
OF FOUR MIXED-DONOR DIOXO MACROCYCLIC LIGANDS  $L^7-L^{10}$ .**

6.1	General Introduction.	223
6.2	Syntheses and Characterisation of $L^7-L^{10}$ .	223
6.3	Co-ordination Studies of $[ML^{7-10}]$ .	235
6.3.1	Spectroscopic Studies of $[ML^{7-10}]$ .	235
6.3.2	Single-Crystal X-ray Structure of $[CuL^{10}] \cdot H_2O$ .	242
	References.	247

**CHAPTER 7 - EXPERIMENTAL.**

7.1	Syntheses - Synthetic Details and Procedures.	249
	References.	265
7.2	Crystallography - Structure Solution of $[CuL^{10}] \cdot H_2O$ .	266
	References.	265

**APPENDIX.**

A	N.M.R. - $AB_2$ Spin System.	273
B	A Brief Resume of Crystallographic Background.	276
C	Crystal Data for $[CuL^{10}] \cdot H_2O$ .	286

**CHAPTER ONE**

**INTRODUCTION TO MACROCYCLIC CHEMISTRY**

### 1.1 General Introduction.

It was at the turn of this century, within the area of co-ordination chemistry<sup>[1]</sup> that the interdependence of structure and reactivity was first realised. The understanding of interactions between metal and ligand has become more complex progressing from simple unidentate to the more complicated multidentate systems and in some instances, ligand designs have imposed unusual co-ordination geometries around metal atoms. Such effects are particularly evident in macrocyclic ligands. Their intrinsic properties as ligands gives them the potential to behave as catalysts,<sup>[2]</sup> semiconductors<sup>[3]</sup> and sequestering agents for use in pollution control and hydrometallurgy.<sup>[4]</sup> In addition, they have impinged on the biomedical field, where they have become likely candidates for therapeutic reagents required for the treatment of metal intoxication,<sup>[5]</sup> or used as diagnostic agents in the form of radio-labelled macrocycle-conjugated antibodies for better tumor imaging<sup>[6]</sup> while their specificity and efficacy prove excellent for enzyme modelling.<sup>[7]</sup> In 1987, achievements in this expanding field culminated in the form of a Nobel prize, awarded to C. J. Pedersen, J. M. Lehn and D. J. Cram and marked the scientific world's recognition of the importance of macrocyclic chemistry.

Having briefly outlined the wealth of research associated with macrocyclic ligands currently being undertaken, one aspect is of special interest to this work. The objective of this project has been to design new selective complexing agents for the toxic heavy metal ions cadmium(II), mercury(II) and lead(II). Resulting observations on the properties of such systems should provide a better insight of how and why certain ligands 'discriminate' or appear selectively to complex

with only certain metal ions. In addition, the project supplements an ongoing study of related work which forms part of a series within a matrix of similar macrocyclic ligands.<sup>[8]</sup>

#### 1.2 Definition of a Macroyclic Ligand.

Macroyclic ligands (whether synthetic or naturally occurring) consist of an organic framework of carbon and heteroatoms arranged in a cyclic manner to form one or more rings. A text book definition is given as "a cyclic compound with nine or more members (including all heteroatoms) and with three or more donor (ligating) atoms".<sup>[9]</sup>

As a result of the voluminous chemistry carried out by macrocyclic chemists, new methods of classification have been developed in order to encompass the vast array of ligands synthesised, all of which conform to the definition of a macrocycle.<sup>[10]</sup>

#### 1.3 Historical Background.

Prior to the 1960s, apart from the well-established phthalocyanines (Figure 1.3a),<sup>[11]</sup> only a limited number of papers concerned with macrocyclic ligands had appeared in the literature.<sup>[12]</sup> At that stage their co-ordinating ability was of little interest, and their potential was not realised. During the 1960s, the field of macrocyclic chemistry underwent rapid development, and several independent workers bridged the gap between incidental,<sup>[13]</sup> deliberate,<sup>[14]</sup> and even accidental<sup>[15]</sup> syntheses of these cyclic ligands and their complexes. At approximately the same time, the natural macrocycles - the cyclic antibiotics, and corrin and porphyrin related systems were being isolated and structurally characterised.

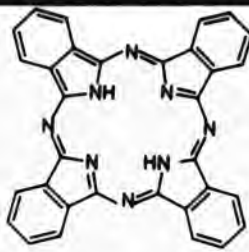


Figure 1.3a Structure of phthalocyanine.

#### 1.3.1 Naturally Occurring Macrocycles.

The antibiotics, valinomycin and enniatin B are composed of alternating  $\alpha$ -amino acid and  $\alpha$ -hydroxy acids which link to form a ring (Figure 1.3b).

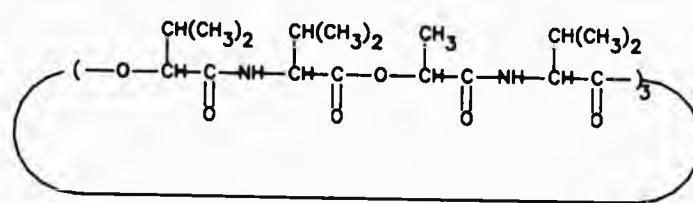


Figure 1.3b The naturally occurring antibiotic valinomycin.

In contrast, the antibiotics monactin and nonactin have four ether and four ester groups incorporated into their ring structure (Figure 1.3c). The key feature of these compounds is that, during complexation, the macrocycles adjust their tertiary conformation so that different environments exist inside and outside the macrocyclic cavity; the inside is hydrophilic whilst the outside is hydrophobic. Upon complexation, the tertiary structure is maintained by a sequence of intra-complex hydrogen bonding. In this way, these macrocycles can selectively transport sodium and potassium ions through the lipid bilayer of cell membranes.<sup>[16]</sup>

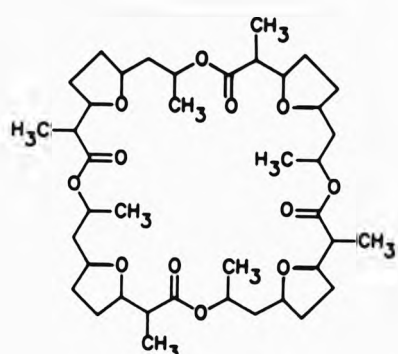


Figure 1.3c The naturally occurring antibiotic nonactin.

Particular derivatives of corrins and porphyrins play a central rôle in photosynthesis, transport and storage of dioxygen, and electron transfer processes. Examples of corrin and porphyrin-based systems are vitamin B<sub>12</sub> and chlorophyll respectively. Additionally, these structures are unusual in being naturally occurring organometallic complexes containing cobalt-carbon (vitamin B<sub>12</sub>) and magnesium-carbon (chlorophyll) linkages (Figure 1.3d).

Further examples of porphyrin-containing systems are the haem proteins haemoglobin, myoglobin and the cytochromes. The prosthetic macro-ring of monomeric sub-units of these proteins permit high- and low-spin states of iron(II) during dioxygen transport and storage, using haemoglobin and myoglobin respectively, whilst the cytochromes perform electron-carrying functions through manipulation of the Fe(II)/Fe(III) redox cycle (Figure 1.3e).

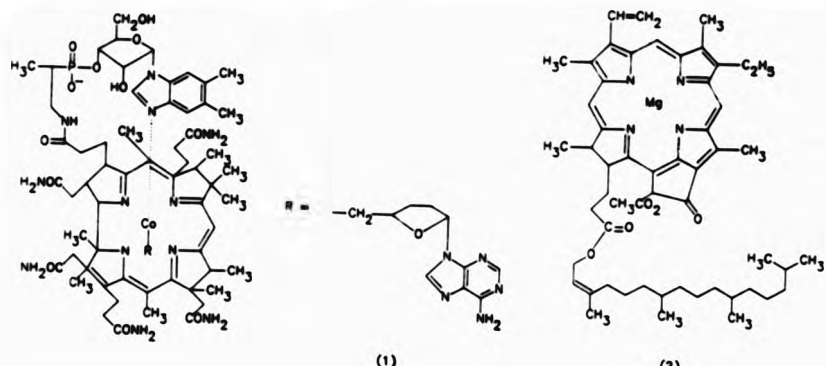


Figure 1.3d Structural features of (1) vitamin B<sub>12</sub> and (2) chlorophyll.

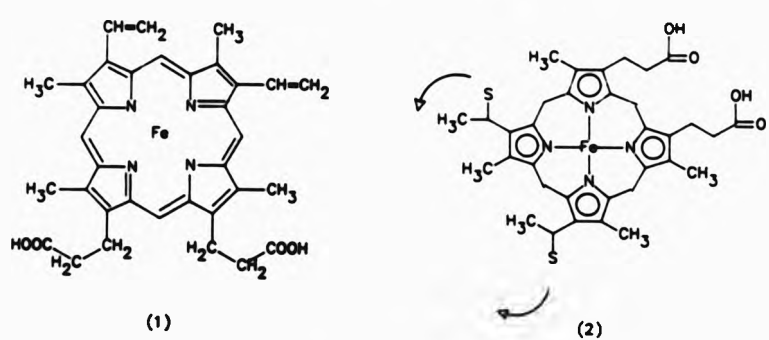


Figure 1.3e A haem unit as contained in (1) haemoglobin and myoglobin and (2) cytochrome C

### 1.3.2 Synthetic Macrocycles.

Initially, work on macrocycles was undertaken without any regard to a possible relationship between the synthetic ligands and the naturally-occurring cyclic ligands and their complexes. The realisation of the significant roles played by these types of ligands fired the imagination of many inorganic chemists to design model complexes to mimic biologically important systems. In view of this, ligands were prepared with the aim of forming stable complexes with

s-block metal ions such as  $\text{Na}^+$ ,  $\text{K}^+$ , and  $\text{Mg}^{2+}$ , and d-block metal ions  $\text{Mn}(\text{II})$ ,  $\text{Co}(\text{II})$ ,  $\text{Fe}(\text{II})$  and  $\text{Fe}(\text{III})$ , commonly encountered in plant and animal organisms. Indeed, until the advent of macrocyclic ligands, the s-block elements were the 'Cinderellas' of metals in so far as co-ordination chemistry was concerned. Countless characteristics of such complexes have since been investigated.<sup>[17]</sup>

In time, ligand design became more diverse and the study of interactions with metal ions unravelled an interesting and varied chemistry, which in turn provided motivation for further investigations. Thus, resulting curiosities led to the development of five distinct areas of macrocyclic chemistry. These new areas may be categorised according to the type of donor atoms incorporated into the macrocyclic ring itself; the divisions being (a) oxygen donor (crown ethers), (b) nitrogen donor (aza macrocycles), (c) sulphur donor (thioethers), (d) phosphorus and arsenic donors and (e) mixed-donor ligands. The intricacy and complexity of macrocyclic ligands has now increased to such an extent that additional structural features like pendant arms,<sup>[18]</sup> compartmental ligands<sup>[19]</sup> and macropolycyclic frameworks<sup>[20]</sup> also exist (Figure 1.3f). These ligand types have forced complexes away from the more common co-ordination numbers of four and six and instead, geometries bearing co-ordination numbers of three, five,<sup>[29]</sup> seven<sup>[30]</sup> or greater are now common-place.

Unsurprisingly, a new area of work rapidly expanded as the awareness of non-stoichiometric compounds became apparent. That is, variable compositions of host-guest complexes were discovered.<sup>[31]</sup> On confirmation of the existence of these host-guest molecules, the next challenge was to design ligands (hosts) which were 'tailor made' for

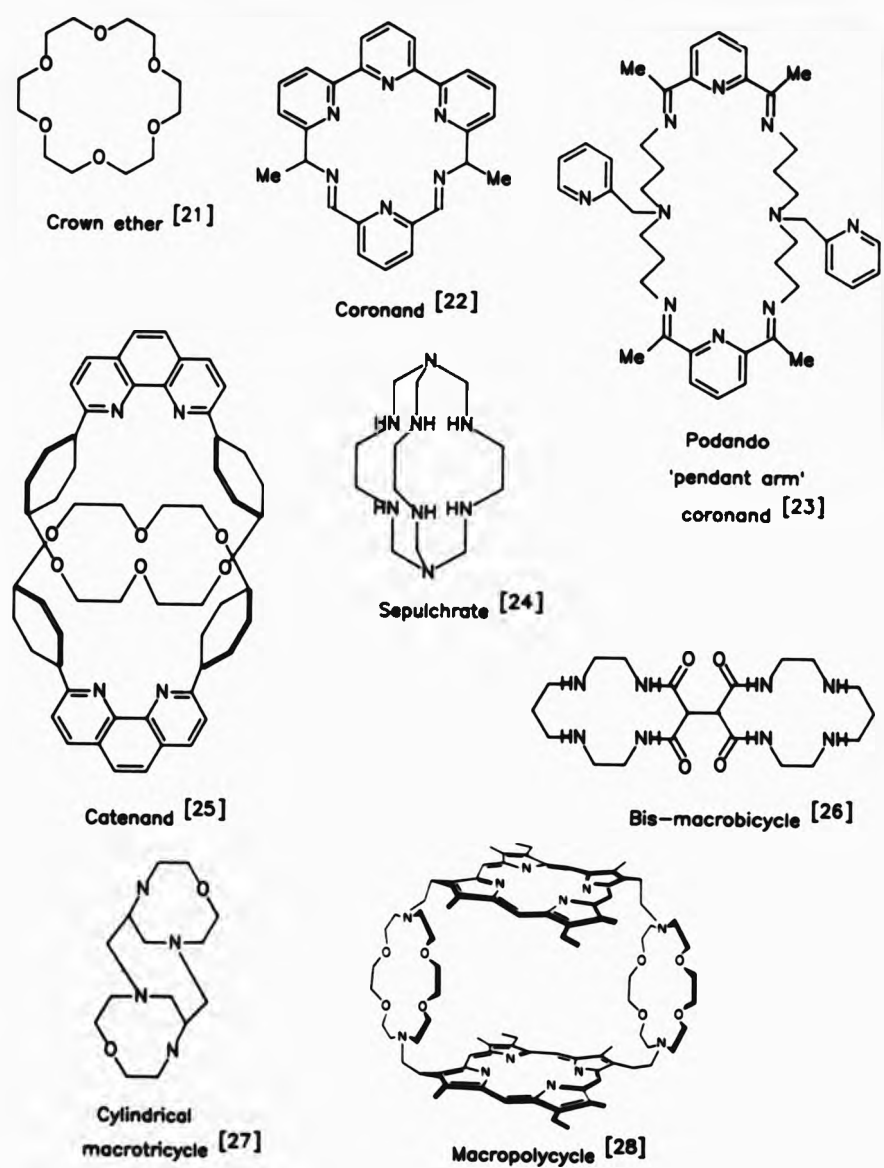


Figure 1.3f Examples of varied dimensionalities exhibited by macrocyclic ligands.

cations,<sup>[32]</sup> anions<sup>[33]</sup> and entire neutral molecules (guests).<sup>[34]</sup>

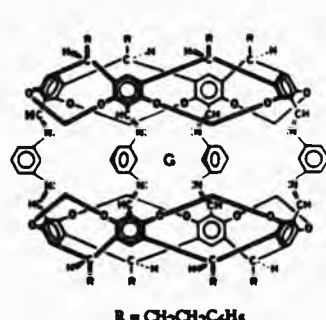
As the twenty-first century approaches, studies now extend beyond the molecule to include supramolecular interactions where the binding of two or more chemical entities is desirable.<sup>[35]</sup> Other synthetic organic hosts (cavitands) containing rigid cavities incorporating redox-active centers, have also received much attention in recent years.<sup>[36]</sup> Macro cyclic receptor molecules that contain a redox centre in close proximity to a metal-ion binding site have been designed to electrochemically recognise the binding of a metal guest either through space interactions or via various bond linkages between the receptor site and redox centre.<sup>[37]</sup>

The formation of hollow, spherical shells (carcerands) capable of incarcerating solvent molecules have been developed, where these incarcerated guests have the ability to communicate with external solvent molecules through the carcereand shell, as well as, with each other in crystal lattices.<sup>[38]</sup> Molecular recognition has been achieved through the making of baskets known as calixarenes, which are the products from the reactions of polyfunctionalised phenol and aldehyde derivatives. Alteration and elaboration of the upper and lower rims of these baskets can give rise to endless but specified cone conformations. Thus, allowing the baskets to be shaped, embroidered and filled.<sup>[39]</sup> For instance, calix[4]arenes have been used as building blocks for applications in membrane transport and field effect transistors. These molecular receptors exhibit a high selectivity for the alkali metal ions.<sup>[40]</sup> Calix[5]arenes are excellent candidates for the incorporation of multi-ring aromatics.<sup>[41]</sup> Syntheses and conformational studies on calix[6]arenes to calix[9]arenes have also

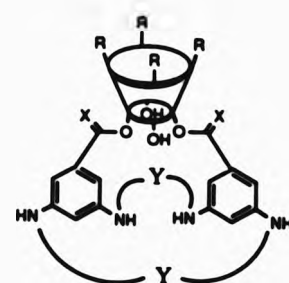
been achieved.<sup>[39]</sup>

The eventual aim is to be able to understand<sup>[42]</sup> the logical approach towards deciphering self-assembly and replication at the molecular level; with this in mind the construction of molecular electronic devices has been undertaken where molecular belts and shuttles based on the self-assembly of [2]rotaxanes has been employed.<sup>[43]</sup>

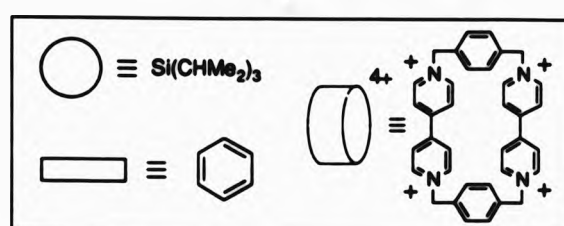
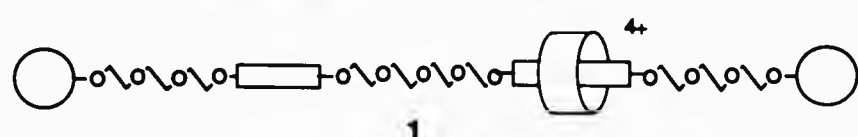
All in all, the basic macrocyclic unit has come along way since the early days of singular flat monocycles and the encapsulation of single metal cations.



Carcerand [38]



Calixarene [39]



Molecular Shuttle [43]

#### 1.4 Metal - Ligand Interactions.

The nature of the interaction between metal and macrocycle is at the source of the special properties displayed by macrocyclic complexes. The 'balance of power' between accommodation of the metal and ligand requirements is still very poorly understood. It is therefore appropriate to look at the development in the thinking and understanding of metal-ligand interactions.

##### 1.4.1 Stability of Metal Complexes.

The term complex is defined as the association between two chemical species linked via a co-ordinate bond. A metal complex consists of a central metal atom (Lewis acid) interacting with a ligand (Lewis base). In a complexation reaction, more than one ligand may complex with a metal atom (which is often the case) e.g.  $ML$ ,  $ML_2$ ,  $ML_3$ . In addition, more than one metal can co-ordinate to a number of ligands e.g.  $M_2L$ ,  $M_2L_3$ ,  $M_4L_2$ .

In solution, the formation of a complex can be expressed by its equilibrium (or stability) constant  $K$ , as follows:



$$K = \frac{[ML]}{[M][L]}$$

Metal ions are usually co-ordinated to solvent molecules in solution, although these are generally omitted from equations for clarity. Displacement of solvent molecules by a number of ligands usually proceeds in a stepwise manner.

$$\begin{aligned}
 M + L &\rightleftharpoons ML \quad K_1 = \frac{[ML]}{[M][L]} \\
 ML + L &\rightleftharpoons ML_2 \quad K_2 = \frac{[ML_2]}{[ML][L]} \\
 ML_2 + L &\rightleftharpoons ML_3 \quad K_3 = \frac{[ML_3]}{[ML_2][L]} \\
 &\vdots \\
 &\vdots \\
 &\vdots \\
 ML_{(i-1)} + L &\rightleftharpoons ML_i \quad K_i = \frac{[ML_i]}{[ML_{(i-1)}][L]}
 \end{aligned}$$

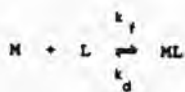
$K_i$  is the stepwise stability constant for each stage in the reaction.  
 Alternatively, the overall stability constant  $\beta_i$  may be employed instead:

$$M + iL \rightleftharpoons ML_i \quad \beta_i = \frac{[ML_i]}{[M][L]^i}$$

Where  $\beta_i$  and  $K_i$  are related in the following way:

$$\beta_i = K_1 K_2 \dots K_i = \prod_{i=1}^{i=i} K_i$$

As thermodynamic and kinetic factors are inter-related, the stability constant ( $K_{ML}$ ) can also be expressed kinetically:

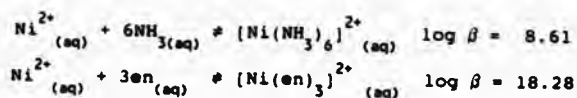


$$K_{ML} = \frac{k_f}{k_d}$$

Where  $k_f$  is the second-order formation constant and  $k_d$  the first-order dissociation rate constant.

#### 1.4.2 The Chelate Effect.

The ability of a multidentate ligand to co-ordinate to a single metal atom and form chelate rings results in the enhanced thermodynamic and kinetic stability of a complex when compared to closely related, non-chelating counterparts. For instance, the overall stability constant ( $\log \beta$ ) for the complexation of nickel(II) with ammonia is much less than that observed for its complexation with 1,2-diaminoethane (en).<sup>(44)</sup>

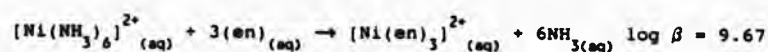


This increase in stability has been termed 'the chelate effect',<sup>(45)</sup> and originates from the enthalpic and entropic contributions given by the thermodynamic relationships:

$$\ln \beta = -\Delta G / RT$$

$$\Delta G = \Delta H - T\Delta S$$

Thus, the more negative  $\Delta H$  or the more positive  $\Delta S$  becomes, the more  $\beta$  increases. However, metathesis reactions indicate that the dominant factor contributing to the chelate effect is found in the entropic term:<sup>[46]</sup>



In this instance  $\Delta H = -12.1 \text{ KJ mol}^{-1}$  and  $T\Delta S = +55.1 \text{ KJ mol}^{-1}$  (both terms are favourable). Since the electronic effects of ammonia and 1,2-diaminoethane (en) are very similar, the ligand-field stabilisation energies (LFSE) of their compounds with the same metal ion will be almost identical, therefore the entropic term will be the most influential factor.

The chelate effect is strengthened when forming several rings with a single metal atom. Additionally, five and six membered chelate rings are known to be far more stable than three, four, seven or eight membered rings.<sup>[47]</sup> Moreover, ancillary effects due to steric restrictions and resonance stabilisation of ligands can also lead to an increase in the chelate effect.<sup>[48]</sup>

#### 1.4.3 The Macroyclic Effect.

An extension of the chelate effect, where a cyclic multidentate ligand encircles a metal atom via the formation of fused metal chelates, has led to the 'macrocyclic effect'.<sup>[49]</sup> That is, an enhanced stability is observed for macrocyclic ligands in comparison with their acyclic analogues which contain an equal number of equivalent donor atoms. It is to be expected that as the number of chelate rings increases (acyclic to macrocyclic) there will be an increase in the stability of

the metal complex. However, the cyclic nature of the ligand exhibits a much greater overall stability, one which exceeds the effect that would be associated with just the presence of an additional metal chelate ring (Figure 1.4a).

The thermodynamic origins of the macrocyclic effect are not clear and the issue is one of great debate. A conflict of ideas led to the belief that in some cases enthalpy factors predominate,<sup>[50]</sup> whilst in other cases, the effect is entirely attributed to entropy factors.<sup>[54]</sup> It is now becoming clear that contributions arising from the enthalpic and entropic terms are significantly different for different cases. Generally, for the tetraamine ligands the entropy term tends to be favourable while the enthalpy term is quite variable.<sup>[55]</sup> For thioether-containing ligands the effect is attributable solely to favourable entropy terms.<sup>[51]</sup> In contrast, the complexes of crown ether ligand types are much more enthalpy-stabilised.<sup>[56]</sup> These differences in origin are thought to be a consequence of the degree of donor atom solvation. Clearly, oxygen and nitrogen donor atoms will interact strongly with polar solvent molecules, whereas it is unlikely that sulphur donor atoms will be strongly solvated in protic solvents. Thus, the variations in stability of these complexes may have their origin in the differences in the solvation of the free ligands and their metal complexes.

Other factors influencing the macrocyclic effect which alter the individual degrees of enthalpic and/or entropic contributions will arise from differences in bond energies, ligand conformational changes, mis-match of metal ion and macrocycle cavity size, and number and randomness (disorder) of components.

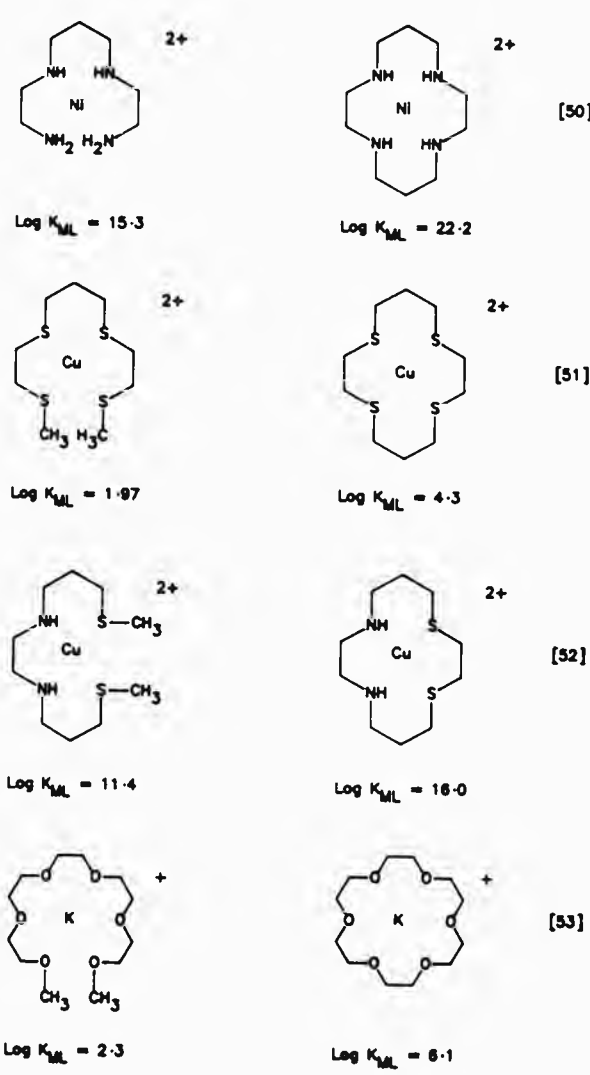


Figure 1.6a Complex stabilities of some open-chain and related macrocyclic ligands.

#### 1.4.4 The Cryptate Effect.

A further enhancement of thermodynamic stability is observed for macrobicyclic complexes over monocyclic ligand complexes. This has been named the 'cryptate effect'.<sup>[57]</sup> Once again, the microscopic origins of this effect cannot be fully elucidated, as they differ from system to system (Figure 1.4b).<sup>[58]</sup>

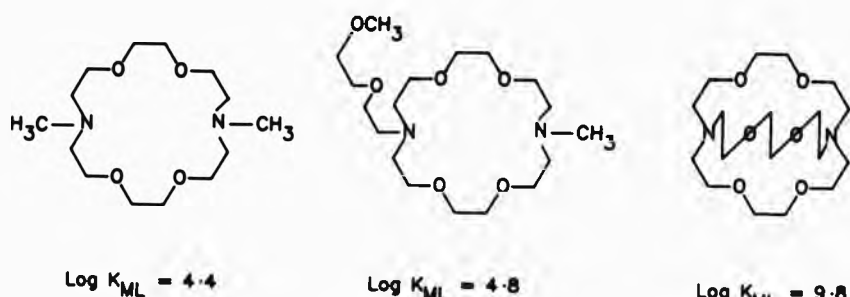


Figure 1.4b Increasing stability of potassium complexes from a monocycle to a cryptand.

As mentioned previously (section 1.4.1) the thermodynamic stability of a complex is the ratio of the rate of formation and dissociation, and therefore, the rate at which a complex dissociates governs the thermodynamic stability of the metal complex. Consequently, an alternative approach has been proposed which can also account for the pronounced stabilities exhibited by macrocyclic complexes i.e. the kinetic origin of the macrocyclic and cryptate effect. The phrase 'multiple juxtapositional fixedness' was introduced,<sup>[59]</sup> based on the very slow rates of metal dissociation (inertness towards substitution) for macrocyclic complexes. The stepwise removal of a cyclic ligand from the co-ordination sphere of a metal atom is more difficult relative to the corresponding non-cyclic complex because the latter

provides an 'end' to initiate ligand substitution ( $S_N1$ ). Conversely, macrocyclic ligand requires distortion (ligand folding) prior to bond breaking and must therefore resemble bimolecular substitution ( $S_N2$ ). Hence, the increase in stabilisation with respect to decomposition (Figure 1.4c).

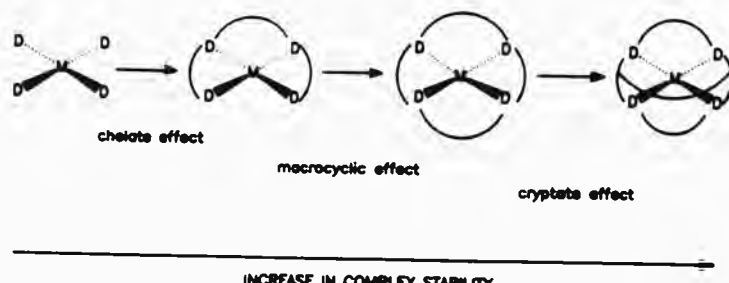


Figure 1.4c Diagrammatic representation of metal complexes in order of increasing stability.

In any system, mechanistic details are clearly dependent on the nature of the metal ion (lability or inertness) and structural features (flexibility or rigidity) of the ligand. For macrocyclic ligands the rate determining step varies with different systems depending on ligand protonation, solvating medium, electrostatic and steric effects. Studies have indicated that rates of formation are affected by the above, whereas rates of dissociation are very much ring size/metal ion dependent.<sup>[60]</sup> In view of these facts, it is apparent that although both thermodynamic and kinetic effects can explain the enhanced stability exhibited by macrocyclic complexes, it is not always possible to definitively trace the source for each and every reaction.

## **1.5 Metal-ion Recognition.**

Many factors contribute in a close-knit and complicated fashion to the success of metal-complex formation. A knowledge of metal-binding preferences, and hence, designation of number, nature and arrangement of binding sites i.e. overall ligand topology, is a requisite for selective complexation.

### **1.5.1 Metal-ion Preferences.**

Any metal ion has three basic properties which will influence its behaviour towards complexation: charge, size and electronic configuration. A crucial feature in the formation of macrocyclic ligands is the size of the metal ion which can be used to influence the reaction course leading to the isolation of the macrocyclic ligand as its complex (section 1.6.2). For instance, the cyclocondensation of Schiff-base reactions (Figure 1.5a) will proceed to form [1+1] complexes (1) in the presence of small metals, whereas, larger metal ions tend to bring about [2+2] condensation products (2).<sup>[61]</sup> Similarly, [4+4] products are also known in which a metal cluster core serves as the template centre.<sup>[62]</sup> According to its co-ordination number - the size of a metal ion will vary. The greater the co-ordination number the larger the ionic radius. The conformation of intermediates such as (3) (Figure 1.5a) will depend on the stereochemical demands of the metal ion, and in turn steer the course of the reaction and hence the products obtained.

One of the main differences between transition and non-transition metal ions is stereochemical preference. Transition metal ions such as iron(II), cobalt(II), and nickel(II) are stereochemically selective and their complexes are very sensitive to ligand field strengths. On the

other hand, non-transition metals have little electronic driving force for geometrical preferences, e.g. zinc(II), silver(I), cadmium(II), mercury(II) and lead(II). It is true that copper(II) can accept a wide variety of geometries but these are a consequence of Jahn-Teller distortions which arise from the removal of degeneracy of the  $t_{2g}$  electrons in an octahedral field. Stereochemically demanding metals will tend to override proposed ligand conformations, and result in either no reaction, ligand rearrangements or constrained ligand conformations. Meanwhile, non-transition metal ions may exhibit unusual and distorted co-ordination geometries imposed by inflexible (particularly macrocyclic) ligand constraints.

In addition, transition metals with six or more d electrons are extremely good soft Lewis acids because these electrons are held in the periphery of the d-orbital lobes and have a greater polarising effect. Consequently, they can also take part in  $\pi$ -d $\pi$  bonding interactions with  $\pi$ -acceptor ligands.

#### 1.5.2 Ligand Framework.

A good starting point for choice of donor atom type is the hard-soft acid-base (HSAB) concept, based on empirical observations.<sup>[63]</sup> Thus, crown ethers (oxygen donors) preferentially co-ordinate to the alkali metal ions through strong electrostatic dipolar interactions, whereas ligands containing nitrogen or sulphur donors (borderline and soft) tend to favourably complex covalently with the late transition metal ions. However, influences that may perturb these interactions also need to be considered. For instance, the presence of electron-withdrawing substituents can reduce the softness of a site, just as the addition of a soft polarisable substituent can often soften

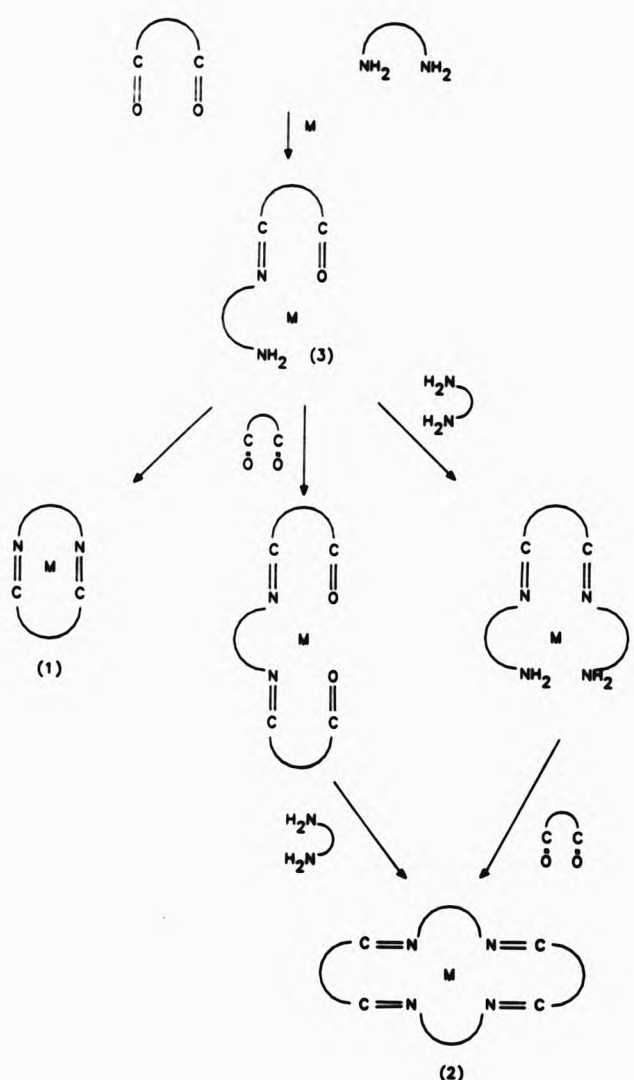


Figure 1.5a Scheme for routes to [1+1] and [2+2] cyclocondensations.

an otherwise hard centre. Simple yet effective results arise from the use of mixed-donor systems, because the metal involved has the possibility of combining with either or both types of donating species present as part of a ligand. Selectivity will, therefore, be enhanced between pairs of metal ions ( $M_a + M_b$ ), where metal  $M_a$  can complex to all donor atoms, while metal  $M_b$  may preferentially co-ordinate to only one type of Lewis base.

It is also worth noting that with a given donor type different reactivities are observed for neutral, anionic, saturated and unsaturated donor atoms. That is, neutral oxygen donors in alcohols, ethers, ketones or amides will have a range of co-ordinating properties which are entirely different when the oxygen donor is negatively charged. The same applies for nitrogen donors (which may be saturated or unsaturated) as well as sulphur donor atoms, where a thioether will behave differently to a thiolate.

On deciding the type of donor atoms to be employed in order to achieve the desired metal-ligand interaction, the number and arrangement of the electron donating binding sites needs to be considered. Obviously, donor atoms must be interspersed with non-co-ordinating atoms of reasonable length, so that an adequate 'bite' is available to the metal ion for effective complexation. As the metal and ligand will both be solvated, and replacement of much of the solvation shell takes place on complexation, the number of ligating atoms should equal the co-ordination number that the metal exhibits with the solvent molecules so that an efficient binding interaction can exist between the two.

The cyclic nature of macrocyclic ligands makes them inherently more

rigid than open-chain ligands. This rigidity can be further increased by the addition of unsaturated groups like imines,<sup>[64]</sup> aromatic ring substituents such as benzene and hetero ring head units like pyridine<sup>[65]</sup> etc. at binding sites. Functional groups can also provide fixed ligand frameworks as well as polar binding sites.

Minimum flexibility is the outcome of highly preorganised ligands, where, in some cases, even solvent molecules are excluded from the cavity of the macrocycles.<sup>[66]</sup> Thus, replacement of the solvent shell is not required prior to complexation, and so conformations in the free ligand and the complexed ligand will effectively be the same.

#### 1.5.3 Ligand Hole Size.

In contrast to the multidentate open-chain ligands, macrocycles have an additional fundamental parameter, their hole size. It was consideration of this property which led to the conclusion that the most stable metal complexes would be formed when the relative sizes of the metal ion and the macrocyclic cavity give the best possible fit. In view of this, a 'goodness of fit' parameter was introduced to specify the match or mis-match of a metal ion for a macrocyclic ligand cavity.<sup>[67]</sup> This is defined as the ratio of the bonding cavity radius ( $R_A$ ) to the Pauling covalent radius ( $R_p$ ) for the metal involved with a perfect match of the metal ion for the bonding cavity occurring when the ratio  $R_A/R_p$  is equal to unity. The actual 'bonding cavity' available to the metal ( $R_A$ ) is obtained from the ligand 'hole size' ( $R_h$ ) (defined by the nuclear positions of the donor atoms), minus the mean effective covalent radii of the donor atoms ( $R_d$ ) (Figure 1.5b). However, such an approach is only useful when the geometrical arrangement of the donor atoms which define the ligand hole size in the

free ligand is similar to that which is required in the metal complex.

The idea of matching hole size (bonding cavity) and metal ion radius works well for the crown ethers and their alkali-metal complexes.<sup>[57]</sup> For such complexes often only small ligand conformational energy changes are involved in complex formation, because these metal ions have no strong preferences for particular co-ordination geometries. Other factors leading to the strong dependence on hole size are the mutual ionic binding preferences of these metals and the ether oxygens, as well as the presence of a single donor type symmetrically positioned within a ligand framework - all of which will interact equally with the central metal ion.

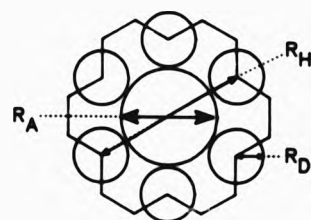


Figure 1.5b Difference in ligand hole size and bonding cavity.

As soon as the cyclic ligands become unsymmetrical either in donor atom disposition or carbon backbone (or both); or donor atoms of different size, reactivity and orbital hybridisation are altered, the metal will not interact uniformly with all the donor atoms. Thus, although a cyclic structure exists within these ligands, twisting and/or folding of the ring to some extent renders the macrocyclic hole/cavity size redundant. For instance, thioether donor atoms prefer to be exodentate in the free ligand state and on complexation, exocyclic as well as endocyclic compounds have been isolated.<sup>[68]</sup>

Alternatively, some views have been expressed in terms of abandoning the notion of the macrocyclic effect, and have instead concentrated on the stability of chelate ring sizes with regard to metal-ion size. The study has concluded that larger chelate rings will lead to greater complex destabilisation for larger metal ions (e.g. lead(II)) than smaller metal ions (e.g. copper(II)), irrespective as to whether the ligands are acyclic or macrocyclic.<sup>(69)</sup>

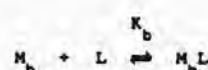
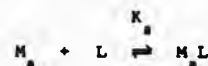
An extension of this study stresses that the selectivity between large and small metals diminishes (as the metal-ion size increases) whilst progressing from 5-membered to 6-membered chelate rings.<sup>(70)</sup> However, discrepancies have been introduced when dealing with flexible ligands, so that the metal can sit above, below, in or out of the donor atom plane, the selectivity apparently being enhanced with more rigidified chelate ring formations. When a macrocyclic ligand has an inflexible backbone, the macrocyclic effect comes into play as opposed to the chelate ring size-based selectivity. More importantly, differing angular requirements of metals are far more pronounced than their actual size in determining complex formation. For instance, nickel(II) is very partial to orthogonal geometries, even if the macrocyclic bonding cavity is a perfect match for its size, non-bonding interactions are likely to result.

Nevertheless, if the electron density of all the donor atoms is directed (focussed) towards the centre of the macrocyclic cavity with the metal ion centrally placed in the plane of the donor atoms, a more stable complex is likely to result. On the other hand, if the radius of the metal ion is too small or much larger than the cavity presented

by the ligand, complexation may occur but with diminished thermodynamic stability.

These differences in stability can and have been exploited to selectively extract particular metal ions from solution, thus providing a basis for the potential industrial application of macrocyclic ligands.

Discrimination may be formally defined as follows, where  $M_a$  and  $M_b$  are two different metals competing for the same ligand L which is available in limited quantity:



Discrimination is achieved when  $K_a/K_b$  or  $\Delta \log K$  is large. It is worth stressing that it is neither necessary nor desirable to have a high log K value in a separation process, but a large difference in log K is required in order to achieve separation via complex formation.

The extensive metal-ion selectivity studies available for macrocycles and cryptands suggest that the underlying enthalpic and entropic terms are quite system dependent. Thus a metal-ion discrimination strategy based solely on the best-fit criterion may not always be appropriate. An alternative approach of structural dislocation has been the subject of recent publications.<sup>[71], [72]</sup>

#### 1.5.4 Structural Dislocation.

This empirical approach for optimising metal-ion discrimination involves the systematic variation of a structural parameter of a ligand. The connectivity of the macrocyclic backbone results in a limited number of stereochemically feasible isomers within the formation of a complex and serves as a basis for structural dislocation.

Typically, the ligand hole size is the most favoured structural parameter altered. However, the degree of unsaturation, type and/or number of donor atoms, sterically influencing substituents etc. could also be employed to systematically vary a matrix of closely related ligands. Along a ligand series, as strain builds up for a given complex geometry, distortion occurs to accommodate the systematic parameterisation, eventually there comes a point where no further changes can take place within the same complex geometry. This in turn triggers a sudden change in ligand conformation resulting in the adaptation of a different co-ordination environment with a different stability. Thus, structural dislocation can be detected as its thermodynamic stability (Figure 1.5c).

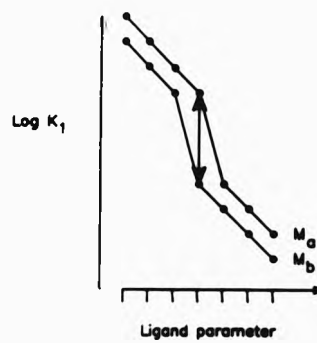
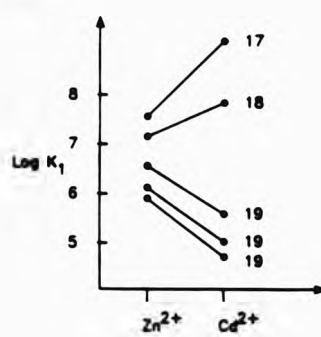


Figure 1.5c Schematic representation of structural dislocation.

Moreover, if two metals  $M_a$  and  $M_b$  promote structural dislocation at different points in the ligand series, substantial discrimination is observed for these ligands.

An illustration of this effect has been provided by the study of a series of tetra-azadioxa donor macrocycles together with their zinc(II) and cadmium(II) complexes based on the changes in ring size of the macrocyclic ligands.<sup>[73]</sup>



A plot of thermodynamic stabilities of these complexes against metal-ion size demonstrates that the zinc(II) complexes of these ligands show only a gradual systematic variation of log K with ligand ring size. As the inner great ring increases in members, there is a decrease in complex stability. In contrast, for cadmium(II) the 17- and 18-membered complexes are more stable than the corresponding zinc complexes, which is quite rare. The trend is reversed for the 19-membered macrocyclic ligands, which show the normal discrimination in favour of zinc(II). These large differences in stability for the cadmium(II) complexes are attributed to a change in bonding environment for the metal atom, from co-ordination to all ligand donor atoms to non-co-ordination of the ether oxygens. The bonding mode throughout

the zinc(II) complexes are thought to be similar. Thus, constraints imposed by the cyclic structure of these ligands are apparent in reversing the relative stabilities of the two metal ions, cadmium(II) and zinc(II). Further characterisations of dislocation behaviour have been investigated for cadmium(II) and zinc(II) where, in addition to increases in ring size, the introduction of bulky substituents gives a series of closely related dibenzo fused tetra-aza macrocycles. In this case, an alteration of ligand flexibility also induce changes in conformational geometry and hence, lead to substantial discrimination.<sup>[74]</sup>

Other elements which are found together either in nature or as a consequence of related solution chemistries e.g. Co(II), Ni(II) and Cu(II) or Ag(I) and Pb(II), require a means of separation and recovery. The interactions of these metal ions have been studied briefly in comparison, using similar approaches.<sup>[71]</sup>

Molecular mechanics calculations have been used as an aid to deduce minimum strain energies in ligands and their metal complexes. Predictions for 'modelling' compounds involves the monitoring of energy variations, related to stretching or compression and deformation from the norm of bond lengths and angles respectively, as well as, intramolecular (van der Waals forces) and molecular dipole interactions.<sup>[71], [74], [75]</sup> Essentially, molecular organisation for effective complexation requires energy expenditure in order to overcome desolvation forces, dipole-dipole interactions, and conformational changes. Thus for any system, minimum energy requirements will lead to a more profitable association.

### **1.6 Synthetic Strategies.**

Two major categories exist for the synthesis of macrocyclic ligand complexes. These are: (i) the 'direct' method and (ii) the '*in situ*' (metal-template) method. The former involves synthesis of the macrocyclic ligand by conventional organic techniques, whereas, the latter makes use of the influence of a metal ion during the cyclisation step. The two methods are not, however, mutually exclusive and the preparation of many macrocyclic systems includes both synthetic categories.

#### **1.6.1 Direct Syntheses.**

This procedure involves isolation of the macrocyclic ligand prior to complexation. In most cases, the reactions are performed under conditions of high dilution. The importance of high dilution becomes apparent when attempting to improve the probability that functional groups within the same molecule react with themselves (intramolecularly), rather than intermolecularly with those in neighbouring molecules in solution, in other words, to ensure cyclisation is favoured over oligomerisation or polymerisation. In view of this, the concentration of reactants at any given time must be extremely small. This is achieved by the slow dropwise addition of reactants over a period of several hours or, on occasions, several days.

Whenever possible, it is always advantageous to isolate, purify and characterise an organic ligand before its metal complexes undergo close scrutiny. For instance, changes in the ligand (solubility, conformation, bonding mode etc.) can be detected prior to, and upon

complexation.

Many macrocyclic ligands can only be synthesised by direct methods; either the intervention of a metal is not required or it disrupts the formation of the desired product. These ligands are stable to oxidation, light and moisture and can be easily isolated for use in further reactions. Examples of these are the dioxo (amide) and thioether macrocycles. Crown ethers and cryptands (polyethers) can be obtained via direct methods, as well as, self-assembly in the presence of templates. In other instances, it is not possible to isolate metal-free macrocycles since they are unstable with respect to hydrolysis. An example of these types of ligands are some of those containing imine functionalities, produced from Schiff-base condensations (*vide infra*).

#### 1.6.2 Metal Template (*In Situ*) Syntheses.

In this approach macrocyclic ligand complex formation is achieved in the presence of a metal ion. Thus, the macrocyclic ligand is generated *in situ*, but only isolated as its metal complex.

For numerous cases of condensations in the absence of a metal-ion, no macrocyclic products are obtained.<sup>[61]</sup> Appropriately, it was concluded that the rôle of the metal ion bears influence on the direction of the synthetic reaction and hence the products obtained.

Two likely mechanistic rôles for the metal have been proposed in terms of the co-ordination template effects. When a metal ion preferentially co-ordinates to one of the components in an equilibrium mixture, and perturbation of this existing equilibrium promotes isolation of the

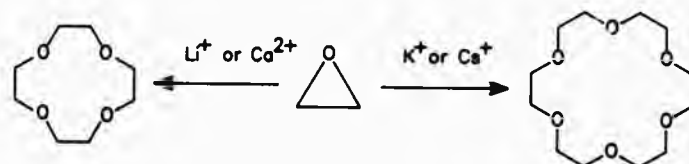
macrocyclic as its complex, a thermodynamic template effect is considered to be operative, i.e. the metal co-ordination geometry matches best that of the product macrocycle. If, on the other hand, a metal ion directs the course of a stepwise reaction by holding the reactive groups in the correct orientation in order to facilitate a stereochemically selective reaction - the action is due to the kinetic template effect. In this case, the metal co-ordination geometry best matches that of the transition-state arrangement of reactants.

Superimposed on this effect, it is possible to envisage an approximation effect, whereby the complexation of both reacting species to the metal converts what would have been a bimolecular reaction into a unimolecular one. Thus, while the reactants are simultaneously complexed in close proximity, they are statistically more likely to react than if mere diffusion were to be relied upon - there is an increase in the effective concentration of the reactants with a consequent increase in the rate of reaction.

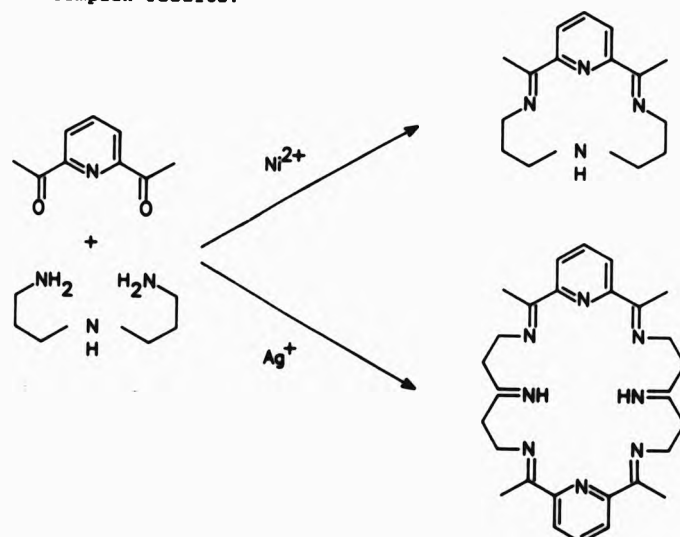
It is possible that both the thermodynamic and kinetic template effects may operate in a given reaction. However, in many cases the detailed rôle of the metal ion has not been defined for the metal template cyclisations.

The size of a templating ion is of fundamental importance to the outcome of a successful synthesis. Consequences of metal-ion/hole size mismatch are evident in a number of macrocyclic products. For instance, the reaction of ethylene oxide with potassium ( $r = 1.38 \text{ \AA}$ ) ions results in the formation of 18-crown-6 ( $R_{\text{H}} = 1.4 \text{ \AA}$ ). Likewise, for the smaller ringed crown compound 12-crown-4 ( $R_{\text{H}} = 0.8 \text{ \AA}$ ), lithium

( $r = 0.76 \text{ \AA}$ ) or calcium ( $r = 0.94 \text{ \AA}$ ) ions are effective templating agents. However, the product of ethylene oxide and caesium ( $r = 1.67 \text{ \AA}$ ) ions does not afford the expected 21-crown-7 ( $R_m = 1.7 \text{ \AA}$ ) complex but yields 18-crown-6 instead.<sup>[76]</sup>

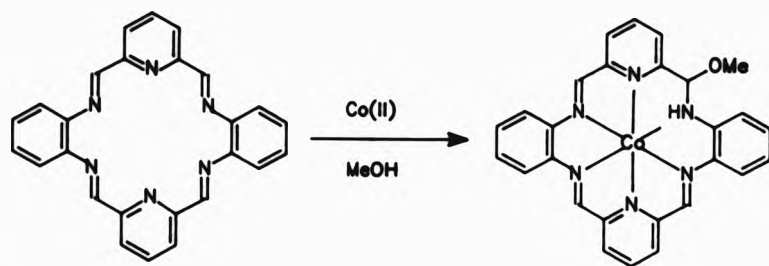


Another example based directly on the metal-ion/hole size concept is the reaction between 2,6-diacetylpyridine and bis(3-aminopropane)amine. In the presence of nickel(II) a mononuclear quadridentate complex is isolated. However, when silver(I) is employed, a bimetallic 28-membered complex results.<sup>[77]</sup>

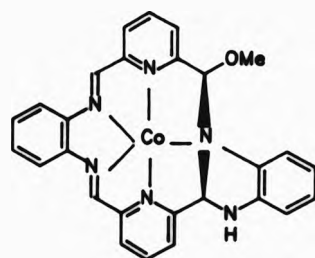


Furthermore, complexation of precursors to the metal ion may also produce an activation or deactivation of the functionalities involved in the cyclisation reaction. Imine-containing macrocycles can undergo

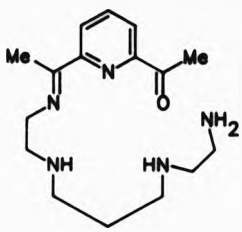
metal-assisted ligand rearrangements, where metal-initiated nucleophilic attack is responsible for intramolecular reorganisation. For example, the preformed hexa-aza macrocycle (non-template procedure) undergoes imine bond solvolysis on treatment with methanolic cobalt(II) solutions.<sup>[78]</sup> Its reaction with cobalt(II) in methanol, initially causes an imine bond to undergo solvolysis:



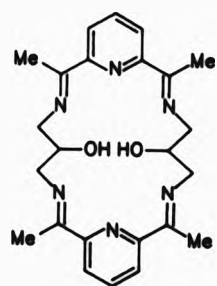
Consequently, there is an increase in ligand flexibility, deviation from planarity and effectively a reduction in bonding cavity. However, this cavity is still unable to accommodate the smaller metal-ion and further nucleophilic attack occurs in response, to eventually yield a smaller 16-membered macrocyclic complex.



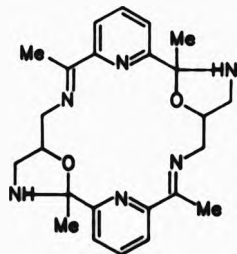
Similarly, in the presence of water, full hydrolysis has been noted to take place which is also known to be metal-induced.<sup>[79]</sup>



The reaction of 2,6-diacetylpyridine with 1,3-diamino-2-hydroxypropane and barium(II) in methanol gives a complex of an octadentate, 20-membered macrocyclic ligand as expected.<sup>[80]</sup>

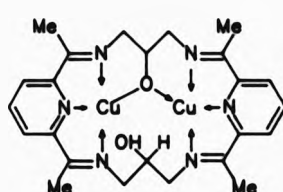


Conversely, in the presence of lead(II) the existence of an oxazolidine resulting in a smaller, sexidentate 18-membered ring unit has been described.

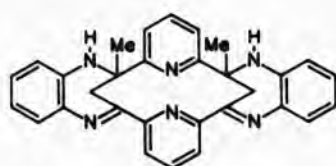


In addition, the reaction with copper(II) does not result in imine solvolysis of the octadentate, 20-membered ligand in order to accommodate the smaller metal ion. Instead, due to its much larger

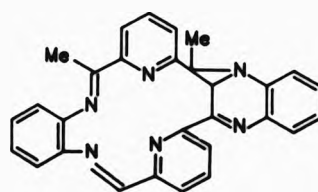
ring size and compartmental nature, the ligand is able to incorporate two copper(II) ions into its bonding cavity.



Rearrangements of increasing complexity have been observed for the methyl analogue of the hexa-aza macrocycle, where steric hindrance promotes ligand alterations.<sup>[81]</sup>



On treatment with excess copper(II) the [7+12+7] inner ring system rearranges to a tricyclic system containing [15+6+3] membered inner rings.<sup>[82]</sup>



When metal ions fail to act as templating agents, an alternate synthetic route to the formation of their complexes can be adopted: transmetallation.<sup>[83]</sup> These are metathetical reactions in which the template metal ion may be substituted for another metal in order to obtain a complex which is not directly available via the template

route.

#### **1.7 Toxic Heavy Metals.**

This section outlines the toxicity of heavy metals and hence, emphasises on the need for 'strongly' selective and efficient complexing agents to aid in their removal and recovery.

Toxic heavy metals are considered to be those of a relatively high density, which show no indication of being an essential trace element in biological processes and have a cumulative effect in living organisms. The metals lead, cadmium and mercury belong to such a category. For centuries, these metals and their compounds have been employed in industry as well as on a household basis. Their applications vary from the specialised, such as fuel antiknock additives (lead), pressure-sensing devices (mercury), heat and light stabilisers in plastics (cadmium), to more common usages such as plating to prevent corrosion (lead and cadmium), batteries (all three), and as preservatives and/or fungicides for antifouling paints (lead and mercury).

##### **1.7.1 Toxicity.**

Lead is a poison in all forms, but finely divided, soluble particles are more hazardous than larger particles with lower solubilities. It is absorbed into the circulatory system of the body by ingestion (10% of ingested lead is absorbed into the blood stream) or after inhalation of dust via the digestive tract and lungs. Normally intake approximately equals output (excretion via urine and faeces); however, disruptions of this balance can occur on prolonged exposure, resulting in malnutrition and constipation, to kidney failure and neuromuscular

dysfunction, the developing fetus being most prone to risk. Strict limitations on airborne lead ( $1.5 \mu\text{g Pb m}^{-3}$  air) are enforced by the Environmental Protection Act, with the acceptable blood level limit dropping each year. In 1983, the blood level limits were set at  $50 \mu\text{g Pb /100 g whole blood}$ .<sup>(84)</sup>

In contrast, cadmium is poorly absorbed by the gastrointestinal tract (only 6 % of the estimated  $40-50 \mu\text{g day}^{-1}$  of ingested cadmium is absorbed), whereas, 25-50 % of ca.  $2-10 \mu\text{g day}^{-1}$  cadmium content of inhaled dust and fumes is absorbed.<sup>(85)</sup> Thus, exposure through the respiratory tract appears to be more effective, with 10-40 % of inhaled cadmium from cigarette smoke being absorbed. Cadmium has a strong affinity for the liver and kidneys and with a half-life of 10-30 years, it is the environmental poison most prone to accumulation. A dose of  $6 \text{ mg m}^{-3}$  air causes severe lung damage after 8 hours exposure. One minute inhalation of  $2500 \text{ mg m}^{-3}$  air is fatal. To date, renewed stricter controls on the use of cadmium (more importantly in the home rather than in industry) have been demanded by Members of the European Parliament in EC legislations. Covering approximately 85 % of community use of cadmium, priority has been given to batteries (containing 28 % Cd by weight) and pigments in polymers, with an absolute ban on items containing more than 0.1 % Cd in the finished product. However, a total ban in some instances is not yet viable, since, the safety of satisfactory substitutes must also be proven.

Metallic mercury and its vapour are more potent than all its compounds, including organic and inorganic. They are all protoplasmic poisons that may enter the body through the skin, gastrointestinal or respiratory tract. On absorption, they dissociate into body fluids,

and in the blood they distribute between the plasma and the erythrocytes. Alkyl derivatives have a half-life of 50-60 days whilst inorganic salts have a half-life of 30-60 days. The former affects the central nervous system and accumulates in the brain where elimination is slow. Salts such as mercuric chloride are very poisonous due to their high solubility and vapour density, which accounts for slow vapour dissipation. Government agencies have imposed severe restrictions on their release in waterways and air and their uses as pharmaceuticals, diuretics and antiseptics has declined sharply in recent years. The maximum atmospheric concentration in all forms is  $0.1 \text{ mg Hg m}^{-3}$  air (except for alkyl =  $0.01 \text{ mg Hg m}^{-3}$  air) with a threshold limit value of  $0.05 \text{ mg Hg m}^{-3}$  air.<sup>[86]</sup> Other applications such as ophthalmic preparations, dentistry, catalysis and intermediates in the formation of other products are still important areas in which mercury and its compounds are still used. Conversely, their usefulness as chromogenic materials has been short lived because of their potential carcinogenic/mutagenic properties. In addition, they are non-biodegradable, this stresses the importance of control, recovery and disposal of a product and not only its manufacturing process.

Lead and zinc ores are intimately mixed and therefore mined together. These mines also sometimes contain cadmium, which pollutes the air when extraction of these metal ores is achieved. Hence the need for commercially viable, recyclable, selective extractants becomes pertinent as the awareness of health and environmental issues increases by public demand.

In 1988, the Control of Substances Hazardous to Health (COSHH), made under provisions of the 'Health and Safety at Work Act, 1974'

regulations came into effect. Under these regulations, in Britain substances such as lead, cadmium and mercury are monitored. The use of lead is dealt by the 'Control of Lead at Work Regulations 1980' and has a maximum exposure limit (MEL), which is the maximum concentration of airbourne substance, averaged over a reference period (8 hrs time-weighted average) that must not exceed  $0.15 \text{ mg m}^{-3}$  of air (for tetraethyl lead 'antiknock' the limit is set at  $0.1 \text{ mg m}^{-3}$  of air). Cadmium also has an MEL which is  $0.05 \text{ mg m}^{-3}$  of air. However, mercury has an occupational exposure standard (OES) of  $0.05 \text{ mg m}^{-3}$  of air.<sup>[87]</sup> This is the concentration of an airbourne substance, averaged over a reference period, at which, according to current knowledge there is no evidence that it is likely to be injurious to employees, if they are exposed by inhalation, day after day to that concentration.

In addition, the Operation of Integrated Pollution Control (IPC), under part 1 of the Environmental Protection Act 1990, is concerned with the control of releases of prescribed substances to air, water and land. As prescribed substances, cadmium and mercury and their compounds must not be released to water, i.e., discharged to the sewer.<sup>[88]</sup>

Interestingly, although silver is not a candidate for toxic heavy metals, it is mined from Zn-Ag-Pb-Cu mines and has similar properties and consequently usages as the aforementioned metals. Silver and its compounds are found in paints, batteries, dental amalgam, mirrors, the photographic industry and as catalysts and powerful bacteriocides. Toxicity of silver salts is dependent on the nature of the counterion present, otherwise they are considered to be without adverse health effects. Irreversible deposition of chemical or colloidal silver on mucus membranes, can nevertheless result in disfigured body

tissues.<sup>[89]</sup>

It is important, therefore, to improve ways of metal extraction with the minimum amount of disturbance to the surrounding environment, be it a mixture of metals from an ore or selective removal of toxic metals (minus the essential trace elements, e.g. zinc) from victims of metal poisoning.

#### *1.7.2 Extraction and Recovery of Heavy Metals.*

Removal of trace quantities of toxic metals (and precious metals) relying on biological systems have been studied. Micro-organisms such as *Chlorella Vulgaris* have been utilised to leach out different metal ions as a result of pH dependence. Several established industrial processes employ sodium tetraborate for the removal and/or recovery of metals from effluent streams: mercury from chloroalkali plants, lead from tetraalkyllead production, and silver and cadmium from photographic film manufacture.<sup>[90]</sup>

For decades, an area that has been exploited for metal-ion recovery is ion-exchange,<sup>[91]</sup> but now procedures involving macrocyclic ligands for solvent extraction purposes are under investigation.<sup>[92]</sup> The ability of macrocyclic ligands to solubilise salts in non-aqueous media has been a major breakthrough in-so-far as mimicking transport of ions through cell membranes in biological systems.<sup>[93]</sup>

Although, macrocyclic ligands have a greater discriminating ability, their interest and uses are at present limited to research because of production costs. It is therefore, doubly important to find newer and better cost-effective synthetic routes leading to the isolation of

these ligands.

#### 1.8 Proposed Program for Ligand Design.

Concluding Chapter One, this section outlines the strategy involved in the syntheses of selective complexing agents for the toxic heavy metal ions.

The initial problems that arise from designing such ligands, is the ability to be selective towards only those metal ions in question. For instance, discrimination is required between Pb/Ag, Cd/Zn and Pb/Hg/Cd. In fact, the chemistry of these metal ions and those which are not of interest to this project directly such as nickel(II) and copper(II) must also be investigated for an overall view of ligand reactivity.

On the basis of hard/soft compatibility nitrogen-sulphur mixed-donor sets were employed for the soft/borderline preferences of the toxic heavy metals. The donor atoms were interspersed with aromatic groups and saturated flexible chains providing a macrocyclic framework of intermediate rigidity, in an attempt to produce restricted co-ordination environments. The ionic radii of lead, cadmium and mercury range from 1.19-0.95 Å for their hexa-co-ordinate complexes. Hence, the importance of having adequate distances between donor atoms so that a bonding cavity may be formed around these metal ions.

Two ring sizes were utilised - fifteen- and eighteen-membered, which would determine metal ion/cavity size preferences, i.e. if smaller metal ions interact with larger macrocyclic ligands by folding etc. or if larger metal ions have the ability to form 'out-of-plane' complexes with the smaller macrocyclic ligands. The general ligand framework was

altered, so that not only could different donor atom types be investigated but also how changes in hybridisation of a particular ligator such as nitrogen ( $sp^2$  to  $sp^3$ ) would lead to a gradation of ligand reactivity due to electron availability and rigidity (amine to imine to amide).

In bioinorganic chemistry, the term entasis is used to describe the state of the active site in metalloenzymes. Entasis conveys a state of tension or stress and gives rise to 'energised' metal centres where they are subjected to unusual bond lengths, geometries and co-ordination numbers. It was thought that on designing ligands for the less stereospecific metal ions like cadmium(II), mercury(II) and lead(II), such effects might be observed. Ideally, a fine balance is required that will ultimately employ the high affinity of the metal ions which compete for active sites on the ligand substrate.

*References - Chapter One.*

1. R. F. Gould (ed), 'Werner Centennial,' American Chemical Society, 1967.
2. R. M. Izatt and J. J. Christensen (eds), 'Synthetic Multidentate Macrocyclic Compounds,' Academic, New York, 1978, Ch 6.
3. B. Girmay, J. D. Kilburn, A. E. Underhill, K. S. Varma, M. B. Hursthouse, M. E. Harman, J. Becher and G. Bojesen, *J. Chem. Soc., Chem. Commun.*, 1989, 1406.
4. D. E. Fenton, U. Casellato and P. A. Vigato, in 'Environmental Inorganic Chemistry,' VCH, 1985, 273.
5. (a) R. A. Bulman, *Struct. Bonding*, 1987, 67, 91; (b) D. Bryce-Smith, *Chem. Soc. Rev.*, 1986, 15, 93.
6. D. Parker, *Chem. Br.*, 1990, 26, 942.
7. J. F. Stoddart, in 'Progress in Macrocyclic Chemistry,' R. M. Izatt and J. J. Christensen (eds), 1981, Vol 2, Ch 4.
8. M. G. B. Drew, J. de O. Cabral, M. F. Cabral, F. S. Esho and S. M. Nelson, *J. Chem. Soc., Chem. Commun.*, 1979, 1033; (b) D. E. Fenton, B. P. Murphy, A. J. Leong, L. F. Lindoy, A. Bashall and M. McPartlin, *J. Chem. Soc., Dalton Trans.*, 1987, 2543.
9. G. A. Nelson (ed), 'Coordination Chemistry of Macrocyclic Compounds', Plenum, New York, 1979.
10. K. B. Mertes and J. M. Lehn, in 'Comprehensive Co-ordination Chemistry,' Pergamon Press, Oxford, 1987, Vol 2, pp. 916-921.
11. (a) R. P. Linstead, and M. Whalley, *J. Chem. Soc.*, 1952, 4839; (b) J. A. Elvidge and J. H. Golden, *J. Chem. Soc.*, 1957, 700.
12. (a) J. Van Alphen, *Rec. Trav. Chim. Pays-Bas*, 1936, 55, 835; (b) D. H. Peacock and Y. S. Gwan, *J. Chem. Soc.*, 1937, 1468.
13. (a) N. F. Curtis, *J. Chem. Soc.*, 1960, 4409; (b) G. A. Nelson and D. H. Busch, *Proc. Chem. Soc.*, 1963, 223.

14. (a) F. Umland and D. Thierig, *Angew. Chem.*, 1962, **74**, 388; (b) M. C. Thompson and D. H. Busch, *J. Am. Chem. Soc.*, 1964, **86**, 3651.
15. (a) C. J. Pedersen, *J. Am. Chem. Soc.*, 1967, **89**, 2495; 7017; (b) R. M. Izatt and J. J. Christensen (eds), 'Synthetic Multidentate Macroyclic Compounds,' Academic Press, New York, 1978, Ch 1.
16. R. W. Hay, 'Bio-Inorganic Chemistry,' Ellis Horwood Ltd, Chichester, 1987, Ch 3.
17. D. E. Fenton, in 'Comprehensive Co-ordination Chemistry,' G. Wilkinson (ed), Pergamon Press, Oxford, 1987, Vol 3, pp. 1-80.
18. P. V. Bernhardt and G. A. Lawrence, *Coord. Chem. Rev.*, 1990, **104**, 297.
19. U. Casellato, P. A. Vigato, D. E. Fenton and M. Vidali, *Chem. Soc. Rev.*, 1979, **8**, 199.
20. K. B. Mertes and J. M. Lehn, in 'Comprehensive Co-ordination Chemistry,' Pergamon Press, Oxford, 1987, Vol 2, pp. 927-957.
21. C. J. Pedersen, *J. Am. Chem. Soc.*, 1967, **89**, 2459, 7017.
22. E. C. Constable and J. M. Holmes, *Polyhedron.*, 1988, **7**, 2531.
23. H. Adams, N. A. Bailey, W. D. Carlisle, D. E. Fenton and G. Rossi, *J. Chem. Soc., Dalton Trans.*, 1990, 1271.
24. A. Hammershoi and A. M. Sargeon, *Inorg. Chem.*, 1983, **22**, 3554.
25. C. O. Dietrich-Buchecker, J. M. Kern and J. P. Sauvage, *J. Am. Chem. Soc.*, 1984, **106**, 3043.
26. L. Fabbrizzi, F. Forlini, A. Perotti and B. Seghi, *Inorg. Chem.*, 1984, **23**, 807.
27. C. T. Lin, D. B. Rorabacher, G. R. Caley and D. W. Margerum, *Inorg. Chem.*, 1975, **11**, 288.
28. A. D. Hamilton, J. M. Lehn and J. Sessler, *J. Chem. Soc., Chem. Commun.*, 1984, 311.
29. R. Bhula, P. Osvath and D. C. Weatherburn, *Coord. Chem. Rev.*, 1988,

91, 89.

30. R. K. Boggess and W. D. Wiegale, *J. Chem. Educ.*, 1978, 55, 156.
31. J. E. Davies, W. Kemula, H. M. Powell and N. O. Smith, *J. Inclusion Phenom.*, 1983, 1, 3.
32. M. J. Gunter and M. R. Johnston, *Tetrahedron Lett.*, 1990, 31, 4801.
33. P. D. Beer and A. D. Keefe, *J. Organomet. Chem.*, 1989, 375, C40.
34. D. J. Cram, J. Weiss, R. C. Helgeson, C. B. Knobler, A. E. Dorigo and K. N. Houk, *J. Chem. Soc., Chem. Commun.*, 1988, 407.
35. J. M. Lehn, *Angew. Chem. Int. Ed. Engl.*, 1988, 27, 89.
36. P. D. Beer, M. G. B. Drew, A. Ibbotson and E. L. Tite, *J. Chem. Soc., Chem. Commun.*, 1988, 1498.
37. P. D. Beer, *Chem. Soc. Rev.*, 1989, 18, 409.
38. (a) M. E. Tanner, C. B. Knobler and D. J. Cram, *J. Am. Chem. Soc.*, 1990, 112, 1659; (b) M. L. C. Quan, C. B. Knobler and D. J. Cram, *J. Am. Chem. Soc.*, 1991, 113, 2754.
39. C. D. Gutsche, 'Calixarenes,' Monograph in Supramolecular Chemistry, J. F. Stoddart (ed), RSC, Cambridge, 1989.
40. (a) D. N. Reinhoudt and E. J. R. Sudhölter, *Adv. Mater.*, 1990, 2, 23; (b) I. Sutherland, *J. Chem. Soc., Chem. Commun.*, 1992, 582.
41. J. L. Atwood, Proceedings of the 16th International Symposium on Macroyclic Chemistry, Sheffield, 1991.
42. D. Philp and J. F. Stoddart, *Synlett.*, 1991, 445.
43. (a) J. F. Stoddart, *Chem. Br.*, 1991, 27, 714; (b) P. L. Anelli, N. Spencer and J. F. Stoddart, *J. Am. Chem. Soc.*, 1991, 113, 5131.
44. F. A. Cotton and G. Wilkinson, 'Advanced Inorganic Chemistry,' Wiley, New York, (5th edn) 1988.
45. G. Schwarzenbach, *Helv. Chim Acta.*, 1952, 35, 2344.
46. D. Munro, *Chem. Br.*, 1977, 13, 100.
47. K. F. Purcell and J. C. Kotz, 'Inorganic Chemistry,' Holt-Sanders

International, London, 1985.

48. J. E. Huheey, 'Inorganic Chemistry-Principles of Structure and Reactivity,' Harper and Row, (3rd edn) 1983, Ch 18.
49. D. K. Cabbiness and D. W. Margerum, *J. Am. Chem. Soc.*, 1969, **91**, 6540.
50. F. P. Hinz and D. W. Margerum, *Inorg. Chem.*, 1974, **13**, 2941.
51. L. S. W. L. Sokol, L. A. Ochrymowycz and D. B. Rorabacher, *Inorg. Chem.*, 1981, **20**, 3189.
52. M. Micheloni, P. Paoletti, L. Siegfried-Hertli and T. A. Kaden, *J. Chem. Soc., Dalton Trans.*, 1985, 1169.
53. (a) H. K. Frensdorff, *J. Am. Chem. Soc.*, 1971, **93**, 600; (b) C. J. Petersen and H. K. Frensdorff, *Angew. Chem. Int. Ed. Engl.*, 1972, **11**, 16.
54. M. Kodama and E. Kimura, *J. Chem. Soc., Dalton Trans.*, 1976, 2341.
55. M. Micheloni, P. Paoletti and A. Sabatini, *J. Chem. Soc., Dalton Trans.*, 1983, 1189.
56. (a) B. L. Haymore, J. D. Lamb, R. M. Izatt and J. J. Christensen, *Inorg. Chem.*, 1982, **21**, 1598; (b) R. M. Izatt, J. S. Bradshaw, S. A. Nielson, J. D. Lamb, J. J. Christensen and D. Sen, *Chem. Rev.*, 1985, **85**, 271.
57. J. M. Lehn and J. P. Sauvage, *J. Am. Chem. Soc.*, 1975, **97**, 6700.
58. L. F. Lindoy, 'The Chemistry of Macrocyclic Ligand Complexes,' Cambridge University Press, 1989, Ch 4.
59. D. H. Busch, K. Farmery, V. Goedken, V. Katovik, A. C. Melnyk, G. R. Sperati and N. Tokel, *Advan. Chem. Ser.*, 1971, **100**, 44.
60. L. F. Lindoy, 'The Chemistry of Macrocyclic Ligand Complexes,' Cambridge University Press, 1989, Ch 7.
61. (a) S. M. Nelson, *Pure Appl. Chem.*, 1980, **52**, 2461; (b) D. E. Fenton, *Pure Appl. Chem.*, 1986, **58**, 1437.

62. J. L. Karn and D. H. Busch, *Nature*, 1966, 211, 160.
63. R. G. Pearson, *J. Chem. Educ.*, 1968, 45, 581; 643.
64. D. St. C. Black, in 'Comprehensive Coordination Chemistry,' G. Wilkinson (ed), Pergamon Press, Oxford, 1987, Vol 6, pp. 155-227.
65. G. R. Newkome, V. K. Gupta and J. D. Sauer, 'Heterocyclic Compounds - Pyridine and its Derivatives,' Wiley, 1984, Vol 14, Ch 3.
66. D. J. Cram, T. Kaneda, R. C. Helgeson, S. B. Brown, C. B. Knobler, E. Maverick and K. N. Trueblood, *J. Am. Chem. Soc.*, 1985, 207, 3645.
67. K. Henrick, P. A. Tasker and L. F. Lindoy, in 'Progress in Inorganic Chemistry,' 1985, 33, pp. 1-58.
68. N. K. Dalley, *J. Chem. Soc., Chem. Commun.*, 1975, 84.
69. R. D. Hancock and M. P. Ngwenya, *J. Chem. Soc., Dalton Trans.*, 1987, 2911.
70. R. D. Hancock, P. W. Wade, M. P. Ngwenya, A. S. de Sousa and K. V. Damu, *Inorg. Chem.*, 1990, 29, 1968.
71. L. F. Lindoy, in 'Progress in Macrocyclic Chemistry,' R. M. Izatt and J. J. Christensen (eds), Wiley-Interscience, New York, 1987, Vol 3, Ch 2.
72. L. F. Lindoy, in 'Current Topics in Macrocyclic Chemistry in Japan,' E. Kimura (ed), Hiroshima University School of Medicine, 1987.
73. K. R. Adam, K. P. Dancey, B. A. Harrison, A. J. Leong, L. F. Lindoy, M. McPartlin and P. A. Tasker, *J. Chem. Soc., Chem. Commun.*, 1983, 1351.
74. K. R. Adam, B. J. McCool, A. J. Leong, L. F. Lindoy, C. W. G. Ansell, P. J. Baillie, K. P. Dancey, L. A. Drummond, K. Henrick, M. McPartlin, D. K. Uppal and P. A. Tasker, *J. Chem. Soc., Dalton Trans.*, 1990, 3435.
75. R. D. Hancock and A. E. Martell, *Chem. Rev.*, 1989, 89, 1875.

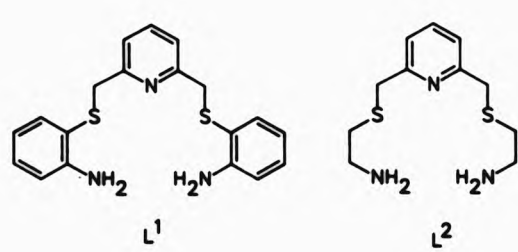
76. E. C. Constable, 'Metal and Ligand Reactivity,' Ellis Horwood Ltd, England, 1990.
77. M. G. B. Drew, C. V. Knox and S. M. Nelson, *J. Chem. Soc., Dalton Trans.*, 1980, 942.
78. S. M. Nelson, F. S. Esho, M. G. B. Drew and P. Bird, *J. Chem. Soc., Chem. Commun.*, 1979, 1035.
79. C. Cairns, S. G. McFall, S. M. Nelson and M. G. B. Drew, *J. Chem. Soc., Dalton Trans.*, 1979, 446.
80. N. A. Bailey, D. E. Fenton, I. T. Jackson, R. Moody and C. Rodriguez de Barbarin, *J. Chem. Soc., Chem. Commun.*, 1983, 1463.
81. J. de O. Cabral, M. F. Cabral, M. G. B. Drew, F. S. Esho, O. Hass and S. M. Nelson, *J. Chem. Soc., Chem. Commun.*, 1982, 1066.
82. J. de O. Cabral, M. F. Cabral, M. G. B. Drew, F. S. Esho and S. M. Nelson, *J. Chem. Soc., Chem. Commun.*, 1982, 1068.
83. S. M. Nelson, S. G. McFall, M. G. B. Drew and A. H. bin Othman, *Proc. Roy. Irish Acad.*, 1977, 77B, 523.
84. Kirk-Othmer, 'Encyclopedia of Chemical technology,' Wiley-Interscience, (3rd edn) 1981, vol 14.
85. Kirk-Othmer, 'Encyclopedia of Chemical technology,' Wiley-Interscience, (3rd edn) 1978, vol 6.
86. Kirk-Othmer, 'Encyclopedia of Chemical technology,' Wiley-Interscience, (3rd edn) 1981, vol 15.
87. EH40/91 Health and Safety Executive (HSE), 'Occupational Exposure limits 1991,' London (HMSO), 1991.
88. Guidance Issued by the D.O.E and the Welsh Office, 'Integrated Pollution control - A practical Guide.'
89. Kirk-Othmer, 'Encyclopedia of Chemical technology,' Wiley-Interscience, (3rd edn) 1983, vol 21.
90. R. Thompson (ed), 'Trace Metal Removal from Aqueous Solution',

Royal Society of Chemistry-Annual Chemical Congress, 1986.

91. J. Starý, 'The Solvent Extraction of Metal Chelates', Pergamon Press, Oxford, 1964.
92. L. F. Lindoy and D. S. Baldwin, *Pure Appl. Chem.*, 1989, 61, 909.

CHAPTER TWO

SYNTHESES, CHARACTERISATION AND CO-ORDINATION STUDIES OF TWO  
QUINQUEDENTATE NITROGEN-SULPHUR ACYCLIC PRECURSOR LIGANDS,  $L^1$  AND  $L^2$ .



## 2.1 General Introduction.

This chapter

describes the synthesis and complexing behaviour of L<sup>1</sup> and L<sup>2</sup>, which were studied prior to any macrocyclic work being undertaken.

## 2.2 Synthesis of L<sup>1</sup>.

The synthetic route leading to L<sup>1</sup> is outlined below (Figure 2.2a). The starting material employed was 2,6-bis(hydroxymethyl)pyridine (1). Attempts to synthesise this precursor from 2,6-pyridine dicarboxylic acid (2) via the ester (3), using the method described in the literature were unsuccessful.<sup>[1]</sup> Thereafter, 2,6-bis(hydroxymethyl)pyridine was obtained commercially.

Preparation of 2,6-bis(bromomethyl)pyridine (4) was carried out using a reported procedure.<sup>[2]</sup> It was found to be essential to use freshly recrystallised material (i.e. within ca. 24 hrs.) otherwise a dark pink colouration developed, which could not be used in any further reactions. The nature of the undesirable pink side-product was difficult to characterise, but is suspected to be a (1+1) cyclic dibromide.<sup>[3]</sup>

It was important to carry out the final step (involving preparation of the sodium salt of 2-aminothiophenol, with subsequent nucleophilic substitution of 2,6-bis(bromomethyl)pyridine) under an inert atmosphere ( $N_2$ ), to prevent the formation of disulphide bridges between two 2-aminothiophenol molecules. This occurred when the reaction was exposed to air (characterised by mass spectrometry m/z 248).

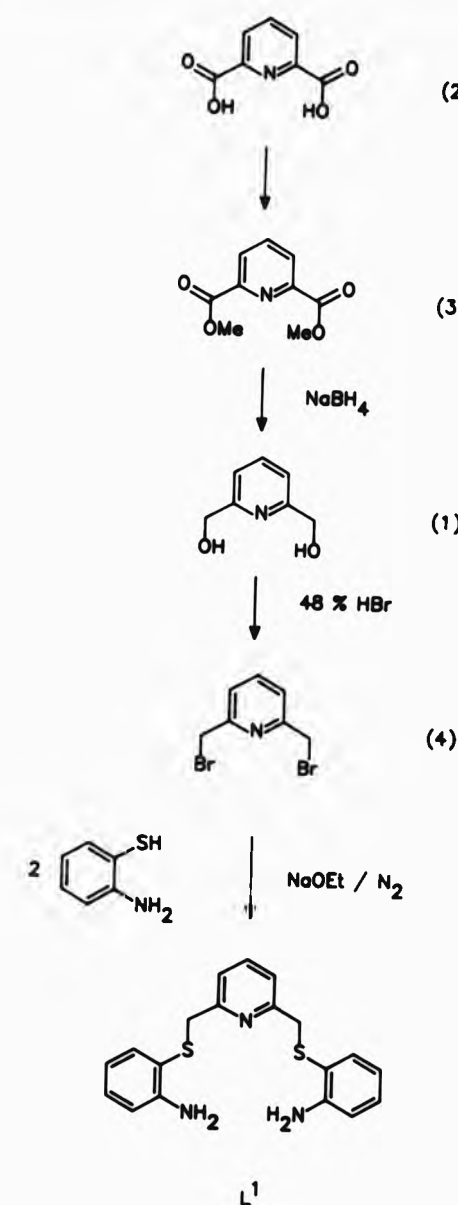
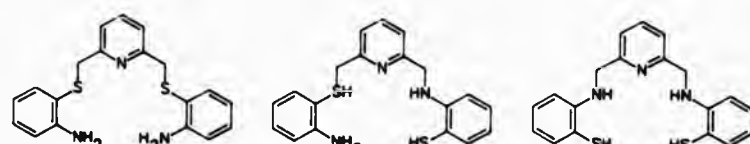


Figure 2.2a Synthetic route for preparation of  $L^1$ .

The insolubility of the final product in water, proved to be an excellent means by which it could be separated from the final reaction mixture to yield 2,6-bis(aminothiophenoxyethyl)pyridine, L<sup>1</sup>.

The reaction afforded white fibrous crystals of good purity and high yield (62 %) when rigorous experimental conditions were maintained, but occasionally, a dark brown caramel-like substance was produced. Repeated recrystallisations (ca. x5) from absolute ethanol and water using decolourising charcoal purified the crude tar to give pale yellow fibrous crystals, albeit in low yield (25 %). Both types of crystals analysed for L<sup>1</sup> and were therefore used in the same way.

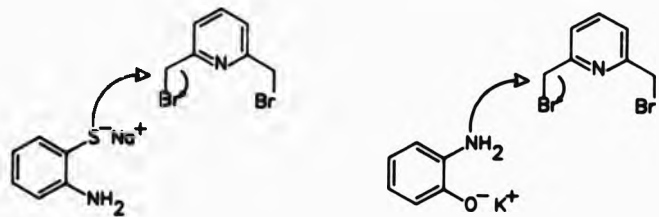
Consideration of the synthetic route indicates that the reaction between 2,6-bis(bromomethyl)pyridine and 2-aminothiophenol can in fact result in any one of three products, depending on which heteroatom of the mercaptoaniline can preferentially act as the nucleophile.



L<sup>1</sup>

The success of the synthetic strategy relies on the fact that the anilino nitrogen acts as a much weaker base when a thiol group is attached at the ortho position. This allows the sodium salt of the thiolate to act as the nucleophile and displace the bromine from 2,6-bis(bromomethyl)pyridine. Therefore the majority of the product was found to be L<sup>1</sup>. In contrast, for a related system in which 2-aminophenol is used, the electron-donating hydroxy function has a

base strengthening effect on the anilino nitrogen; this then becomes the stronger nucleophile of the two and attacks the 2,6-bis(bromomethyl)pyridine ( $pK_a = 2.73^{(5)}$ , 4.62, 4.72 for aminothiophenol, aniline and aminophenol respectively).<sup>(6)</sup>



In this instance, it is always necessary either to protect the anilino function prior to nucleophilic attack or, more usually, 2-nitrophenol is employed initially and the nitro groups are then subsequently reduced.

### 2.3 Characterisation of L<sup>1</sup>.

Infrared analysis shows two bands typical of symmetric and asymmetric stretching for primary amines  $\nu(N-H)$  at ca. 3440 and 3340  $\text{cm}^{-1}$ , with a sharp band at 1600  $\text{cm}^{-1}$  attributed to  $\nu(C=C)$  of pyridine and/or the phenylene rings. The absence of thiol absorptions between ca. 2600-2500  $\text{cm}^{-1}$  precludes the presence of any reactants in the product. The mass spectrum gives a parent ion peak at  $m/z$  353 corresponding to the molecular weight of L<sup>1</sup>. Elemental analysis has the required compositions for carbon, hydrogen and nitrogen (section 7.1). The proton (Table 2.3a) and carbon-13 (Table 2.3b) n.m.r. data were also in agreement with the given structure.

Full assignment of the proton and carbon-13 n.m.r. spectra of L<sup>1</sup> was achieved through hetero-nuclear correlation spectroscopy (<sup>1</sup>H,<sup>13</sup>C-COSY),

first-order spin-spin coupling multiplicities and substituent-induced shift parameters.<sup>[7]</sup> The proton n.m.r. spectra of L<sup>1</sup> were run in different deuterated solvents, d<sub>1</sub>-chloroform and d<sub>3</sub>-acetonitrile. There were two reasons for this. Firstly, to observe how L<sup>1</sup> would interact with solvent molecules in solution. Secondly, the metal complexes of L<sup>1</sup> were synthesised and recrystallised in either acetonitrile and/or methanol. Hence, the complexes of the diamagnetic metal ions of L<sup>1</sup> would preferentially solubilise in d<sub>3</sub>-acetonitrile or d<sub>4</sub>-methanol; comparative conclusions could then be drawn between L<sup>1</sup> and its metal complexes.

The proton n.m.r. spectrum (Figure 2.3a) in both solvents gave resonance signals representing eight different chemical environments. The total number of protons present in L<sup>1</sup> are nineteen, but as the two halves of the molecule are chemically equivalent, one would expect ten signals instead of eight. This is suggestive of rapid rotation about the C-S and C-N bonds in solution; hence, the protons of CH<sub>2</sub> and NH<sub>2</sub> are magnetically equivalent on the n.m.r. time scale.

Analyses of both proton n.m.r. spectra (d<sub>1</sub>-chloroform and d<sub>3</sub>-acetonitrile) showed the signals of L<sup>1</sup> (except for NH<sub>2</sub>) to be chemically shifted either upfield or downfield by a maximum of ± 0.10 p.p.m. only. There was no evidence to suggest that the various solvents had drastically affected the structural or chemical nature of L<sup>1</sup>. Interpretation of the proton n.m.r. of L<sup>1</sup> has been described for both solvents simultaneously. The first parameter ( $\delta$  or J) refers to the d<sub>1</sub>-chloroform spectrum, whilst values for d<sub>3</sub>-acetonitrile are quoted directly thereafter, in parentheses in bold.

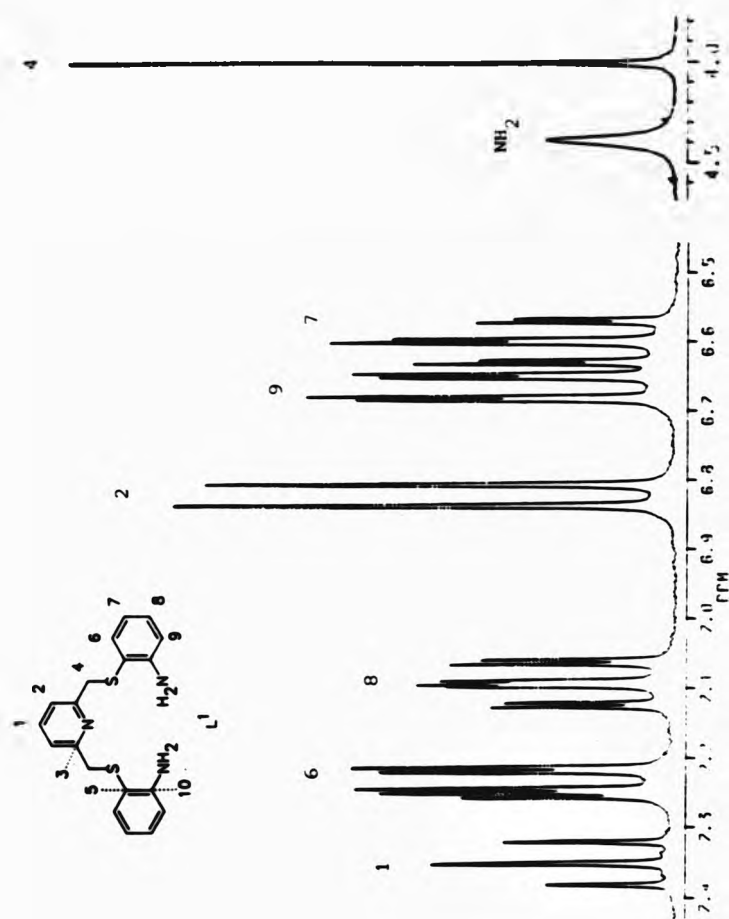
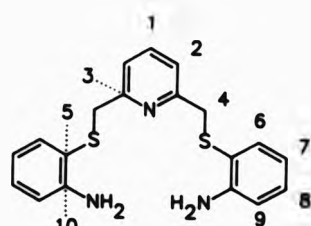


Figure 2.3a  $^1\text{H}$  n.m.r. spectrum of  $\text{L}$  in  $d_6$ -chloroform.

Table 2.3a  $^1\text{H}$  n.m.r. data<sup>a</sup> for L<sup>1</sup> in  $\text{CDCl}_3$  (250.133 MHz) and  $\text{CD}_3\text{CN}$  (250.134 MHz) at ambient temperature.



Chemical shift <sup>a</sup> $\text{CDCl}_3$	Chemical shift <sup>a</sup> $\text{CD}_3\text{CN}$	equivalent nuclei (by integration)	multiplicity	assignment
7.35	7.42	1H	t	$\text{H}^1$
7.23	7.15	2H	dd	$\text{H}^6$
7.09	7.05	2H	ddd <sup>b</sup>	$\text{H}^8$
6.82	6.92	2H	d	$\text{H}^2$
6.66	6.69	2H	dd	$\text{H}^9$
6.60	6.50	2H	td	$\text{H}^7$
4.39	4.70	4H	s	$\text{NH}_2$
4.00	3.94	4H	s	$\text{H}^4$

<sup>a</sup>In p.p.m., relative to  $\text{SiMe}_4$ . <sup>b</sup>Different ortho couplings  $^3\text{J}(\text{H}-\text{H}^{7,9})$  give rise to extra signals.

The pyridyl proton  $\text{H}^1$  is ortho coupled to the magnetically equivalent protons  $\text{H}^2$ , with a three-bond coupling constant of 7.7(7.7) Hz giving rise to a triplet centered at  $\delta$  7.4(7.4) p.p.m. Consequently, the pyridyl protons  $\text{H}^2$  are ortho coupled to  $\text{H}^1$ , with a three-bond coupling constant of 7.7(7.7) Hz present as a doublet at  $\delta$  6.82(6.92) p.p.m.

The remaining aromatic protons H<sup>6</sup>-H<sup>9</sup>, show splitting patterns in accordance with three- and four-bond coupling. H<sup>6</sup> and H<sup>9</sup> each appear as a doublet of doublets. Both types of proton show ortho [ $J = 7.7(7.7)$  and  $8.0(8.1)$  Hz respectively], as well as meta [ $J = 1.6(1.6)$  and  $1.3(1.3)$  Hz respectively] coupling. At the same time, both H<sup>7</sup> and H<sup>8</sup> are ortho coupled to two adjacent protons; H<sup>6</sup>, H<sup>8</sup> [ $J = 7.5(7.5)$  Hz] and H<sup>7</sup>, H<sup>9</sup> [ $J = 7.3(7.3)$  and  $8.0(8.1)$  Hz (see below)], with meta coupling to H<sup>8</sup> [ $J = 1.3(1.4)$  Hz] and H<sup>6</sup> [ $J = 1.6(1.6)$  Hz] respectively. Hence H<sup>7</sup> is a triplet of doublets. It is interesting to note that the signal for H<sup>8</sup> is a result of slightly different ortho couplings to H<sup>7</sup> and H<sup>9</sup>, which is reflected by  $J(H^8-H^7$  or H<sup>9</sup>) = 7.3 and 8.0 Hz, and displays a doublet of doublet of doublets multiplicity (Figure 2.3b).

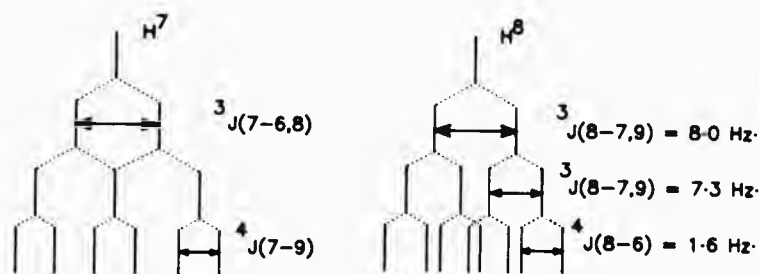
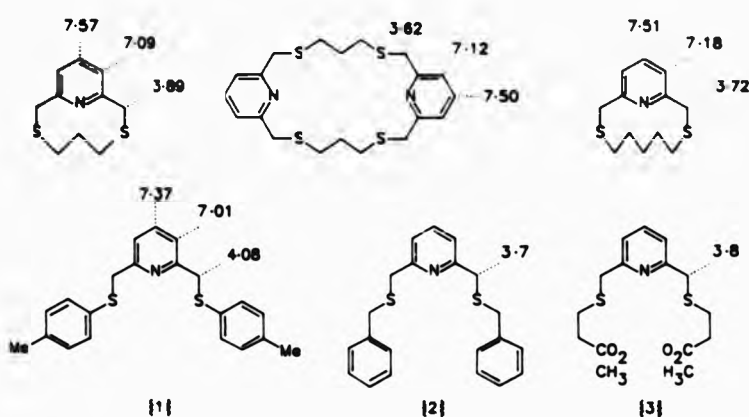


Figure 2.3b Multiplet splitting pattern for H<sup>7</sup> and H<sup>8</sup>.

The methylene protons H<sup>4</sup> appear as a singlet in the expected region, which is an indication of the conformational flexibility of the mercaptoaniline substituents. The anilino signal is broad which is characteristic of acidic protons as a result of fast exchange with solvent molecules. Similar ligands containing the py-NS<sub>2</sub> donor atoms,

give comparable chemical shifts for proton signals in  $d_6$ -chloroform. [8], [9]



For the carbon-13 broad band decoupled spectra of  $L^1$ , a total number of ten resonance signals were obtained, denoting ten unique carbon environments. This is in agreement of one half of the molecule being chemically equivalent to the other half (as expected). Assignment of the carbon-13 n.m.r. was achieved through  $^1H$ ,  $^{13}C$ -COSY spectra (Figure 2.3c). Where quaternary carbon atoms could not be unambiguously assigned, correlation tables containing substituent-induced shift parameters were consulted.

As a consequence of changing the nature of the solvent, the resonance signals were chemically shifted either upfield or downfield by approximately 1-2 p.p.m. only. In  $d_6$ -chloroform, the signals for  $C^1$  and  $C^6$  were almost indistinguishable, being chemically shifted by only 0.07 p.p.m. However, in  $d_3$ -acetonitrile, the signals for  $C^1$  and  $C^6$  were chemically shifted by 0.79 p.p.m. Carbon-13 resonances are more

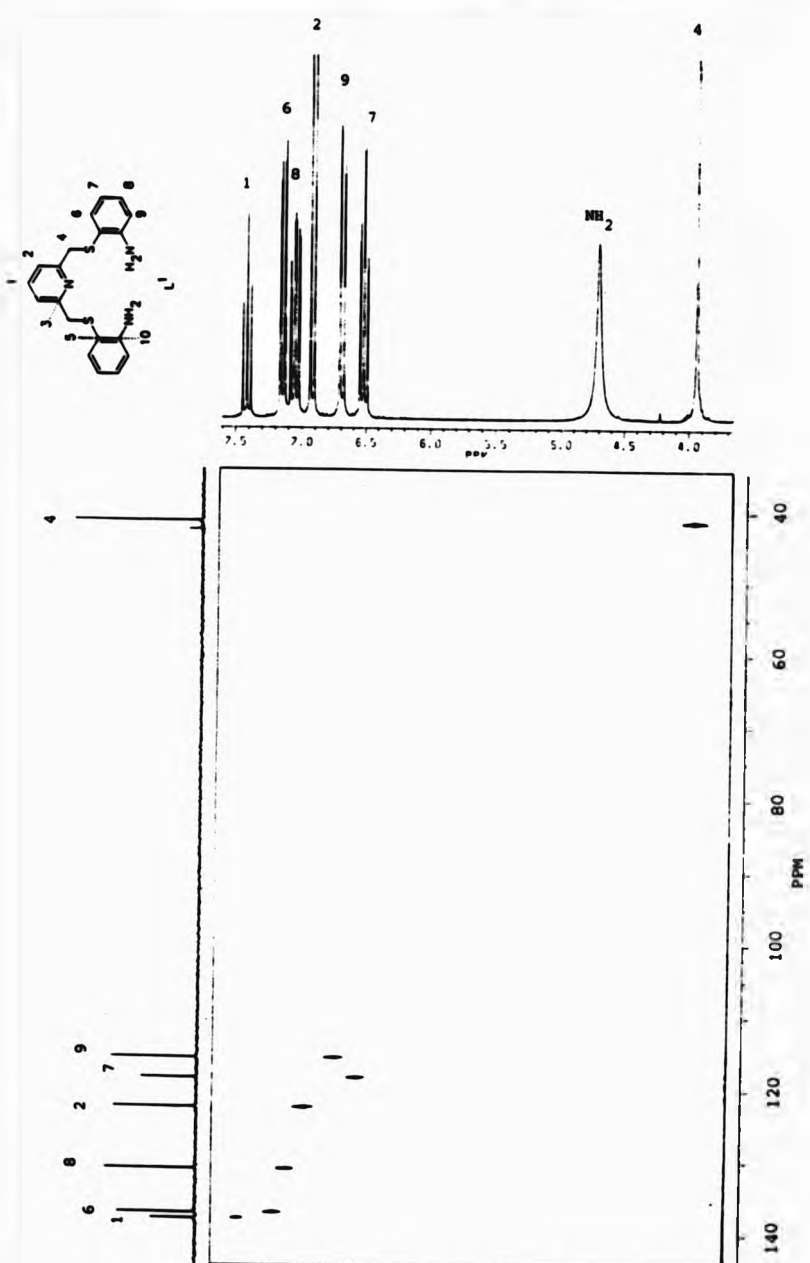


Figure 2.3c  $^1\text{H}, ^{13}\text{C}$ -COSY n.m.r. spectrum of  $\text{L}^1$  in  $d_3$ -acetonitrile.

sensitive to structural changes, because they have a greater shift dispersion in comparison to proton n.m.r. Therefore, the proton signals shift to a lesser degree in different solvents than do the carbon-13 signals.

Table 2.3b  $^{13}\text{C}$  n.m.r. data<sup>a</sup> for  $\text{L}^1$  in various solvents (62.896 MHz) at ambient temperature.

$\text{CDCl}_3$	$\text{CD}_3\text{CN}$	$\text{CD}_3\text{OD}$	Assignment <sup>b</sup>
157.87	158.75	159.06	c <sup>3</sup>
148.83	150.40	150.90	c <sup>10</sup>
136.65	137.75	138.34	c <sup>1</sup>
136.58	136.96	137.64	c <sup>6</sup>
130.20	130.94	131.25	c <sup>8</sup>
121.48	122.32	123.21	c <sup>2</sup>
118.25	118.29	118.74	c <sup>7</sup>
117.00	117.10	117.26	c <sup>5</sup>
114.93	115.54	116.14	c <sup>9</sup>
41.35	41.38	40.95	c <sup>4</sup>

<sup>a</sup>In p.p.m., relative to  $\text{SiMe}_4$ . <sup>b</sup>Numbering scheme as for Table 2.3a.

#### 2.4 Co-ordination studies of $[\text{ML}]^{m+}$ .

As a Lewis base,  $\text{L}^1$  has five potential donor atoms: an  $\text{sp}^2$  pyridyl nitrogen, two  $\text{sp}^3$  thioether donors and two  $\text{sp}^2$  anilino nitrogens (which will become  $\text{sp}^3$  on co-ordination). Hence, three different types of donor atom are available to the metal ion for co-ordination. The flexibility of  $\text{L}^1$  allows for many conformations to be adopted on complexation (Figure 2.4a).

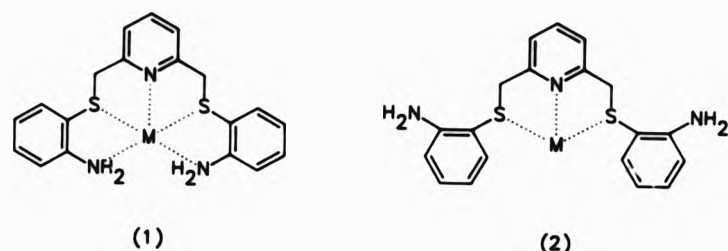


Figure 2.4a Pictorial representation of extreme conformations of L<sup>1</sup>.

Two extreme conformations of L<sup>1</sup> may be depicted, where in the first, the ligand is quinquedentate to the central metal ion, forming four five-membered chelate rings (1). In the second, free rotation about the C-S bond allows the anilino nitrogens to separate as far away as possible, rendering the ligand terdentate to the central metal ion and adopts a more 'linear' arrangement (2).

The co-ordination chemistry of  $L^1$  was investigated with a series of metal ions to elucidate the conformation assumed by the ligand, and the co-ordination sphere around the central metal ion in question.

$L'$  was found to be soluble in most common organic solvents. Complexation reactions were carried out in methanol or acetonitrile, either at room temperature or under refluxing conditions. Perchlorate, thiocyanate and/or chloride salts of the metal ions: lead(II), silver(I), mercury(II), cadmium(II), copper(II), nickel(II), zinc(II), manganese(II), calcium(II), strontium(II) and barium(II) were employed.

#### 2.4.1 Spectroscopic Studies of $[ML^1]^{m+}$ .

Reactions of  $L^1$  with calcium(II), strontium(II) and barium(II) perchlorate were unsuccessful, with only the starting materials being isolated, as indicated by infrared and mass spectrometry. At this stage, the most obvious explanation could be the incompatibility of the soft/borderline donor atoms with the harder metal ions.<sup>[10]</sup> Manganese(II) also showed no complexing behaviour towards  $L^1$ . Once again, the factor appears to be differences according to the hard-soft concept and not due to differences in metal-ion size, since the effective ionic radius of manganese(II) is nearly half that of barium(II) ( $r_{Mn^{(II)}} = 0.67\text{ (ls)}$  and  $r_{Ba^{(II)}} = 1.35 \text{ \AA}$  respectively). On the other hand, the borderline metal ions such as lead(II), cadmium(II) and zinc(II) gave no isolable products under the conditions employed, resulting instead in oily polymeric residues.

##### 2.4.1.1 Electronic Spectra of $[ML^1]^{m+}$ .

$L^1$  was found to react with copper(II), nickel(II), silver(I) and mercury(II). The transition-metal ion complexes isolated gave a wide range of colours as expected (Table 2.4.1a). For both the d<sup>8</sup> and d<sup>9</sup> metal ions, nickel(II) and copper(II) respectively, d-d transitions are standard. However, the non-transition metal ions silver(I) and mercury(II) have d<sup>10</sup> electrons in their outer valence shell. In this case d-d transitions are, of course, not possible. The dark inky-blue colour of the  $[AgL^1]ClO_4$  and the  $[HgL^1(Cl)_2]$  complexes must therefore arise from charge transfer between the metal and the ligand.<sup>[11]</sup>

The room temperature magnetic moments for the copper(II) and nickel(II) products indicates the isolation of paramagnetic complexes with effective magnetic moments equal to 2.00 (copper(II)), 3.24 and

3.18 B.M. [nickel(II)]. These values are typical for  $d^9$  [copper(II)] and  $d^8$  [nickel(II)] metal ions with one and two unpaired electrons respectively. Although, the spin-only magnetic moments are 1.73 B.M. for  $d^9$  and 2.83 B.M. for  $d^8$  metal ions (temperature independent), mixing of spin-coupling and contributions from orbital angular momenta will always lead to  $\mu_{\text{eff}} > \mu_{\text{spin-only}}$  (the former is temperature dependent).

Table 2.4.1a Electronic<sup>a</sup> and magnetic<sup>b</sup> data for the  $[\text{ML}]^{n+}$  complexes.

COMPLEX	COLOUR	$\lambda_{\text{max}}/\text{nm}$	$\epsilon/\text{m}^2\text{mol}^{-1}$	$\mu_{\text{eff}}/\text{B.M.}^c$
$[\text{CuL}^1][\text{ClO}_4]_2$	Green	637.5	20.85	2.00
$[\text{NiL}^1(\text{Cl})]\text{Cl}\cdot\text{MeOH}$	Purple	-*	-	3.24
$[\text{NiL}^1][\text{ClO}_4]_2$	Purple	529.0	1.02	3.18
$[\text{AgL}^1]\text{ClO}_4$	Blue	-	CT <sup>d</sup>	-
$[\text{Ag}_2\text{L}^1][\text{NO}_3]_2$	Pink	-	CT	-
$[\text{HgL}^1(\text{Cl})_2]$	Blue	-	CT	-
$[\text{HgL}^1][\text{ClO}_4]_2$	Green	-	CT	-

<sup>a</sup>In methanol. <sup>b</sup>Corrected for diamagnetism of ligand. <sup>c</sup>At 298 K.

<sup>d</sup>Charge transfer bands, obscured by ligand bands. \*Insoluble in methanol.

In each case, any copper(II) species isolated will be paramagnetic in nature. In practice, the magnetic moments for copper(II) are in the range 1.9-2.2 B.M., with moments at the lower or higher end due to compounds approaching an octahedral or tetrahedral geometry respectively. For the  $d^8$  system a square planar geometry is readily favoured if the crystal field is sufficiently strong enough to split the  $d_{x^2-y^2}$  and  $d_z^2$  orbitals so that all eight d electrons can be paired

and accommodated in the four lower orbitals -  $d_{xz}$ ,  $d_{yz}$ ,  $d_z^2$  and  $d_{xy}$ , leaving the  $d_{x^2-y^2}^2$  orbital unoccupied. The resultant complexes are consequently diamagnetic due to spin-pairing. Thus, a four-co-ordinate square planar geometry does not exist between nickel(II) and L<sup>1</sup>. The magnetic moments for octahedral complexes of nickel(II) lie in the range 2.9-3.3 B.M. and between 3.2-4.1 B.M. for tetrahedral complexes.<sup>[12]</sup>

The electronic spectra obtained in methanol for  $[\text{CuL}^1](\text{ClO}_4)_2$  and  $[\text{NiL}^1](\text{ClO}_4)_2$  give rise to absorptions at ca. 637.5 nm and 529 nm respectively. The d<sup>9</sup> configuration gives rise to only one term, that of  $^2D$ . In a cubic field, this term splits to yield a doublet  $^2E$  and a triplet  $^2T_2$  state. Depending on the ligand field (tetrahedral or octahedral) the energy levels of these states become inverted and the separation between these states is dependent on the ligand field strength. Thus, a single main absorption is expected for copper(II) in cubic fields, which is equal to 10Dq (crystal-field splitting). Jahn-Teller distortions will exclude a true octahedral stereochemistry and the complex geometry will be intermediate or distorted. A band between 900-625 nm ( $11000-16000 \text{ cm}^{-1}$ ) is usually found for octahedral fields, whereas, bands below 500 nm ( $20000 \text{ cm}^{-1}$ ) are attributed to tetrahedral fields. Hence, for  $[\text{CuL}^1](\text{ClO}_4)_2$  the absorption band at 640.5 nm has been assigned to a  $^2E_g \rightarrow ^2T_{2g}$  transition as found for an octahedral environment.<sup>[12]</sup>

The d<sup>8</sup> configuration gives rise to the  $^3F$  ground term and higher-energy terms  $^3P$ ,  $^1G$ ,  $^1D$  and  $^1S$ . In the presence of cubic fields the degeneracy of these terms is lifted and further split states are obtained. In all, three spin-allowed transitions are expected for both

tetrahedral and octahedral complexes. In general,  $^3A_{2g}(F) \rightarrow ^3T_{2g}(F)$  ( $= 10Dq$ ) lies between  $7000-13000 \text{ cm}^{-1}$ ,  $^3A_{2g}(F) \rightarrow ^3T_{1g}(F)$  in the range  $11000-20000 \text{ cm}^{-1}$  and  $^3A_{2g}(F) \rightarrow ^3T_{1g}(F)$  between  $19000-27000 \text{ cm}^{-1}$  in octahedral fields. For tetrahedral complexes the transitions  $^3T_1(F) \rightarrow ^3A_2(F)$  gives a band in the near infrared and  $^3T_1(F) \rightarrow ^3T_1(P)$  a band at  $15000 \text{ cm}^{-1}$ , whilst the lowest-energy band is rarely observed.<sup>[13]</sup> However, for  $[\text{NiL}^1](\text{ClO}_4)_2$  only one absorption band is observed at 529 nm in the electronic spectrum. Tentatively, this band has been assigned to the  $^3A_{2g}(F) \rightarrow ^3T_{1g}(F)$  transition for an octahedral co-ordination environment.

#### 2.4.1.2 Infrared Studies.

The infrared spectra (Table 2.4.1b) of  $[\text{ML}]^{m+}$  were compared to that of  $\text{L}^1$  in relation to two main types of absorption areas;  $\nu(\text{N-H})$  and  $\nu(\text{py})$ . Any shift observed in these bands would be due to co-ordination of the metal ion by the ligand via the respective donor atoms of these organic substituents.

No changes in  $\nu(\text{py})$  absorption bands at ca.  $1580 \text{ cm}^{-1}$  from  $\text{L}^1$  to  $[\text{ML}]^{m+}$  were observed. However, this does not totally exclude the probability of pyridine co-ordination via the nitrogen donor to the metal atoms. Since, pyridine and benzene ring deformation modes appear in the same region, this could mask any  $\text{C}_5\text{H}_5\text{N}:\rightarrow \text{M}^{m+}$  co-ordination that may be present in the  $[\text{ML}]^{m+}$  complexes. In addition,  $\nu(\text{N-H})$  bending modes occur between  $1650-1560 \text{ cm}^{-1}$  which would also obscure pyridine co-ordination or vice versa. No doubt co-ordination to the pyridyl nitrogen is more than likely for all complexes obtained. However, for a similar ligand containing the sub-unit  $\text{py-NS}_2$  as the only donating species, the metal ion palladium(II) is co-ordinated to both sulphur

donor atoms leaving the pyridyl nitrogen unbound.<sup>[8]</sup>

In comparing the symmetric and asymmetric  $\nu(\text{N-H})$  stretching frequencies between  $\text{L}^1$  and its complexes, two distinct features became apparent. For  $[\text{CuL}^1](\text{ClO}_4)_2$  and  $[\text{HgL}^1](\text{ClO}_4)_2$ , the metal ions are, undoubtedly, bound to the anilino nitrogens. Changes in the  $\nu(\text{N-H})$  vibration modes for the nickel complexes,  $[\text{NiL}^1](\text{ClO}_4)_2$  and  $[\text{NiL}^1(\text{Cl})]\text{Cl}\cdot\text{MeOH}$  are not so pronounced, but the metal is still considered to be co-ordinated to the anilino nitrogen donor atoms in both complexes. In contrast, for  $[\text{AgL}^1]\text{ClO}_4$ ,  $[\text{Ag}_2\text{L}^1](\text{NO}_3)_2$  and  $[\text{HgL}^1(\text{Cl})_2$ , comparable stretching frequencies for  $\text{L}^1$  and  $[\text{ML}^1]^{m+}$  are an indication of a lack of bonding interactions between the metal ions and the anilino nitrogens in these complexes.

Table 2.4.1b Infrared data<sup>a,c</sup> for the  $[\text{ML}^1]^{m+}$  complexes.

	$\nu(\text{N-H})$ <sup>b</sup>		$\nu(\text{counterion})$	
$\text{L}^1$	3440s	3340s		
$[\text{CuL}^1](\text{ClO}_4)_2$	3280m	3240m	1100-1090(sp)	620m
$[\text{NiL}^1(\text{Cl})]\text{Cl}\cdot\text{MeOH}$	3400s	3280s	-	-
$[\text{NiL}^1](\text{ClO}_4)_2$	3440m(br)	3240s	1100m(br)	630s
$[\text{AgL}^1]\text{ClO}_4$	3440m	3340m	1110m(br)	630s
$[\text{Ag}_2\text{L}^1](\text{NO}_3)_2$	3440s	3340s	1380m(br)	
$[\text{HgL}^1(\text{Cl})_2$	3440m	3360s	-	
$[\text{HgL}^1](\text{ClO}_4)_2$	3280m(br)	3220m	1110m(br)	630s

<sup>a</sup>In  $\text{cm}^{-1}$ , as KBr disc. <sup>b</sup>Symmetric and asymmetric stretches.

Anion co-ordination is often misconstrued, especially in relation to the perchlorate counterion. Ionic perchlorate has a regular

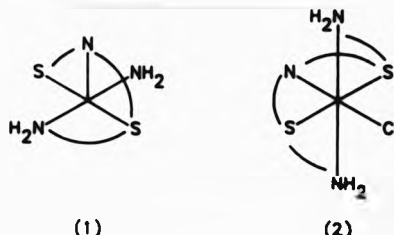
tetrahedral geometry with a point group symmetry  $T_d$ . Associated with this symmetry are four normal modes of vibration, of which only  $\nu_3$  ( $1110 \text{ cm}^{-1}$ ) and  $\nu_4$  ( $626 \text{ cm}^{-1}$ ) are infrared active. Usually,  $\nu_3$  is a very strong band with a poorly defined maximum, and is often split.<sup>[14]</sup> For  $[\text{CuL}^1](\text{ClO}_4)_2$ ,  $\nu_3(\text{ClO}_4)$  is split (ca.  $1110$  and  $1090 \text{ cm}^{-1}$ ), and the appearance of split shoulders on the perchlorate bands between ca.  $1100$  and  $1090 \text{ cm}^{-1}$  for  $[\text{NiL}^1](\text{ClO}_4)_2$ ,  $[\text{AgL}^1]\text{ClO}_4$  and  $[\text{HgL}^1](\text{ClO}_4)_2$ , are also observed. In general when complexation reactions are not carried out under anhydrous conditions, the perchlorate ion is rarely co-ordinated since, the metal ion will preferentially interact with the aquo ions in solution.<sup>[15]</sup> Thus, neither of the perchlorate complexes of  $L^1$  are thought to contain a co-ordinated counterion despite the split  $\nu_3$  bands. Splitting may also arise if two perchlorate counterions are in different environments or involved in hydrogen bonding.

For  $[\text{Ag}_2\text{L}^1](\text{NO}_3)_2$ , the  $\nu(\text{NO}_3)$  band centered at ca.  $1380 \text{ cm}^{-1}$  is broad. This is characteristic of asymmetric  $\nu(\text{N-O})$  stretching for ionic nitrate ions.<sup>[16]</sup> The other infrared active vibration modes,  $\nu_2$  at  $831 \text{ cm}^{-1}$  (out of plane deformation) and  $\nu_4$  at  $720 \text{ cm}^{-1}$  (in-plane bending) of ionic nitrates are obscured by ligand absorptions. Broadening of the counterion absorbances are usually due to the presence of hydrogen bonding, in this case between the oxyanions and the anilino hydrogens or they could be due to both nitrate ions being located in different lattice environments.<sup>[17]</sup> The complexes  $[\text{NiL}^1(\text{Cl})]\text{Cl}\cdot\text{MeOH}$  and  $[\text{HgL}^1(\text{Cl})_2]$ , will obviously show no infrared-active modes for the unco-ordinated chloride counterions; co-ordinated chloride gives rise to  $\nu(\text{M-Cl})$  vibrations in the far-infrared region ( $350-200 \text{ cm}^{-1}$ ).<sup>[18]</sup>

Differences in free-ligand and metal-complex spectra between 1280-660  $\text{cm}^{-1}$  are attributable to  $\nu(\text{C-S})$  stretching vibrations. Generally, carbon-sulphur absorbances decrease in frequency and lower in intensity (and sometimes even disappear) when metal-sulphur bonding occurs. However, no significant conclusions could be drawn from this area of the infrared spectra for the  $[\text{ML}]^{m+}$  complexes. In addition, a weak band due to  $\nu(\text{M-S})$  stretching vibrations between 490-470  $\text{cm}^{-1}$  may further serve to confirm metal-sulphur interactions.<sup>[19]</sup> Unfortunately, infrared spectral data could only be obtained between 4000-600  $\text{cm}^{-1}$ .

In summary, the infrared data implies that both silver(I) complexes  $[\text{AgL}^1]\text{ClO}_4$  and  $[\text{Ag}_2\text{L}^1][\text{NO}_3]_2$ , and the mercury(II) complex  $[\text{HgL}^1(\text{Cl})_2]$  are co-ordinated to the pyridyl nitrogen and to both thioether donor atoms [Figure 2.4a mode (2)] leaving the anilino nitrogens unco-ordinated. This is consistent with the tendency of silver(I) and mercury(II) to form low co-ordinate complexes, although some four, five and six co-ordinate mercury(II) and silver(I) complexes are also well known depending on the rigidity of the ligand and the counterion present.<sup>[20]</sup> Thus, co-ordination of the chloride anions is very likely (though not detected by infrared) because of the preference of mercury(II) for covalent bonds to chlorine over nitrogen atoms in solution.

Meanwhile, both nickel(II) complexes  $[\text{NiL}^1](\text{ClO}_4)_2$  and  $[\text{NiL}^1(\text{Cl})]\text{Cl}\cdot\text{MeOH}$  are believed to have orthogonal geometries, such that the co-ordination sphere is either *nido*-octahedral (1) or that the metal is bound in a distorted octahedral fashion (2).



(1)

(2)

In the above cases, the anilino nitrogens are in a *trans* relationship to one another. This is supported by the fact that addition of 2,6-bis(bromomethyl)pyridine<sup>(21)</sup> or 2,6-diformylpyridine<sup>(22)</sup> in an attempt to cyclise the open-chain product, does not result in a closed macrocyclic ligand complex (infrared and microanalytical data are identical to that of  $[NiL]^{\text{m}}$ ).

Likewise, in  $[HgL^{\text{l}}](ClO_4)_2$  and  $[CuL^{\text{l}}](ClO_4)_2$ , all five ligand donor atoms are co-ordinated to the central metal ion. Since, mercury(II) tends to interact more favourably with softer, more polarisable, donor atoms, the metal co-ordinates to the ligand anilino nitrogens instead of the smaller, harder oxygen donors of the perchlorate counterions. This is in contrast to  $[HgL^{\text{l}}(Cl)_2]$ , where mercury(II) prefers to co-ordinate to the chloride anions rather than the anilino nitrogen donors, because the latter are now harder than the available chloride ions in solution. However, hydrogen bonding between the anilino nitrogens and the perchlorate oxygens is evident.

Microanalytical data (section 7.1.1 and 7.1.2) for the  $[ML]^{\text{m}}$  complexes denotes a metal-to-ligand ratio of 1:1, with the exception of  $[Ag_2L^{\text{l}}](NO_3)_2$ . The bimetallic nature of this complex may attribute to the differences in colour exhibited by  $[Ag_2L^{\text{l}}](NO_3)_2$  and  $[AgL^{\text{l}}]ClO_4$  (Table 2.4.12). Only the  $[NiL^{\text{l}}(Cl)]Cl \cdot MeOH$  complex has a methanol solvate associated within its lattice.

2.4.1.3 Fast-atom bombardment mass spectral studies.

F.a.b. mass data (Table 2.4.1c) obtained for five complexes of L<sup>1</sup> also suggest a 1:1 (metal-to-ligand ratio) formulation, with the exception of [HgL<sup>1</sup>(Cl)<sub>2</sub>]. In this case, the mass spectral parent-ion is absent for the complex. Instead, the most stable peak observed is at m/z 354, corresponding to the free ligand [L<sup>1</sup>]<sup>+</sup>, possibly implying the presence of relatively weak interactions between mercury(II) and L<sup>1</sup>.

Table 2.4.1c F.a.b. mass spectral data<sup>a</sup> for the [ML<sup>1</sup>]<sup>m</sup> complexes.

COMPLEX	FRAGMENTATION ASSIGNMENT	MASS <sup>b</sup>	RELATIVE PERCENTAGE	
[CuL <sup>1</sup> ][ClO <sub>4</sub> ] <sub>2</sub>	[CuL <sup>1</sup> ][ClO <sub>4</sub> ] <sub>2</sub> <sup>+</sup>	617	5	
	[CuL <sup>1</sup> ][ClO <sub>4</sub> ] <sup>+</sup>	517	15	
	[CuL <sup>1</sup> ] <sup>+</sup>	417	100	
	[L <sup>1</sup> ] <sup>+</sup>	354	6	
[NiL <sup>1</sup> (Cl)]Cl.MeOH	[NiL <sup>1</sup> ]Cl <sup>+</sup>	446	32	
	[NiL <sup>1</sup> ] <sup>+</sup>	410 <sup>c</sup>	100	
[HgL <sup>1</sup> (Cl) <sub>2</sub> ]	[L <sup>1</sup> ] <sup>+</sup>	354	100	
[AgL <sup>1</sup> ]ClO <sub>4</sub>	[AgL <sup>1</sup> ] <sup>+</sup>	462	95	
	[L <sup>1</sup> ] <sup>+</sup>	354	45	
[Ag <sub>2</sub> L <sup>1</sup> ][NO <sub>3</sub> ] <sub>2</sub>	[AgL <sup>1</sup> ] <sup>+</sup>	462	31	

<sup>a</sup>In NOBA matrix. <sup>b</sup>Positive-ion mode. <sup>c</sup>Different isotopic masses of Nickel and Chlorine contribute to this mass number.

For [AgL<sup>1</sup>]ClO<sub>4</sub> and [Ag<sub>2</sub>L<sup>1</sup>][NO<sub>3</sub>]<sub>2</sub>, a relatively more stable metal-ligand mass peak is observed for these complexes. [NiL<sup>1</sup>(Cl)]Cl.MeOH has a mass peak correlating to [NiL<sup>1</sup>]Cl<sup>+</sup> which may be suggestive of chloride

co-ordination to the nickel(II) ion. For  $[\text{CuL}^1](\text{ClO}_4)_2$ , four fragmentation patterns are observed for the degradation of the complex. Hence, the following order of increase in relative stability for the complexes of  $\text{L}^1$  could be tentatively proposed as being  $[\text{CuL}^1](\text{ClO}_4)_2 > [\text{NiL}^1(\text{Cl})]\text{Cl} \cdot \text{MeOH} > [\text{AgL}^1]\text{ClO}_4 > [\text{Ag}_2\text{L}^1](\text{NO}_3)_2 > [\text{HgL}^1(\text{Cl})_2]$ .

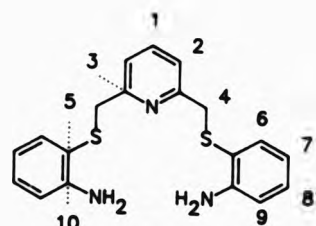
#### 2.4.1.4 Nuclear magnetic resonance studies.

Those diamagnetic complexes of  $\text{L}^1$  which were sufficiently soluble in deuterated solvent were further characterised by high field n.m.r. in order to determine their structures in solution (Tables 2.4.1d and 2.4.1f). The difference in chemical shift ( $\Delta\delta$ ) between a free ligand ( $\text{L}$ ) and its metal complex ( $\text{ML}$ ) is defined for the purpose of this discussion as:

$$\Delta\delta = \delta_{\text{ML}} - \delta_{\text{L}}$$

In comparing  $\text{L}^1$  with its metal complexes,  $[\text{AgL}^1]\text{ClO}_4$  (Figure 2.4.1a),  $[\text{HgL}^1](\text{ClO}_4)_2$  (Figure 2.4.1b), and  $[\text{HgL}^1(\text{Cl})_2]$  (Figure 2.4.1c), the most notable difference is the position of the methylene protons  $\text{H}^4$ . On complexation, these protons resonate at a higher frequency. This effect is typical of metal co-ordination and is therefore a useful criterion for ligand denticity, showing here that the metal ions are co-ordinated to the sulphur donor atoms. In addition, the  $\text{H}^4$  protons still appear as a singlet, denoting either weak metal-ligand interactions which sustain ligand flexibility via rapid rotation about the C-S bond, or that fast exchange of the methylene protons between the non-equivalent axial and equatorial sites is caused by chelate ring flipping.

Table 2.4.1d  $^1\text{H}$  n.m.r. data<sup>a</sup> for  $[\text{ML}]^{m+}$  and  $\text{L}^1$  (250.134 MHz) in  $\text{CD}_3\text{CN}$  at ambient temperature.



$\text{L}^1$		$(\text{AgL}^1)\text{ClO}_4$	$(\text{HgL}^1)(\text{ClO}_4)_2$	$(\text{HgL}^1(\text{Cl})_2)$
7.42	$\text{H}^1$	7.52	$\text{H}^1$	7.70
7.15	$\text{H}^6$	7.07	$\text{H}^8$	- <sup>b</sup>
7.05	$\text{H}^8$	7.02	$\text{H}^2$	7.41
6.92	$\text{H}^2$	6.91	$\text{H}^6$	7.33
6.69	$\text{H}^9$	6.79	$\text{H}^9$	7.26
6.50	$\text{H}^7$	6.46	$\text{H}^7$	7.23
4.70	$\text{NH}_2$	4.76	$\text{NH}_2$	6.12
3.94	$\text{H}^4$	4.16	$\text{H}^4$	4.60
				4.27
				$\text{H}^4$

<sup>a</sup>In p.p.m., relative to  $\text{SiMe}_4$ . <sup>b</sup>Unobserved due to signal overlap.

The values of  $\Delta\delta$  (Table 2.4.1e) for  $\text{H}^4$  between  $\text{L}^1$  and its complexes are 0.22, 0.33 and 0.66 p.p.m. for  $(\text{AgL}^1)\text{ClO}_4$ ,  $(\text{HgL}^1(\text{Cl})_2)$  and  $(\text{HgL}^1)(\text{ClO}_4)_2$  respectively. Proton deshielding of the mercury(II) complexes in comparison to the silver(I) complex is expected, on account of the greater effective nuclear charge on the mercury(II) atom.

As expected the pyridyl protons  $\text{H}^1$  and  $\text{H}^2$  for each metal complex also

resonate at higher frequencies, consistent with metal-pyridine co-ordination.  $\Delta\delta$  for these protons, H<sup>1</sup> and H<sup>2</sup> are  $\Delta\delta\text{H}^1 = 0.10, 0.09, 0.28$  p.p.m. and for  $\Delta\delta\text{H}^2 = 0.10, 0.09, 0.34$  p.p.m. for  $[\text{AgL}^1]\text{ClO}_4$ ,  $[\text{HgL}^1(\text{Cl})_2]$  and  $[\text{HgL}^1][\text{ClO}_4]_2$  respectively. In both the above cases, for protons H<sup>4</sup>, H<sup>1</sup> and H<sup>2</sup>, the  $[\text{HgL}^1][\text{ClO}_4]_2$  complex has the largest chemical shift differences ( $\Delta\delta$ ).

In this connection, the order of upfield resonances for the phenylene protons H<sup>6</sup>-H<sup>9</sup> are different for the metal complexes when compared to L<sup>1</sup>, except for  $[\text{HgL}^1(\text{Cl})_2]$ . In this instance, signals are chemically shifted within  $\pm 0.05$  p.p.m. for protons H<sup>6</sup>-H<sup>9</sup>. It would appear that the presence of mercury(II) in solution has a minimal effect on L<sup>1</sup>. That is to say, the mercury(II) atoms are covalently bound to chloride atoms in solution for periods longer than the n.m.r. time scale. For  $[\text{AgL}^1]\text{ClO}_4$ , the order of the phenylene protons is disrupted by H<sup>6</sup> ( $\Delta\delta = -0.24$  p.p.m.) which is ortho to the thioether donor atom and meta to the anilino nitrogen. The proton is shielded and resonates at lower frequencies. Since non co-ordination of the anilino nitrogens to silver(I) has been established by infrared analysis (*vide supra*), the o-phenylene rings are free to rotate and tumble in solution. Depending on the orientation of the rings with respect to the applied magnetic field, anisotropic shielding effects will occur for the aromatic protons. A possible explanation for the cause of extra shielding on proton H<sup>6</sup> could be ascribed to a balance between the degree of 'tilt' of the phenylene ring (due to metal-sulphur co-ordination), the electron donating effect of the anilino substituent at the meta position and the closeness of the lone pair on the sulphur atom which is ortho to H<sup>6</sup>.

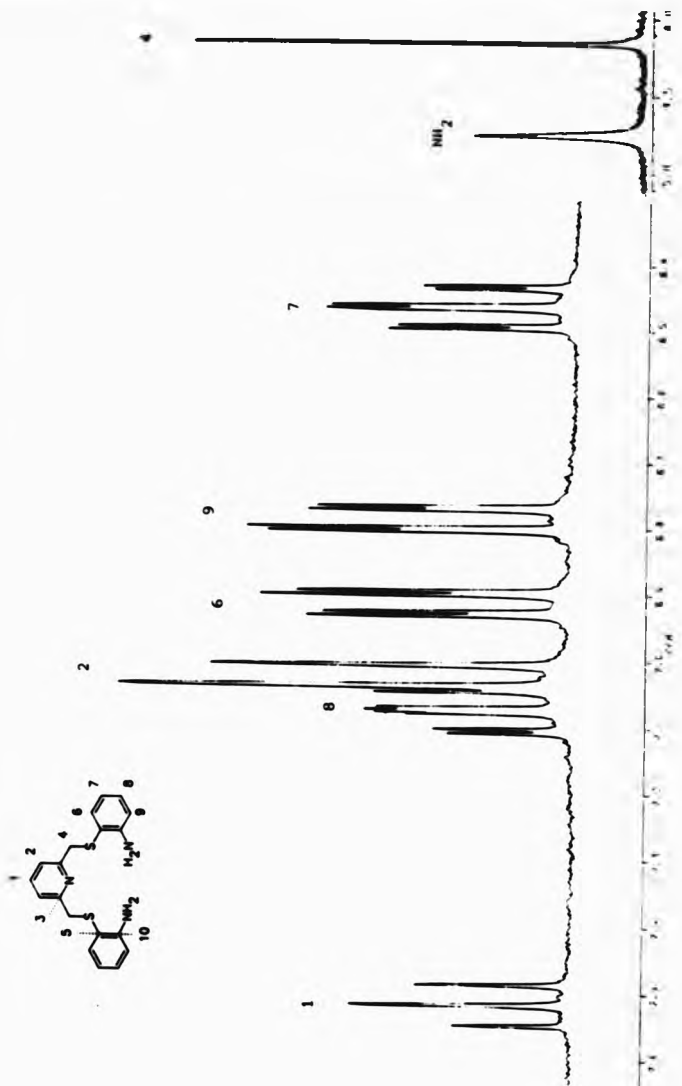


Figure 2.4.1a  $^1\text{H}$  n.m.r. spectrum of  $[\text{AgL}]^+\text{ClO}_4^-$  in  $\text{d}_3$ -acetonitrile.

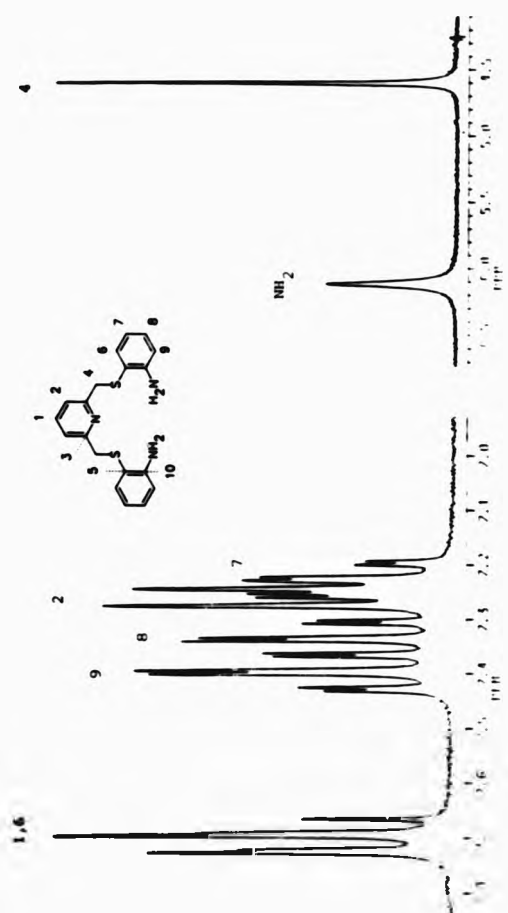


Figure 2.4.1b  $^1\text{H}$  n.m.r. spectrum of  $[\text{MgL}](\text{ClO}_4)_2$  in  $d_3$ -acetonitrile.

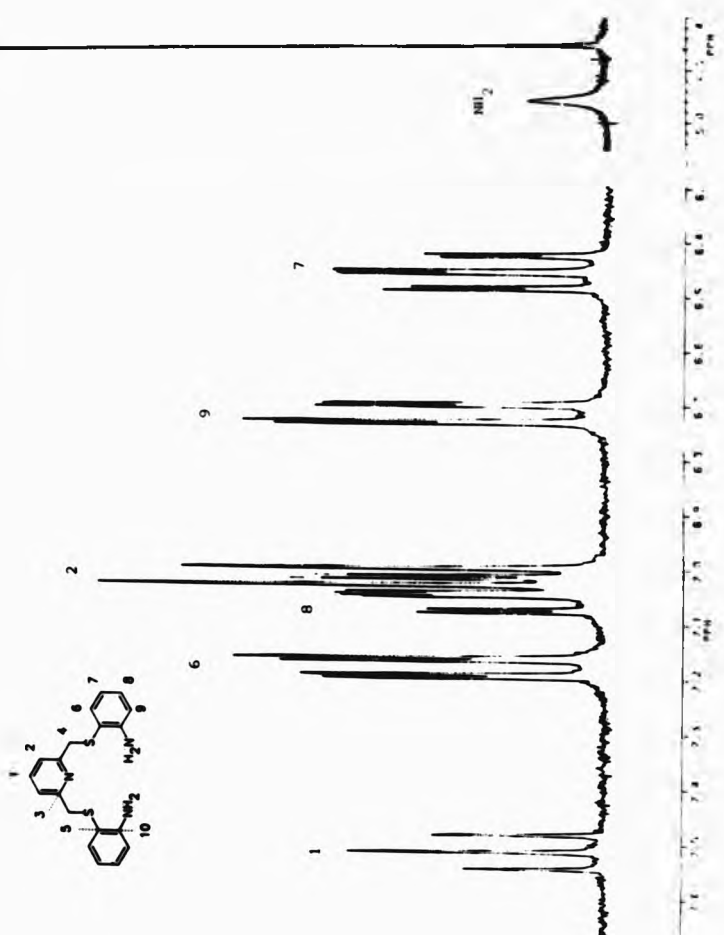
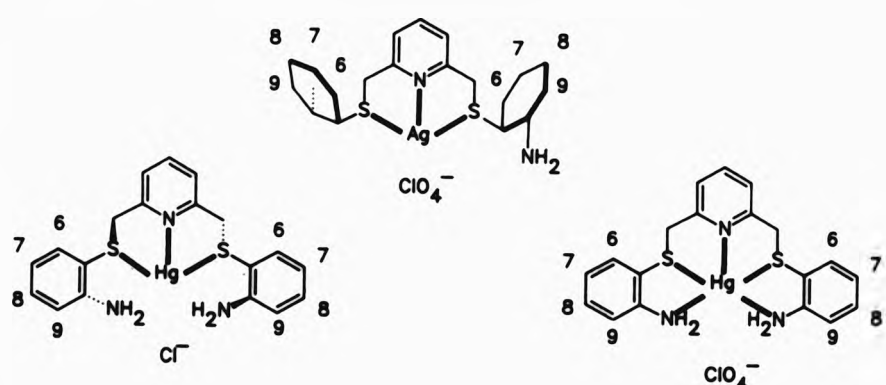


Figure 2.4.1c  $^1\text{H}$  n.m.r. spectrum of  $[\text{HgL}(\text{Cl})_2]$  in  $\text{d}_3$ -acetonitrile.

Meanwhile, for  $[HgL^1][ClO_4]_2$ , all the phenylene protons  $H^6-H^9$  (except  $H^7$ ) have been chemically shifted downfield ( $\Delta\delta H^6 = -0.45$ ,  $\Delta\delta H^7 = -0.05$ ,  $\Delta\delta H^8 = 0.28$  and  $\Delta\delta H^9 = 0.72$  p.p.m.). Co-ordination of all five ligand donor atoms to mercury(II) has been realised by infrared analysis (vide supra) for this complex also. Hence, a more planar conformation must be adopted by the o-phenylene rings in relation to the position of the ligand donor atoms (i.e. no tilting), and therefore anisotropic shielding/deshielding will occur approximately to the same extent, at the same time, for the protons  $H^6-H^9$ . Interestingly, the largest  $\Delta\delta$  value occurs for  $H^9$  which now resonates between  $\delta H^6$  and  $\delta H^8$ , instead of  $\delta H^8$  and  $\delta H^7$  as previously noted for the free ligand  $L^1$ . In this respect, extra deshielding of  $H^9$  must be due to the electron withdrawing effects of the co-ordinated metal ion on the o-phenylene ring via the sulphur and nitrogen donor atoms. Since  $H^9$  is only three bonds away from the anilino nitrogen, its higher frequency resonance is justified.



Additionally, multiplicities for  $L^1$  and its complexes are the same for all proton signals except  $H^8$ . For  $[HgL^1][ClO_4]_2$ , the doublet of doublet of doublet signal is reduced to a triplet of doublets

(identical to H<sup>7</sup>). Hence, co-ordination of mercury(II) to both sulphur and nitrogen donor atoms of the phenylene ring results in a notable change in coupling constant values.

Assignment of the carbon-13 broad band decoupled spectra, revealed trends similar to those observed in the proton n.m.r. spectra. For all three [ML]<sup>m</sup> complexes, the resonance signals for C<sup>5</sup> and C<sup>9</sup> are interchanged in relation to the spectrum of L<sup>1</sup>. Both C<sup>5</sup> and C<sup>9</sup> are ortho to the anilino group of the benzene ring. In addition, C<sup>5</sup> is ipso to the sulphur donor atom. The order of the other carbon signals for [AgL<sup>1</sup>(Cl)<sub>2</sub>] and [AgL<sup>1</sup>]ClO<sub>4</sub> are comparable to those of L<sup>1</sup>, being chemically shifted by no more than  $\pm$  1-2 p.p.m. In contrast, for [HgL<sup>1</sup>][ClO<sub>4</sub>]<sub>2</sub>,  $\Delta\delta$  ranges from +10.58 to -11.00 p.p.m. The carbon atoms C<sup>3</sup>, C<sup>10</sup> and C<sup>6</sup> have become shielded ( $\Delta\delta$  = -6.39, -11.00 and -3.60 p.p.m. respectively) in the mercury(II) complex, the rest of the signals are deshielded and resonate at higher frequencies.

Table 2.4.1e  $\Delta\delta$  for the [ML]<sup>m</sup> complexes ( $\Delta\delta$  =  $\delta_{ML} - \delta_L$ ). \*

	[AgL <sup>1</sup> ]ClO <sub>4</sub>	[HgL <sup>1</sup> (Cl) <sub>2</sub> ]	[HgL <sup>1</sup> ][ClO <sub>4</sub> ] <sub>2</sub>
H <sup>1</sup>	0.10	0.09	0.28
H <sup>2</sup>	0.10	0.09	0.34
H <sup>4</sup>	0.22	0.33	0.66
H <sup>6</sup>	-0.24	0.03	0.45 <sup>b</sup>
H <sup>7</sup>	-0.04	-0.05	-0.05
H <sup>8</sup>	0.02	-0.01	0.28
H <sup>9</sup>	0.10	0.02	0.72

\*In p.p.m. <sup>b</sup>Approximate value due to signal overlap.

The sizeable differences between [HgL<sup>1</sup>(Cl)<sub>2</sub>] and [HgL<sup>1</sup>][ClO<sub>4</sub>]<sub>2</sub> also

become apparent in solution. In essence, it is the nature of the counterion that appears to dictate the bonding mode of mercury(II). As previously mentioned,  $HgCl_2$  is distinctly molecular in solution, showing marked solubility in many organic solvents. Meanwhile, the highly ionic nature of  $Hg(ClO_4)_2$  will lead to complete dissociation in solution with stabilisation of the resultant ion pairs through solvation. Thus, in the former situation, mercury(II) is favourably associated with the chloride ions in solution rather than  $L^1$ , whereas in the latter case, mercury(II) and the perchlorate ions are solvated and hence mercury(II) opts for co-ordination to the nitrogen/sulphur donor atoms of  $L^1$ .

Table 2.4.1f  $^{13}C$  n.m.r. data<sup>a</sup> for  $[ML^1]^{m+}$  and  $L^1$  (62.896 MHz) in  $CD_3CN$  at ambient temperature.

$L^1$	$[AgL^1]ClO_4$	$[HgL^1](ClO_4)_2$	$[HgL^1(Cl)]_2$
158.75	c <sup>3</sup>	157.30	c <sup>3</sup>
150.40	c <sup>10</sup>	149.28	c <sup>10</sup>
137.75	c <sup>1</sup>	139.38	c <sup>1</sup>
136.96	c <sup>6</sup>	135.78	c <sup>6</sup>
130.94	c <sup>8</sup>	131.37	c <sup>8</sup>
122.32	c <sup>2</sup>	124.85	c <sup>2</sup>
118.29	c <sup>7</sup>	119.57	c <sup>7</sup>
117.10	c <sup>5</sup>	117.28	c <sup>9</sup>
115.54	c <sup>9</sup>	115.62	c <sup>5</sup>
41.38	c <sup>4</sup>	41.18	c <sup>4</sup>
		41.52	c <sup>4</sup>
			39.87

<sup>a</sup>In p.p.m., relative to  $SiMe_4$ . <sup>b</sup>Two resonance signals observed.

Having gathered some knowledge of ligand flexibility, donor atom

co-ordination and metal-ion preferences towards  $L^1$ , where possible, conclusive structural analyses were undertaken as an aid to confirm the preceding observations.

#### 2.4.2 Single-Crystal X-ray Structure of $[HgL^1(Cl)_2]$ .

The interaction between mercury(II) and  $L^1$  in the solid state is revealed by the single-crystal X-ray structural analysis of  $[HgL^1(Cl)_2]$  (Figure 2.4.2a). The mercury(II) atom is co-ordinated to three of the five available ligand donor atoms, the pyridyl nitrogen N(1c), and the thioether donors S(1a) and S(1b). The co-ordination sphere is completed by two chlorine atoms, Cl(1) and Cl(2) (Table 2.4.2a). The co-ordination geometry around the mercury(II) atom is best described as distorted arachno-pentagonal bipyramidal, with the ligand donor atoms in the equatorial plane [ $N(1c)$ -Hg-S(1a)  $71.1(2)^\circ$  and  $N(1c)$ -Hg-S(1b)  $63.8(2)^\circ$ ] and the chlorine atoms occupying the axial sites [Cl(1)-Hg-Cl(2)  $157.2(1)^\circ$ ].

Bond lengths between the mercury(II) atom and the sulphur donor atoms S(1a) and S(1b) are  $2.942(3)$  and  $3.310(4)$  Å respectively. These bonding interactions are relatively long, but within the estimated sum of the van der Waals radii for Hg-S =  $3.58$  Å ( $Hg(II)$  =  $1.73$  Å<sup>[23]</sup> + S =  $1.85$  Å). The differences in mercury-sulphur bond distances show the mercury(II) atom to be displaced towards S(1b), which gives  $L^1$  an unsymmetrical ligand conformation.

Co-ordination of mercury(II) to N(1c), S(1a) and S(1b) results in the formation of two five-membered chelate rings. Puckering of these chelate rings causes the pyridyl ring to twist relative to the S(1a)-Hg-S(1b) donor plane by  $23.12^\circ$ , due to the restriction of

pyramidal geometry imposed by the sulphur donor atoms. As a consequence, the position of both phenylene rings display a 'zig-zag' pattern (Figure 2.4.2b) as opposed to the 'linear' representation depicted previously (Figure 2.4a). In addition, this unsymmetrical arrangement permits both anilino nitrogen donor atoms N(2a) and N(2b) to be orientated away from each other on different sides of the plane of the pyridyl ring.

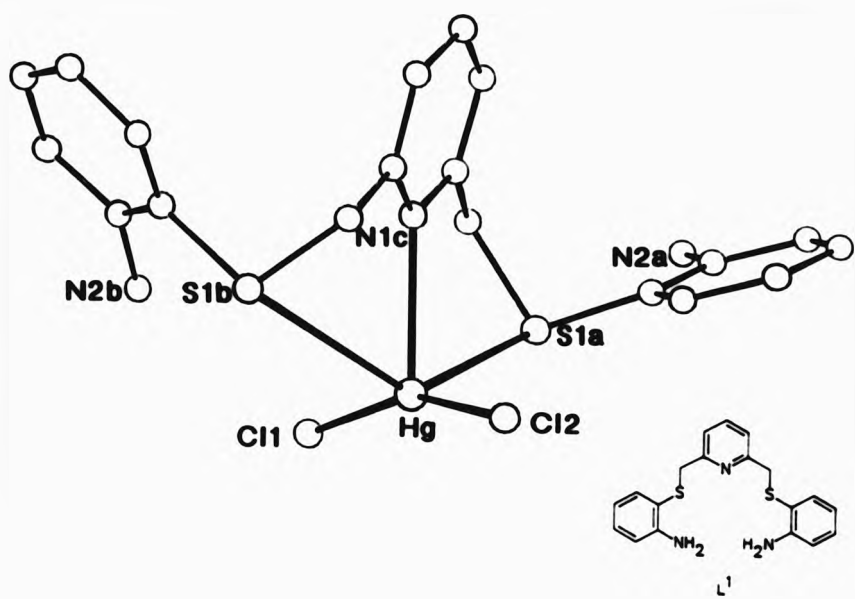


Figure 2.4.2a Single-crystal X-ray structure of  $[HgL^1(Cl)_2]$ .

In this connection, the anilino nitrogen N(2b) and the chlorine atom Cl(1) have a contact distance N(2b)...Cl(1) of 3.31 Å, whereas, the anilino nitrogen N(2a) points away from the chlorine atom Cl(2). The close proximity of N(2b) and Cl(1) may give rise to very weak hydrogen bonding between the anilino hydrogen atoms and the chlorine atom. The

Table 2.4.2a Selected co-ordination sphere bond distances and bond angles for  $[\text{HgL}^{\dagger}(\text{Cl})_2]$ .

Bond distances ( $\text{\AA}$ )		Bond angles ( $^{\circ}$ )	
Hg - N(1c)	2.583(9)	N(1c) - Hg - S(1a)	71.1(2)
Hg - S(1a)	2.942(3)	N(1c) - Hg - S(1b)	63.8(2)
Hg - S(1b)	3.310(4)	S(1a) - Hg - S(1b)	133.2(1)
Hg - Cl(1)	2.336(4)	Cl(1) - Hg - Cl(2)	157.2(1)
Hg - Cl(2)	2.333(4)	N(1c) - Hg - Cl(1)	104.6(2)
		N(1c) - Hg - Cl(2)	97.7(2)
		S(1a) - Hg - Cl(1)	84.2(1)
		S(1a) - Hg - Cl(2)	107.8(1)
		S(1b) - Hg - Cl(1)	95.3(1)
		S(1b) - Hg - Cl(2)	90.4(1)

actual positions of the anilino hydrogens could not be located in the difference maps using low angle reflections ( $\sin\theta < 0.35$ ). Their geometrically idealised positions were not calculated either, since, free rotation about the C-N bonds can occur. Hydrogen bonding between N(2b) and Cl(1) would help stabilise the longer bonding interaction of Hg-S(1b), with the formation of a pseudo six-membered chelate ring. On the other hand, the 'pull' of Cl(1) on the hydrogens of N(2b) may attribute to the longer length of the Hg-S(1b) bond in order to minimise steric hindrance. However in general, when hydrogen bonding between terminal chlorine atoms and nitrogen amine donors occurs, longer bond distances ( $> 2.57 \text{ \AA}$ ) for Hg-Cl have been found.<sup>(24), (25), (26)</sup>

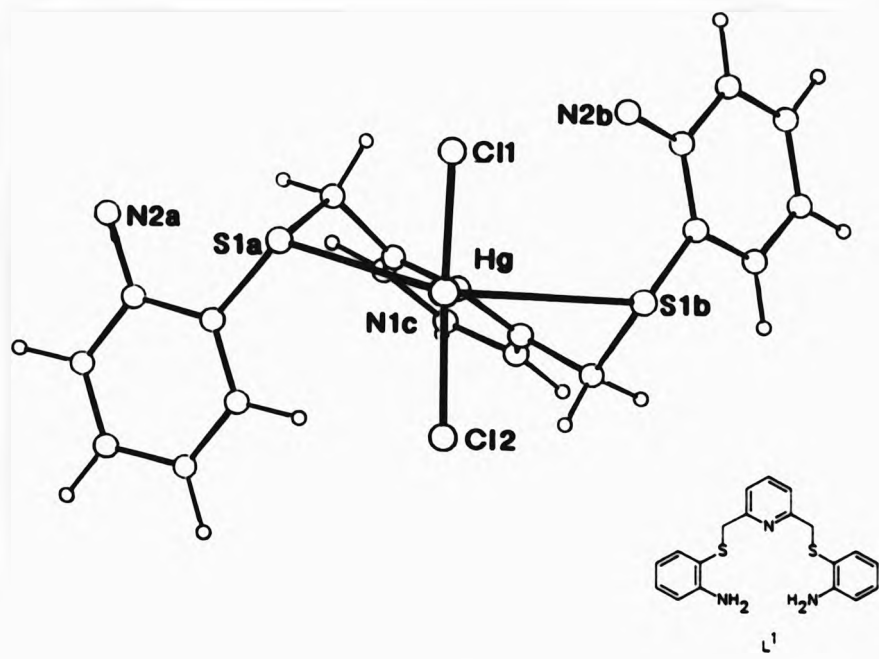
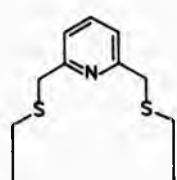


Figure 2.4.2b Single-crystal X-ray structure of  $[\text{HgL}^1(\text{Cl})_2]$ .

Although  $\text{L}^1$  is potentially quinquedentate, it behaves as a terdentate ligand in forming this complex. It is therefore interesting to compare this data with that reported for the metal complexes of a related terdentate acyclic ligand (4), containing the py- $\text{NS}_2$  donor atoms (Table 2.4.2b). It is not surprising that, as the metal ions decrease in size, the metal-nitrogen bonds and the metal-sulphur interactions also get progressively shorter. As a consequence, the smallest metal ion copper(II), has the largest S-M-S angle.

Table 2.4.2b Selected bond distances ( $\text{\AA}$ ) and angles ( $^\circ$ ) for complexes of (4) and  $[\text{HgL}^1\text{Cl}]_2$  for comparison.



{4}

COMPLEX	$r_{\text{M}(II)}$	M-N(1c)	M-S(1a)	M-S(1b)	S(1a)-M-S(1b)	Reference
$[\text{Cd}\{4\}\text{Cl}]_2$	0.95 <sup>b</sup>	2.380(3)	2.703(1)	2.724(1)	148.5(1)	9
$[\text{Zn}\{4\}\text{Br}]_2$	0.68 <sup>c</sup>	2.083(5)	2.741(2)	2.632(2)	157.0(1)	27
$[\text{Cu}\{4\}\text{Cl}]_2$	0.65 <sup>c</sup>	2.016(10)	2.344(4)	2.358(4)	161.3(1)	28
$[\text{HgL}^1\text{Cl}]_2$	1.02 <sup>d</sup>	2.583(9)	2.942(3)	3.310(4)	133.2(1)	This work

<sup>a</sup>Effective ionic radii in  $\text{\AA}$ . <sup>b</sup>Six co-ordinate. <sup>c</sup>five co-ordinate.

<sup>d</sup>Six co-ordinate (four co-ordinate 0.96  $\text{\AA}$ ).

Other mercury(II) crystal structures containing thioether donor atoms in macrocyclic and linear ligands have been reported. Although, none are similar systems for comparative purposes, they do give some idea of geometrical preferences with regard to mercury(II)-sulphur interactions (Figure 2.4.2c).

The flexible macrocyclic ligand, (5) contains four thioether donor atoms, which co-ordinate separately to two molecules of mercuric chloride,  $[(\text{HgCl}_2)_2\{5\}]$ .<sup>[29]</sup> Both mercury(II) atoms are co-ordinated to two sulphur donors [Hg-S(1) 2.580(3), Hg-S(2) 2.699(2)  $\text{\AA}$ ] in an exo-conformation with the formation of two five-membered chelate rings. Two chloride counterions complete the co-ordination sphere [Hg-Cl(1)

2.407(3), Hg-Cl(2) 2.419(3) Å] giving a near tetrahedral geometry about the metal atom. For  $[\text{HgL}^1(\text{Cl})_2]$ , the mercury(II)-sulphur bond lengths are much longer and the mercury(II)-chloride distances shorter than those in  $[(\text{HgCl}_2)_2\{\text{S}\}]$ . In both cases however, there is a stronger bonding interaction between mercury(II) and the chloride ions than with mercury(II) and the thioether donor atoms.

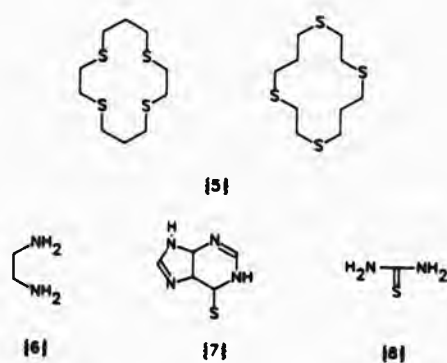


**Figure 2.4.2c Comparable ligands for structurally characterised mercury(III) complexes.**

On replacing chlorides with perchlorate counterions, the interaction with ligand (5) yields a very different structure,  $[\text{Hg}(5)(\text{H}_2\text{O})][\text{ClO}_4]_2$ .<sup>[30]</sup> On this occasion, a single mercury(II) atom is co-ordinated to all four sulphur donor atoms of the same ligand. This imposes a square-pyramidal geometry around the metal atom, with a co-ordinating water molecule perpendicular to the basal plane. Here, the four mercury(II)-sulphur bond lengths are 2.581(4), 2.51(5), 2.60(5) and 2.71(4) Å. These distances are comparable to those of  $[(\text{HgCl}_2)_2(5)]$ . Thus the presence of different counterions in solution, dictates the geometry around the mercury(II) co-ordination sphere. If the ligand is flexible enough to do so, the thioether donor atoms

conform to the requirements of the metal atom.

The structures for mercury(II) and 1,2-diaminoethane (6) with different counterions have also been analysed. For  $[\text{Hg}(6)(\text{SCN})_2]$ ,<sup>[31]</sup> the mercury(II) atom is co-ordinated to both amine nitrogen atoms and to both sulphur donor atoms of the thiocyanate molecules giving an effectively tetrahedral geometry about the metal atom. The mercury(II)-sulphur bond distances are 2.428(10) and 2.529(11) Å ( $\text{SCN}^-$ ) in this complex. In contrast, when (6) is reacted with  $\text{Hg}(\text{ClO}_4)_2$  anion co-ordination does not take place. Instead, the mercury(II) atom is co-ordinated to two molecules of (6) (all four ligand nitrogen atoms), to give the formulation  $[\text{Hg}(6)_2](\text{ClO}_4)_2$ .<sup>[32]</sup> The co-ordination sphere around the mercury(II) atom for this complex resembles an elongated and twisted tetrahedron (orthorhombic disphenoid). Once again, the hard/soft properties of the counterion affect the bonding mode of the mercury(II) atom.

Similarly, the potentially bidentate ligand 6-mercaptopurine (7), exhibits monodentate character in the presence of  $\text{HgCl}_2$  to give  $[\text{Hg}(7)_2\text{Cl}_2]$ .<sup>[25]</sup> Thus, the mercury(II) atom is co-ordinated to the sulphur donor atom from each molecule of (7) and to both chloride ions displaying a distorted tetrahedral environment, with bond distances mercury(II)-sulphur 2.460(3) Å and mercury(II)-chloride 2.622(2) Å. The longer bonding interactions are attributed to hydrogen bonding involvement of the chlorine atom. It was proposed that the monodentate behaviour of the ligand was not due to geometrical constraints, but the preference of mercury(II) for chlorine over nitrogen, the other donor atom of (7).

It is noteworthy in this context, that ligand L<sup>1</sup> can also adopt two different conformations depending on the mercury(II) counterion present, as previously discussed by infrared and n.m.r. spectroscopy (*vide ante*). Thus, the individual solution and solid state structures of [HgL<sup>1</sup>(Cl)<sub>2</sub>] and [HgL<sup>1</sup>](ClO<sub>4</sub>)<sub>2</sub> are appreciably similar, but between the two complexes substantial differences exist.

Several mercury(II) complexes of  $\gamma$ -mercaptoamine ligands have been reported, where the geometry around the metal atom ranges from linear to pseudo-octahedral. The mercury(II)-sulphur bond distances range from 2.33-2.45 for linear, 2.59-2.66 for tetrahedral, 2.44-2.47 for distorted octahedral, to 2.38-2.43 Å for pseudo-octahedral complexes.<sup>[24]</sup> In all cases, the bonding interactions are much shorter in these co-ordination compounds in comparison to those of L<sup>1</sup> and (4). Only one complex having a mercury(II)-sulphur bond length over 3 Å could be found in the literature. Where mercury(II) interacts with three molecules of thiourea (8) to give mercury(II)-sulphur bond distances of 2.37(3), 2.61(3) and 3.10(3) Å for [Hg(8)<sub>3</sub>Cl<sub>2</sub>].<sup>[25]</sup> Although, in this case the sulphurs are thiolates rather than thioether donor atoms.

#### 2.4.3 Single-Crystal X-ray Structure of [NiL<sup>1</sup>(Cl)]Cl.MeOH.

The single-crystal X-ray analysis of [NiL<sup>1</sup>(Cl)]Cl.MeOH has revealed an octahedral co-ordination geometry around the central nickel(II) atom with N(2a), N(2b), S(1a) and S(1b) in the equatorial plane and N(1c) and Cl(1) occupying the axial sites. All five ligand donor atoms are co-ordinated to the metal ion with the formation of four, five-membered chelate rings. Additionally, a chloride ion completes the co-ordination sphere (a methanol solvate is also associated with the

crystal lattice) (Figure 2.4.3a).

The flexible open-chain ligand  $L^1$  assumes a *trans* donor atom arrangement, this is expected if co-ordination to the pyridyl nitrogen N(1c) is to take place and for an orthogonal conformation to exist, which is desirable to nickel(II) (section 5.3.2).<sup>[33]</sup> Otherwise, *cis* relationships are also known.<sup>[34]</sup> The shortest metal-nitrogen bond distance is Ni-N(2b) 2.027(8) Å, followed by Ni-N(1c) 2.081(6) Å with a slightly longer bonding interaction between Ni-N(2a) 2.166(8) Å. Metal-sulphur interactions are much longer with the thioether donor atoms almost equidistant from the nickel(II) atom [Ni-S(1a) 2.389(3) and Ni-S(1b) 2.385(3) Å] (Table 2.4.3a).

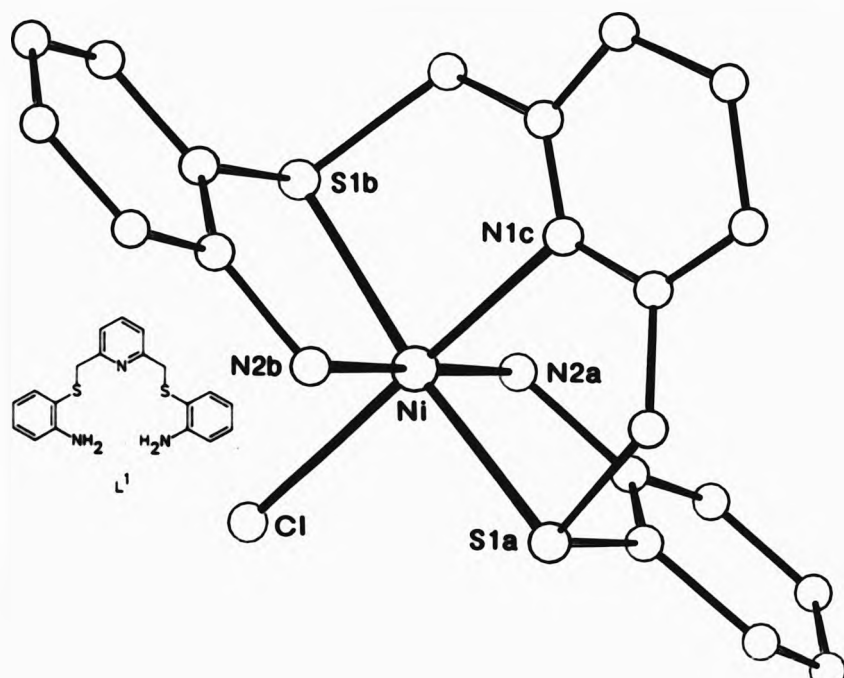


Figure 2.4.3a Single-crystal X-ray structure of  $[NiL^1(Cl)]Cl \cdot MeOH$ .

**Table 2.4.3a Selected co-ordination sphere bond distances and bond angles for  $[NiL^1(Cl)]Cl\cdot MeOH$ .**

Bond distances ( $\text{\AA}$ )		Bond angles ( $^\circ$ )	
Ni - N(1c)	2.081(6)	N(1c) - Ni - Cl(1)	176.1(4)
Ni - N(2a)	2.166(8)	S(1a) - Ni - Cl(1)	92.6(1)
Ni - N(2b)	2.027(8)	S(1a) - Ni - N(1c)	84.0(3)
Ni - S(1a)	2.389(3)	N(2a) - Ni - Cl(1)	90.3(3)
Ni - S(1b)	2.385(3)	N(2a) - Ni - N(1c)	87.6(6)
Ni - Cl(1)	2.422(2)	N(2a) - Ni - S(1a)	84.1(3)
O(1m) - C(1m)	2.027(8)	S(1b) - Ni - Cl(1)	98.6(1)
		S(1b) - Ni - N(1c)	84.8(3)
		S(1a) - Ni - S(1b)	168.7(1)
		S(1b) - Ni - N(2a)	94.2(3)
		N(2b) - Ni - Cl(1)	87.3(2)
		N(2b) - Ni - N(1c)	95.0(6)
		N(2b) - Ni - S(1a)	96.7(3)
		N(2b) - Ni - N(2a)	177.4(3)
		N(2b) - Ni - S(1b)	85.5(3)

Essentially, the metal ion, anilino nitrogens and sulphur donor atoms are coplanar with the two phenylene rings, which in turn are perpendicular to the pyridyl ring (Figure 2.4.3b).

The previously described modes of co-ordination possible for  $L^1$  (Figure 2.4a) have both been displayed by the crystal structures of  $[HgL^1(Cl)_2]$  and  $[NiL^1(Cl)]Cl\cdot MeOH$ . In the former,  $L^1$  is terdentate to mercury(II) whilst in the latter case, nickel(II) is co-ordinated to all five donor

atoms of  $L^1$ .

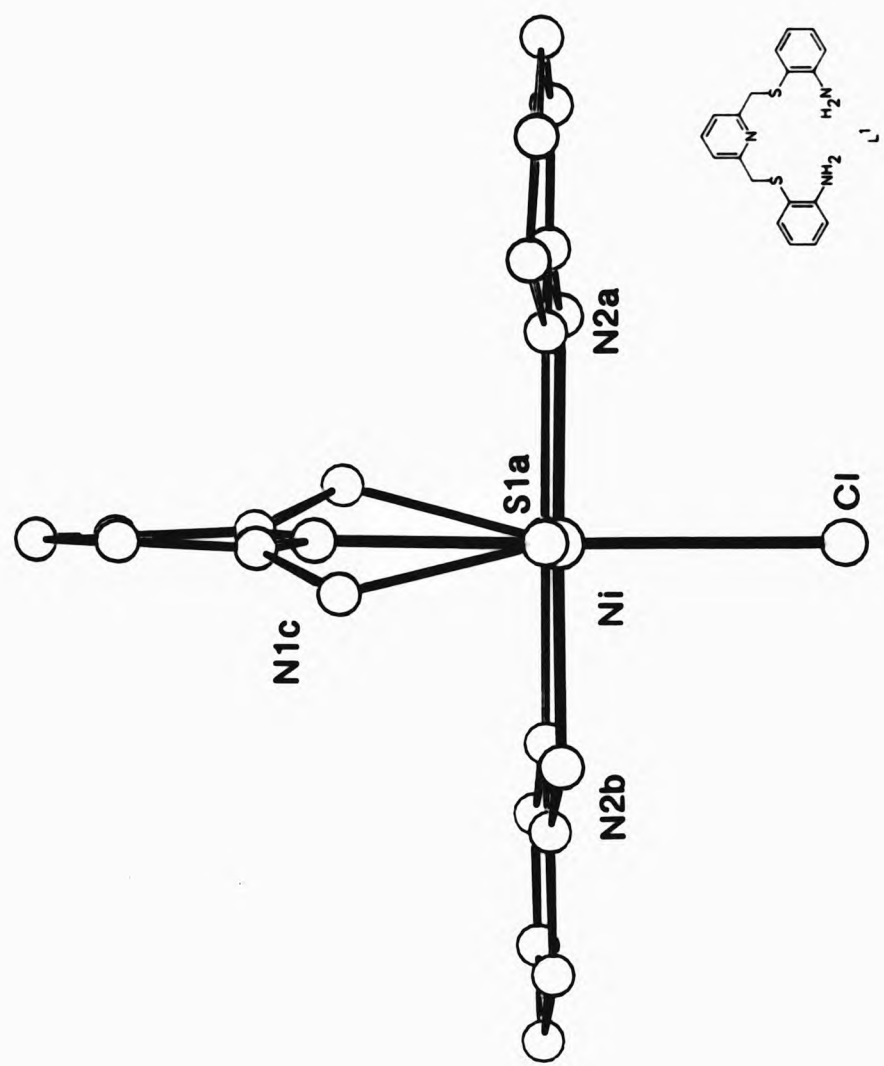


Figure 2.4.3b Single-crystal X-ray structure of  $[NiL^1(Cl)]Cl \cdot MeOH$ .

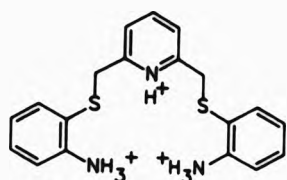
#### 2.4.4 Stability Constant Measurements for $[\text{CuL}^1](\text{ClO}_4)_2$ .

The thermodynamic stability constants for  $\text{L}^1$  were determined potentiometrically using a computer controlled titration system.<sup>[35]</sup> The data files were analysed with the FORTRAN 77 program SUPERQUAD<sup>[36]</sup> which was carried out on the DEC VAX11-780 mainframe computer (VMS version 5.4-3).

Two types of equilibrium constants were investigated; the reaction of  $\text{L}^1$  with (i) protons and (ii) Cu(II) ions.

##### (i) Protonation equilibria.

$\text{L}^1$  has three sites for protonation, the pyridyl nitrogen and two anilino nitrogen donors (of which both sites are expected to be identical).

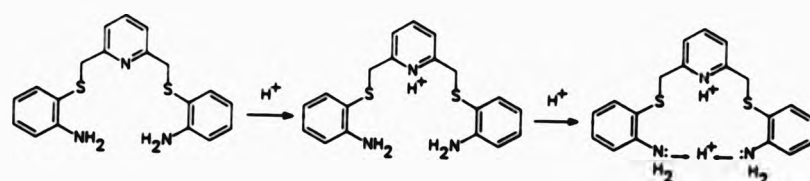


However, only two protonation constants were successfully refined,  $\log K_1 = 4.26$  and  $\log K_2 = 2.39$  which correspond to a ligand-to-proton stoichiometry of 1:1 and 1:2 respectively.

$$\text{L} + \text{H} \rightleftharpoons \text{LH} \quad K_1 = \frac{[\text{LH}]}{[\text{L}][\text{H}]}$$
$$\text{LH} + \text{H} \rightleftharpoons \text{LH}_2 \quad K_2 = \frac{[\text{LH}_2]}{[\text{LH}][\text{H}]}$$

The individual protonation constants for pyridine and aniline are

5.52(0.03) and 4.78(0.02)<sup>[37]</sup> respectively. It is therefore expected that the pyridine nitrogen of L<sup>1</sup> will become protonated first, followed by the anilino nitrogens.



The species plot indicates the relative percentages of L<sup>1</sup>, L<sup>1</sup>H and L<sup>1</sup>H<sub>2</sub> in solution between pH 2 and 12 (Figure 2.4.4a).

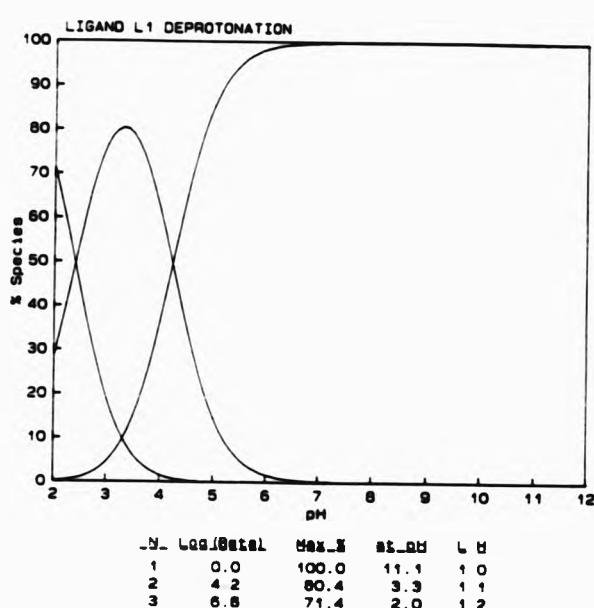
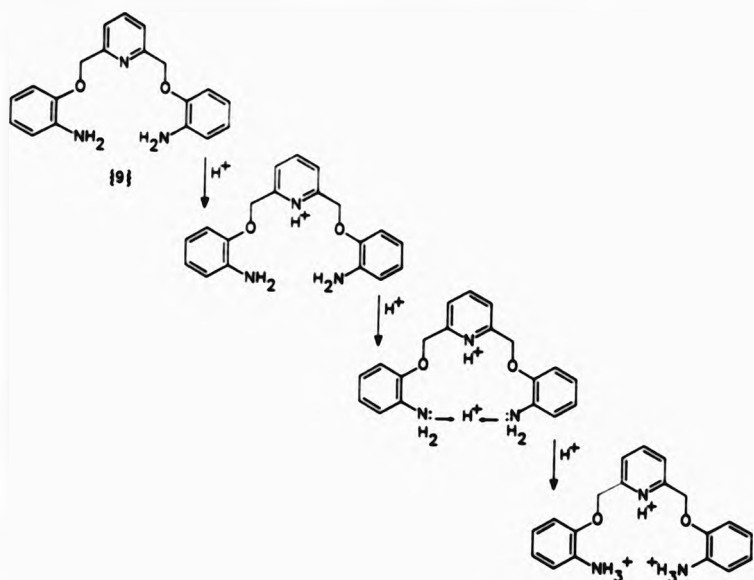


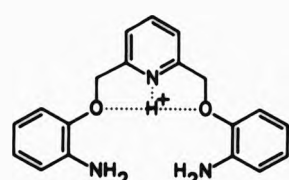
Figure 2.4.4a Distribution of L<sup>1</sup>, L<sup>1</sup>H and L<sup>1</sup>H<sub>2</sub> species in solution.

In contrast, for the reported ligand {9},<sup>[4], [38]</sup> which is the oxygen analogue of L<sup>1</sup>, three protonation constants are obtained:

$\log K_1 = 4.80$ ,  $\log K_2 = 3.94$  and  $\log K_3$  ca. 2.08. As a consequence, the following protonation scheme is proposed,

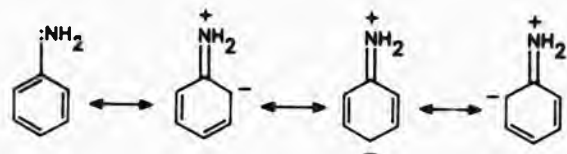


On comparing the protonation constants for  $L^1$  and (9), in both instances the values for (9) are higher (by 0.54 and 0.55 log units respectively). A high log  $K$  value may be attributed to the enhanced stabilisation provided to the initial proton by the more electronegative ether oxygens via hydrogen-bonding interactions;

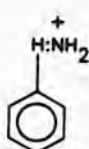


whereas, thioether donor atoms will form very weak interactions with the pyridyl-nitrogen proton. In the case of aniline, the lone pair on the nitrogen atom can interact with the delocalised  $\pi$  orbitals of the

benzene nucleus.



Thus, if aniline is protonated, the lone pair of electrons on the nitrogen atom are no longer available to stabilise the resultant anilinium ion,



Aniline is therefore, reluctant to act as a base, since, it is 'energetically unprofitable' to take up a proton. However, the presence of an electron-donating substituent such as OH or OMe at the ortho or para position in relation to aniline, will strengthen its basic properties.<sup>[6]</sup> In this connection,  $\log K_2$  for (9) is larger than that for L<sup>1</sup>. Accordingly, it is conceivable for this reason that  $\log K_3$  for (9) is observed, but has not been found for L<sup>1</sup>H<sub>3</sub>.

#### (ii) Copper(II) complex equilibria.

Synthetically, the reaction between L<sup>1</sup> and copper(II) initially gave a dark green complex which on standing, rapidly decomposed to give a black solid residue. These observations were also noted for the potentiometric titration procedures.

Four models were proposed for the complexation of copper(II) with L<sup>1</sup>: ML, MLH, ML<sub>2</sub> and ML<sub>2</sub>H<sub>2</sub>. However, only two were successfully refined,

$\text{ML}_2$  and  $\text{ML}_2\text{H}_2$ . The resulting  $\log K$  values are 8.24 and 4.19 respectively. It appears that under the potentiometric titration conditions employed, the most thermodynamically stable species detected are those for a 1:2 metal-to-ligand ratio. Under the circumstances it is difficult to determine the exact structures of the protonated species for the copper(II) complexes of  $\text{L}^1$  -  $\text{CuL}_2^1$  and  $\text{CuL}_2^1\text{H}_2$ , and why a metal-to-ligand ratio of 1:1 cannot be detected in solution (i.e. modelled by computer analyses) (Figure 2.4.4b).

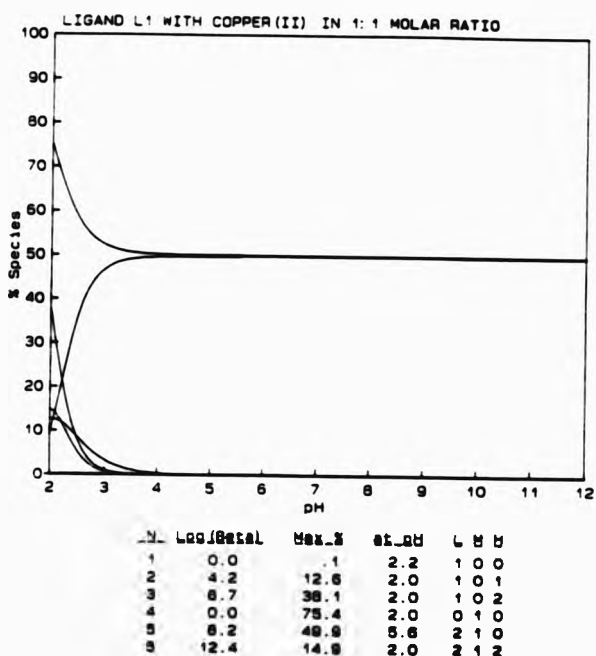


Figure 2.4.4b Distribution curves for  $\text{Cu}(\text{II})-\text{L}^1$  species present in solution between pH 2 and 12.

### 2.5 Synthesis of $\text{L}^2$ .

The synthesis of  $\text{L}^2$  has been previously reported, but isolation and

hence characterisation of the free ligand has not been accomplished. The ligand was always obtained as an oil and characterisation was achieved through its cadmium(II), cobalt(II), nickel(II) and copper(II) complexes. However, physical and analytical data were not presented in the publication.<sup>(27)</sup>

In this work also, attempts to isolate L<sup>2</sup> as the free ligand have failed. Instead of obtaining an oil however, on gradual reduction of the reaction mixture, a white solid precipitated which was subsequently isolated.

The method employed for the synthesis of L<sup>2</sup> was similar to that used for the preparation of L<sup>1</sup> (Figure 2.5a). The only modification of the synthetic route is the filtration of sodium chloride, this is necessary since the hydrochloride salt of the starting material 2-mercaptopoamine has been employed instead.

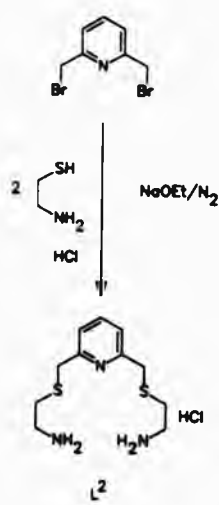


Figure 2.5a Synthetic route for preparation of L<sup>2</sup>.

## 2.6 Characterisation and Co-ordination Studies of L<sup>2</sup>.

The infrared spectrum of L<sup>2</sup> was inconclusive, since broadness obscured the thiol absorption region between ca. 2600-2500 cm<sup>-1</sup>. Elemental analysis (section 7.2) suggested an L<sup>2</sup>.2HCl composition. The salt formation of L<sup>2</sup> is possible as the white solid readily dissolves in water. Mass spectrometry indicated the presence of L<sup>2</sup> in the white solid, m/z 257 (46 %), but higher mass peaks were also observed.

Table 2.6a Infrared and f.a.b. mass data for [NiL<sup>2</sup>](ClO<sub>4</sub>)<sub>2</sub>.

INFRARED <sup>a</sup>		FRAGMENTATION	MASS <sup>b</sup>	RELATIVE
$\nu$ (NH)	$\nu$ (ClO <sub>4</sub> )	ASSIGNMENT		PERCENTAGE
3260s	1100s	[NiL <sup>2</sup> ]ClO <sub>4</sub> <sup>+</sup>	414	100
3240s	630s	[NiL <sup>2</sup> ] <sup>+</sup>	315	29

<sup>a</sup>In cm<sup>-1</sup>, as KBr disc. <sup>b</sup>In NOBA matrix, positive-ion mode.

Unsuccessful isolation and characterisation of L<sup>2</sup> prevented further stoichiometrically controlled reactions from being carried out. Nevertheless, the nickel(II) and copper(II) complexes of L<sup>2</sup> were isolated with the addition of the appropriate metal ion salt in methanol to an aqueous solution of L<sup>2</sup>. However, microanalytical data were not in agreement with the proposed formulations. The reasons for these discrepancies became apparent with f.a.b. mass spectrometry. F.a.b. mass spectra were consistent with the isolation of the metal-ion complexes, but a mixture of counterions were present. On one occasion only (section 7.2.1), was [NiL<sup>2</sup>](ClO<sub>4</sub>)<sub>2</sub> obtained as a pure complex (Table 2.6a). At other times, on the addition of perchlorate or chloride salts of the metal ions, the resultant highest mass peaks observed corresponded to those of the bromide complexes of L<sup>2</sup>, as [ML<sup>2</sup>]Br<sup>+</sup>.

No further attempts were made to isolate complexes of  $L^2$ , but the isolation of an eighteen-membered macrocyclic ligand  $L^5$  (section 4.5), has been effected via an *in situ* process in the presence of  $L^2$  and lead(II) salts.

However, recently the isolation of  $L^2$  has also led to the preparation of a number of macrocyclic ligands.<sup>[39]</sup>

*References - Chapter Two.*

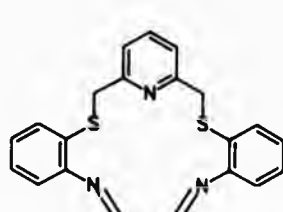
1. T. Shimamoto, M. Ishikawa, H. Ishikawa and M. Inoue, *Chem. Abstr.*, 1968, **68**, 2815X.
2. W. Baker, K. M. Buggie, J. F. W. McOmie and D. A. M. Watkins, *J. Chem. Soc.*, 1958, 3595.
3. E. C. Constable, presented at the U.K. Macrocyclic Conference, Warwick, 1989.
4. D. E. Fenton, B. P. Murphy, A. J. Leong, L. F. Lindoy, A. Bashall and M. McPartlin, *J. Chem. Soc., Dalton Trans.*, 1987, 2543.
5. B. W. Buddeinsky and J. Svec, *J. Inorg. Nucl. Chem.*, 1971, **33**, 3795.
6. P. Sykes, 'A Guidebook to Mechanism in Organic Chemistry,' Longman, London-New York, (5th edn) 1981.
7. D. H. Williams and I. Fleming, 'Spectroscopic Methods in Organic Chemistry,' McGraw-Hill, London, (4th edn) 1988.
8. D. Parker, J. M. Lehn and J. Rimmer, *J. Chem. Soc., Dalton Trans.*, 1985, 1517.
9. F. Teixidor, L. Escriche, I. Rodriguez, J. Casabó, J. Ríos, E. Molins, B. Martínez and C. Miravitles, *J. Chem. Soc., Dalton Trans.*, 1989, 1381.
10. R. G. Pearson, *J. Chem. Educ.*, 1968, **45**, 581; 643.
11. D. Nicholls, 'Complexes and First-row Transition elements,' Macmillan Press Ltd, London, 1974.
12. N. N. Greenwood and A. Earnshaw, 'Chemistry of the Elements,' Pergamon Press, Oxford, 1984.
13. B. N. Figgis in 'Comprehensive Coordination Chemistry,' ed G. Wilkinson, Pergamon Press, Oxford, 1987, Vol 1, pp. 213-279.
14. B. J. Hathaway and A. E. Underhill, *J. Chem. Soc.*, 1961, 3091.
15. M. R. Rosenthal, *J. Chem. Educ.*, 1973, **50**, 331.

16. N. F. Curtis and Y. M. Curtis, *Inorg. Chem.*, 1965, 4, 804.
17. K. Nakamoto, 'Infrared Spectra of Inorganic and Co-ordination Compounds,' Wiley-Interscience, New York, (2nd edn) 1970.
18. S. S Mitra and S. Nudelman, 'Far-infrared Properties of Solids,' Plenum Press, New York-London, 1970.
19. D. Sevdic, M. Curic and L. Tušek-Božić, *Polyhedron.*, 1989, 8, 505.
20. P. A. Cotton and G. Wilkinson, 'Advanced Inorganic Chemistry,' Wiley, New York, (5th edn) 1988.
21. See for example; M. C. Thompson and D. H. Busch, *J. Am. Chem. Soc.*, 1964, 86, 3651.
22. See for example; E. K. Barefield, *Inorg. Chem.*, 1972, 11, 2273.
23. A. J. Canty and G. B. Deacon, *Inorg. Chim. Acta.*, 1980, 45, L225.
24. I. Casals, P. González-Duarte and J. Sola, *Polyhedron.*, 1988, 7, 2509.
25. P. Lavertue, J. Hubert and A. L. Beauchamp, *Inorg. Chem.*, 1976, 15, 322.
26. C. Chish, *Can. J. Chem.*, 1977, 55, 1583.
27. F. Teixidor, L. Escriche, J. Casabó, E. Molins and C. Miravitles, *Inorg. Chem.*, 1986, 25, 4060.
28. L. Escriche, M. Sanz, J. Casabó, F. Teixidor, E. Molins and C. Miravitles, *J. Chem. Soc., Dalton Trans.*, 1989, 1739.
29. N. W. Alcock, N. Herron and P. Moore, *J. Chem. Soc., Chem. Commun.*, 1976, 886.
30. N. W. Alcock, N. Herron and P. Moore, *J. Chem. Soc., Dalton Trans.*, 1978, 394.
31. M. Cannas, A. Christini and G. Marongiu, *Inorg. Chim. Acta.*, 1976, 18, L10.
32. T. Duplanic, D. Grdenic, B. Kamenar, P. Matkovic and M. Sikirica, *J. Chem. Soc., Dalton Trans.*, 1976, 887.

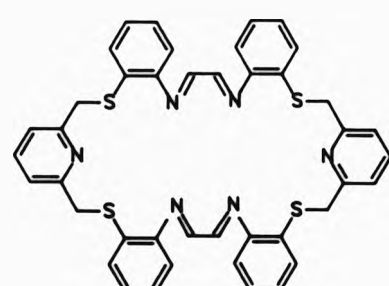
33. (a) M. G. B. Drew, J. Nelson S. M. Nelson, *J. Chem. Soc., Dalton Trans.*, 1981, 1691; (b) S. M. Nelson, M. McCann and C. Stevenson, *J. Chem. Soc., Dalton Trans.*, 1979, 1477.
34. (a) R. W. Hay, A. L. Galyer and G. A. Lawrence, *J. Chem. Soc., Dalton Trans.*, 1976, 939; (b) R. W. Hay, G. A. Lawrence and U. R. Shone, *J. Chem. Soc., Dalton Trans.*, 1976, 942; (c) P. D. Donaldson, P. A. Tasker and N. W. Alcock, *J. Chem. Soc., Dalton Trans.*, 1976, 2262.
35. (a) P. L. Biggins and S. E. Edwards, 'S.SCMCAL,' unpublished BBC BASIC programme, 1987; (b) P. L. Biggins, S. E. Edwards, T. A. Lucas, I. J. Scowen and C. J. L. Silwood, 'S.SCMTITR,' unpublished BBC BASIC program, 1990; (c) P. L. Biggins, S. E. Edwards, I. J. Scowen and C. J. L. Silwood, 'DECDATA,' unpublished BBC BASIC program, 1988; 'TERMULATOR,' terminal emulation for BBC MICRO, University of Surrey, 1984.
36. P. Gans, A. Sabatini and A. Vacca, *J. Chem. Soc., Dalton Trans.*, 1985, 1195.
37. R. M. Smith and A. E. Martell, 'Critical Stability Constants,' Plenum Press, New York, 1975, Vol 2.
38. K. R. Adam, S. Donnelly, A. J. Leong, L. F. Leong, B. J. McCool, A. Bashall, M. R. Dent, B. P. Murphy, M. McPartlin, D. E. Fenton and P. A. Tasker, *J. Chem. Soc., Dalton Trans.*, 1990, 1635.
39. E. Constable, Proceedings of the 16th International Symposium on Macroyclic Chemistry, Sheffield, 1991.

CHAPTER THREE

SYNTESSES, CHARACTERISATION AND CO-ORDINATION STUDIES OF (1+1) AND  
[2+2] NITROGEN-SULPHUR SCHIFF-BASE MACROCYCLIC LIGANDS  $L^3$  AND  $L^{33}$ .



$L^3$



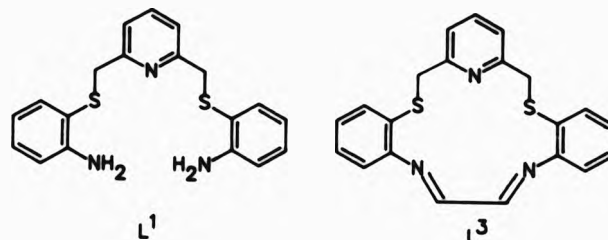
$L^{33}$

### 3.1 General Introduction.

The macrocyclic ligands studied in this chapter all contain the di-imine functionality and are derived from the condensation of a primary diamine with a dialdehyde. In practice, it does not always prove possible to isolate metal-free, imine-containing macrocyclic ligands. As a result, the co-ordination chemistry of these ligands is discussed in relation to their complexes and not to the free macrocycles.

### 3.2 Introduction to L<sup>3</sup>.

This section describes the synthesis of a potentially quinquedentate, N<sub>3</sub>S<sub>2</sub> fifteen-membered macrocyclic ligand L<sup>3</sup>. The donor set of L<sup>3</sup> differs from L<sup>1</sup> (Chapter Two), in that two of the nitrogen donor atoms are chemically dissimilar. These nitrogens are no longer anilino sp<sup>3</sup> donors but part of an sp<sup>2</sup> methine unit.

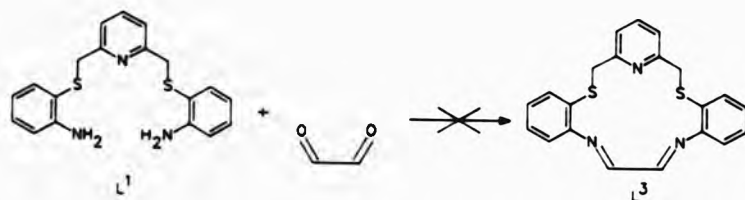


Constraints imposed by ring closure on complexation will restrict free rotation of single bonds to some extent. In turn, limited bonding modes may result from the intermediate rigidity, steric hindrance and macrocyclic cavity size of L<sup>3</sup>.

### 3.3 Template Synthesis of L<sup>3</sup>.

In the absence of a metal ion, the reaction of L<sup>1</sup> with glyoxal in ethanol or acetonitrile did not yield the target di-imine macrocyclic

ligand  $L^3$ , even under conditions of high dilution. This was not entirely unexpected, since solvolysis and general nucleophilic attack (section 1.6.2) of imines is well-documented. At times, when a pale yellow solid could be isolated, characterisation proved to be inconclusive; the mass spectral parent ion was m/z 353, corresponding to that of  $L^1$ .



The next approach to the synthesis of  $L^3$  was to carry out the reaction in the presence of a metal ion; this proved to be more productive. Reactions were carried out in either methanol, ethanol or acetonitrile, under reflux or at room temperatures. For effective complexation, it was necessary to dissolve glyoxal and the metal salt in refluxing solvent, then allow the solution to cool to room temperature prior to the addition of  $L^1$ .

Under the reaction conditions employed, lead(II), mercury(II), cadmium(II), zinc(II), manganese(II) and nickel(II) gave no isolable complexes of  $L^3$ . The reaction solutions varied from pale yellow to dark orange in colour (characteristic of imine compounds) but the colours were transient and the solutions readily formed black oily tars within ca. 30s to ten mins. The only templated products isolated from the reaction of  $L^1$  and glyoxal were the complexes of silver(I) and copper(I), these are discussed in detail in the next section.

### 3.6 Co-ordination Studies of $[AgL^3]ClO_4$ and $[Cu_2L^{33}][ClO_4]_2$ .

The metal-ion salts of silver(I) and copper(II) perchlorate were found to be effective templating agents in the presence of  $L^1$  and glyoxal. Ideally, the silver(I) complex was obtained when the reaction mixture was refluxed for no more than half an hour. In contrast, the copper(I) complex required no heating. In both instances, prolonged refluxing resulted in the formation of black solids of unknown composition.

#### 3.4.1 Spectroscopic Studies of $[AgL^3]ClO_4$ and $[Cu_2L^{33}][ClO_4]_2$ .

Table 3.6a Infrared data<sup>a</sup> for the isolated silver and copper complexes.

COMPLEX	COLOUR	$\nu(C=N)$	$\nu(bz)/(py)$	$\nu_3(ClO_4)$	$\nu_4(ClO_4)$
Silver(I)	Orange	1640w(br)	1600m, 1580m	1100s	630s
Copper(I)	Brown	1640w(br)	1600m, 1575m	1130, 1090s <sup>b</sup>	640s, 620s

<sup>a</sup>In cm<sup>-1</sup>, as KBr disc. <sup>b</sup>Shoulder to 620 cm<sup>-1</sup>.

For the complexes isolated under gentle refluxing conditions [silver(I) complex] and at room temperature [copper(II) complex], the following characterisations were achieved. In the infrared spectra (Table 3.4a), absence of any amine (ca. 3500-3300 cm<sup>-1</sup>) or carbonyl (ca. 1715-1695 cm<sup>-1</sup>) peaks and the presence of an absorbance at ca. 1640 cm<sup>-1</sup> confirmed the formation of imine-containing complexes. The bands between ca. 1600 and 1575 cm<sup>-1</sup> were attributed to the stretching modes of benzene and pyridine.<sup>[1]</sup> Metal-imine or metal-pyridine co-ordination cannot be deciphered at this stage. For the silver(I) complex absorbances at ca. 1110 and 630 cm<sup>-1</sup> were assigned to the  $\nu_3$  and  $\nu_4$  stretching modes of ionic perchlorate. In the copper(I) complex,  $\nu_3$  is split at ca. 1130 and 1090 cm<sup>-1</sup> and  $\nu_4$  at ca. 620 cm<sup>-1</sup>.

possess a shoulder at ca. 640 cm<sup>-1</sup>. However, counterion co-ordination is not conclusive since, broadness may be due to asymmetry within the two perchlorate sites in the solid state.<sup>[2]</sup>

Elemental analyses for both complexes (section 7.3) denote a metal-to-ligand-to-perchlorate ratio of 1:1:1. Therefore, the copper complex contains the metal ion in its +1 oxidation state. It is interesting to note that L<sup>3</sup> appears to be stabilised by the d<sup>10</sup> metal ions silver(I) and copper(I).

Table 3.4b F.a.b. mass spectral data<sup>a</sup> for [AgL<sup>3</sup>]ClO<sub>4</sub> and [Cu<sub>2</sub>L<sup>33</sup>](ClO<sub>4</sub>)<sub>2</sub>.

COMPLEX	FRAGMENTATION ASSIGNMENT	MASS <sup>b</sup>	RELATIVE
			PERCENTAGE
[AgL <sup>3</sup> ]ClO <sub>4</sub>	[AgL <sup>3</sup> ] <sup>+</sup>	484	100
	[L <sup>3</sup> ] <sup>+</sup>	377	7
[Cu <sub>2</sub> L <sup>33</sup> ](ClO <sub>4</sub> ) <sub>2</sub>	[Cu <sub>2</sub> L <sup>33</sup> ](ClO <sub>4</sub> ) <sub>2</sub> <sup>+</sup>	1077	7
	[Cu <sub>2</sub> L <sup>33</sup> - ClO <sub>4</sub> ] <sup>+</sup>	977	31
	[Cu <sub>2</sub> L <sup>33</sup> ] <sup>+</sup>	876	14
	[Cu(L <sup>33</sup> /2)] <sup>+</sup> = [CuL <sup>3</sup> ] <sup>+</sup>	438	100
	[CuL <sup>3</sup> - C <sub>2</sub> H <sub>4</sub> N] <sup>+</sup>	399	15

<sup>a</sup>In NOBA matrix. <sup>b</sup>Positive-ion mode.

For the silver(I) complex, f.a.b. mass spectrometry (Table 3.4b) confirms formation of the expected [1+1] mononuclear macrocyclic ligand complex, [AgL<sup>3</sup>]ClO<sub>4</sub>. No higher mass peaks, e.g. for a (2+2) cyclocondensation, were observed in the spectrum. In contrast, f.a.b. data for the copper(I) complex shows higher mass peaks (exactly double

the expected formulation) which suggests the existence of a binuclear, [2+2] Schiff-base condensation product,  $[\text{Cu}_2\text{L}^{33}](\text{ClO}_4)_2$  (Figure 3.4a).

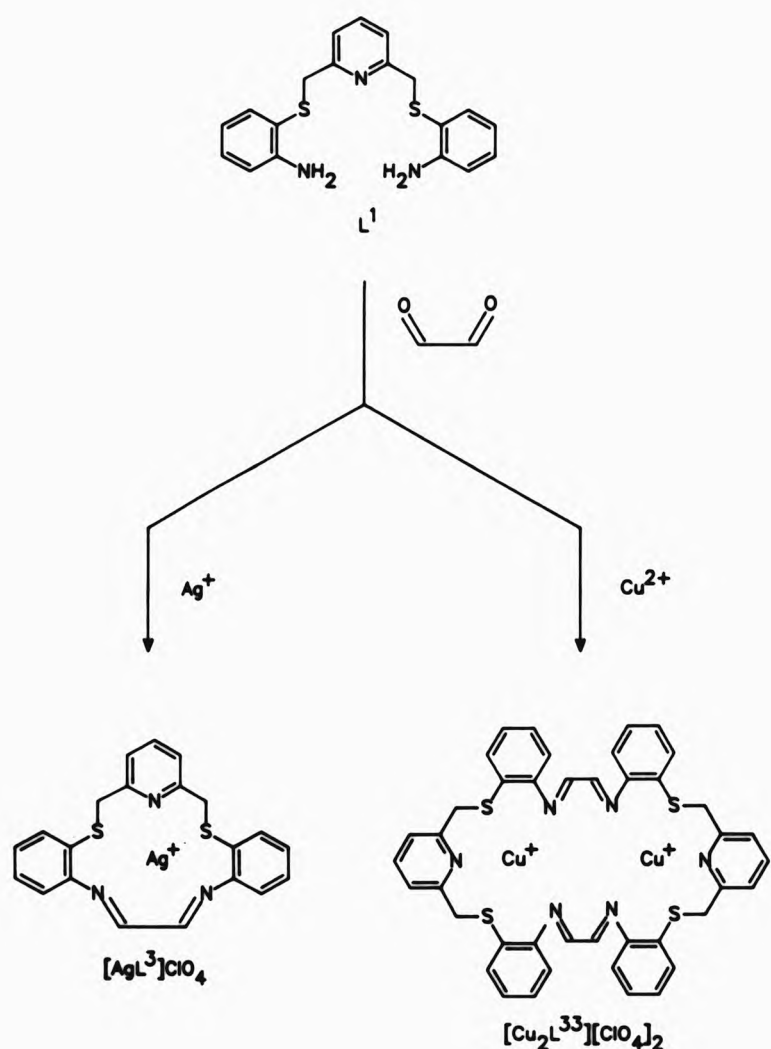
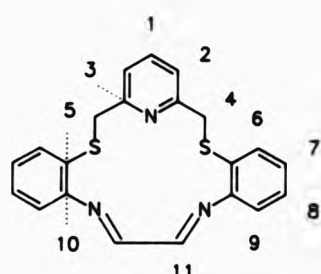


Figure 3.4a Schematic route to  $[\text{AgL}^3]\text{ClO}_4$  and  $[\text{Cu}_2\text{L}^{33}](\text{ClO}_4)_2$ .

Further characterisation of both complexes has been achieved through n.m.r. assignments (Table 3.4c and 3.4e).

Table 3.4c  $^1\text{H}$  (250.134 MHz) and  $^{13}\text{C}$  n.m.r. (62.896 MHz) data<sup>a</sup> for  $[\text{AgL}^3]\text{ClO}_4$  at ambient temperature in  $\text{CD}_3\text{CN}$ .



$^1\text{H}$	$\text{H}^{11}$	$\text{H}^1$	$\text{H}^{6/9}\text{d}$	$\text{H}^{\text{Ph}}\text{e}$	$\text{H}^2$	$\text{H}^4$
$\delta/\text{p.p.m.}$	8.49(s)	7.75(t) <sup>b</sup>	7.49(dd)	7.36 - 7.16(m)	7.35(d) <sup>c</sup>	4.27(s)

$^{13}\text{C}$  ABSOLUTE ASSIGNMENT NOT POSSIBLE.

$\delta/\text{p.p.m.}$  155.90 140.59 132.49 131.11 130.88 130.63 125.79 119.88 118.39

<sup>b</sup>Relative to  $\text{SiMe}_4$ . <sup>c</sup> $J(\text{H}^1-\text{H}^2) = 7.7 \text{ Hz}$ . <sup>d</sup> $J(\text{H}^2-\text{H}^1) = 7.7 \text{ Hz}$ . <sup>e</sup>Could be either proton - see text. <sup>f</sup>Remaining phenylene protons.

The proton n.m.r. (Figure 3.4b) for  $[\text{AgL}^3]\text{ClO}_4$  integrates for seventeen protons in total; the molecule having a  $C_2$  axis of symmetry. Three distinct areas were noted in the spectrum. The most downfield singlet ( $\delta$  8.49 p.p.m.) was attributed to the imine protons  $\text{H}^{11}$  (2 H, s,  $\text{CH}=\text{N}$ ). As expected, the most upfield singlet ( $\delta$  4.27 p.p.m.) was assigned to the methylene protons  $\text{H}^4$  (4 H, s,  $\text{CH}_2\text{S}$ ). In this respect, the singlets denote fast exchange of the metal between ligand and solvent molecules as a result of weak silver(I) and  $\text{L}^3$  donor interactions. Additionally, the metal must be co-ordinated to the ligand donor atoms in a

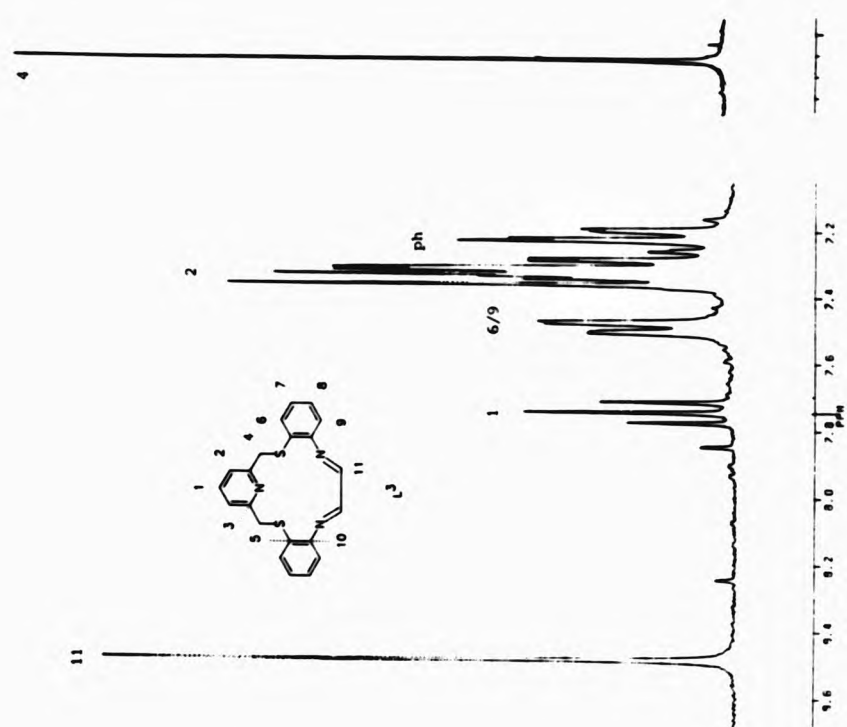


Figure 3.4b  $^1\text{H}$  n.m.r. spectrum of  $[\text{AgL}^3]\text{ClO}_4$  in  $d_3$ -acetonitrile.

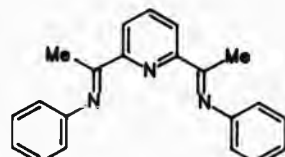
symmetrical manner. Typically, the region between  $\delta^{11}$  and  $\delta^4$  ( $\delta$  7.75-7.16 p.p.m.) accounts for the aromatic protons. Signals corresponding to the pyridyl protons  $\delta^1$  and  $\delta^2$  were assigned on the basis of their characteristic first-order splitting patterns, namely a triplet and doublet respectively. A signal centered at  $\delta$  7.49 p.p.m. is reminiscent of a doublet of doublets (dd) which may be attributable to the phenylene proton  $\delta^6$  or  $\delta^9$ . The remaining signals appear as complicated overlapped multiplets due to second-order coupling effects.

Although, substituent-induced n.m.r. shift parameters are readily attainable for mono-substituted benzene,<sup>[1]</sup> data is not available for the imino substituent. For instance, an  $-\text{NH}_2$  substituent will have an electron-donating as well as an ortho-/para-directing effect towards the remaining proton sites around the benzene ring. As a result, the protons of aniline will be shielded and they are predicted to resonate upfield relative to benzene; the ortho and para protons being shifted further upfield than the meta protons (section 2.3: used for assignment of  $\delta^1$ ). In contrast, an  $-\text{SMe}$  substituent is known to have a deshielding effect on all ortho, meta and para positions relative to benzene; the ortho proton being shifted furthest downfield.

In order to identify the inductive effects of an imino ( $\text{C}=\text{N}$ ) substituent towards the aromatic protons of a benzene nucleus, an already characterised phenylimino compound (1)<sup>[3]</sup> was employed (Figure 3.4c).

From the reported ortho, meta and para resonances of (1), together with the known shift for an unsubstituted benzene proton ( $\delta$  7.27 p.p.m.),<sup>[1]</sup> predicted imino ( $\text{C}=\text{N}$ ) shift parameters were obtained for each position,

*ortho* = -0.37, *meta* = 0.13 and *para* = -0.12 p.p.m.. The protons *ortho* and *para* to the imino substituent have been predicted to shift upfield and the *meta* protons to resonate at a low field relative to benzene. It is now possible to predict the relative shielding effects of an *ortho*-disubstituted thiophenylimino fragment. Referring back to the n.m.r. assignment of  $[AgL^3]ClO_4$ , calculations suggest that  $H^6$  should be further downfield ( $\delta$  7.77 p.p.m.) than  $H^9$  ( $\delta$  7.10 p.p.m.). The appropriateness of these interpretations needs to be treated with caution, since changes in solvent, temperature, concentration etc. all contribute to the appearance and relative position of a resonance signal. Furthermore, metal co-ordination of donor atoms will undoubtedly influence the shielding or deshielding effects of neighbouring proton sites. Substituent-induced shift parameters can also be applied to carbon-13 signals. However, the carbon-13 spectrum obtained in this instance was very weak and only nine (as opposed to eleven) different environments were noted. Therefore, no further attempt was made to assign the  $[AgL^3]ClO_4$  complex.

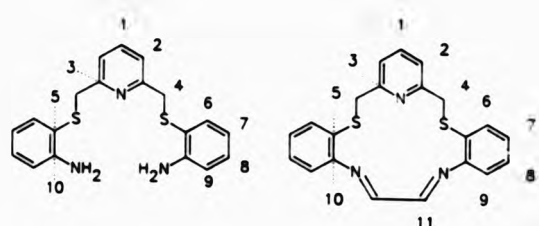


{1}

Figure 3.6c Ligand {1}, used to deduce imino induced chemical shifts.

Comparison of the proton n.m.r. spectrum of  $[AgL^1]ClO_4$  (section 2.4.1.2) with that of  $[AgL^3]ClO_4$ , shows the signals for  $H^1$ ,  $H^2$  and  $H^4$  to be shifted further downfield in the latter complex as a consequence of the extended  $\pi$ -delocalisation system covering the phenylene and methine units of  $L^3$  (Table 3.4d).

Table 3.4d Selected proton n.m.r. data for  $[\text{AgL}^1]\text{ClO}_4$  and  $[\text{AgL}^3]\text{ClO}_4$ .



$[\text{AgL}^1]\text{ClO}_4$                      $[\text{AgL}^3]\text{ClO}_4$

$\delta/\text{p.p.m.}$

H <sup>1</sup>	7.52	7.75
H <sup>2</sup>	7.02	7.35
H <sup>4</sup>	4.16	4.27

Although the silver(I) ion is not thought to be co-ordinated to the anilino nitrogens of L<sup>1</sup>, but only to the pyridyl nitrogen and thioether donor atoms, it is suspected that the silver(I) atom in its L<sup>3</sup> complex may be five co-ordinate. The sp<sup>2</sup> imino nitrogens involved in the π-system are 'softer' than the sp<sup>3</sup> anilino nitrogen donor atoms which due to their 'softer nature' may encourage co-ordination to silver(I). Further, it is a classical feature of macrocyclic chemistry that the cyclic constraints imposed by these ligands make it unlikely that any one donor could remain outside the first co-ordination sphere while the rest stay within.

Other comparable silver(I) macrocyclic ligand complexes which have been structurally characterised display co-ordination numbers from three to six (Figure 3.4d).

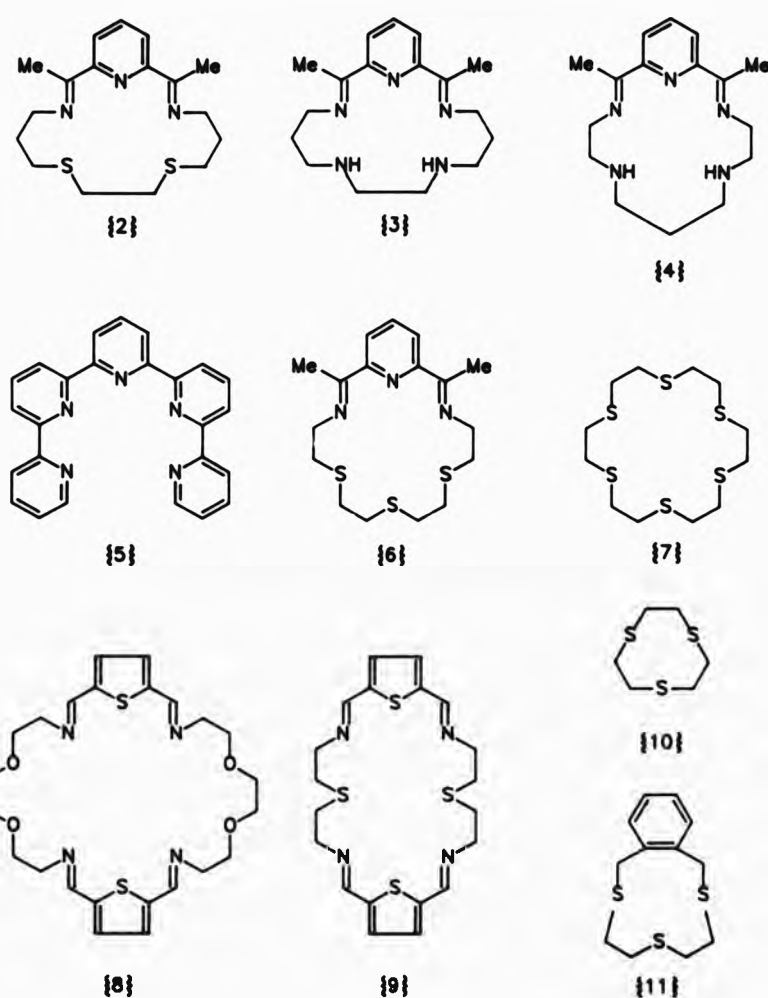


**Figure 3.44 Comparable ligands for structurally characterised silver(I) complexes.**

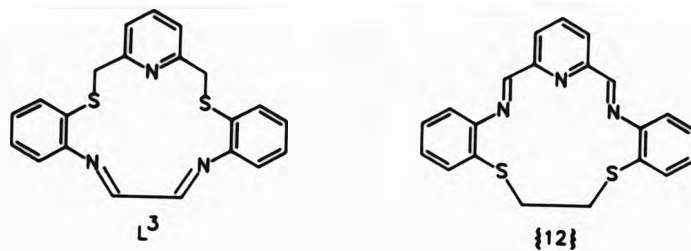
The quinquedentate seventeen-membered ligands {2}<sup>[4]</sup> and {3}<sup>[5]</sup> have a trigonal bipyramidal (both sulphur atoms in equatorial positions) conformation and two cations, with a similarly distorted pentagonal planar geometry around the metal ion respectively. In both cases, the size of the metal ion [ $r_{\text{Ag(I)}} = 1.09 \text{ \AA}$  (penta-co-ordinate)] was found to be a good fit for the seventeen-membered macrocyclic cavity. For the sixteen-membered macrocycle {4},<sup>[6]</sup> all five potential donor atoms are co-ordinated to the central metal ion defining a pentagonal plane. Additionally, the silver(I) atom interacts axially with a co-ordinatively saturated nitrogen atom of another identical [Ag(4)]<sup>+</sup> cation to form a face-to-face dimer. Thus, the co-ordination sphere around each silver(I) atom becomes pentagonal pyramidal. A rigid, acyclic quinquedentate ligand {5},<sup>[7]</sup> is also closely planar (slight helical twist) as a result of a good metal ion/bonding cavity match. The potentially sexidentate eighteen-membered macrocyclic ligands {6}<sup>[8]</sup> and {7}<sup>[9]</sup> can also comfortably accommodate the silver(I) ion [ $r_{\text{Ag(I)}} = 1.15 \text{ \AA}$  (hexa-co-ordinate)] because they are flexible enough to effectively moderate their bonding cavity dimensions. These structures also illustrate the ease with which silver(I) can increase its co-ordination number in the presence of soft donor ligands. Accordingly, in the presence of an unfavourable donor set such as in ligand {8},<sup>[10]</sup> each silver(I) atom of the disilver(I) complex is bound only to two imino nitrogens and a water molecule.

Under metal-ion templating conditions, twelve to fourteen-membered macrocyclic ligands are ineffective complexing agents towards silver(I). Instead, the formation of disilver(I), [2+2] condensation products is usually observed e.g. {9}<sup>[10]</sup>. On the other hand, two molecules of a pre-formed nine-membered macrocyclic ligand {10},<sup>[9]</sup>

co-ordinate facially to one Ag(I) metal centre in an octahedral manner. For a more rigid pre-formed eleven-membered macrocyclic ligand (11),<sup>[11]</sup> with a 1:2 metal-to-ligand ratio the complex conformation is dictated by the non-co-ordinating counterion, presumably due to crystal-packing compatibility.

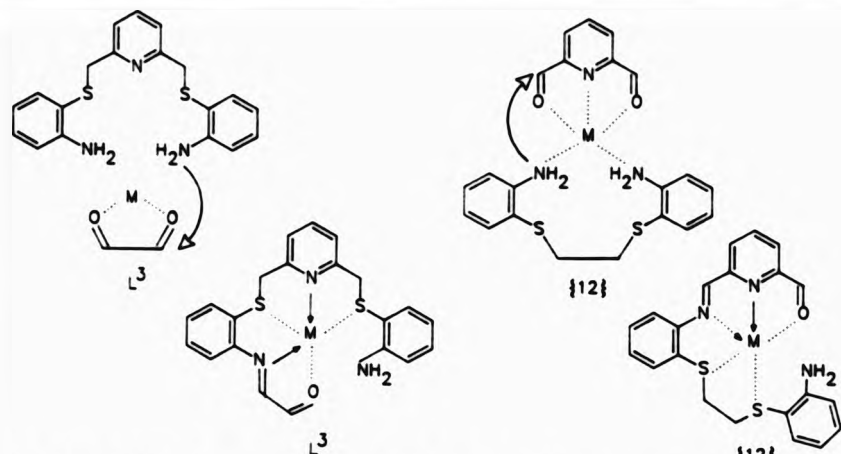
Despite the fact, that silver(I) complexes of fifteen- to eighteen-membered macrocyclic ligands can be isolated, as far as selectivity is concerned, the fifteen-membered macrocyclic ligand L<sup>3</sup>, in this work appears to discriminate against the toxic heavy metal ions lead(II), mercury(II) and cadmium(II). As lead(II) has a larger ionic radius than silver(I) ( $r_{\text{Pb}(II)} = 1.19 \text{ \AA}$  (hexa-co-ordinate)), it was not expected to complex with L<sup>3</sup>. However, both mercury(II) and cadmium(II) are smaller than silver(I) ( $r_{\text{Hg}(II)} = 1.02$ ,  $r_{\text{Cd}(II)} = 0.95 \text{ \AA}$  (hexa-co-ordinate)), in ionic radii. Non-co-ordination of mercury(II) to L<sup>3</sup> is somewhat surprising, since mercury(II) has an affinity for thioether donor atoms. Conversely, cadmium(II) is a borderline metal ion with a preference towards nitrogen and/or oxygen donor sets. Although, these predictions are based purely on an enthalpic premise to the formation of a stable isolable complex, entropic contributions and geometry of the transition state may also be unfavourable.

An isomeric ligand (12), of L<sup>3</sup> has also been investigated.<sup>[12], [13], [14]</sup> Like L<sup>3</sup>, (12) has an N<sub>3</sub>S<sub>2</sub> donor set, a fifteen-membered inner great ring and di-imino functionalities, the only difference being donor atom arrangement.



Work reported on ligand {12} was investigated with the metal complexes of manganese(II) and zinc(II).<sup>[12]</sup> It is striking that each isomer  $L^3$  and {12} appears to be stabilised by a different type of metal ion; in this work, complexation with only the softer metal ions silver(I) and copper(I) was achieved, whereas, {12} co-ordinates to the harder metal ions manganese(II) and zinc(II). At first it seems strange that isomers differing in only donor atom disposition should have such different 'bites'. But some insight into the origin of this anomaly is obtained by considering the differences in delocalisation of the two ligands.

The potentially quinquedentate ligands both have regions of delocalisation. However,  $L^3$  only has two donor atoms involved in the  $\pi$ -system since, the pyridyl ring is fragmented from the imine functions whereas, {12} is far more rigid with one pyridyl and two imino nitrogens forming a trimethine head-unit capable of being a strong  $\pi$ -acceptor ligand upon complexation. The apparent 'softness' and 'hardness' of  $L^3$  and {12} respectively may not necessarily be due to polarisability of the donor atoms, but the sequence of synthetic steps leading to the isolation of the products (i.e. involvement of metal-ion in the transition-state).

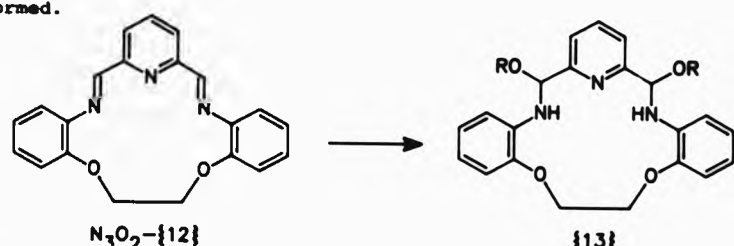


In the formation of  $L^3$  or  $\{12\}$ , the metal ion is thought to be initially co-ordinated to the carbonyl oxygens of glyoxal or 2,6-diformylpyridine. In doing so, the metal draws electron density away from the carbon atoms inducing an even greater  $\delta+$  charge to initiate nucleophilic attack by the anilino nitrogens. It appears that the 'jaw' or 'bite' of the glyoxal chelate may be too wide for the small metal ions manganese(II) and zinc(II) ( $r_{Mn(II)} = 0.83$ ,  $r_{Zn(II)} = 0.68 \text{ \AA}$  (penta-co-ordinate)), i.e. the angular requirements of these metal ions are not being met. Unlike 2,6-diformylpyridine which has the extra pyridyl nitrogen to serve as an 'anchor' for initial co-ordination to the metal and allows for a more stable (but labile) association and possibly a smaller 'bite' due to its terdentate nature.

Schiff-base condensations are known to proceed via the formation of carbinolamines,<sup>[15]</sup> that is the carbon atoms under nucleophilic attack are initially  $sp^3$  rather than  $sp^2$  hybridised. Therefore, this step would permit co-ordination of the smaller metal ions due to increased flexibility of the 'ethylene bridge'. However, loss of water in the final step with concomitant increase in rigidity (due to imine

formation) may force manganese(II) and zinc(II) out of co-ordination in the synthesis of  $L^3$ .

Surprisingly, the  $N_3O_2$  analogue of {12}, although initially isolated as its manganese(II) complex, readily undergoes solvolysis across the imine linkages to yield the alcohol adduct {13}.<sup>{16}</sup> In addition, the metal ion is not required for the cyclisation step and may have no organisational influence but merely complexes the macrocyclic product once formed.



The  $N_5$  analogue of {12} has also been isolated as its manganese(II) and zinc(II) complexes. It has been noted, that both high-spin manganese(II) ( $3d^5$ ) and zinc(II) ( $3d^{10}$ ) will form planar, pentagonal five co-ordinate complexes with the potentially quinquedentate ligands just mentioned since their crystal-field stabilisation energy (CFSE) is zero.<sup>{17}</sup> More importantly, lack of CFSE for any conformation provides an energetically favourable situation for ligand-imposed geometries to prevail.

The copper(I) complex  $[Cu_2L^{33}][ClO_4]_2$ , containing two copper(I) ions is diamagnetic ( $d^0$ ) and hence suitable for characterisation by n.m.r. (Table 3.4e). Although  $L^{33}$  is twice  $L^3$  in molecular weight, the number of equivalent environments for both proton and carbon-13 will be the same if the proposed structure is true. Instead of two halves of the molecule being magnetically and symmetrically equivalent as in  $L^3$ , one

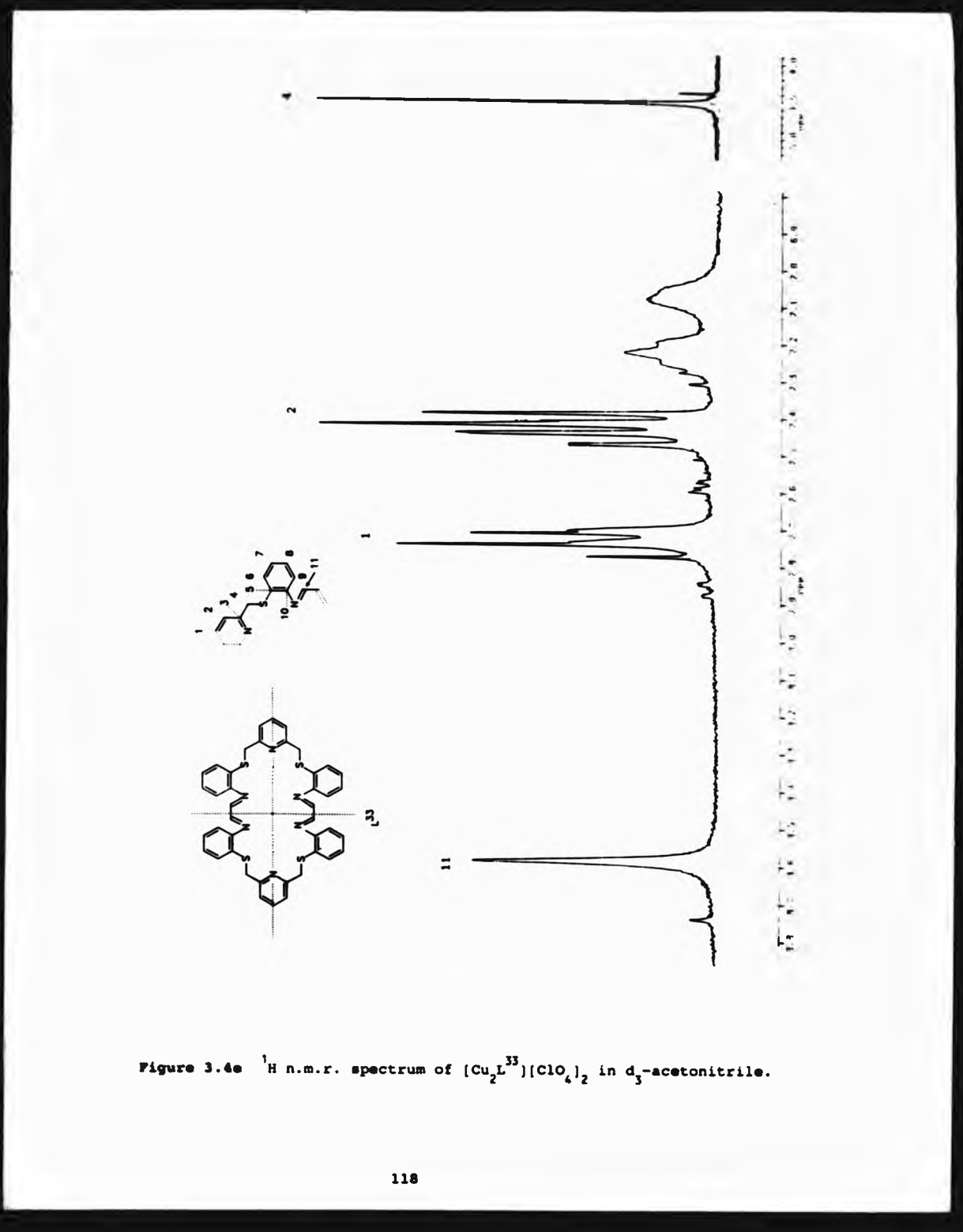
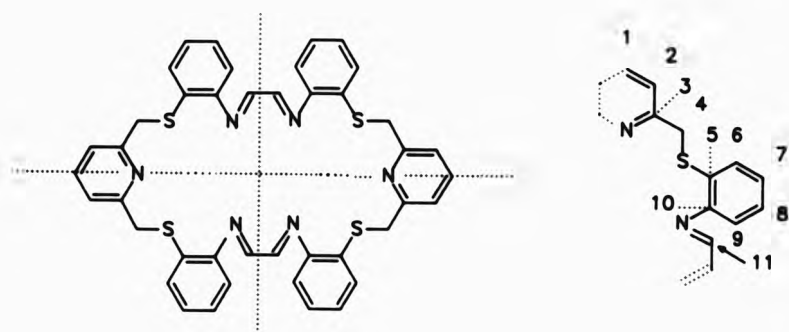


Figure 3.4e  $^1\text{H}$  n.m.r. spectrum of  $[\text{Cu}_2\text{L}^{33}](\text{ClO}_4)_2$  in  $d_3$ -acetonitrile.

quarter of L<sup>33</sup> was found to be unique in this instance.

Table 3.4e <sup>1</sup>H (250.134 MHz) and <sup>13</sup>C (62.896 MHz) n.m.r. data<sup>a</sup> for [Cu<sub>2</sub>L<sup>33</sup>](ClO<sub>4</sub>)<sub>2</sub> at ambient temperature in CD<sub>3</sub>CN.



<sup>1</sup> H	H <sup>11</sup>	H <sup>1</sup>	H <sup>2</sup>	H <sup>6-9</sup>	H <sup>4</sup>
δ/p.p.m. 8.59(s)	7.74(t) <sup>b</sup>	7.40(d) <sup>c</sup>	7.77 - 7.08(m)	4.53(s)	
<sup>13</sup> C ABSOLUTE ASSIGNMENT NOT POSSIBLE.					
δ/p.p.m. 160.38 156.17 147.13 140.35 132.29 131.54 130.76 129.68 125.59 124.90 42.94					

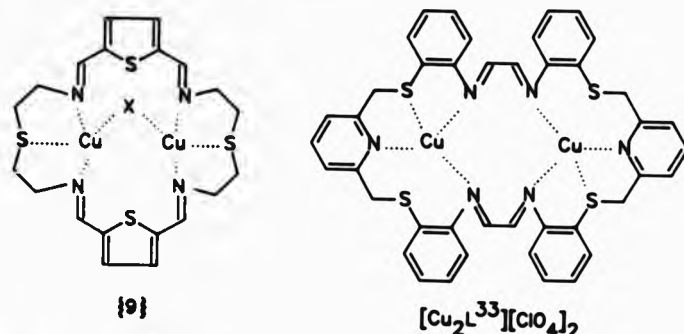
<sup>a</sup>Relative to SiMe<sub>4</sub>. <sup>b</sup>J(H<sup>1</sup>-H<sup>2</sup>) = 7.8 Hz. <sup>c</sup>J(H<sup>2</sup>-H<sup>1</sup>) = 7.7 Hz.

The proton n.m.r. spectrum of [Cu<sub>2</sub>L<sup>33</sup>](ClO<sub>4</sub>)<sub>2</sub> integrates for thirty five protons, of which only thirty four could be accounted for (Figure 3.4e). The most downfield singlet (δ 8.59 p.p.m.) was assigned to the imine protons H<sup>11</sup> (4 H, s, CH=N), whilst the most upfield singlet (δ 4.53 p.p.m.) was attributed to the methylene protons H<sup>4</sup> (4 H, s, CH<sub>2</sub>S). The pyridyl protons H<sup>1</sup> and H<sup>2</sup> are characteristically a triplet and doublet respectively. For the remaining aromatic protons H<sup>6-9</sup>, four distinct areas were noted. However, the signals appear broadened

with ill-defined multiplet splitting patterns. Nevertheless, some structural features and outlines of the broadened resonance signals could be identified as either belonging to a doublet of doublets (dd) or a triplet of doublets (td). Thus, the ranges  $\delta$  7.77-7.70, 7.47-7.39, 7.30-7.18 and 7.10-7.05 p.p.m. are thought to correspond to (dd), (td), (td) and (dd) splitting patterns respectively. Tentatively, each proton H<sup>6</sup> and H<sup>9</sup> should give a doublet of doublets signal and the protons H<sup>7</sup> and H<sup>8</sup> show a triplet of doublets splitting.

Also noteworthy in the proton n.m.r. spectrum of  $[\text{Cu}_2\overset{33}{\text{L}}](\text{ClO}_4)_2$  is the appearance of 'shadow' patterns downfield from the main characterised signals at ca. one tenth the intensity. These signals are also broad and may be due to a copper(I) or copper(II) [1+1] (i.e. L<sup>3</sup>) impurity. This may also account for the extra proton in the integration trace. The origins of broadening in the spectrum are unlikely to be a result of copper(II) species in solution, because of the absence of paramagnetic shifts and the microanalytical data obtained. If L<sup>3</sup> is present in solution, it must be as its copper(I) complex. Other causes of spectrum broadening are interchange between ligand conformation of the stable complex or exchange of metal environment (i.e. with solvent molecules). The carbon-13 n.m.r. spectrum also contained broadened signals that could not be identified. In all, twelve signals were observed where only eleven were expected. The most downfield and upfield carbon signals should be C<sup>11</sup> and C<sup>6</sup> respectively. No further assignment of the carbon-13 spectra of  $[\text{Cu}_2\overset{33}{\text{L}}](\text{ClO}_4)_2$  was attempted. A general feature of the n.m.r. spectra points to the flexibility of the macrocyclic ligand L<sup>33</sup> which is reflected in the imine and methylene signals (H<sup>11</sup> and H<sup>6</sup>) appearing as singlets (no geminal or vicinal couplings observed).

The n.m.r. spectra of dicopper(I) complexes of the macrocyclic ligand (9),<sup>[18]</sup> are quoted as having ranges from δ 9.30-8.63 p.p.m. for the imino protons. Additionally, crystal-structure analysis of one of these complexes reveals that each copper(I) atom is co-ordinated to two imino nitrogens and a thioether donor atom, with the remaining fourth site being occupied by a bridging anion.



Likewise, for  $[\text{Cu}_2\text{L}^{33}][\text{ClO}_4]_2$  the co-ordination geometry around each copper(I) atom is also thought to be tetrahedral. Thus, leaving two of the ten potential donor atoms unco-ordinated. Additionally, it may be possible for the thirty-membered macrocyclic ligand L<sup>33</sup> to twist and assume a helical geometry on co-ordination.<sup>[19]</sup>

In order to account for the binuclear {2+2} cyclocondensation product, it is thought that copper(II) co-ordinates preferentially to L<sup>1</sup> (section 2.4.1) rather than glyoxal. In doing so, the lone pairs of the anilino nitrogens may reduce copper(II) to copper(I). Additionally, mercaptocaniline has vacant π-orbitals which can accept electron density from the filled metal orbitals. In turn, π-acceptor ligands tend to stabilise low oxidation states and copper(I) will be favoured. Consequently, L<sup>1</sup> will assume a tetrahedral geometry around

copper(I). The anilino nitrogens may now be too far away or not in an idealised *cis* relationship to allow closure of the ring by the same molecule of glyoxal. Hence, two open-ended [1+1] moieties effect ring-closure.

Interestingly, isolation of the copper(II) complex of the fifteen-membered macrocyclic ligand (12) has also been reported.<sup>[13]</sup> According to e.s.r. spectra the compound has a roughly rectangular pyramidal  $N_3S_2$  co-ordination geometry with one of the sulphur atoms axially co-ordinated. However, the experimental conditions employed for the synthesis of  $[\text{Cu}(12)](\text{ClO}_4)_2$ , i.e. refluxing temperatures, were found in this work to lead to reduction of copper(II) to copper(I) or degradation of products.

Isolation of the copper(I) complex of the seventeen-membered macrocyclic ligand (2) (Figure 3.4b), has been afforded via transmetallation of the  $[\text{Ag}(2)]^+$  complex using  $\text{Cu}(\text{ClO}_4)_2 \cdot 6\text{H}_2\text{O}$  followed by chemical reduction.<sup>[4]</sup> It is thought that nucleophilic attack on the complex may be initiated by  $[\text{Ph}]^-$  or  $[\text{MeO}]^-$  species, after which electron transfer to the copper(II) centre to generate copper(I) is accompanied by radical formation. A crystal structure determination of the copper(I) complex indicates that the metal ion is tightly bound to the pyridyl nitrogen and to both sulphur atoms, with the remaining donors fitting in as best they can. The penta-co-ordinate complex assumes a trigonal bipyramidal (both sulphurs are in the equatorial plane) geometry. Conversely, in the copper(II) complexes (also five co-ordinate) of the macrocyclic ligand (2),<sup>[20]</sup> the metal ion is strongly bound to the three nitrogens of the trimethine unit, with longer bonding interactions to the thioether donor atoms. Furthermore,

one sulphur atom of the macrocycle remains unco-ordinated in the presence of an N-bonded thiocyanate molecule.

Transport of oxygen or transfer of electrons arising from mutual interactions between dinuclear active sites via bridging ligands is a widespread occurrence in biological systems.<sup>[21]</sup> Formation of the thirty-membered  $N_6S_4$  ligand  $L^3$ , isolated as its dicopper(I) complex is potentially useful as a model system for copper proteins.<sup>[22]</sup>

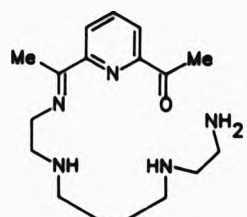
### 3.5 Transmetallation Reactions of $[AgL^3]ClO_4$ .

Those metal complexes of  $L^3$  which were not accessible via the template route were attempted through metal exchange (transmetallation) reactions.

The addition of lead(II), mercury(II), cadmium(II), zinc(II) or manganese(II) salts to  $[AgL^3]ClO_4$  were not successful. Even when a chloride salt was used in order to precipitate silver chloride, no other complexes of  $L^3$  were isolated. A reaction did take place on the addition of nickel(II) chloride to  $[AgL^3]ClO_4$ ; however, on analysis of the purple crystalline solid the product was confirmed to be  $[NiL^1(Cl)]Cl \cdot MeOH$ , as the elemental, infrared and f.a.b. mass data were identical to the analysis of the product that had been isolated previously (section 2.4.1). Clearly, ligand constraints imposed by the orthogonal geometries favoured by nickel(II) have led to the hydrolysis of  $L^3$  at the imine linkages to give an open-chain complex of the ligand  $L^1$ .

Transmetallation of the dimer  $[Ag(4)]_2[ClO_4]_2$  with  $Ni[ClO_4]_2 \cdot 6H_2O$  has led to the isolation of a ring-opened nickel(II) complex of ligand

{14}.<sup>[23]</sup> Here too, the strong stereochemical preferences of nickel(II) have been invoked as the driving force for the ligand rearrangements.



{14}

The reactions between L<sup>1</sup> and glyoxal in the presence of metal ion salts has underlined the importance of metal-ion size and electronic effects involved during the syntheses of [AgL<sup>3</sup>]ClO<sub>4</sub> and [Cu<sub>2</sub>L<sup>33</sup>](ClO<sub>4</sub>)<sub>2</sub>.

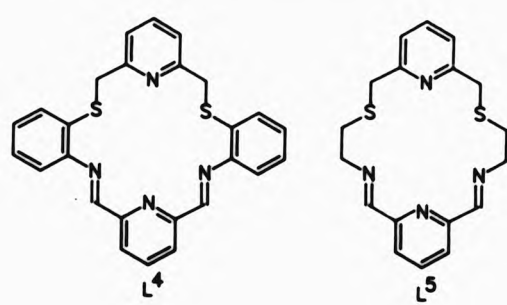
*References - Chapter Three.*

1. D. H. Williams and I. Fleming, 'Spectroscopic Methods in Organic Chemistry,' McGraw-Hill, London, (4th edn) 1988.
2. K. Nakamoto, 'Infrared Spectra of Inorganic and Co-ordination Compounds, Wiley-Interscience, New York, (2nd edn) 1970.
3. (a) D. A. Edwards, M. F. Mahon, W. R. Martin, K. C. Molloy, P. E. Panwick and R. A. Walton, *J. Chem. Soc., Dalton Trans.*, 1990, 3161;  
(b) I. J. Scowen and R. W. Matthews, personal communication.
4. M. G. B. Drew, C. Cairns, S. G. McFall and S. M. Nelson, *J. Chem. Soc., Dalton Trans.*, 1980, 2020.
5. S. M. Nelson, S. G. McFall, M. G. B. Drew, A. H. Bin Othman and N. B. Mason, *J. Chem. Soc., Chem. Commun.*, 1977, 167.
6. S. M. Nelson, S. G. McFall, M. G. B. Drew and A. H. Bin Othman, *J. Chem. Soc., Chem. Commun.*, 1977, 370
7. E. C. Constable, M. G. B. Drew, G. Forsyth and M. D. Ward, *J. Chem. Soc., Chem. Commun.*, 1988, 1450
8. S. Bin Silong, J. D. Kildea and A. H. White, *Aust. J. Chem.*, 1989, 42, 1387
9. A. J. Blake, R. O. Gould, A. J. Holder, T. I. Hyde and M. Schröder, *Polyhedron.*, 1989, 8, 513.
10. N. A. Bailey, M. M. Eddy, D. E. Fenton, S. Moss, A. Mukhopadhyay and G. Jones, *J. Chem. Soc., Dalton Trans.*, 1984, 2281.
11. B. de Groot, H. A. Jenkins and S. J. Loeb, *Inorg. Chem.*, 1992, 31, 203.
12. N. W. Alcock, D. C. Liles, M. McPartlin and P. A. Tasker, *J. Chem. Soc., Chem. Commun.*, 1974, 727.
13. A. W. Addison, T. N. Rao and E. Sinn, *Inorg. Chem.*, 1984, 23, 1957.
14. D. C. Liles, M. McPartlin and P. A. Tasker, *J. Chem. Soc., Dalton Trans.*, 1987, 1631.

15. Z. P. Haque, M. McPartlin and P. A. Tasker, *Inorg. Chem.*, 1979, 18, 2920.
16. D. H. Cook and D. E. Fenton, *Inorg. Chim. Acta.*, 1977, 25, L95.
17. R. K. Boggess and W. D. Wiegand, *J. Chem. Educ.*, 1978, 156.
18. A. Lavery, S. M. Nelson and M. G. B. Drew, *J. Chem. Soc., Dalton Trans.*, 1987, 2975.
19. (a) J. M. Lehn, J. P. Sauvage, J. Simon, R. Ziessel, C. Piccinni-Leopardi, G. Germain, J. P. Declercq and M. V. Meerssche, *Nouv. J. Chim.*, 1983, 7, 413; (b) J. M. Lehn and A. Rigault, *Angew. Chem., Int. Ed. Engl.*, 1988, 27, 1095.
20. M. G. B. Drew, C. Cairns, S. M. Nelson and J. Nelson, *J. Chem. Soc., Dalton Trans.*, 1981, 942.
21. R. W. Hay, 'Bio-inorganic Chemistry', Ellis Horwood Ltd, Chichester, 1987.
22. See for example: (a) M. G. Burnett, V. McKee, S. M. Nelson and M. G. B. Drew, *J. Chem. Soc., Chem. Commun.*, 1980, 829; (b) M. G. B. Drew, S. M. Nelson and J. Reedijk, *Inorg. Chim. Acta.*, 1982, L189; (c) J. de O. Carbal, M. F. Cabral, M. McCann and S. M. Nelson, *Inorg. Chim. Acta.*, 1984, L15; (d) M. F. Cabral, J. Cabral, J. Trocha-Grimshaw, K. P. McKillop, S. M. Nelson and J. Nelson, *J. Chem. Soc., Dalton Trans.*, 1989, 1351; (e) R. Meniff and A. E. Martell, *J. Chem. Soc., Chem. Commun.*, 1989, 1521.
23. C. Cairns, S. G. McFall, S. M. Nelson and M. G. B. Drew, *J. Chem. Soc., Dalton Trans.*, 1979, 446.

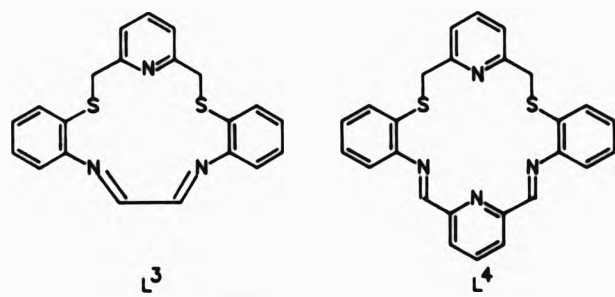
CHAPTER FOUR

**SYNTHESSES, CHARACTERISATION AND CO-ORDINATION STUDIES OF TWO  
SEXIDENTATE NITROGEN-SULPHUR SCHIFF-BASE MACROCYCLIC LIGANDS  $L^4$  AND  $L^5$**



#### 4.1 Introduction to L<sup>4</sup>.

As the underlying interest of this project is in the co-ordination chemistry of the toxic heavy metals cadmium(II), mercury(II) and lead(II), an eighteen-membered macrocyclic ligand L<sup>4</sup> was synthesised. In doing so, the interactions of L<sup>4</sup> also serve to shed some light on the binding preferences of these metal ions, as opposed to their unsuccessful union with L<sup>3</sup>. In the previous chapter, the smaller fifteen-membered macrocyclic ligand L<sup>3</sup>, could only be stabilised by the silver(I) metal ion while a larger thirty-membered macrocyclic ligand L<sup>33</sup> containing two metal sites was formed with copper(I).



Model studies show that for L<sup>4</sup>, the six donor atoms available cannot conform to an octahedral arrangement, nor does the ligand as a whole have a near planar geometry. The large thioether groups strain the inner great ring causing the phenylene rings to 'sit proud' out of the donor plane of the macrocycle which gives a 'puckered' ligand arrangement. The conjugated half of the macrocycle, containing one pyridyl and two imino substituents is likely to be planar. On the other hand, free rotation about the methylene carbons at the 2- and 6-positions of the other pyridine ring, allows the ring itself to be above or below the plane of the trimethine unit.

#### 4.2 Non-template and Template Syntheses of L<sup>4</sup>.

The non-template synthesis of L<sup>4</sup> using L<sup>1</sup> and 2,6-diformylpyridine was carried out in acetonitrile rather than alcoholic solutions (in order to limit imine hydrolysis/solvolytic) with ca. 5 cm<sup>3</sup> of 2,2-dimethoxypropane to eliminate water (side product) from the equilibrium mixture. Unfortunately, the dark orange solid isolated did not analyse for L<sup>4</sup>.

Templating the above reaction with calcium(II), strontium(II) and barium(II) (which were not expected to form final macrocyclic products with L<sup>4</sup>), was also attempted. Once again, the pale yellow solids isolated did not analyse for L<sup>4</sup> (nor [ML<sup>4</sup>]<sup>2+</sup> where M = Ca, Sr or Ba) however, the mass spectrum did indicate the presence of L<sup>4</sup>. Nevertheless, the addition of silver(I), mercury(II) or lead(II) to the crude orange or pale yellow solids isolated in the above reactions yielded characterisable complexes of known composition. Notwithstanding this, yields were low and thereafter complexation reactions were carried out via the *in situ* procedure.

Interestingly, complexation reactions of an analogous eighteen-membered potentially sexidentate N<sub>6</sub> macrocyclic ligand (1), with alkali and alkaline earth metal ions, followed by ligand exchange in the presence of a ten molar excess of 18-crown-6 has afforded the metal-free macrocyclic ligand (1).<sup>(1)</sup>

#### 4.3 Co-ordination Studies of [PbL<sup>4</sup>]<sup>2+</sup>, [AgL<sup>4</sup>]<sup>+</sup>, and [MgL<sup>4</sup>]<sup>2+</sup>.

As expected, L<sup>4</sup> formed complexes with the larger heavy-metal ions, silver(I), mercury(II), cadmium(II) and lead(II); but also formed complexes with the smaller metal ions copper(II), nickel(II) and zinc(II). Interactions between cadmium(II) and zinc(II) salts with L<sup>4</sup>

are discussed in section 4.4. However, copper(II) and nickel(II) gave rearranged products under the same reaction conditions and will therefore be dealt with separately in Chapter Five.

As before, complexation reactions were carried out in alcohol or acetonitrile, utilising metal-ion perchlorate, thiocyanate, nitrate and/or chloride salts. All complexes were brightly coloured, characteristic of the imines and the extended conjugation available through the benzene and pyridine rings. The complexes were isolated as crystalline or amorphous solids, and in some instances it was possible to undertake crystallographic structural determinations.

#### 4.3.1 Spectroscopic Studies of $[PbL^4]^{2+}$ , $[AgL^4]^+$ and $[HgL^4]^{2+}$ .

##### 4.3.1.1 Infrared studies.

The infrared spectra (Table 4.3.1a) for these complexes, show no amine or carbonyl stretching frequencies (due to the reactants) in their respective absorbance regions. Instead, a weak-to-medium band in the range ca.  $1630$ - $1620\text{ cm}^{-1}$  was observed and is indicative of  $\nu(C=N)$ . The pyridyl/phenyl absorbances are found between ca.  $1590$ - $1580\text{ cm}^{-1}$ .<sup>[2]</sup> In both cases, it is not possible to ascertain metal-imine or metal-pyridine co-ordination, since a reliable free ligand infrared spectrum of  $L^4$  is unavailable.

Spectra for the lead(II) and silver(I) perchlorate complexes of  $L^4$  give no intimation of anion co-ordination. However, for the lead(II) complex, a strong sharp band at ca.  $3465\text{ cm}^{-1}$  is considered to arise from vibrations due to the O-H stretchings of a water molecule, co-ordinated to the metal atom.<sup>[2]</sup>

The lead(II), silver(I) and mercury(II) thiocyanate complexes of  $L^4$  all show a single, sharp absorbance corresponding to the  $\nu(C-N)$  stretching frequency of [NCS] at ca. 2040, 2090 and 2120  $\text{cm}^{-1}$  respectively. Where more than one thiocyanate is known to be present in a complex, single, unsplit absorbances are an indication of identical co-ordination environments about both the thiocyanate anions. Moreover, the thiocyanate group is ambidentate since, both nitrogen and sulphur may co-ordinate to a metal atom and act as a unidentate ligand or the anion may bridge between two metal centres in a bidentate fashion. The linear disposition of the thiocyanate molecule together with its ambidentate nature, leading to linkage isomerism arising from different types of (hard/soft) ligating atoms, must encourage anion co-ordination in the majority of its complexes.

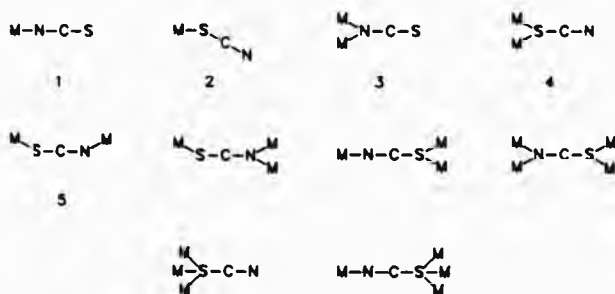
Table 4.3.1a Infrared data<sup>a</sup> for  $[PbL^4]^{2+}$ ,  $[AgL^4]^+$  and  $[HgL^4]^{2+}$ .<sup>b</sup>

COMPLEX	COLOUR	$\nu(C=N)$	$\nu(\text{py/Bz})$	$\nu(\text{counterion})$
$[PbL^4(H_2O)(MeOH)][ClO_4]_2$	ORANGE	1622w	1585m	1060s 624s
$[PbL^4(SCN)]_2$	"	1620w	1580m	2040s
$[PbL^4][NO_3]_2$	"	1630m	1585m	1390s <sup>c</sup> 822m
$[PbL^4]Cl_2$	"	1620m	1585m	-
$[AgL^4]ClO_4$	"	1630m	1590m	1100s 630s
$[AgL^4(SCN)]$	"	1630m	1580m	2090s
$[AgL^4]NO_3$	YELLOW	1630m	1580m	1390s
$[HgL^4(SCN)]_2 \cdot MeOH$	"	1622w	1580m	2120s

<sup>a</sup>In  $\text{cm}^{-1}$ . <sup>b</sup>KBr disc. <sup>c</sup>Absorbance is broad and split.

As inorganic ions, the thiocyanate stretches give rise to strong bands between 2200-2000  $\text{cm}^{-1}$ .<sup>[2]</sup> For metal-thiocyanate complexes, in all,

ten potential bonding modes have been cited for the thiocyanate molecule.<sup>[3]</sup> Thus, for mononuclear complexes the metal-thiocyanate bonding mode is either (1) or (2). Whilst, three modes of co-ordination (3), (4) or (5) can exist for binuclear complexes.



Numerous correlations between thiocyanate bonding modes and infrared spectroscopy have been reported for macrocyclic complexes. However, only one type of bonding mode has been established without ambiguity. That is, frequencies observed below  $2000\text{ cm}^{-1}$  correspond to single-atom, nitrogen-only bridging (3) between metal centres.<sup>[4]</sup> Although, there is an exception where proton transfer from the macrocyclic ligand has resulted in the formation of an isothiocyanic acid complex.<sup>[5]</sup> Additionally, there is only one structurally characterised complex containing sulphur-only bridges (4) to date.<sup>[6]</sup>

Generally, the thiocyanate mode of co-ordination to a metal atom follows the HSAB principle. That is, harder metal ions will preferentially co-ordinate to nitrogen and softer metal ions will tend to ligate the sulphur donor atoms. Once again, however, discrepancies arise for the borderline cases and steric constraints imposed by crowded complexes where either mode of co-ordination may be present.

In the infrared region, depending on the metal-donor atom interaction, the individual bond vibrations within the thiocyanate molecule give rise to three fundamental frequency ranges:<sup>[7]</sup>

	$\nu_1$ (C-N) stretch	$\nu_2$ (N-C-S) bend	$\nu_3$ (C-S) stretch
N-bonded	2040-2080	465-480	780-860
S-bonded	2080-2120	410-470	690-720

Correlation of the HSAB concept and the infrared data available would suggest that metal-sulphur co-ordination exists for the silver(I)<sup>[7]</sup> and mercury(II)<sup>[8]</sup> complexes of L<sup>4</sup>. The lead(II) thiocyanate complex, on the other hand, is more difficult to assess. Lead(II) is a borderline metal ion and has been found to co-ordinate to thiocyanate via both nitrogen and/or sulphur donor atoms. Although metal-sulphur co-ordination will be bent and metal-nitrogen co-ordination can be linear or bent, there should not be any ligand constraints preventing either of these spatial arrangements from taking place. Based on the single, sharp absorbance at ca. 2040 cm<sup>-1</sup>, trans metal-nitrogen co-ordination is favoured. Unfortunately, the value is also close to that observed for ionic thiocyanates (absorbances at ca. 2050 cm<sup>-1</sup> have been noted - although these tend to be broader),<sup>[9],[10]</sup> a possibility which cannot be ruled out in this case. Furthermore, ligand bands of L<sup>4</sup> obscure the  $\nu$ (N-C-S) bending and  $\nu$ (C-S) stretching regions which sometimes prove to be more diagnostic.

In the absence of crystallographic data, it is not always possible to deduce categorically thiocyanate bonding modes in a complex. Factors which further complicate structure elucidation of thiocyanate complexes result from  $\nu$ (C-N) stretches being sensitive to the presence of other

ligands, dx-p<sub>z</sub> back bonding,<sup>[6]</sup> type of bonding (i.e. terminal or bridging),<sup>[11]</sup> nature of bonding interaction (i.e. covalent or ionic), spatial arrangement (i.e. cis- or trans-),<sup>[9]</sup> steric ligand constraints and presence of solvent if in solution.<sup>[7]</sup>

The nitrate complexes differ greatly in their infrared spectra.  $[\text{AgL}^4]\text{NO}_3$  shows a single sharp vibration at ca.  $1390 \text{ cm}^{-1}$ . On the other hand, for  $[\text{PbL}^4][\text{NO}_3]_2$  a very broad but structured band which centres at ca.  $1390 \text{ cm}^{-1}$  is observed. For the silver(I) complex, the nitrate counterion is ionic. In the case of the lead(II) complex, since an absorption is present at ca.  $1390 \text{ cm}^{-1}$ , the nitrates are still considered to be unco-ordinated,<sup>[12]</sup> even though fine structure at ca.  $1290$ ,  $1310$  and  $1360 \text{ cm}^{-1}$  exist. Broadness and extra absorbances may be caused by the presence of two nitrate groups in different environments for this compound as opposed to only one nitrate group being associated with the silver(I) complex.

Elemental compositions (section 7.4.1-3) analyse for the formation of a (1+1) ligand product, with a metal-to-ligand ratio of 1:1. In addition,  $[\text{HgL}^4(\text{SCN})_2]\cdot\text{MeOH}$  has a methanol solvate associated with its formulation.

#### 4.3.1.2. Fast atom bombardment mass spectrometry.

F.a.b. mass spectral data (Table 4.3.1b) are consistent with the formulation of (1+1) Schiff base condensation products for mononuclear complexes. All complexes showed the highest, most stable (100 %) mass peaks for the loss of a counterion molecule, with the exception of  $[\text{PbL}^4][\text{NO}_3]_2$ . The loss of counterion for this complex was also indicated but the relative intensity of the corresponding species was

almost half (55 %) that of the other complexes. Sequential counterion loss is apparent for each complex, followed by presence of the free imine ligand  $L^+$ , in some instances.

Table 4.3.1b Fast-atom bombardment mass spectra<sup>a</sup> for  $[PbL^4]^{2+}$ ,  $[AgL^4]^+$  and  $[HgL^4]^{2+}$  complexes.

COMPLEX	FRAGMENTATION ASSIGNMENT	MASS <sup>b</sup>	RELATIVE
			PERCENTAGE
$(PbL^4(H_2O)(MeOH)) [ClO_4]_2$	$[PbL^4]ClO_4^+$	759	100
	$[PbL^4]^+$	659	55
	$[PbL^4]ClO_4^+$	759	6 <sup>c</sup>
	$[L^4]^+$	453	100 <sup>c</sup>
$(PbL^4(SCN)_2$	$[PbL^4]SCN^+$	718	100
	$[PbL^4]^+$	660	35
$(PbL^4)[NO_3]_2$	$(PbL^4)NO_3^+$	722	55
	$[PbL^4]^+$	660	21
$(AgL^4)ClO_4$	$(AgL^4)^+$	561	100
$(AgL^4)NO_3$	$(AgL^4)^+$	561	100
$(HgL^4(SCN)_2 \cdot MeOH$	$(HgL^4)SCN^+$	712	100
	$(HgL^4)^+$	652	6
	$[L^4]^+$	453	35

<sup>a</sup>In NOBA matrix unless stated otherwise. <sup>b</sup>Positive-ion mode. <sup>c</sup>In thioglycerol.

There are differences in the spectra of  $(PbL^4(H_2O)(MeOH)) [ClO_4]_2$ , depending on the nature of the matrix used. In thioglycerol,  $[PbL^4]ClO_4^+$  accounts for only 6 %, whereas, the highest, most stable mass peak corresponds to that of  $[L^4]^+$ , which is in total contrast to

the spectrum obtained in 3-nitrobenzyl alcohol.

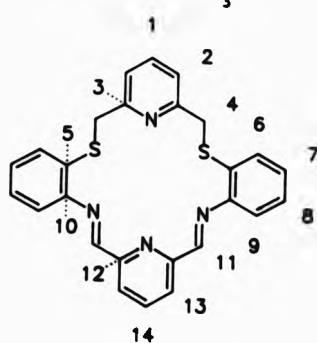
#### 4.3.1.3 Nuclear magnetic resonance spectroscopy.

The solution structures for those metal complexes having sufficient solubility for n.m.r. studies were investigated. The proton n.m.r. (Table 4.3.1c) spectra of  $[\text{PbL}^4(\text{H}_2\text{O})(\text{MeOH})]\text{ClO}_4$ ,  $[\text{AgL}^4]\text{ClO}_4$  and  $[\text{HgL}^4(\text{SCN})_2]\text{MeOH}$  show similarities for the lead(II) and mercury(II) complexes, whilst the silver(I) complex is slightly better resolved.

The proton spectrum (Figure 4.3.1a) of the  $[\text{PbL}^4(\text{H}_2\text{O})(\text{MeOH})]\text{ClO}_4$  complex has resonance signals integrating for twenty protons (consistent with the given formulation). The most downfield resonance ( $\delta$  9.57 p.p.m.) observed is attributed to the imino protons  $\text{H}^{11}$  (2 H, s,  $\text{CH}=\text{N}$ ). The singlet at  $\delta$  4.75 p.p.m. is attributed to the methylene protons  $\text{H}^4$  (4 H, s,  $\text{CH}_2\text{S}$ ) and are still magnetically equivalent (as for  $[\text{ML}^1]^{m+}$  or  $[\text{ML}^3]^{m+}$  n.m.r. discussion, section 2.4.2 or 3.4) by way of free rotation about the C-S bond, even though a more rigid moiety exists, for the latter part of the molecule in  $\text{L}^4$ .

Signals at  $\delta$  8.62 and 8.35 p.p.m. are assignable to  $\text{H}^{14}$  [1 H, t,  $^3J(\text{H}^{14}-\text{H}^{13})$  7.8 Hz,  $\gamma\text{pyH}$ ] and  $\text{H}^{13}$  [2 H, d,  $^3J(\text{H}^{13}-\text{H}^{14})$  7.7 Hz,  $\beta\text{pyH}$ ] which are characteristically a triplet and doublet respectively. The other pyridine protons,  $\text{H}^1$  [1 H, t,  $^3J(\text{H}^1-\text{H}^2)$  7.8 Hz,  $\gamma\text{pyH}$ ] and  $\text{H}^2$  [2 H, d,  $^3J(\text{H}^2-\text{H}^1)$  7.7 Hz,  $\beta\text{pyH}$ ] are overlapped with the rest of the aromatic protons  $\text{H}^6\text{-H}^9$ . However, it is still possible to locate the triplet and doublet for  $\text{H}^1$  and  $\text{H}^2$  with added confirmation from coupling constant comparisons. Distinctions between  $\text{H}^{14}$  and  $\text{H}^1$ , as well as,  $\text{H}^{13}$  and  $\text{H}^2$  are based on delocalisation of pyridyl and imino electrons leading to an overall deshielding effect.

Table 4.3.1c  $^1\text{H}$  n.m.r. data<sup>a</sup> for  $[\text{PbL}^4(\text{H}_2\text{O})(\text{MeOH})][\text{ClO}_4]_2$ ,  $[\text{AgL}^4]\text{ClO}_4$  and  $[\text{HgL}^4(\text{SCN})_2]\cdot\text{MeOH}$  (250.134 Hz) in  $\text{CD}_3\text{CN}$  at ambient temperature.



	$[\text{PbL}^4(\text{H}_2\text{O})(\text{MeOH})][\text{ClO}_4]_2$	$[\text{AgL}^4]\text{ClO}_4$	$[\text{HgL}^4(\text{SCN})_2]\cdot\text{MeOH}$
9.57(s)	$\text{H}^{11}$	8.86(s)	$\text{H}^{11}$
8.62(t)	$\text{H}^{14}$	8.31(t) <sup>b</sup>	$\text{H}^{14}$
8.35(d)	$\text{H}^{13}$	8.05(d) <sup>b</sup>	$\text{H}^{13}$
7.91-7.83(m)	$\text{H}^1, \text{ph}^c$	7.77(dd)	7.82-7.75(m) $\text{H}^1, \text{ph}^c$
7.49(d)	$\text{H}^2$	7.65(t)	7.53-7.40(m) $\text{ph}^d$
7.63-7.48(m)	$\text{ph}^d$	7.53-7.36(m)	$\text{ph}^c$
4.75(s)	$\text{H}^4$	7.25(d)	$\text{H}^2$
		4.35(s)	4.55(s) $\text{H}^4$
			3.27(s) $\text{H}^4$

<sup>a</sup>In p.p.m., relative to  $\text{SiMe}_4$ . <sup>b</sup>Assigned as  $\text{AB}_2$  spin system. <sup>c</sup>Any phenylene proton. <sup>d</sup>Remaining phenylene protons. <sup>e</sup>Could be either proton - see text. <sup>f</sup>Origin unknown - integrates for one proton.

Lead ( $^{207}\text{Pb}$ ) too, has a nucleus of spin  $I = 1/2$  and is known to couple with protons. Consequently lead(II) is found to couple with the imino protons,  $\text{H}^1$  to give  $^3J(^{207}\text{Pb}-\text{H}^1) = 16.7$  Hz. The intensity ratios of the satellites are proportional to the natural abundance of  $^{207}\text{Pb}$  (Table 4.3.1d). This is strongly suggestive of lead(II)-imino nitrogen co-ordination.

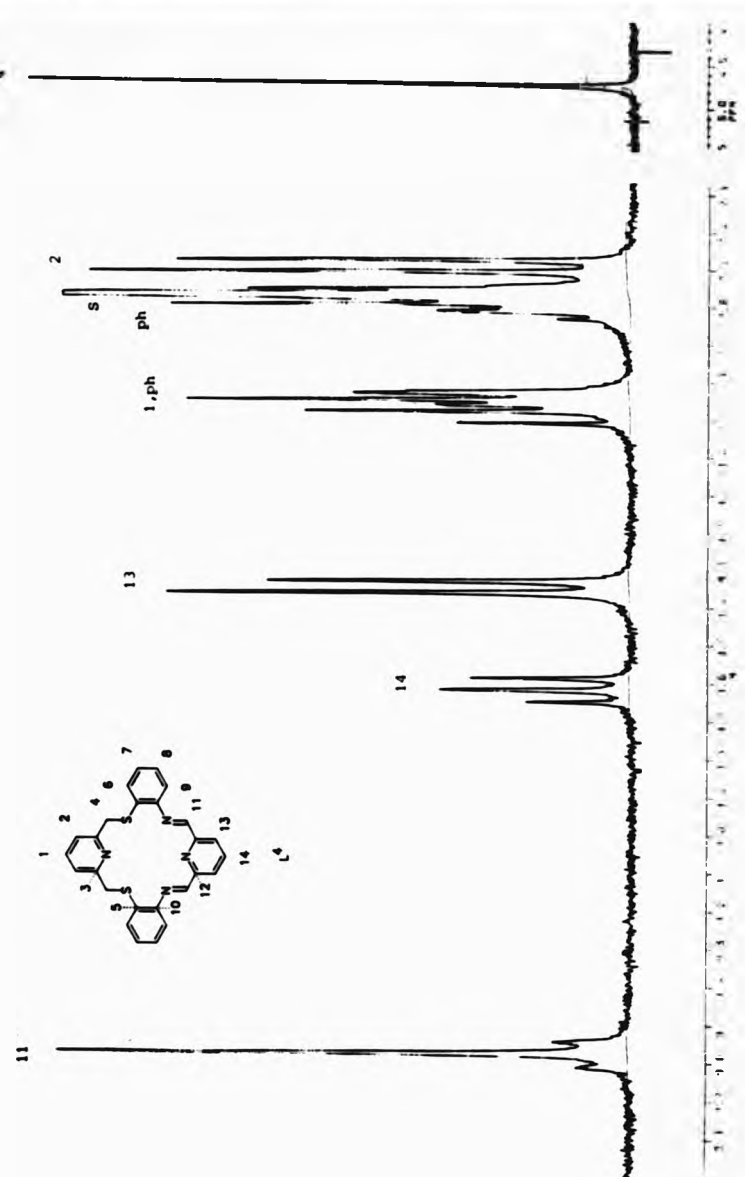


Figure 4.3.1a  $^1\text{H}$  n.m.r. spectrum of  $[\text{PbL}^4(\text{H}_2\text{O})(\text{MeOH})][\text{ClO}_4]_2$  in  $d_3$ -acetonitrile.

The carbon-13 (Table 4.3.1a) broad band proton decoupled spectrum for  $[PbL(H_2O)(MeOH)][ClO_4]_2$ , gave fifteen resonance signals. However, only fourteen chemically distinct carbon environments had been ascertained. No  $^{207}Pb-^{13}C$  satellites have been observed (sample may be too dilute), although the pyridyl and imino carbon signals do appear broadened at the base. The protonated carbons were assigned through  $^1H, ^{13}C$ -COSY spectra. It was not possible to identify the phenylene carbons,  $C^6-C^9$  individually. Non-protonated carbons (quaternary),  $C^{12}, C^3, C^{10}$  and  $C^5$  were designated as such, according to deshielding effects caused by electronegativity of the heteroatoms ( $N>S>>C$ ).

Table 4.3.1d Isotopic abundances for metals with  $I = 1/2$  nuclear spins.

	NATURAL ABUNDANCE (%)	INTENSITY RATIOS (%) OF SATELLITES	
		CALCULATED	OBSERVED
$^{207}Pb$	22.60	11.30	8.60
$^{199}Hg$	16.84	8.42	8.79

The proton and carbon-13 n.m.r. shifts have been reported for the analogous eighteen-membered  $N_6$  donor macrocyclic ligand (1).<sup>(13)</sup> The imino protons resonate at  $\delta$  9.72 p.p.m. (4 H, s,  $CH=N$ ), whilst the pyridyl protons at  $\delta$  8.56 p.p.m. (2 H, t,  $\gamma_{PyH}$ ) and  $\delta$  8.33 p.p.m. (4 H, d,  $\beta_{PyH}$ ) display a three-bond coupling constant of J 7.5 Hz. Two multiplets centered at  $\delta$  7.88 and 7.72 p.p.m. are assigned to the phenylene protons. Seven unique carbon-13 environments were observed; the most downfield signal at  $\delta$  160.59 p.p.m. corresponds to the imino carbon, signals at  $\delta$  152.57, 140.98, 131.12 and 143.25, 130.36, 119.52 p.p.m. are assigned to the pyridyl and phenylene carbon sites respectively.

The proton n.m.r. (Figure 4.3.1b) of the  $[HgL^4(SCN)_2] \cdot MeOH$  complex, was also indicative of the given structure, bar one resonance signal at 3.27 p.p.m. (1H, s). Elemental analysis agreed with the presence of a methanol molecule in its formulation. However, this upfield resonance integrates for one proton only, even though the region corresponds to that for methyl resonance signals.

Thus as before, protons H<sup>11</sup>, H<sup>4</sup>, H<sup>14</sup> and H<sup>13</sup> can be readily assigned. In relation to  $(PbL^4(H_2O)(MeOH))(\text{ClO}_4)_2$ , these four proton signals resonate at lower frequencies (ranging from 0.20-0.51 p.p.m.). The rest of the aromatic protons appear as complicated, overlapped multiplets, approximating to second-order, except for H<sup>2</sup> at δ 7.40 p.p.m. (2 H, d,  $J(H^2-H^1)$  7.7 Hz,  $\beta_{pyH}$ ) which is easily identified by height and appearance as a doublet. In addition, mercury-proton coupling is evident, denoting three-bond coupling via the imine nitrogens [ $J(^{119}\text{Hg}-H^{11})$  = 7.2 Hz]. Once again, intensity ratios correlate to the natural isotopic abundances of <sup>119</sup>Hg (Table 4.3.1d). It is interesting to note, that the one side of the doublet for H<sup>13</sup>, which does not overlap with other proton resonances, also exhibits a mercury satellite (with diminished intensity), which must arise from four-bond coupling either via the imino nitrogens or the pyridyl nitrogen donor. The latter is more viable and metal-to-nitrogen co-ordination in solution is therefore exemplified.

The carbon-13 (Table 4.3.1e) broad band proton decoupled spectrum for  $[HgL^4(SCN)_2] \cdot MeOH$  shows fifteen carbon resonance signals. Fourteen of these signals arise from the macrocyclic ligand L<sup>4</sup>. The other signal at δ 126.70 p.p.m. is due to the thiocyanante ions co-ordinated to the metal atom (both must be chemically and magnetically equivalent).

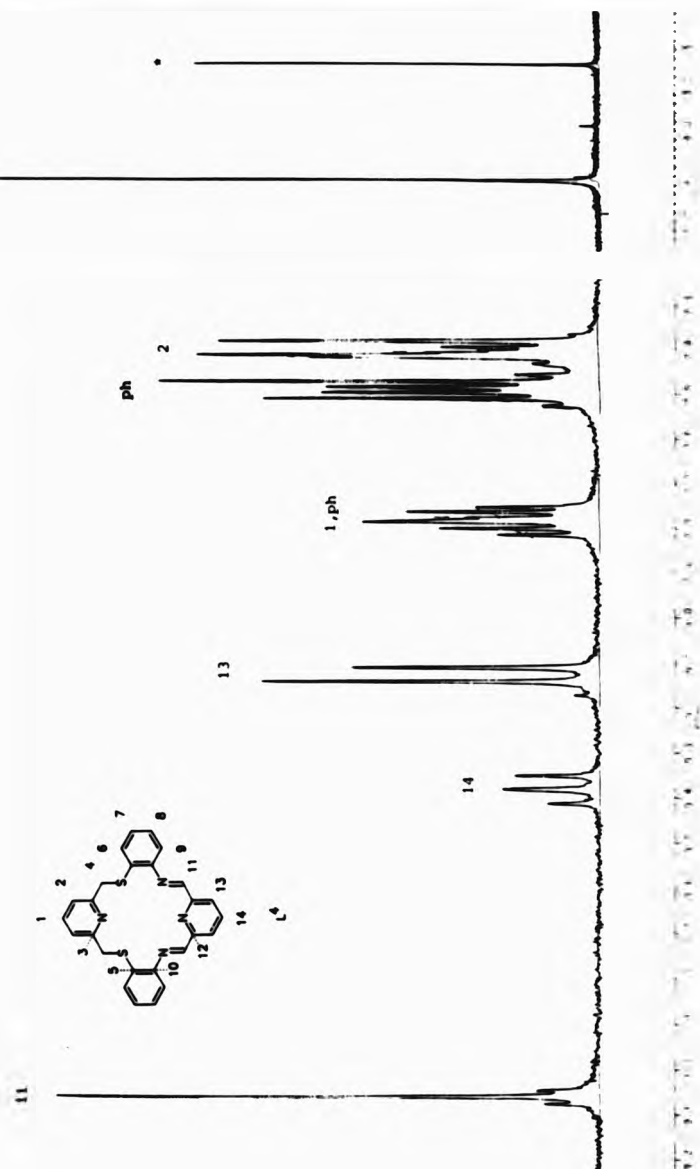


Figure 4.3.1b  $^1\text{H}$  n.m.r. spectrum of  $[\text{HgL}^4(\text{SCN})_2]\cdot\text{MeOH}$  in  $\text{d}_3$ -acetonitrile.

Apart from the differences in counterion the lead(II) and mercury(II) complexes have similar solution structures.

The spectrum (Figure 4.3.1c) for  $[AgL^4]ClO_4$  integrates for twenty protons, incorporated into ten resonance signals, indicating that one half of the molecule is chemically and magnetically equivalent to the other half. The most downfield resonance at  $\delta$  8.86 p.p.m. is attributed to  $H^{11}$  (2 H, s,  $CH=N$ ), and the most upfield resonance at  $\delta$  4.35 p.p.m. to the methylene protons  $H^4$  (4 H, s,  $CH_2S$ ).

As previously, the pyridyl protons  $H^1$  ( $\delta$  7.65 p.p.m.) and  $H^2$  ( $\delta$  7.25 p.p.m.) appear characteristically as a triplet and doublet respectively according to  $(n+1)$  selection rules for first-order spectra. In contrast, the other set of pyridyl protons  $H^{14}$  and  $H^{13}$  give rise to second-order effects within the spectrum and are assigned as an  $AB_2$  spin system (Appendix A).

In comparison to the n.m.r. spectrum of  $[AgL^1]ClO_4$ , proton signals for  $H^1$ ,  $H^2$  and  $H^4$  resonate at higher frequencies for  $[AgL^4]ClO_4$  which must be due to the deshielding effects of the conjugated  $\pi$ -system involving the phenylene ( $H^6-H^9$ ), imino ( $H^{11}$ ) and pyridyl protons ( $H^{13}-H^{14}$ ). However,  $H^1$  and  $H^2$  for  $[AgL^3]ClO_4$  are 0.1 p.p.m. downfield in relation to  $[AgL^4]ClO_4$ . This may be a reflection of weaker bonding interactions between silver(I) and the pyridyl nitrogen (between thioether donor atoms) in the latter complex, even though a stronger interaction may exist for silver(I) and the thioether donor atoms themselves (Table 4.3.1f). Unfortunately, the limited solubility of  $[AgL^4]ClO_4$  in  $d_3$ -acetonitrile, prevented adequate data from being collected in order to obtain a carbon-13 broad band proton decoupled spectrum.

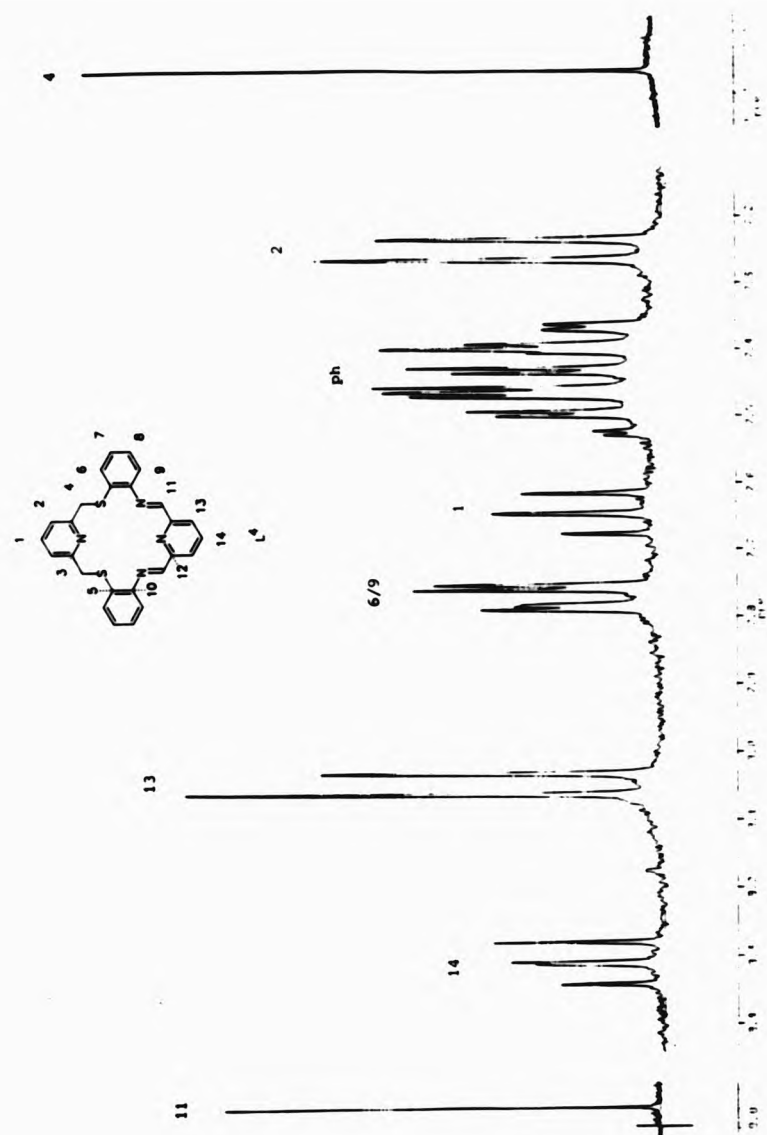


Figure 4.3.1c  $^1\text{H}$  n.m.r. spectrum of  $[\text{AgL}^4]\text{ClO}_4$  in  $\text{d}_3$ -acetonitrile.

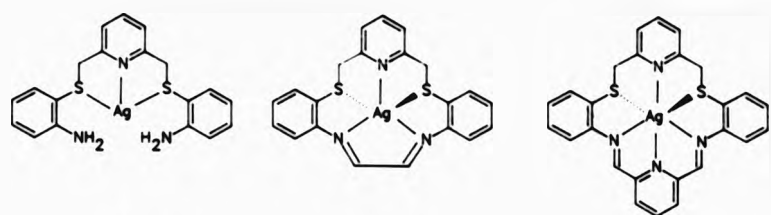
Table 4.3.1a  $^{13}\text{C}$  n.m.r. data<sup>a</sup> for  $[\text{PbL}^4(\text{H}_2\text{O})(\text{MeOH})][\text{ClO}_4]_2$  (62.896 Hz) and  $[\text{HgL}^4(\text{SCN})_2]\cdot\text{MeOH}$  (62.896 Hz) in  $\text{CD}_3\text{CN}^b$  at ambient temperature.

$[\text{PbL}^4(\text{H}_2\text{O})(\text{MeOH})][\text{ClO}_4]_2$		$[\text{HgL}^4(\text{SCN})_2]\cdot\text{MeOH}$	
164.46	$\text{C}^{11}$	158.39	$\text{C}^{11}$
161.98	$\text{C}^c$		
157.22	$\text{C}^{12}$	156.64	$\text{C}^{12}$
153.97	$\text{C}^3$	151.01	$\text{C}^3$
149.76	$\text{C}^{10}$	148.18	$\text{C}^{10}$
143.54	$\text{C}^{14}$	142.15	$\text{C}^{14}$
140.46	$\text{C}^1$	139.59	$\text{C}^1$
133.60	$\text{C}^{13}$	133.59	ph
133.08	ph	133.40	$\text{C}^5$
132.83	$\text{C}^5$	132.25	$\text{C}^{13}$
131.20	$\text{C}^2$	130.13	$\text{C}^2$
130.68	ph	130.05	ph
		126.70	$\text{C}^d$
124.85	ph	124.13	ph
121.94	ph	121.48	ph
42.86	$\text{C}^{11}$	43.75	$\text{C}^{11}$

<sup>a</sup>In p.p.m., relative to  $\text{SiMe}_4$ . <sup>b</sup> $[\text{AgL}^4]\text{ClO}_4$  too insoluble to obtain  $^{13}\text{C}$  n.m.r. <sup>c</sup>Origin unknown. <sup>d</sup>-S-C≡N signal.

According to n.m.r. studies of  $[\text{ML}^4]^m$ , there appear to be differences in the bonding mode of the silver(I) complex in comparison to the lead(II) and mercury(II) solution structures.

Table 4.3.1f Selected proton n.m.r. data for  $[\text{AgL}^1]\text{ClO}_4$ ,  $[\text{AgL}^3]\text{ClO}_4$  and  $[\text{AgL}^4]\text{ClO}_4$ .



$[\text{AgL}^1]\text{ClO}_4$	$[\text{AgL}^3]\text{ClO}_4$	$[\text{AgL}^4]\text{ClO}_4$
$\delta/\text{p.p.m.}$	$\delta/\text{p.p.m.}$	$\delta/\text{p.p.m.}$
H <sup>11</sup>	-	8.49
H <sup>1</sup>	7.52	7.75
H <sup>2</sup>	7.02	7.35
H <sup>4</sup>	4.16	4.27
		4.35

Crystal structure determinations were performed on the complexes  $[\text{PbL}^4(\text{H}_2\text{O})(\text{MeOH})]\text{[ClO}_4]_2$  and  $[\text{HgL}^4(\text{SCN})_2]\cdot\text{MeOH}$  in order to deduce solid state conformations of the macrocyclic ligand towards these metal ions.

#### 4.3.2 Single-Crystal X-ray Structure of $[\text{PbL}^4(\text{H}_2\text{O})(\text{MeOH})]\text{[ClO}_4]_2$ .

A full single-crystal X-ray structure (Figure 4.3.2a) of  $[\text{PbL}^4(\text{H}_2\text{O})(\text{MeOH})]\text{[ClO}_4]_2$  shows that the lead(II) atom is co-ordinated to three of the four available nitrogen donors N(1c), N(2a) and N(2b), and to both sulphur donors S(1a) and S(1b), with one molecule of water O(w) and one molecule of methanol O(m) completing the co-ordination sphere. The bond lengths for Pb-N(1c), Pb-N(2a) and Pb-N(2b) are 2.567(11), 2.695(11) and 2.690(11) Å respectively, which are typical metal-nitrogen bond distances found in macrocyclic ligands containing

the trimethine unit.<sup>(14)-(21)</sup> The fourth nitrogen donor, N(3c) is not co-ordinated to the lead(II) atom, the Pb-N(3c) interatomic distance being 3.25 Å. In comparison, the bond distances Pb-S(1a) and Pb-S(1b) are 3.145(4) and 3.193(10) Å respectively, and although they are rather long, they still represent considerable bonding interaction because the bond lengths are within the sum (3.82 Å) of the estimated van der Waals radii. The 'soft' character of both the lead(II) atom and the sulphur donor atoms indicates that some interaction is likely to be present between them (Table 4.3.2a). The closest approach for an oxygen atom of a perchlorate molecule to the metal centre is 3.03 Å.

It can be seen that, to a first approximation, the lead(II) atom may be described as having a very distorted *nido*-hexagonal bipyramidal co-ordination geometry. The two axial sites are occupied by a water molecule [Pb-O(w) 2.512(10) Å] and a methanol oxygen atom [Pb-O(m) 2.751(10) Å]. Five of the equatorial positions are occupied by the macrocycle donor atoms - N(1c), N(2a), N(2b), S(1a), S(1b), and the vacant sixth equatorial site is between the two sulphur donor atoms [S(1a)-Pb-S(1b) 107.0(1) °]. The distortions from a regular *nido*-hexagonal bipyramidal arrangement can be seen in the 'side-on' view (Figure 4.3.2b).

The lead(II) atom is asymmetrically positioned in the macrocyclic cavity, lying closer to, and in the same plane as, the imino nitrogens N(2a) and N(2b) and the pyridyl nitrogen N(1c). The lead(II) atom is -0.69 Å below the mean plane defined by the atom N(1c), N(2a), N(2b), S(1a) and S(1b). Due to their pyramidal bonding geometry the sulphur atoms are forced below the plane of nitrogens containing the lead(II) atom, distorting the macrocycle. The position of the sulphur donors

forces the phenylene rings to be 'tilted upwards', and gives the appearance of 'pulling' the N(3c) donor containing pyridine ring towards the metal centre, effectively bringing themselves closer to the lead(II) atom, to allow co-ordination to take place.

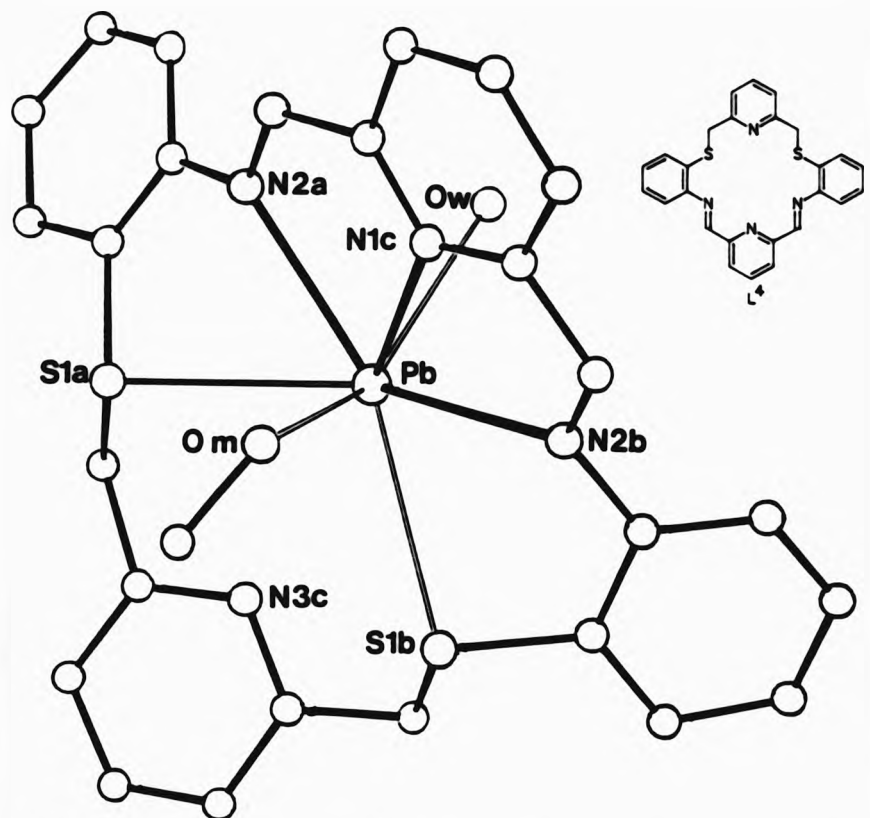


Figure 4.3.2a Single-Crystal X-ray structure of  $[PbL(H_2O)(MeOH)][ClO_4]_2$ .

One feature of the lead(II) atom is of particular interest - the 'inert pair' effect, which is due to a pair of non-bonding electrons. In the stereochemical sense they may be active or inactive.

Table 4.3.2a Selected co-ordination sphere bond distances and angles for  $[PbL^4(H_2O)(MeOH)][ClO_4]_2$ .

Bond distances ( $\text{\AA}$ )		Bond angles ( $^\circ$ )	
Pb - N(1c)	2.567(11)	N(1c) - Pb - N(2a)	63.9(3)
Pb - N(2a)	2.695(11)	N(1c) - Pb - N(2b)	62.1(3)
Pb - N(2b)	2.690(11)	N(2a) - Pb - S(1a)	59.2(3)
Pb - S(1a)	3.145(4)	N(2b) - Pb - S(1b)	58.6(2)
Pb - S(1b)	3.193(10)	S(1a) - Pb - S(1b)	107.0(1)
Pb - O(W)	2.512(10)	O(W) - Pb - O(M)	142.1(3)
Pb - O(M)	2.751(10)	O(M) - Pb - N(1c)	73.3(3)
Pb - N(3c)	....3.25		

For  $[PbL^4(H_2O)(MeOH)][ClO_4]_2$ , a consequence of the stereochemically active lone pair becomes apparent as the co-ordinating water and methanol molecules are bent [ $O(W)-Pb-O(M)$  142.1(3)  $^\circ$ ] away from the non-co-ordinating pyridyl nitrogen and thioether sulphur atoms, towards the imine-half of the macrocycle. Thus, a vacant area exists about the lead(II) atom which is represented in the space filling diagram (Figure 4.3.2c).

A number of structurally characterised eighteen-membered, lead(II) macrocyclic ligand complexes have been published (Figure 4.3.2d).

Ligand (1)<sup>[14]</sup> providing an  $N_6$  donor set, containing four  $sp^2$  imino nitrogens and two  $sp^2$  pyridyl nitrogens, has quite a different structure compared to  $[PbL^4(H_2O)(MeOH)][ClO_4]_2$ . The lead(II) atom is co-ordinated to all six available nitrogen donors and sits close to the

centre of the macrocyclic ring just below the plane of best fit, almost equidistant from all six donor atoms. Its co-ordination geometry is best described as a distorted hexagonal pyramid. On this occasion the stereochemically active lone pair on the lead(II) atom appears to prevent the close approach of a perchlorate counterion which consequently becomes disordered [closest approach Pb....O(ClO<sub>4</sub>) 2.83(3) Å].

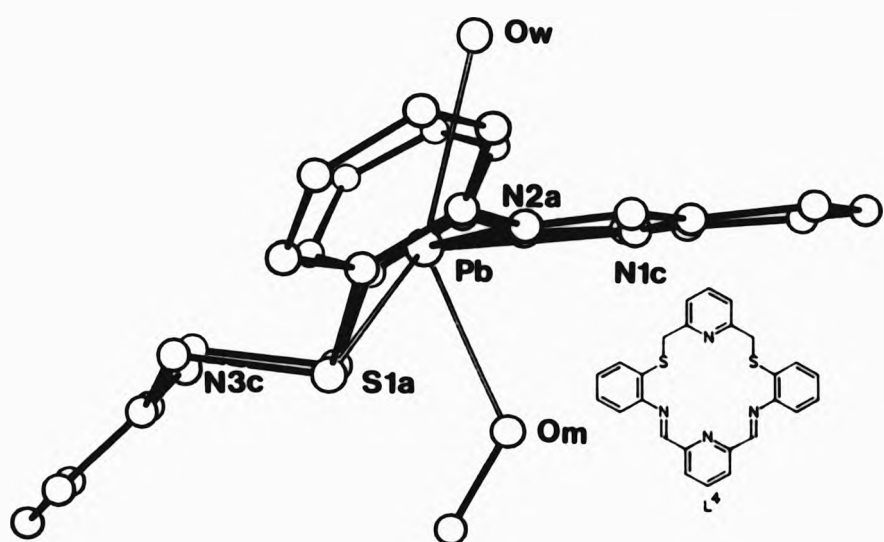


Figure 4.3.2b Single-crystal X-ray structure of [PbL<sup>4</sup>(H<sub>2</sub>O)(MeOH)][ClO<sub>4</sub>]<sub>2</sub>.

The differences in the metal-ion geometry and ligand conformation between  $[\text{PbL}^4(\text{H}_2\text{O})(\text{MeOH})][\text{ClO}_4]_2$  and  $[\text{Pb(l)}(\text{H}_2\text{O})][\text{ClO}_4]_2$  are two-fold. Firstly, the exchange of two imino nitrogen donors for two thioether donors gives increased flexibility to the macrocycle, which is permitted since there is a break in conjugation. Secondly, replacement of a smaller donor atom by a larger one does not necessarily strain the ligand framework if the number of members of the inner great ring are kept constant. This is because although the larger donor size will cause slight ring-expansion due to increase in bond length, the lead(II) atom will not have a larger cavity size available to it due to the additional volume required by the donor. In addition, the preferred geometry of the individual donor atoms, from trigonal ( $-\text{N}=$ ) to pyramidal ( $-\text{S}-$ ) i.e  $\text{sp}^2$  to  $\text{sp}^3$  will also be displayed.

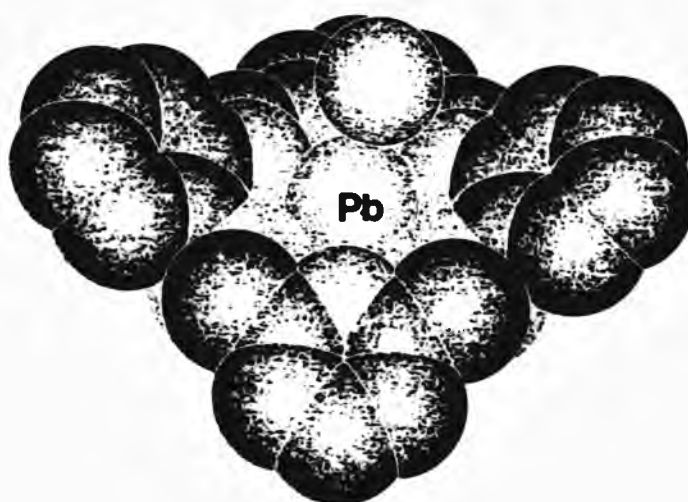
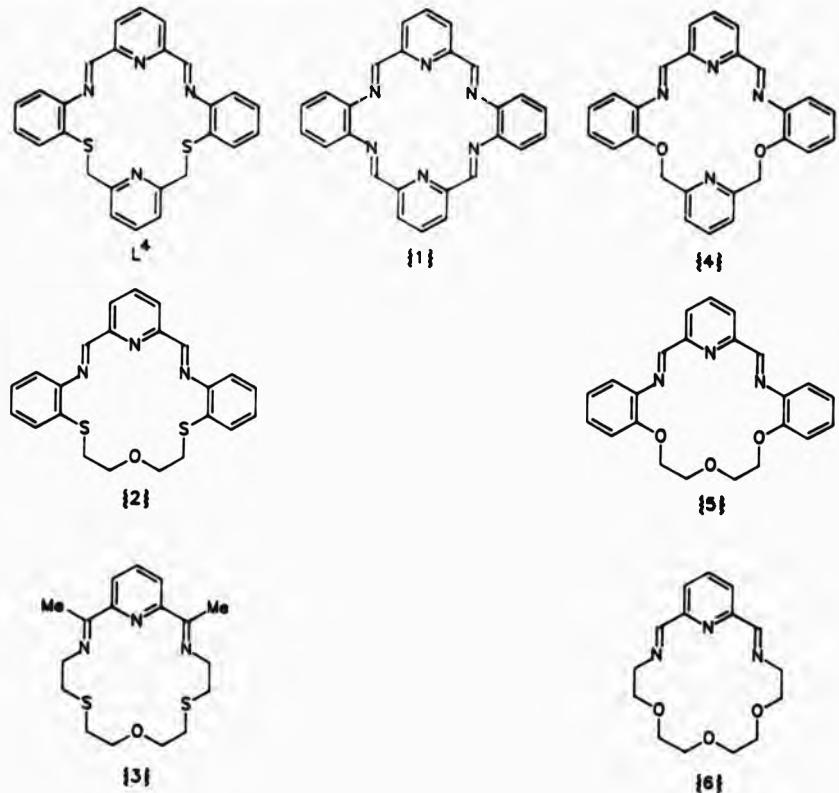


Figure 4.3.2c Space filling representation of  $[\text{PbL}^4(\text{H}_2\text{O})(\text{MeOH})][\text{ClO}_4]_2$ .

For  $[\text{Pb}\{2\}(\text{NO}_3)_2] \cdot \text{H}_2\text{O}$ ,<sup>[15]</sup> where the ligand has an  $\text{N}_3\text{S}_2\text{O}$  donor set, the lead(II) atom is co-ordinated to all three nitrogens and both the sulphurs leaving the oxygen unco-ordinated. The co-ordination sphere is completed by two nitrate ions co-ordinated in a bidentate fashion. The lead(II) atom sits in the same plane as the nitrogen donors, with one sulphur atom above and one below the mean plane. The lead(II)-sulphur distances are also long ( $\text{Pb-S}(1a)$  3.079(2) and  $\text{Pb-S}(1b)$  3.167(2) Å) but comparable to those of  $[\text{PbL}^4(\text{H}_2\text{O})(\text{MeOH})][\text{ClO}_4]_2$ . One of the main differences between  $[\text{PbL}^4(\text{H}_2\text{O})(\text{MeOH})][\text{ClO}_4]_2$  and  $[\text{Pb}\{2\}(\text{NO}_3)_2] \cdot \text{H}_2\text{O}$  is the position of the phenylene rings. In the former, both are *syn* above the mean donor plane. Whereas, in the latter the phenylene rings are in an *anti* position, one above and one below the donor plane. This *anti* arrangement of the phenylene rings is possible because of the increased flexibility available from the diethoxy ether linkage, unlike the pyridyl unit present in  $[\text{PbL}^4(\text{H}_2\text{O})(\text{MeOH})][\text{ClO}_4]_2$  and  $[\text{Pb}\{1\}(\text{H}_2\text{O})][\text{ClO}_4]_2$ .

Given a ligand with even more flexibility for the same donor set  $\text{N}_3\text{S}_2\text{O}$ ,  $[\text{Pb}\{3\}(\text{H}_2\text{O})(\text{ClO}_4)][\text{ClO}_4]$ <sup>[16]</sup> shows the lead(II) atom co-ordinated to all six available donor atoms. In addition, a co-ordinated water and perchlorate molecule complete the co-ordination sphere. Once again, the lead(II) atom sits in the same plane as the nitrogen donors, with both sulphur donors just below it. Here too, the Pb-S distances ( $\text{Pb-S}$  3.21 and 3.41 Å) are of the same order as in  $[\text{PbL}^4(\text{H}_2\text{O})(\text{MeOH})][\text{ClO}_4]_2$  and  $[\text{Pb}\{2\}(\text{NO}_3)_2] \cdot \text{H}_2\text{O}$ .



**Figure 4.3.2d** Comparable ligands for structurally characterised lead(II) complexes.

Unfortunately, the lead complex of ligand {4}<sup>(17)</sup> with an N<sub>4</sub>O<sub>2</sub> donor set analogous to [PbL<sup>4</sup>(H<sub>2</sub>O)(MeOH)][ClO<sub>4</sub>]<sub>2</sub> has not been structurally determined. Though, one would not expect the structure to be as planar as that of [Pb{1}(H<sub>2</sub>O)][ClO<sub>4</sub>]<sub>2</sub> since the ligand is not fully conjugated, nor as distorted as [PbL<sup>4</sup>(H<sub>2</sub>O)(MeOH)][ClO<sub>4</sub>]<sub>2</sub> because oxygen tends to have a planar geometry as opposed to the pyramidal arrangement preferred by sulphur. For example, the lead(II) complex of ligand

{5}<sup>[18]</sup> which has an N<sub>3</sub>O<sub>3</sub> donor set is far more planar, with both phenylene rings on the same side of the mean donor plane. This contrasts with the crystal structure of [Pb{2}(NO<sub>3</sub>)<sub>2</sub>]H<sub>2</sub>O which has the same ligand framework but an N<sub>3</sub>S<sub>2</sub>O donor set as already mentioned.

Finally, for the [Pb{6}(SCN)<sub>2</sub>] complex where {6}<sup>[19]</sup> also has an N<sub>3</sub>O<sub>3</sub> donor set similar to {5}, the lead(II) atom is co-ordinated to all six macrocycle donor atoms non-centrosymmetrically towards the trimethine unit. Additionally, the co-ordination sphere is completed by thiocyanate ions exhibiting linkage isomerism. Furthermore, the N-bonded ion interacts via the sulphur atom with a neighbouring [Pb{6}(SCN)<sub>2</sub>] molecule to give loosely held dimers.

It is also probable that all the lead(II) complexes of L<sup>4</sup> that were isolated have a similar co-ordination geometry about the metal ion.

#### 4.3.3 Single-Crystal X-ray Structure of [HgL<sup>4</sup>(SCN)<sub>2</sub>].MeOH.

A full single-crystal X-ray structure of [HgL<sup>4</sup>(SCN)<sub>2</sub>].MeOH revealed a similar structure to that of [PbL<sup>4</sup>(H<sub>2</sub>O)(MeOH)][ClO<sub>4</sub>]<sub>2</sub>. The mercury(II) atom is co-ordinated to three of the four available nitrogen donors, N(1c), N(2a) and N(2b), and to both sulphur donor atoms S(1a) and S(1b). However, this time the co-ordination sphere is completed by two thiocyanate molecules. The mercury(II) atom is seven co-ordinate (Figure 4.3.3a).

Here too, the mercury(II) atom is asymmetrically placed in the macrocyclic cavity, lying closer to the imine nitrogens [Hg-N(2a) 2.713(9) Å and Hg-N(2b) 2.737(9) Å], and the pyridyl nitrogen [Hg-N(1c) 2.558(9) Å]. The bond distances Hg-S(1a) and Hg-S(1b) are

3.094(3) and 3.164(3) Å respectively. Whereas, the bond distances to the sulphur atoms of the thiocyanate molecules are Hg-S(2a) 2.491(3) Å and Hg-S(2b) 2.438(3) Å (Table 4.3.3a).

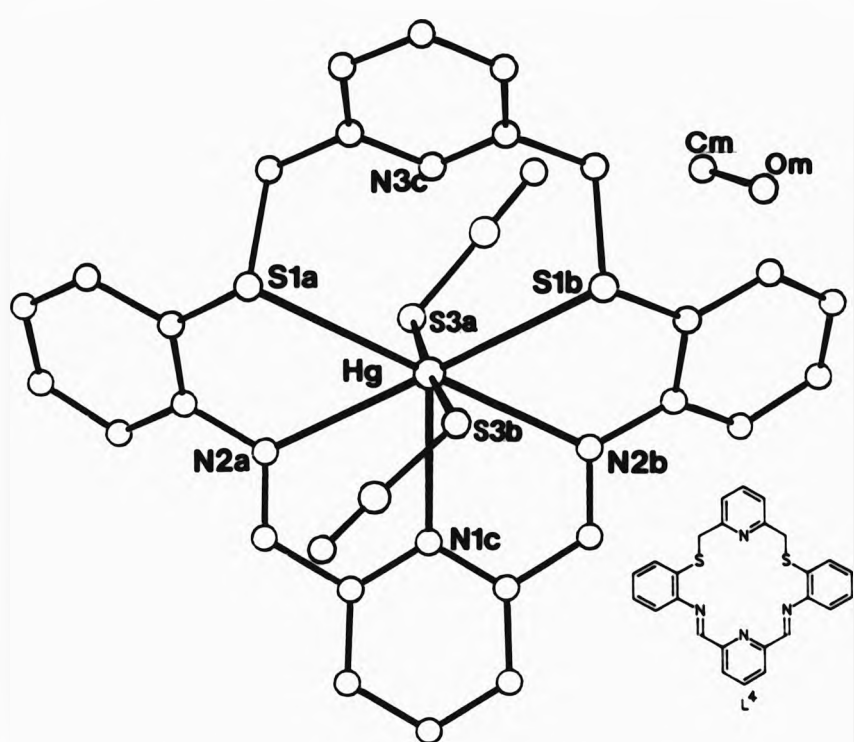


Figure 4.3.3a Single-crystal X-ray structure of  $[\text{HgL}^4(\text{SCN})_2] \cdot \text{MeOH}$ .

The geometry around the mercury(II) atom is also *nido*-hexagonal bipyramidal. The five equatorial positions are occupied by the macrocycle donor atoms - N(1c), N(2a), N(2b), S(1a) and S(1b), with both axial sites being occupied by thiocyanate molecules (Figure 4.3.3b).

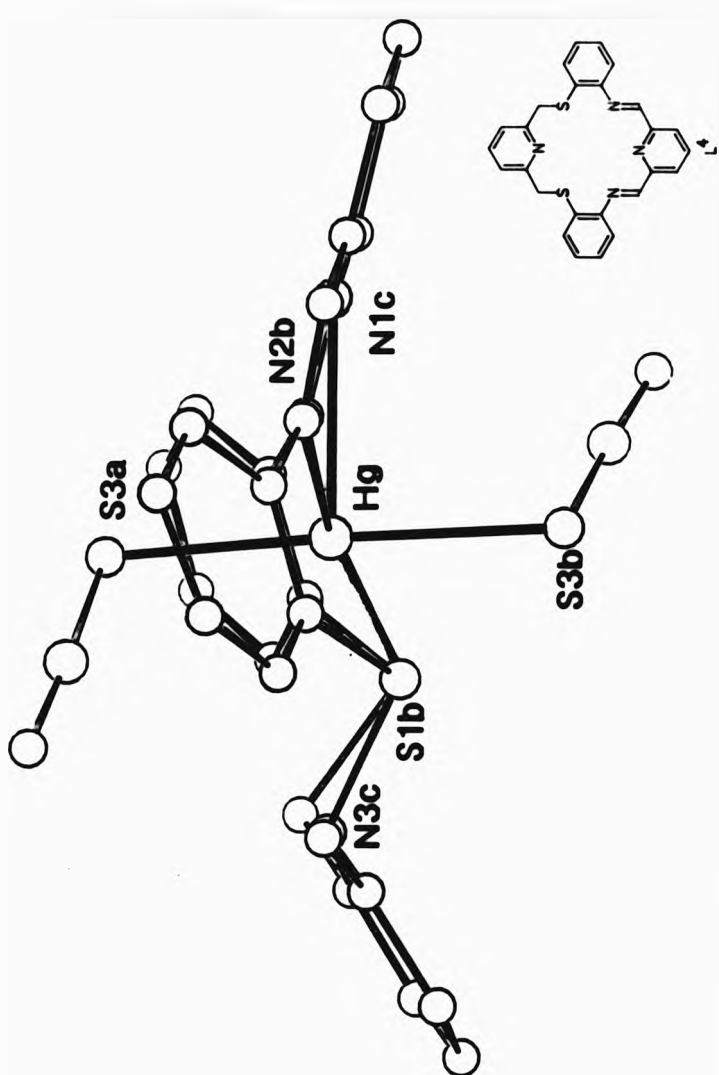


Figure 4.3.3b Single-crystal X-ray structure of  $[\text{HgL}^4(\text{SCN})_2] \cdot \text{MeOH}$ .

**Table 4.3.3a Selected co-ordination sphere bond distances and angles for  $\text{[HgL}^4(\text{SCN})_2\text{]}\cdot\text{MeOH}$ .**

Bond distances ( $\text{\AA}$ )		Bond angles ( $^\circ$ )	
Hg - N(1c)	2.558(9)	N(1c) - Hg - N(2a)	63.5(3)
Hg - N(2a)	2.713(9)	N(1c) - Hg - N(2b)	62.5(3)
Hg - N(2b)	2.737(9)	N(2a) - Hg - S(1a)	60.5(2)
Hg - S(1a)	3.094(3)	N(2b) - Hg - S(1b)	60.3(2)
Hg - S(1b)	3.164(3)	S(1a) - Hg - S(1b)	114.7(1)
Hg - S(2a)	2.491(3)	S(2a) - Hg - S(2b)	175.9(1)
Hg - S(2b)	2.438(3)		

The axial thiocyanate ligands are near vertical [ $S(2a)\text{-Hg-S}(2b)$   $175.9(1)^\circ$ ] and almost perpendicular to the trimethine head unit [ $S(2a)\text{-Hg-N}(1c)$   $86.4(2)^\circ$ ]. Linearity of the  $S(2a)\text{-Hg-S}(2b)$  bond contrasts with the bent  $O(w)\text{-Pb-O}(m)$  bond present in  $[\text{PbL}^4(\text{H}_2\text{O})(\text{MeOH})]\text{[ClO}_4\text{]}_2$ . In fact, the mercury(II) atom is totally engulfed by the macrocycle donors in the equatorial plane and by the thiocyanates axially (Figure 4.3.3c). In contrast to the lead(II) complex, the mercury(II) atom is not coplanar with the delocalised  $\pi$ -system and sits below the mean donor [N(1c), N(1a), N(1b)] plane with bent bonds to the trimethine head unit. The mercury(II) atom is  $-0.27 \text{ \AA}$  below the mean plane defined by the atoms N(1c), N(2a), N(2b), S(1a) and S(1b).

There is also a methanol solvate present in the unit cell which has no intermolecular associations with the macrocyclic cation. The 'face-on'

view (Figure 4.3.3a) of  $[\text{HgL}^4(\text{SCN})_2]\cdot\text{MeOH}$  shows that each thiocyanate is S-bonded as indicated by the infrared vibrational frequency.

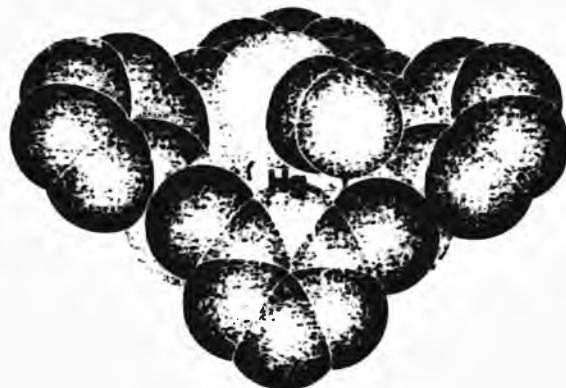


Figure 4.3.3c Space filling representation of  $[\text{HgL}^4(\text{SCN})_2]\cdot\text{MeOH}$ .

A very limited number of crystal structures have been determined for mercury(II) complexes of macrocyclic ligands (Figure 4.3.3d).

The seventeen-membered  $\text{N}_5$  donor ligand (7),<sup>[22]</sup> assumes a distorted pentagonal pyramidal geometry about the mercury(II) atom. The metal-ion is co-ordinated to all five macrocycle donor atoms with an axial bromide completing the co-ordination sphere. Mercury(II)-nitrogen distances are shorter [2.25(5)-2.44(5) Å] than those found in  $[\text{HgL}^4(\text{SCN})_2]\cdot\text{MeOH}$ . Although there are no intermolecular contacts, the unit cell consists of two equivalent cations,  $[\text{Hg}(7)(\text{Br})]^+$  and one centrosymmetric anion  $[\text{Hg}_2\text{Br}_6]^{2-}$ . In addition, the pyridine nitrogen is displaced below the mean donor plane and the metal atom rests above this plane towards the bromide ion.

For the analogous sixteen-membered  $\text{N}_5$  ligand (8),<sup>[23]</sup> the mercury(II) complex was found to be isomorphous with the cadmium(II) complex. The

existence of a seven co-ordinate polymeric cation  $(\text{Hg(8Br)}_n)^{m+}$  with bridging bromide ions has been deduced. Two bridging bromide ions of different distances between the closely planar macrocyclic girdles are presumably a consequence of the metal ion being too large for the macrocyclic cavity.

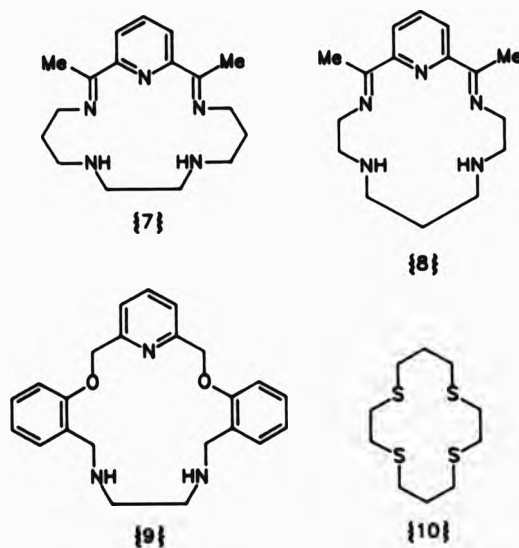


Figure 4.3.3d Comparable ligands for structurally characterised mercury(II) complexes.

A seventeen-membered  $\text{N}_3\text{O}_2$  macrocyclic ligand (9),<sup>[24]</sup> has been found to co-ordinate exocyclically to mercury(II) via the secondary amine nitrogens with the tetrahedral co-ordination sphere being completed by two iodide ions.

The interaction of mercury(II) and a fourteen-membered  $\text{S}_4$  macrocyclic ligand (10)<sup>[25]</sup> has previously been discussed in relation to the

$\{\text{HgL}^1(\text{Cl})_2\}$  complex (section 2.4.2).

Surprisingly, the solution and solid state structures for both the lead(II) and mercury(II) complexes of  $\text{L}^4$  were found to be similar. In the presence of sulphur donor atoms, mercury(II) is expected to interact more strongly with these ligators rather than the trimethine nitrogen head unit. When  $\text{Hg}(\text{NO}_3)_2$  was employed in the template synthesis, no reaction was observed. This may be due to the incompatibility of the harder donor atoms of the nitrate ions and the water and methanol molecules available in solution that are required for axial ligation on complexation.

Non-co-ordination of lead(II) or mercury(II) to N(3c) may be attributed to different reasons. For lead(II), the lone pair is found to be stereochemically active. In the case of mercury(II), a combination of its slightly smaller size [ $r_{\text{Pb}(II)} = 1.19$ ;  $r_{\text{Mg}(II)} = 1.02 \text{ \AA}$  (hexa-co-ordinate)] and long M-S(thioether) contacts which cannot distort due to macrocyclic constraints will hold N(3c) (with inherent rigidity of pyridyl ring) further away.

#### 4.4 Co-ordination Studies of $[\text{CdL}^4]^{2+}$ and $[\text{ZnL}^4]^{2+}$ .

Complexation reactions of  $\text{L}^4$  with cadmium(II) and zinc(II) salts have led to the isolation of macrocyclic, open-chain and rearrangement products depending on the type of counterion present in solution during the metal-ion template syntheses of  $[\text{ML}^4]^{2+}$ .

##### 4.4.1 Spectroscopic Studies of $[\text{CdL}^4]^{2+}$ and $[\text{ZnL}^4]^{2+}$ .

###### 4.4.1.1 Infrared studies.

The infrared spectra (Table 4.4.1a) of the cadmium(II) and zinc(II)

complexes all show the expected vibrational frequency between ca. 1630-1620 cm<sup>-1</sup> attributable to stretching  $\nu(C=N)$  bands. Aromatic  $\nu(C=C)$  and  $\nu(C=N)$  absorbances were found in the range ca. 1590-1565 cm<sup>-1</sup> assignable to the pyridine and/or benzene rings. Counterion co-ordination is much the same in both sets of compounds. The perchlorate<sup>[11]</sup> and nitrate<sup>[12]</sup> anions in each complex are suggested to be equivalent and ionic. The thiocyanate complex of cadmium(II) [CdL<sup>4</sup>(NCS)<sub>2</sub>], gives rise to a strong, unsplit absorbance at ca. 2070 cm<sup>-1</sup> which may signify *trans*-N-bonded thiocyanate co-ordination to the metal centre (section 4.3.1.1).<sup>[7]</sup> Additionally, for the perchlorate complex of cadmium(II) [CdL<sup>40</sup>][ClO<sub>4</sub>]<sub>2</sub>, a strong, sharp band at ca. 1700 cm<sup>-1</sup> was also observed. It is apparent that reactant [ $\nu(C=O)$  of 2,6-diformylpyridine] impurities are still present in the isolated complex. However, there are no bands between ca. 3500-3300 cm<sup>-1</sup> to indicate the presence of  $\nu(N-H)$  stretching vibrations possibly due to any unused reactant, L<sup>1</sup>. Lack of amine in the spectrum precludes the likelihood of a ring-opened hydrolysis product, since both carbonyl and amine bands would be observed in the infrared.<sup>[26]</sup>

Table 4.4.1a Infrared data<sup>a</sup> for [CdL<sup>4</sup>]<sup>2+</sup> and [ZnL<sup>4</sup>]<sup>2+</sup> complexes.

COMPLEX	COLOUR	$\nu(C=N)$	$\nu(py/Bz)$	$\nu(counterion)$
[CdL <sup>40</sup> ][ClO <sub>4</sub> ] <sub>2</sub> <sup>c</sup>	YELLOW	1630s	1590s	1090s 620s
[CdL <sup>4</sup> ][NO <sub>3</sub> ] <sub>2</sub> ·CH <sub>3</sub> CN	"	1630s	1590s	1390s
[CdL <sup>4</sup> (NCS) <sub>2</sub> ]	"	1620w	1580m	2070s
[ZnL <sup>4</sup> ][ClO <sub>4</sub> ] <sub>2</sub>	"	1635m	1600s	1100s 615s
[ZnL <sup>4</sup> ][NO <sub>3</sub> ] <sub>2</sub> ·CH <sub>3</sub> CN	"	1640m	1590m	1385s

<sup>a</sup>In cm<sup>-1</sup>, as KBr disc. <sup>b</sup>ca. 1700 cm<sup>-1</sup> also present for this complex.

Elemental analyses (section 7.4.4-5) give formulations corresponding to (1+1) cyclocondensations, with a metal to ligand ratio of 1:1. Additionally, both nitrate complexes have an acetonitrile molecule associated within their crystal lattice.

#### 4.4.1.2 Fast atom bombardment mass spectrometry.

F.a.b. mass spectral data (Table 4.4.1b) obtained for five of the complexes gave the highest mass peaks corresponding to  $[ML]^4X^+$  ( $X$  = counterion) with the exception of  $[CdL]^{40}[\text{ClO}_4]_2$ . In this instance, the highest mass peak observed appeared to be one molecule of 2,6-diformylpyridine higher than anticipated. Presence of the dicarbonyl could also account for the strong, sharp absorbance at ca.  $1700 \text{ cm}^{-1}$  in the infrared spectrum of the cadmium(II) perchlorate complex (section 4.4.1.1). The two structural modes of co-ordination environment possible for this type of complex can either be acyclic (1) or macrocyclic (2) (Figure 4.4.1a).

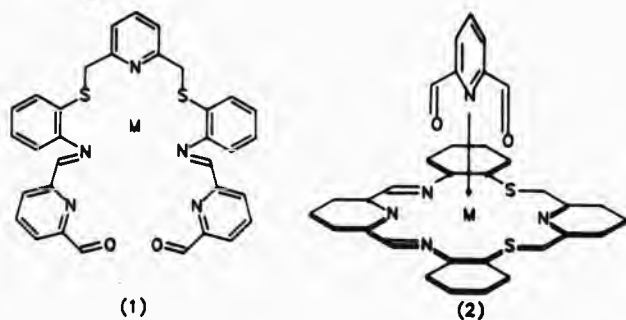


Figure 4.4.1a Structural modes for  $[CdL]^{40}[\text{ClO}_4]_2$ .

Mode (2) is not considered favourable since, the angular requirements of the terdentate nature of the 2,6-diformylpyridine unit may be hindered by the encircling macrocyclic ligand. Thus, mode (1) is a more promising suggestion. Significantly, the open-chain dicarbonyl

ligand  $L^{40}$ , exists only in the presence of the perchlorate counterion.

Table 4.4.1b Fast atom bombardment mass spectra<sup>a</sup> for  $[CdL^4]^{2+}$  and  $[ZnL^4]^{2+}$  complexes.

COMPLEX	FRAGMENTATION ASSIGNMENT	MASS <sup>b</sup>	RELATIVE
			PERCENTAGE
$(CdL^4)[ClO_4]_2$	$[CdL^{40}]ClO_4^+$	800	54
	$[CdL^4]^+$	700	28
	$[CdL^4]^+$	565	5
	$[L^1 + H^+]^+$	355	100
$(CdL^4)[NO_3]_2 \cdot CH_3CN$	$[CdL^4]NO_3^+$	628	100
	$[CdL^4]^+$	565	90
$(CdL^4(NCS))_2$	$[CdL^4]NCS^+$	624	96
	$[CdL^4]^+$	565	56
$(ZnL^4)[ClO_4]_2$	$[ZnL^4]ClO_4^+$	617	100
	$[ZnL^4]^+$	517	88

<sup>a</sup>In NOBA matrix. <sup>b</sup>Positive-ion mode.

While the existence of  $L^{40}$  is in accord with an increase in co-ordination number of the large cadmium(II) ion, solvent molecules e.g. water, acetonitrile (or methanol) are also present in solution and available for co-ordination. Consequently, for the other cadmium(II) complexes of  $L^4$ , thiocyanate bonding has already been established and the chloride ions are also thought to be co-ordinated to the metal centre. There is no intimation of nitrate co-ordination in the infrared spectrum, although the absorbance is broad and slightly structured.

#### 4.4.1.3 Nuclear magnetic resonance spectroscopy.

The complexes of  $[CdL^{40}][ClO_4]_2$  and  $[ZnL^4][ClO_4]_2$  were soluble enough for n.m.r. studies. However, analysis of the proton (Table 4.4.1c) and carbon-13 (Table 4.4.1e) spectra of the cadmium(II) product revealed solely the presence of  $[CdL^4][ClO_4]_2$  in solution and not of  $[CdL^{40}][ClO_4]_2$ .

The proton spectrum (Figure 4.4.1b) of  $[CdL^4][ClO_4]_2$  integrates for twenty protons. The most downfield singlet at  $\delta$  9.15 p.p.m. is attributed to the imino protons  $H^{11}$  (2 H, s,  $CH=N$ ). Additionally, satellites were observed on either side of this singlet which must be due to metal-proton couplings via the imino nitrogen [ $J(^{113}Cd-H^{11}) = 30.4$  Hz]. Intensity ratios are proportional to the natural abundances of  $^{113}Cd$  and  $^{111}Cd$  (Table 4.4.1d). For the corresponding eighteen-membered  $N_6$  analogue (1), a three-bond coupling constant = 22 Hz to the imine protons has been quoted in the  $^{113}Cd$  n.m.r.<sup>[27]</sup> There were no resonance signals downfield from the imine singlet corresponding to the presence of an aldehydic carbonyl ( $CH=O$ ) group. The methylene protons  $H^4$  (4 H, s,  $CH_2S$ ) were assigned to the most upfield signal in the spectrum ( $\delta$  4.36 p.p.m.).

Table 4.4.1d Isotopic abundances for cadmium(II); I = 1/2 nuclear spin.

	NATURAL ABUNDANCE (%)	INTENSITY RATIOS (%) OF SATELLITES	
		CALCULATED	OBSERVED
$^{113}Cd$	12.26		
$^{111}Cd$	12.75	6.26(AV)	5.60

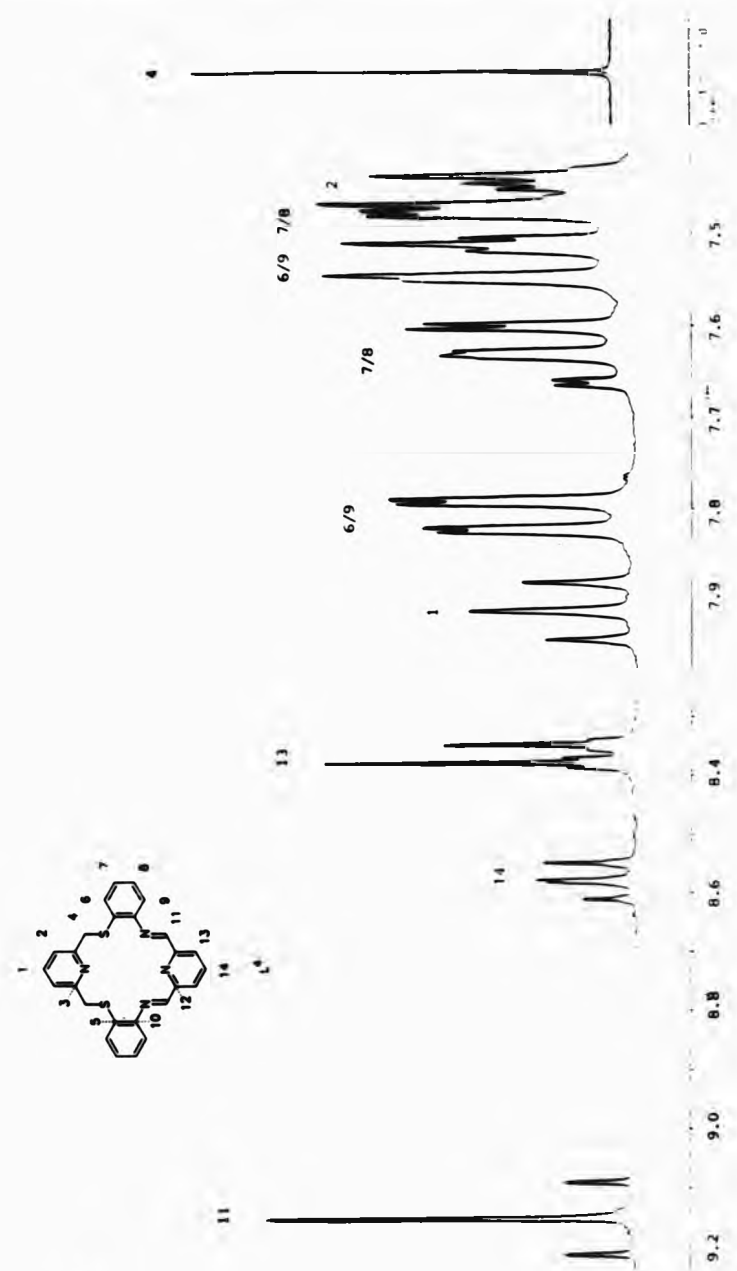
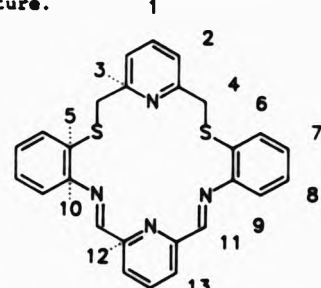


Figure 4.4.1b  $^1\text{H}$  n.m.r. spectrum of  $[\text{CdL}^4][\text{ClO}_4]_2$  in  $\text{d}_3$ -acetonitrile.

Table 4.4.1c  $^1\text{H}$  n.m.r. data<sup>a</sup> for  $[\text{CdL}^4](\text{ClO}_4)_2$  (250.134 MHz) in  $\text{CD}_3\text{CN}$  at ambient temperature.



	$\delta/\text{p.p.m.}$	$14$	$J/\text{Hz}$
9.15(s)	$\text{H}^{11}$		$^3J(\text{H}^{11}-\text{H}^{11}) = 30.4$
8.58(t) <sup>b</sup>	$\text{H}^{14}$		$^3J(\text{H}^{14}-\text{H}^{13}) = 7.7$
8.36(d) <sup>b</sup>	$\text{H}^{13}$		$^3J(\text{H}^{13}-\text{H}^{14}) = 7.7$
7.91(t)	$\text{H}^1$		$^3J(\text{H}^1-\text{H}^2) = 7.7$
7.81(dd) <sup>c</sup>	$\text{H}^{6/9}$		$^3J = 7.71; ^4J = 1.3$
7.63(td) <sup>c</sup>	$\text{H}^{7/8}$		$^3J = 7.65; ^4J = 1.3$
7.53(dd) <sup>c</sup>	$\text{H}^{6/9}$		$^3J = 8.63; ^4J = 2.0$
7.48(td) <sup>c</sup>	$\text{H}^{7/8}$		$^3J = 7.42; ^4J = 1.5$
7.45(d)	$\text{H}^2$		$^3J(\text{H}^2-\text{H}^1) = 8.0$
4.36(s)	$\text{H}^4$		

<sup>a</sup>Relative to  $\text{SiMe}_4$ . <sup>b</sup>Assigned as  $\text{AB}_2$  spin system. <sup>c</sup>Cannot assign protons.

The pyridyl protons  $\text{H}^{14}$  ( $\delta$  8.58 p.p.m.) and  $\text{H}^{13}$  ( $\delta$  8.36 p.p.m.) are assigned as an  $\text{AB}_2$  spin system (Appendix A). In addition, the doublet of  $\text{H}^{13}$  also possesses satellites presumably through four-bond coupling via metal-pyridine co-ordination [ $^4J(\text{H}^{13}-\text{Cd}) = 4.1$  and 3.8 Hz]. Five-bond coupling via metal-imine co-ordination may also contribute to the presence of these satellites. The pyridyl protons  $\text{H}^1$

( $\delta$  7.91 p.p.m.) and H<sup>2</sup> ( $\delta$  7.45 p.p.m.) show characteristic first-order splittings - a triplet and doublet respectively. No extra aromatic protons to account for the additional molecule of 2,6-diformylpyridine were present in the spectrum.

The remaining aromatic protons H<sup>6</sup>-H<sup>9</sup>, although fairly well resolved into doublet of doublets and triplet of doublets, could not be assigned with absolute certainty. Application of the calculated imine-induced shift parameters (cf.  $[\text{AgL}^3\text{ClO}_4]$  - section 3.4.1.3) for substituted benzene rings, predict the following resonances for the phenylene protons H<sup>6</sup>-H<sup>9</sup>:

	$\delta_c$		$\delta_o$
H <sup>6</sup>	7.77(dd)	H <sup>6</sup>	7.81(dd)
H <sup>7</sup>	7.50(td)	H <sup>7</sup>	7.63(td)
H <sup>8</sup>	7.35(td)	H <sup>9</sup>	7.53(dd)
H <sup>9</sup>	7.10(dd)	H <sup>8</sup>	7.48(td)

The signals observed in the cadmium(II) complex have been tentatively assigned, and they do not follow the same order as the calculated shifts (H<sup>8</sup> and H<sup>9</sup> are reversed). The reasons for this are two-fold. Firstly, the predicted shifts ( $\delta_c$ ), are those you would expect for the free ligand spectrum. Secondly, the observed shifts ( $\delta_o$ ) resonate at higher frequencies which is due to either solvent dependence or metal co-ordination.

The carbon-13 spectrum (Table 4.4.1e) was assigned on the basis of <sup>1</sup>H, <sup>13</sup>C-COSY and DEPT 45 spectra. Additionally, several carbon signals also display satellites arising from <sup>113</sup>Cd - <sup>13</sup>C couplings.

Observations of these couplings has aided in the elucidation of the co-ordination environment around the metal atom. For instance, two-bond couplings to C<sup>10</sup>, C<sup>11</sup> and C<sup>12</sup>, and a three-bond coupling to C<sup>13</sup> is evidence for cadmium(II) co-ordination towards the donor atoms of the trimethine head unit. Also noteworthy, is the two- or three-bond coupling to C<sup>3</sup> and three-bond coupling to C<sup>2</sup> which strongly suggest that cadmium(II) co-ordination to the pyridyl ring between the thioether donor atoms may be present. Whether the metal atom is also co-ordinated to the thioether donor atoms is debatable. Models indicate that due to its smaller ionic radius ( $r_{Cd(II)} = 0.95 \text{ \AA}$  (hexa-co-ordinate)) compared to lead(II), silver(I) and mercury(II) ( $r_{Pb(II)} = 1.19$ ;  $r_{Ag(I)} = 1.15$ ;  $r_{Hg(II)} = 1.02 \text{ \AA}$  (hexa-co-ordinate)) it may not be possible for cadmium(II) to be co-ordinated to both pyridyl nitrogens at the same time, unless the thioether donor atoms are extruded from the macrocyclic cavity effectively bringing the four nitrogen donor atoms into close proximity.

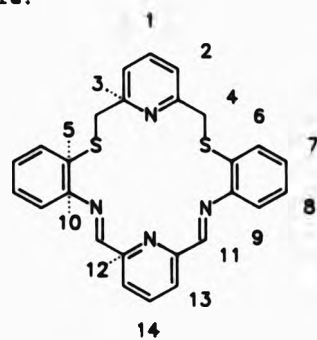
A quarter of cadmium nuclei have spin I = 1/2, arising from two isotopes <sup>113</sup>Cd and <sup>111</sup>Cd of roughly equal abundance. Generally, couplings due to both nuclei may not be resolved and although slightly less in abundance, <sup>113</sup>Cd will give rise to larger coupling constants.

Thus, in the solid state, through infrared and f.a.b. mass spectrometry, the presence of an open-chain ligand L<sup>60</sup> containing cadmium(II) has been suggested. Conversely in solution, n.m.r. studies have confirmed the existence of the macrocyclic complex [CdL<sup>6</sup>][ClO<sub>4</sub>]<sub>2</sub>.

Very few nitrogen-sulphur mixed donor complexes of cadmium(II) are known and in the majority of cases the ligands are

non-macrocyclic (Figure 4.4.1c).

Table 4.4.1e  $^{13}\text{C}$  n.m.r. data<sup>a</sup> for  $[\text{CdL}^4](\text{ClO}_4)_2$  (62.906 Hz) in  $\text{CD}_3\text{CN}$  at ambient temperature.



$\delta/\text{p.p.m.}$		$J/\text{Hz}$
160.64	$\text{C}^{11}$	$^2J(^{113}\text{Cd}-\text{C}^{11})$ = 16.2
155.54	$\text{C}^{12}$	$^2J(^{113}\text{Cd}-\text{C}^{12})$ = 11.7
148.30	$\text{C}^3$	$^2J(^{113}\text{Cd}-\text{C}^3)$ = 23.4
147.42	$\text{C}^{10}$	$^2J(^{113}\text{Cd}-\text{C}^{10})$ = 15.7
145.01	$\text{C}^{14}$	
142.45	$\text{C}^1$	
135.29	$\text{C}^6$	
133.25	$\text{C}^{13}$	$^3J(^{113}\text{Cd}-\text{C}^{13})$ = 8.6
132.49	$\text{C}^7$	
130.75	$\text{C}^8$	
126.47	$\text{C}^5$	
126.38	$\text{C}^2$	$^3J(^{113}\text{Cd}-\text{C}^2)$ = 3.9 <sup>b</sup>
122.13	$\text{C}^9$	
42.77	$\text{C}^4$	

<sup>a</sup>Relative to  $\text{SiMe}_4$ . <sup>b</sup>approximately equal to only half the coupling constant, obscured due to signal overlap.

The sixteen- and seventeen-membered, potentially quinquedentate  $N_5$  macrocyclic ligands {7}<sup>(23)</sup> and {8}<sup>(22), (23)</sup> have already been discussed in relation to their mercury(II) complexes (section 4.3.1.1).  $[Cd\{7\}Br]Br \cdot H_2O$  is mononuclear with a six-co-ordinate distorted pentagonal pyramidal structure. In contrast,  $[Cd\{8\}Br]_{2n}[CdBr_4]_n$  is polymeric in nature, the metal ion is five co-ordinate to the macrocycle donor atoms and additionally axially co-ordinated to two bridging bromide ions of different bond lengths. This has been attributed to the larger size of the cadmium(II) ion for the sixteen-membered ligand where the metal ion is displaced from the  $N_5$  donor plane. Structural data on the analogous eighteen-membered potentially sexidentate  $N_6$  macrocyclic ligand {1}<sup>(14)</sup> indicates that the metal ion is co-ordinated to all six donor atoms of the macrocycle with water and perchlorate completing the co-ordination sphere in an approximately hexagonal bipyramidal geometry.  $[Cd\{1\}(H_2O)(ClO_4)][ClO_4] \cdot MeOH$  can only be isolated by transmetallation reactions and not via a template synthesis. Furthermore, the cadmium(II)-nitrogen bond lengths are long in comparison to those found for ligands {7} and {8} and the metal ion is asymmetrically positioned in the macrocyclic cavity. These observations have led to the conclusion that this eighteen-membered ring size is too large for the cadmium(II) ion, notwithstanding the added inflexibility of the highly conjugated and planar conformation of the ligand. Thus, a sixteen-membered macrocycle is too small for cadmium(II) and an eighteen-membered cavity is too large. The seventeen-membered ligand appears to be more appropriate for cadmium(II). However, although L<sup>4</sup> is an eighteen-membered macrocycle like {1}, the increased flexibility arising from the replacement of thioether donor atoms for nitrogen donor atoms was designed to be a better fit for the cadmium(II) ion. A

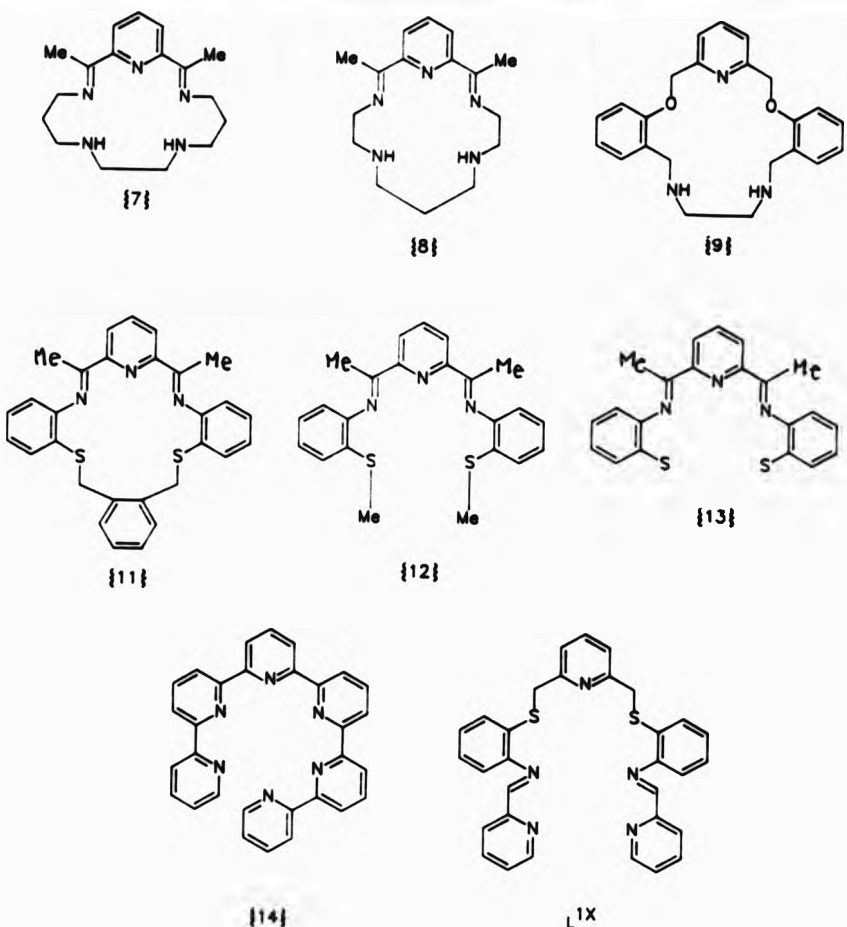


Figure 4.4.1c Comparable ligands of isolated cadmium(II) complexes.

seventeen-membered quinquedentate  $N_3S_2$  macrocyclic ligand {11}<sup>(28)</sup> has also been isolated as its cadmium(II) complex, no structural data is available and structure elucidation has not been accomplished. The donor atoms of the seventeen-membered quinquedentate  $N_3O_2$  macrocyclic ligand {9},<sup>(24)</sup> conform to an approximately pentagonal bipyramidal geometry around cadmium(II) with axial sites being occupied by a

methanol and an asymmetrical nitrate anion. Likewise, the eighteen-membered analogue of (9) is also approximately pentagonal bipyramidal in its geometry with acetonitrile and a perchlorate anion occupying the axial sites.<sup>[24]</sup>

The N<sub>3</sub>S<sub>2</sub> acyclic ligand (12)<sup>[29]</sup>, interacts with cadmium(II) in a trigonal bipyramidal fashion with only the trimethine head unit co-ordinating to the metal ion, iodide ions in the axial sites complete the co-ordination geometry. However, a related ligand (13)<sup>[30]</sup> and the potentially sexidentate ligand (14)<sup>[31]</sup> have been shown to display helical geometries in their cadmium(II) complexes.

Consequently, it is possible for [CdL<sup>40</sup>][ClO<sub>4</sub>]<sub>2</sub> to also have a helical structure. Furthermore, as the helix increases, the proportion of carbonyl would be reduced in comparison to the rest of the molecule and the n.m.r. may approximate to that of [CdL<sup>4</sup>][ClO<sub>4</sub>]<sub>2</sub>. This would still account for the presence of a ν(C=O) in the infrared and agree with the microanalytical data. The fact that the complex is only isolated when the perchlorate counterion is employed may indicate a thermodynamic effect, i.e. due to its insolubility L<sup>40</sup> becomes a 'trapped' intermediate. Likewise, the ligand L<sup>1x[32]</sup> is also believed to have a helical conformation in the presence of Cd[ClO<sub>4</sub>]<sub>2</sub>.6H<sub>2</sub>O.

The proton spectrum (Figure 4.4.1d) of [ZnL<sup>4</sup>][ClO<sub>4</sub>]<sub>2</sub> integrates for twenty protons, as expected (Table 4.4.1f). The most downfield singlet ( $\delta$  8.99 p.p.m.) was assigned to the imino protons H<sup>11</sup> (2 H, s, CN=N), whilst the most upfield singlet ( $\delta$  4.32 p.p.m.) is considered to arise from resonances due to the methylene protons H<sup>4</sup> (4 H, s, CH<sub>2</sub>S). The pyridyl protons H<sup>16</sup> ( $\delta$  8.69 p.p.m.) and H<sup>1</sup> ( $\delta$  7.88 p.p.m.) are both

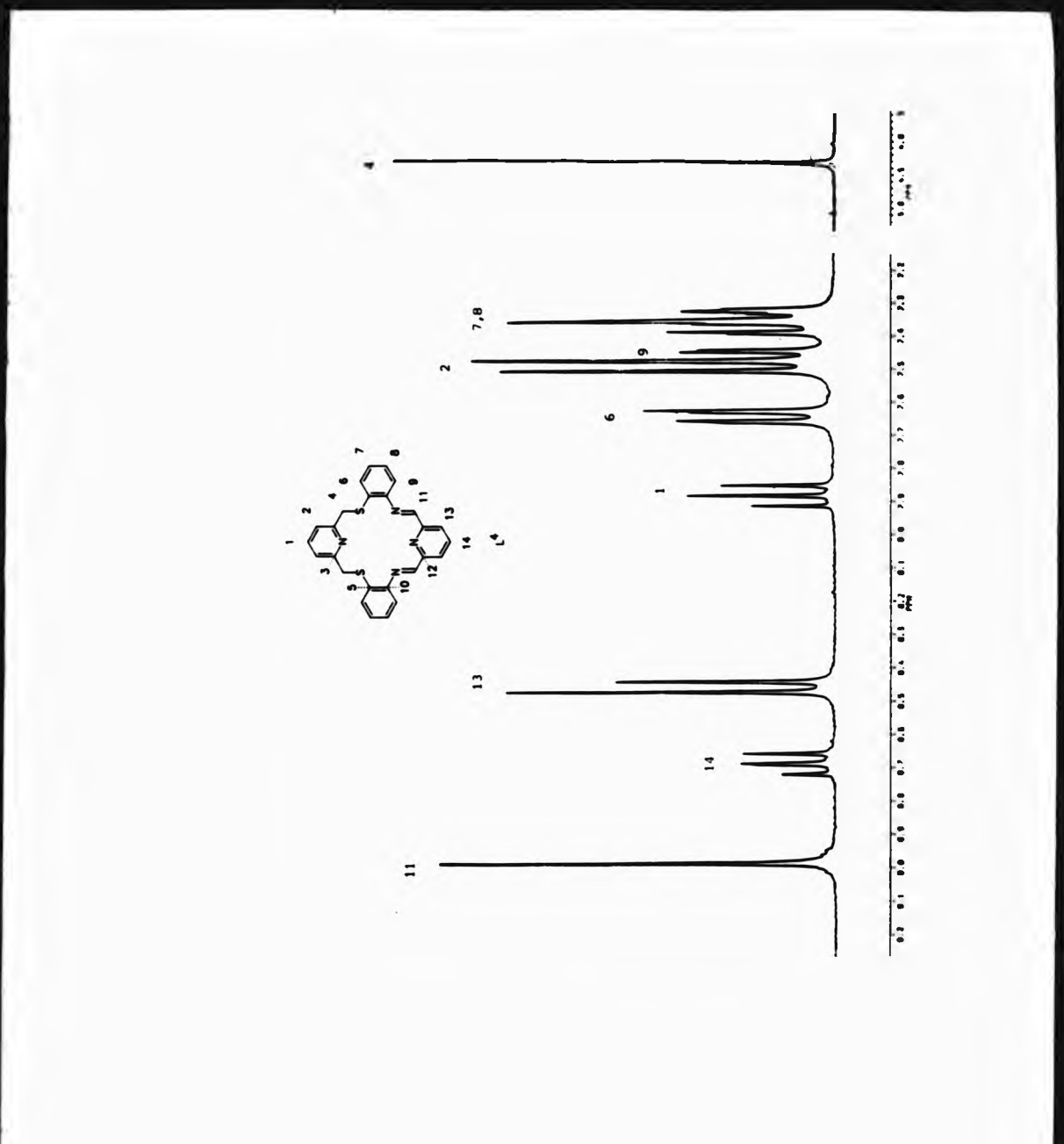


Figure 4.4.1d  $^1\text{H}$  n.m.r. spectrum of  $[\text{ZnL}^4](\text{ClO}_4)_2$  in  $d_3$ -acetonitrile.

recognised as triplets, with both  $H^{13}$  ( $\delta$  8.46 p.p.m.) and  $H^2$  ( $\delta$  7.49 p.p.m.) characteristically dominating the aromatic region as a pair of doublets. The remaining aromatic protons  $H^6-H^9$ , appear as complicated overlapped multiplets with the exception of a doublet of doublets signal at  $\delta$  7.64 p.p.m.. As in the n.m.r. spectrum of the silver(I) and cadmium(II) complexes of  $L^4$ , the most downfield doublet of doublets has been assigned to  $H^6$ .

Assignment of the carbon-13 (Table 4.4.1f) broad band decoupled spectrum was achieved through  $^1H$ ,  $^{13}C$ -COSY and DEPT 45 spectra. Fourteen unique carbon environments as expected for the macrocyclic ligand  $L^4$ , were observed. Each carbon resonance is comparable to those found in the spectrum of the cadmium(II) complex of  $L^4$ , apart from the order of the phenylene carbons  $C^6-C^9$ .

It is the differences in the order and chemical shift of the phenylene protons and carbon sites which are diagnostic of structures in solution. Clearly, if the general features/outline of spectra vary from metal to metal for the same ligand, their solution structures may differ considerably. These clues are beneficial not only for establishing the existence of ligands but also towards discerning metal co-ordination environments.

The ionic radius of zinc(II) [ $r_{Zn(II)} = 0.74 \text{ \AA}$  (hexa-co-ordinate)] is even smaller than that of cadmium(II) [ $r_{Cd(II)} = 0.95 \text{ \AA}$  (hexa-co-ordinate)], consequently, zinc(II) is not large enough and  $L^4$  is not flexible enough for six-co-ordinate metal-ligand interactions to occur. Thus, the bonding mode of zinc(II) towards  $L^4$  is thought to be five-co-ordinate with a distorted trigonal bipyramidal or square

pyramidal co-ordination geometry. However, only three of the potential six macrocycle donor atoms are proposed to be bound to the metal centre with counterions or solvent molecules completing the co-ordination

Table 4.4.1f  $^1\text{H}$  (250.134 Hz) and  $^{13}\text{C}$  n.m.r. (62.896 Hz) data<sup>a</sup> for  $[\text{ZnL}^4][\text{ClO}_4]_2$  in  $\text{CD}_3\text{CN}$  at ambient temperature.

		1		
8.99(s)	$\text{H}^{11}$	2		
8.69(t)	$\text{H}^{14}$	3	4	
8.46(d)	$\text{H}^{13}$	5	6	
7.88(t)	$\text{H}^1$	7	8	
7.64(dd)	$\text{H}^6$	10	9	
7.49(d)	$\text{H}^2$	11	12	
7.46(dd)	$\text{H}^9$	13	14	
7.36(2xtd)	$\text{H}^{7,8}$ <sup>b</sup>			
4.32(s)	$\text{H}^4$			
			160.42	$\text{C}^{11}$
			157.23	$\text{C}^{12}$
			147.89	$\text{C}^3$
			147.53	$\text{C}^{10}$
			146.48	$\text{C}^{14}$
			142.85	$\text{C}^1$
			134.05	$\text{C}^6$
			132.50	$\text{C}^{13}$
			131.29	$\text{C}^9$
			130.28	$\text{C}^{7,8}\text{c}$
			127.12	$\text{C}^5$
			126.93	$\text{C}^2$
			121.52	$\text{C}^{7,8}\text{c}$
			40.42	$\text{C}^4$

<sup>a</sup>In p.p.m., relative to  $\text{SiMe}_4$ . <sup>b</sup>Both protons present under same signal. <sup>c</sup>Cannot distinguish between  $\text{C}^7$  and  $\text{C}^8$ .

sphere. The strong  $\pi$ -acceptor properties of the trimethine head unit makes these nitrogen donor atoms more likely candidates for co-ordination rather than the thioether end of the macrocycle.

For instance, the reaction between zinc(II) and a number of open-chain terdentate ligands containing the trimethine linkages, such as in (15)<sup>[33]</sup> or (16),<sup>[34]</sup> comfortably result in the formation of five-co-ordinate trigonal bipyramidal complexes in the presence of strongly co-ordinating anions e.g. Cl<sup>-</sup> and NCS<sup>-</sup>. On the other hand, the perchlorate counterion forces two molecules of ligand to be co-ordinated to the metal centre in an octahedral manner.<sup>[33]</sup> In contrast, zinc(II) salts were not found to complex with the open-chain ligand L<sup>1</sup> alone (section 2.4). However, the isolation of related pyridyl-thioether-containing ligands with zinc(II) salts have been reported.<sup>[35]</sup>

The trimethine mode of co-ordination between zinc(II) and L<sup>4</sup> would also be consistent with those found for other related acyclic and macrocyclic ligands (Figure 4.4.1e).

Crystallographically determined structures for zinc(II) complexes of the fifteen- and sixteen-membered quinquedentate N<sub>3</sub>S<sub>2</sub> macrocyclic ligands (17)<sup>[36]</sup> and (18)<sup>[37]</sup> reveal a pentagonal bipyramidal co-ordinate complex in each case. It is of interest to note, that on going from a sixteen-membered to a potentially quinquedentate N<sub>3</sub>S<sub>2</sub> seventeen-membered macrocyclic ligand (19),<sup>[29]</sup> there is a change in co-ordination sphere for the metal ion, promoting structural dislocation. Prompted by the larger cavity size, the zinc(II) atom is unable to effectively co-ordinate all five donor atoms of the

macrocycle and leaves the thioether donor atoms unco-ordinated. Instead, two iodide ions interact with the metal centre to display a square pyramidal environment. The analogous, potentially quinquedentate  $N_3S_2$  seventeen-membered macrocyclic ligand (11)<sup>(28)</sup> has also been isolated as its zinc(II) complex. Although no structural data are available, a pentagonal bipyramidal co-ordination geometry was proposed. In hind sight, this may not be true and the possibility of a five-co-ordinate complex may be more appropriate.

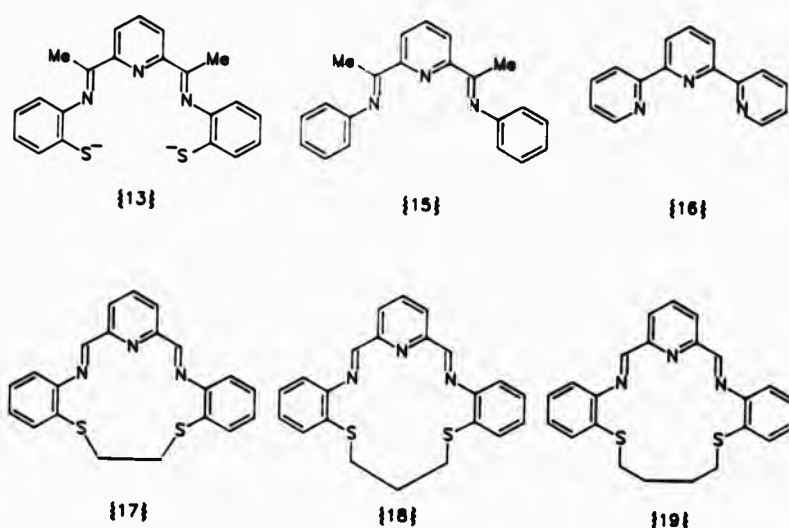


Figure 4.4.1e Comparable ligands for structurally characterised zinc(II) complexes.

The quinquedentate  $N_3S_2$  acyclic ligand (13),<sup>(38)</sup> is also five-co-ordinate (to all ligand donor atoms) and exhibits a helical geometry, whereas, (16)<sup>(34)</sup> is terdentate in nature but boasts a trigonal bipyramidal structure as just mentioned (*vide supra*).

Furthermore, for all five zinc(II) complexes the metal-nitrogen bond distances are comparable, indicating the propensity of zinc(II) towards the  $\pi$ -acceptor properties of the trimethine ligating unit regardless of whether in addition, the ligand contains thioether donor atoms or is acyclic or macrocyclic.

#### 4.4.2 Single-Crystal X-ray Structure of L<sup>48</sup>.

Under slow, mixed solvent (acetonitrile, methanol and water) recrystallisation conditions, a minor side product was also obtained in the presence of Zn(ClO<sub>4</sub>)<sub>2</sub>.6H<sub>2</sub>O during the preparation of [ZnL<sup>48</sup>][ClO<sub>4</sub>]<sub>2</sub>. Since, the low yield precluded any other studies from being undertaken the product was analysed by a single-crystal structure determination (Figure 4.4.2a).

Table 4.4.2a Selected bond distances ( $\text{\AA}$ ) and angles ( $^{\circ}$ ) for L<sup>48</sup>.

Bond distances		Bond angles	
O - C(4a)	1.228(7)	C(5a) - N(2a) - C(4a)	129.0(4)
N(2a) - C(4a)	1.360(6)	C(7a) - S(1a) - C(6a)	101.3(3)
N(2b) - C(4b)	1.444(7)	N(2a) - C(4a) - O	124.8(5)
C(3a) - C(4a)	1.490(8)	C(3a) - C(4a) - O	122.4(4)
C(3b) - C(4b)	1.521(7)	C(9a) - C(8a) - C(7a)	121.6(5)
N(2a) - C(5a)	1.401(7)	C(3b) - C(4b) - N(2b)	114.7(4)
N(2b) - C(5b)	1.390(7)	C(7b) - C(4b) - C(3b)	111.8(4)
S(1a) - C(6a)	1.776(5)	C(6b) - C(5b) - N(2b)	122.6(4)
S(1b) - C(6b)	1.756(5)	C(5b) - C(6b) - S(1b)	122.8(4)
S(1a) - C(7a)	1.822(6)	C(8b) - C(7b) - S(1b)	110.4(3)
S(1b) - C(7b)	1.822(6)	C(8b) - C(7b) - C(4b)	111.7(4)
C(4b) - C(7b)	1.544(6)	C(9b) - C(8b) - C(7b)	124.5(4)

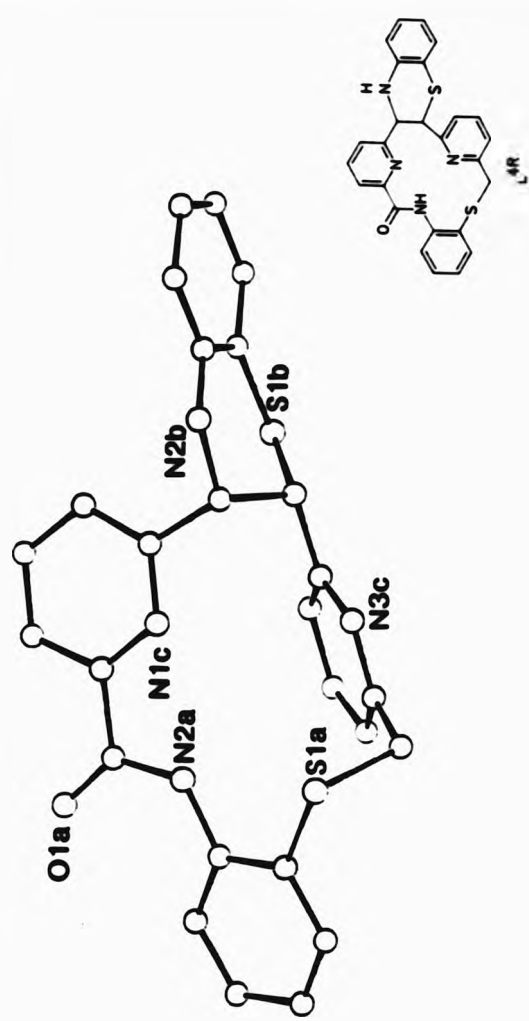
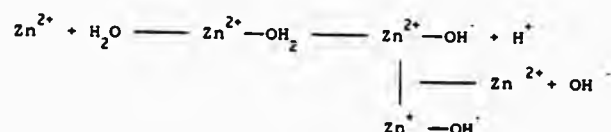


Figure 4.4.2a Single-crystal X-ray structure of  $L^{48}$ .

The crystal structure revealed that the isolated side product was a purely organic molecule  $L^{48}$ , and not an inorganic zinc(II) complex of  $L^4$  as initially suspected.  $L^{48}$  is still macrocyclic in nature, however, an internal cyclisation has led to the formation of a thiazole ring, leaving a fourteen-membered inner great ring comprising of an  $N_3S$  donor set which includes an amide function. Thus, a rearrangement of the parent di-imine macrocyclic ligand  $L^4$  to yield  $L^{48}$  is more than likely and suspected to be metal assisted.

Zinc(II) co-ordinated to water can be a potent nucleophile<sup>[55]</sup> or release free hydroxide ions in solution for base catalysed reactions.



Thus, one possible mechanistic route to the formation of  $L^{48}$  (Figure 4.4.2b) could be the initial isolation of  $[\text{ZnL}^4(\text{H}_2\text{O})_2](\text{ClO}_4)_2$ . Hydrolysis of  $L^4$  may occur at the imine linkages in the presence of water (1). The carbinolamine (2) could undergo air oxidation or possibly chemical oxidation by perchloric acid in solution to yield an amide carbonyl (3), giving the corresponding dioxo macrocyclic ligand (4). Proton abstraction of the methylene carbon by hydroxide ions (5) would generate a nucleophile within the macrocycle at the partially polarised carbon atom of the carbonyl group (6). Furthermore, it seems likely that zinc(II) ions in solution may possibly co-ordinate to the carbonyl oxygen and render the carbon site even more susceptible to nucleophilic attack. Hence, the enclosure of a six-membered ring could occur with the formation of a new carbon-carbon bond leaving a larger

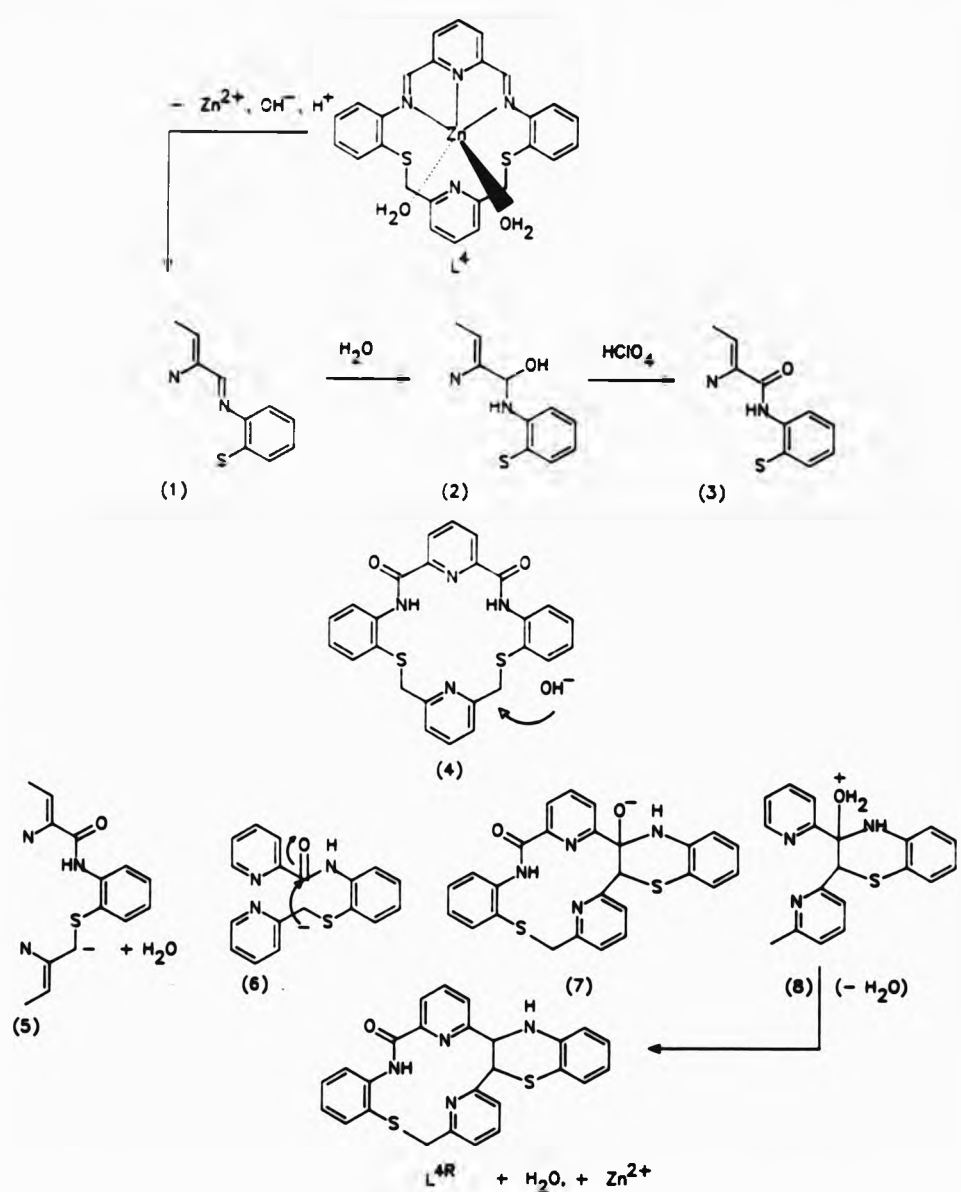
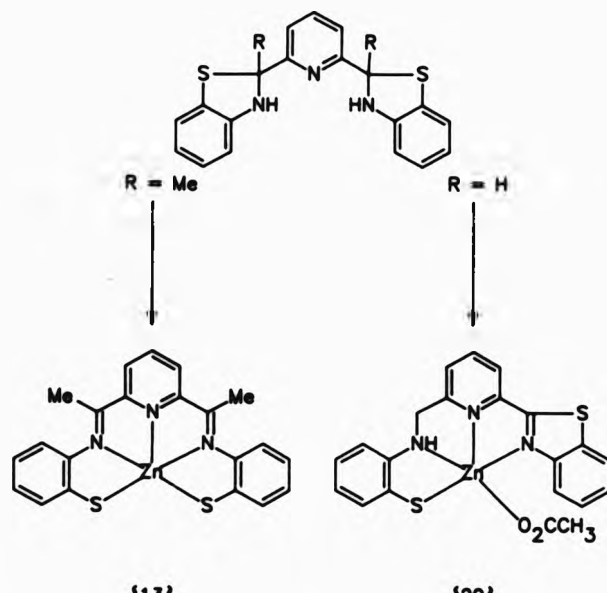


Figure 4.4.2b Mechanism for formation of  $L^{4R}$ .

fourteen-membered ring as well (7). Finally, combination of oxide and hydrogen ions to yield hydronium ions (8) which are released to solution as water molecules may produce the ligand L<sup>48</sup>. The existence of only one six-membered ring may be attributed to the fact that model studies indicate that two thiazole rings would be sterically unfavourable since, the lone pairs of the pyridyl nitrogens would be in close proximity. There will of course be any one of several chemical reactions being executed in solution, but without further evidence any mechanistic route suggested will be purely speculative.

Interestingly, the major product between the reaction of zinc(II) and the acyclic ligand (13-H) gives the zinc(II) complex of the rearranged ligand (20).<sup>[40]</sup> Ring opening of one of the thiazolinyl rings gives an imino thiolate chelate accompanied by a net 'internal hydrogen transfer' to account for dehydrogenation of the other benzothiazolinyl ring and the rehydrogenation of the imino linkage.

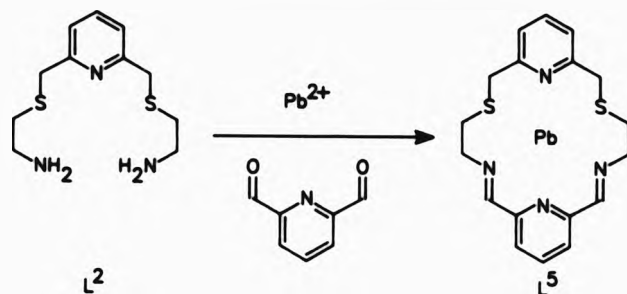


{13}

{20}

#### 4.5 Co-ordination Studies of $[PbL]^{\pm 2+}$ .

An analogous eighteen-membered potentially sexidentate  $N_4S_2$  donor macrocycle  $L^5$ , has been isolated as its lead(II) complexes. Isolation of the acyclic precursor ligand  $L^2$  has not been achieved (section 2.5). Consequently, the  $[PbL]^{\pm 2+}$  complexes have been prepared under conditions of non-stoichiometry.



##### 4.5.1 Spectroscopic Studies of $[PbL]^{\pm 2+}$ .

###### 4.5.1.1 Infrared studies.

Two characterisable lead(II) complexes of the macrocyclic ligand  $L^5$  were isolated (Table 4.5.1a). In both cases, the absence of stretching frequencies for  $\nu(C=O)$  at ca.  $1700\text{ cm}^{-1}$  and  $\nu(N-H)$  between  $3500-3300\text{ cm}^{-1}$  and the presence of bands at ca.  $1660$ ,  $1650$  and  $1620\text{ cm}^{-1}$  is indicative of the formation of a Schiff-base condensation reaction product.<sup>[2]</sup> For the  $[PbL^5(SCN)_2]$  complex, the split imine absorbances may be due to unsymmetrical metal co-ordination to the imino nitrogens. Furthermore, a band at ca.  $2080\text{ cm}^{-1}$  was assigned to the  $\nu(C-N)$  stretching mode of the thiocyanate molecule.<sup>[7]</sup> Absorptions in this region arise from terminally bonded sulphur-metal co-ordination (cf.  $[PbL^4(NCS)_2] = 2040\text{ cm}^{-1}$ , trans N-bonded (section 4.3.1.1)).

Although there is no conclusive evidence that the anions are

co-ordinated in both complexes, a preference towards high co-ordination numbers, large metal ion size and anion geometry would suggest this to be true.

Table 4.5.1a Infrared data<sup>a</sup> for  $[PbL^5]^{2+}$  complexes.

COMPLEX	COLOUR	$\nu(C=N)$	$\nu(py)$	$\nu(\text{counterion})$
$[PbL^5(Br)_2]$	Pale yellow	1660m	1590s	-
$[PbL^5(SCN)_2]$	Bright yellow	1650s, 1620s	1580s	2080s

<sup>a</sup>In  $\text{cm}^{-1}$ , as KBr disc.

Microanalytical data (section 7.5.2) were consistent with the formulations  $[PbL^5(Br)_2]$  and  $[PbL^5(SCN)_2]$ , indicating the presence of a  $(1+1)$  cyclocondensation product to give a lead(II) to  $L^5$  ratio of 1:1.

#### 4.5.1.2 Fast-atom bombardment mass spectrometry.

The f.a.b. mass spectral data (Table 4.5.1b) for both compounds confirm the existence of  $L^5$  as its lead(II) complexes. No higher mass peaks were observed in either spectrum.

Table 4.5.1b F.a.b. mass spectral data<sup>a</sup> for  $[PbL^5]^{2+}$  complexes.

COMPLEX	FRAGMENTATION ASSIGNMENT	MASS <sup>b</sup>	RELATIVE
			PERCENTAGE
$[PbL^5(Br)_2]$	$[PbL^5(Br)]^+$	643	89
	$[PbL^5]^+$	564	11
$[PbL^5(SCN)_2]$	$[PbL^5(SCN)]^+$	622	75
	$[PbL^5]^+$	564	14

<sup>a</sup>In NOBA matrix. <sup>b</sup>Positive ion mode.

#### 4.5.1.3 Nuclear magnetic resonance studies.

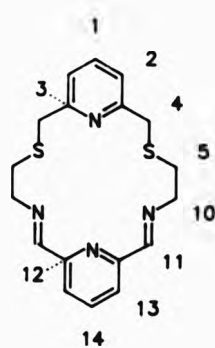
The  $[PbL^5(SCN)_2]$  complex was sufficiently soluble in  $d_7$ -dimethylformamide in order to obtain  $^1H$  and  $^{13}C$  n.m.r. (Table 4.5.1c) spectra.

The proton n.m.r. spectrum (Figure 4.5.1a) integrates for twenty protons which is in accordance with the proposed structure. The most downfield singlet at  $\delta$  9.60 p.p.m. was assigned to the imino proton  $H^{11}$ . In addition, the observance of satellites on either side of the imino signal are thought to arise from lead-imino proton couplings ( $^3J(^{207}Pb-C^{11}) = 15.9$  Hz) implying metal-imino nitrogen co-ordination (section 4.3.1.3).

As previously, the protons of the pyridyl ring (which is part of the trimethine head unit) are chemically shifted further downfield than the protons of the second pyridyl ring. The sub-spectrum of the pyridyl protons  $H^{14}$  and  $H^{13}$ , shows a four-line multiplet for  $H^{14}$  and a doublet for  $H^{13}$  which indicates significant second-order character and has therefore been assigned as an AB<sub>2</sub> spin system (Appendix A). Identical multiplets were observed for the silver(I) and cadmium(II) complexes of L<sup>4</sup> (sections 4.3.1.3 and 4.4.1.3). Meanwhile, protons  $H^1$  and  $H^2$  are characteristically a triplet and doublet respectively and display first-order spin-spin couplings to each other with a three-bond coupling constant of 7.7 Hz.

Finally, the three sets of methylene signals for  $H^4$ ,  $H^5$  and  $H^{10}$  appear as complicated multiplets. Additionally, two of the proton sites have similar chemical shifts. Consequently, assignment of these protons was

Table 4.5.1c  $^1\text{H}$  (250.134 MHz) and  $^{13}\text{C}$  (62.896 MHz) n.m.r. data<sup>a</sup> for  $(\text{PbL}^3(\text{SCN})_2)$ <sup>b</sup> in  $(\text{CD}_3)_2\text{NCDO}$  at ambient temperature.



$\delta/\text{p.p.m.}$		$J/\text{Hz}$	$\delta/\text{p.p.m.}$	$J/\text{Hz}$
9.60(s)	$\text{H}^{11}$	$^3J(^{207}\text{Pb}-\text{H}^{11})$	= 15.9	164.21 $\text{C}^{11}$
8.63(t) <sup>c</sup>	$\text{H}^{14}$	$^3J(\text{H}^{14}-\text{H}^{13})$	= 7.7	157.52 $\text{C}^{12}$
8.38(d) <sup>c</sup>	$\text{H}^{13}$	$^3J(\text{H}^{13}-\text{H}^{14})$	= 7.7	153.40 $\text{C}^3$
7.90(t)	$\text{H}^1$	$^3J(\text{H}^1-\text{H}^2)$	= 7.7	142.65 $\text{C}^{14}$ $^4J(^{207}\text{Pb}-\text{H}^1)$ = 4.8
7.53(d)	$\text{H}^2$	$^3J(\text{H}^2-\text{H}^1)$	= 7.7	139.68 $\text{C}^1$
4.46(m)	$\text{H}^{10,4}$			130.87 $\text{C}^{13}$ $^3J(^{207}\text{Pb}-\text{H}^{13})$ = 7.4
3.32(m)	$\text{H}^5$			123.67 $\text{C}^2$ $^3J(^{207}\text{Pb}-\text{H}^2)$ = 13.1 58.35 $\text{C}^{10}$
				37.29 $\text{C}^4$
				33.75 $\text{C}^5$

<sup>a</sup>Relative to  $\text{SiMe}_4$ . <sup>b</sup>Numbering scheme comparable to L<sup>4</sup>. <sup>c</sup>Assigned as  $\text{AB}_2$  spin system.

based on the relative shielding of the individual protons depending on the electronegativity of adjacent donor atoms attached to the respective methylene carbons. Thus, protons  $\text{H}^4$  and  $\text{H}^{10}$  were assigned

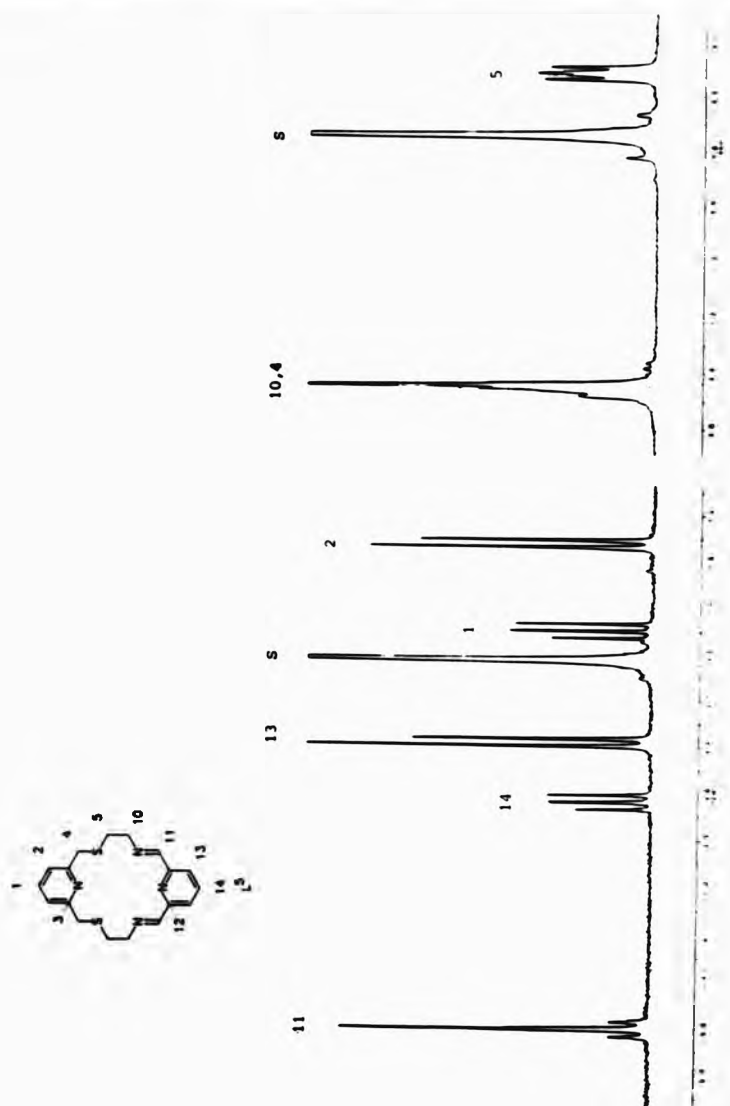


Figure 4.5.1a  $^1\text{H}$  n.m.r. spectrum of  $[\text{PbL}^5(\text{SCN})_2]$  in  $d_7\text{-DMF}$ .

to the multiplet centered at  $\delta$  4.46 p.p.m. (signal integrates for 8 H) whilst  $H^5$  must therefore be the most upfield multiplet at  $\delta$  3.32 p.p.m. (signal integrates for 4 H). The appearance of multiplets rather than a singlet for  $H^4$  and the other methylene protons  $H^5$  and  $H^{10}$  may be attributed to geminal and/or vicinal couplings. Perhaps folding and unfolding of the macrocyclic ligand upon co-ordination in solution due to metal exchange of ligand and solvent molecules may result in the appearance of complicated multiplets.

The carbon-13 spectrum of  $[PbL(SCN)_2]$  was found to have ten resonance signals corresponding to ten unique carbon environments. Assignment of the spectrum was achieved by the analyses of the  $^1H$ ,  $^{13}C$ -COSY and DEPT 45 spectra. Carbon signals  $C^{14}$ ,  $C^{13}$  and  $C^2$  also show signs of being coupled to  $^{207}Pb$ . The signal for  $C^{14}$  has satellites corresponding to a coupling constant of 4.8 Hz which may be attributable to four- or five-bond coupling via the pyridyl or imino nitrogen donor atoms respectively. The magnitude of lead(II) couplings to the  $\beta$ -pyridyl carbon sites  $C^{13}$ ,  $J(^{207}Pb-C^{13}) = 7.4$  Hz and  $C^2$ ,  $J(^{207}Pb-C^2) = 13.1$  Hz are distinctly different. In both instances, metal-carbon coupling may occur through the pyridyl nitrogens and/or the imino nitrogens or the thioether donor atoms. The pyridyl ring of the trimethine head unit has the larger metal- $\beta$ -carbon coupling with the  $\gamma$ -carbon also being involved in some metal couplings (Figure 4.5.1b).

Flexibility of the macrocyclic ligand  $L^5$  and the size of its eighteen-membered inner great ring should allow the lead(II) atom to interact with all six potential donor atoms to give a distorted hexagonal bipyramidal co-ordination sphere (counterions included).

Moreover, comparison of n.m.r spectra of the  $[ML^4]^{m+}$  complexes with that of  $[PbL^5(SCN)_2]$  indicate metal-nitrogen co-ordination to all four methine donor atoms of the macrocyclic ligand. Metal-sulphur co-ordination is suspected but cannot be proven.

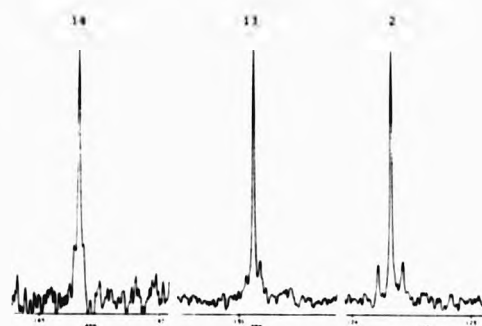


Figure 4.5.1b  $^{13}\text{C}$  n.m.r. spectrum of  $[PbL^5(SCN)_2]$  displaying  $^{207}\text{Pb}-^{13}\text{C}$  couplings only.

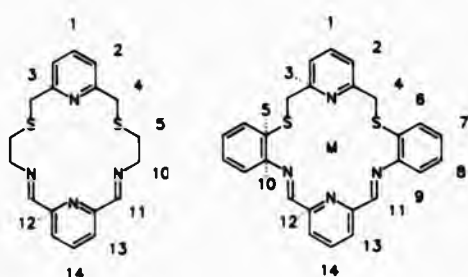
Although the n.m.r. spectra for  $[PbL^4(\text{H}_2\text{O})(\text{MeOH})][\text{ClO}_4]_2$  and  $[PbL^5(SCN)_2]$  were obtained in different deuterated solvents, d<sub>3</sub>-acetonitrile and d<sub>7</sub>-dimethylformamide respectively, selected proton resonances are comparable in both complexes (Table 4.5.1d).

The differences in splitting patterns exhibited by protons H<sup>1</sup> and H<sup>4</sup> for both complexes can be attributed to the increased flexibility of the macrocyclic ligand L<sup>5</sup> compared to L<sup>4</sup>. X-ray analysis has shown lead(II) to be co-ordinated to only three of the four available nitrogen donor atoms of L<sup>4</sup> (section 4.3.2). In contrast, L<sup>5</sup> is suspected to be co-ordinated by all four available nitrogen donor atoms to the lead(II) atom.

The eighteen-membered potentially sexidentate N<sub>6</sub> macrocyclic ligand

{21},<sup>[21]</sup> has been isolated as its lead(II) complex. A crystal structure determination has revealed the complex to be eight

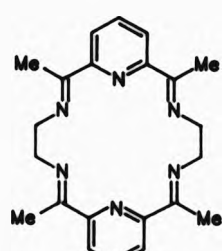
Table 4.5.1d Selected proton n.m.r. data<sup>a</sup> for  
 $[\text{PbL}^4(\text{H}_2\text{O})(\text{MeOH})](\text{ClO}_4)_2$ <sup>b</sup> and  $[\text{PbL}^5(\text{SCN})_2]$ .<sup>c</sup>



$[\text{PbL}^4(\text{H}_2\text{O})(\text{MeOH})](\text{ClO}_4)_2$        $[\text{PbL}^5(\text{SCN})_2]$

H <sup>11</sup>	9.57(s)	9.60(s)
H <sup>14</sup>	8.62(t)	8.63(t)
H <sup>13</sup>	8.35(d)	8.38(d)
H <sup>1</sup>	7.91(m) <sup>d</sup>	7.90(t)
H <sup>2</sup>	7.49(d) <sup>d</sup>	7.53(d)
H <sup>4</sup>	4.75(s)	4.46(m)
$^3J(^{207}\text{Pb}-\text{H}^{11})$	16.74 Hz	15.92 Hz

<sup>a</sup>In p.p.m., relative to SiMe<sub>4</sub>.    <sup>b</sup>In CD<sub>3</sub>CN.    <sup>c</sup>In (CD<sub>3</sub>)<sub>2</sub>NCDO.    <sup>d</sup>Assigned as AB<sub>2</sub> spin system.



{21}

co-ordinate, its geometry best described as hexagonal bipyramidal. All six macrocycle donor atoms define the equatorial girdle and two thiocyanate anions occupy the axial positions. Additionally, one anion is N-bonded and the other is S-bonded (cf.  $[PbL^5(SCN)_2]$ ). Under identical experimental conditions or via transmetallation reactions, isolation of the calcium(II), strontium(II) and barium(II) complexes of (21) have also been achieved. However, silver(I), mercury(II) and cadmium(II) were ineffective templating ions which instead yielded complexes consisting of a ring-opened ligand. In the presence of copper(II) and nickel(II), rearrangements as well as ring hydrolysis have occurred in these systems.<sup>[41]</sup>

The synthesis of L<sup>4</sup> in the presence of the diamagnetic metal ions zinc(II), silver(I), cadmium(II), mercury(II) and lead(II) has led to the isolation of complexes where the metal ion preferentially associates with the trimethine head unit rather than the thioether donor atoms. The stability of the conjugated system is attributed to back-donation of electrons from the metal d orbitals into the ligand  $\pi^*$  orbital. Such di-imines function as very efficient  $\pi$ -acceptors, as the  $\pi^*$  orbitals associated with the unsaturation extend over both ligand atoms and can therefore overlap with a filled orbital on the metal and form a cyclic, delocalised  $6\pi$ -electron system.

The mixed-donor set and the intermediate rigidity of L<sup>4</sup> has given rise to different bonding modes towards metal ions of various sizes. Meanwhile, the HSAB concept remains important in the sense that the strong  $\pi$ -acceptor properties of the trimethine head unit (due to extensive delocalisation) are able to stabilise metal ions whether they have a preference towards hard or soft ligating atoms. Differences in

chemical reactivity for L<sup>5</sup> compared to that of L<sup>4</sup>, cannot be fully appreciated since the number of isolated complexes have been limited.

*References - Chapter Four.*

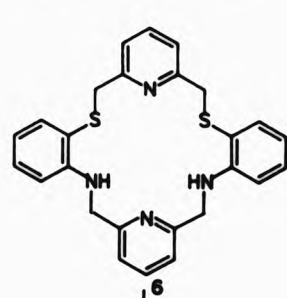
1. T. W. Bell and F. Guzzo, *J. Chem. Soc., Chem. Commun.*, 1986, 769.
2. D. H. Williams and I. Fleming, 'Spectroscopic Methods in Organic Chemistry,' McGraw-Hill, London, (4th edn) 1988.
3. J. L. Burmeister, *Coord. Chem. Rev.*, 1990, 105, 77.
4. (a) J. Hunter, B. P. Murphy and J. Nelson, *J. Chem. Educ.*, 1991, 68, 59, and references therein. (b) S. Raghunathan, C. Stevenson and V. McKee, *J. Chem. Soc., Chem. Commun.*, 1989, 5.
5. M. G. B. Drew, B. P. Murphy, J. Nelson and S. M. Nelson, *J. Chem. Soc., Dalton Trans.*, 1987, 873.
6. S. M. Nelson, F. S. Esho and M. G. B. Drew, *J. Chem. Soc., Chem. Commun.*, 1981, 388.
7. A. H. Norbury and A. I. P. Sinha, *Quart. Rev.*, 1970, 24, 69.
8. D. E. Fenton and R. Leonardi, *Inorg. Chim. Acta.*, 1981, 55, L51.
9. D. H. Cook and D. E. Fenton, *J. Chem. Soc., Dalton Trans.*, 1979, 266.
10. D. H. Cook, D. E. Fenton, M. G. B. Drew, A. Rodgers, M. McCann and S. M. Nelson, *J. Chem. Soc., Dalton Trans.*, 1979, 414.
11. K. Nakamoto, 'Infrared Spectra of Inorganic and Co-ordination Compounds, Wiley-Interscience, New York, (2nd edn) 1970.
12. P. H. Merrel, E. C. Alyea and L. Ecott, *Inorg. Chim. Acta.*, 1982, 59, 25.
13. F. Benetollo, G. Bombieri, K. K. Fonda, A. Polo, J. R. Quagliano and L. M. Vallarino, *Inorg. Chem.*, 1991, 30, 1345.
14. M. G. B. Drew, J. de O. Cabral, M. F. Cabral, F. S. Esho and S. M. Nelson, *J. Chem. Soc., Chem. Commun.*, 1979, 1033.
15. S. J. Kitchen, Ph.D Thesis, University of Sheffield, 1990.
16. M. G. B. Drew, personal communication.
17. D. E. Fenton, B. P. Murphy, A. J. Leong, L. F. Lindoy, A. Bashall

- and M. McPartlin, *J. Chem. Soc., Dalton Trans.*, 1987, 2543.
18. A. Bashall, M. McPartlin, B. P. Murphy, D. E. Fenton, S. J. Kitchen and P. A. Tasker, *J. Chem. Soc., Dalton Trans.*, 1990, 505.
19. I. W. Nowell, *Acta Crystallogr., Sect B*, 1979, B35, 1891.
20. (a) B. P. Murphy, J. Nelson, S. M. Nelson, M. G. B. Drew and P. C. Yates, *J. Chem. Soc., Dalton Trans.*, 1987, 123; (b) J. Nelson, B. P. Murphy, M. G. B. Drew, P. C. Yates and S. M. Nelson, *J. Chem. Soc., Dalton Trans.*, 1988, 1001; (c) M. G. B. Drew, A. Rodgers, M. McCann and S. M. Nelson, *J. Chem. Soc., Chem. Commun.*, 1978, 415; (d) N. A. Bailey, D. E. Fenton, I. T. Jackson, R. Moody and C. Rodriguez de Barbarin, *J. Chem. Soc., Chem. Commun.*, 1983, 1463.
21. J. de O Cabral, M. F. Cabral, W. J. Cummins, M. G. B. Drew, A. Rodgers and S. M. Nelson, *Inorg. Chim. Acta*, 1978, L313.
22. M. G. B. Drew, S. G. McFall and S. M. Nelson, *J. Chem. Soc., Dalton Trans.*, 1979, 575.
23. S. M. Nelson, S. G. McFall, M. G. B. Drew, A. bin Othman and N. B. Mason, *J. Chem. Soc., Chem. Commun.*, 1977, 167.
24. H. Adams, N. A. Bailey, D. E. Fenton, I. G. Ford, S. J. Kitchen, M. G. Williams, P. A. Tasker, A. J. Leong and L. F. Lindoy, *J. Chem. Soc., Dalton Trans.*, 1991, 1665.
25. N. W. Alcock, N. Herron and P. Moore, *J. Chem. Soc., Dalton Trans.*, 1978, 394.
26. C. Cairns, S. G. McFall, S. M. Nelson and M. G. B. Drew, *J. Chem. Soc., Dalton Trans.*, 1979, 446.
27. P. S. Marchetti, S. Bank, T. W. Bell, M. A. Kennedy and P. D. Ellis, *J. Am. Chem. Soc.*, 1989, 111, 2063.
28. L. F. Lindoy and D. H. Busch, *Inorg. Chem.*, 1974, 13, 2494.
29. M. G. B. Drew and S. Hollis, *J. Chem. Soc., Dalton Trans.*, 1978, 511.

30. L. F. Lindoy, D. H. Busch and V. Goedken, *J. Chem. Soc., Chem. Commun.*, 1972, 683.
31. E. C. Constable, M. D. Ward and D. A. Tocher, *J. Chem. Soc., Dalton Trans.*, 1991, 1675.
32. M. Constantinou, personal communication.
33. (a) D. A. Edwards, M. F. Mahon, W. R. Martin, K. C. Molloy, P. E. Fanwick and R. A. Walton, *J. Chem. Soc., Dalton Trans.*, 1990, 3161; (b) E. C. Alyea and P. H. Merrell, *Syn. React. Inorg. Metal-Org. Chem.*, 1974, 4(6), 535.
34. F. W. Einstein and B. R. Penfold, *Acta Cryst.*, 1966, 20, 924.
35. (a) F. Teixidor, L. Escriche, I. Rodriguez, J. Casabó, J. Rius, E. Molins, B. Martínez and C. Miravitles, *J. Chem. Soc., Dalton Trans.*, 1989, 1381; (b) F. Teixidor, L. Escriche, J. Casabó, E. Molins and C. Miravitles, *Inorg. Chem.*, 1986, 25, 4060.
36. N. W. Alcock, D. C. Liles, M. McPartlin and P. A. Tasker, *J. Chem. Soc., Chem. Commun.*, 1974, 727.
37. D. C. Liles, M. McPartlin and P. A. Tasker, *J. Chem. Soc., Dalton Trans.*, 1987, 1631.
38. V. L. Goedken and G. G. Christoph, *Inorg. Chem.*, 1973, 12, 2316.
39. D. Bryce-smith, *Chem. Brit.*, 1989, 25, 783.
40. D. C. Liles, M. McPartlin and P. A. Tasker, *J. Am. Chem. Soc.*, 1977, 99, 7704.
41. S. M. Nelson, F. S. Esho and M. G. B. Drew, *J. Chem. Soc., Dalton Trans.*, 1982, 407.

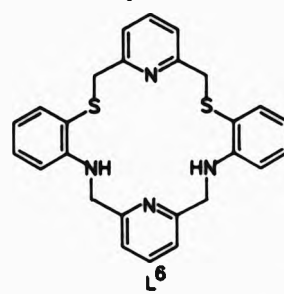
CHAPTER FIVE

SYNTHESSES, CHARACTERISATION AND CO-ORDINATION STUDIES OF A SEXIDENTATE  
NITROGEN-SULPHUR MACROCYCLIC LIGAND  $L^6$  AND ITS DERIVATIVES  $L^{6A-D}$ .



### 5.1 General Introduction.

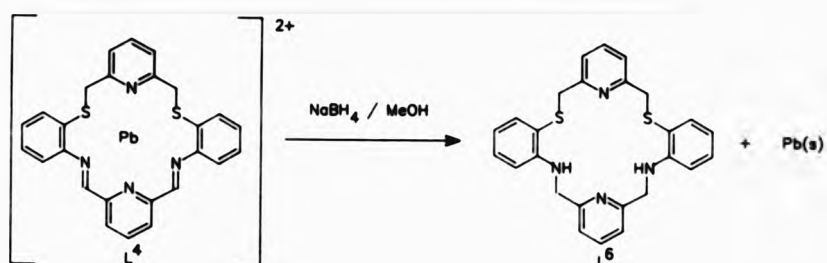
Isolation of the Schiff-base (di-imine) macrocyclic ligands described so far has only been accomplished via their metal complexes (Chapters Three and Four). Although these systems are useful for investigating metal-ion preferences they would not be suitable in the field of hydrometallurgy where metal-ion selectivity and regeneration is required; nor are they capable of the metal-ion specificity necessary for their use as effective therapeutic reagents for metal detoxification in biological systems. For cost effectiveness and minimal pollution, recovery of metal-free macrocyclic ligands is desirable. Furthermore, free-ligand characterisation followed by monitoring of changes upon complexation will lead to a better understanding of ligand reactivity.



In an attempt to address this point, this chapter presents the synthesis of a metal-free macrocyclic ligand  $L^6$  together with some complexation reactions, and also includes the isolation of metal complexes of its carbinolamine derivatives  $[ML^6]^{2+}$  which were synthesised under metal-ion template conditions (Chapter Four).

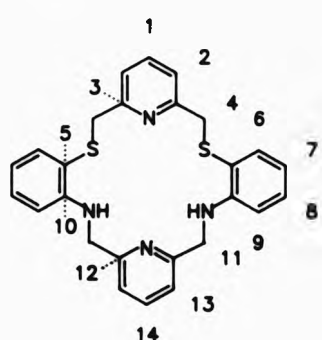
### 5.2 Synthesis and Characterisation of $L^6$ .

The synthesis of  $L^6$  has been achieved through the reductive demetallation of  $[PbL^6](H_2O)(MeOH)][ClO_4]_2$  (section 4.3) with sodium tetrahydroborate using a known reported procedure.<sup>[1]</sup>



In the infrared spectrum, a single, sharp absorbance at ca.  $3320\text{ cm}^{-1}$  can be attributed to the  $\nu(\text{N-H})$  stretching frequency of an amino function. The lack of absorptions in the region ca.  $1690\text{-}1640\text{ cm}^{-1}$  indicate absence of  $\nu(\text{C=N})$  stretching vibrations and denotes hydrolysis or reduction of the imino linkage {cf.  $[\text{PbL}^4](\text{H}_2\text{O})(\text{MeOH})][\text{ClO}_4]_2$ } in the isolated product. Additionally, the absence of bands at ca.  $1100$  and  $625\text{ cm}^{-1}$  assignable to  $\nu(\text{ClO}_4)$  ( $\nu_3$  and  $\nu_4$  of ionic perchlorate) were also absent in the spectrum which suggests removal of  $\text{Pb}(\text{ClO}_4)_2$  from the initial complex. The presence of three strong bands of equal intensities at ca.  $1600$ ,  $1510$  and  $1460\text{ cm}^{-1}$  are typical of six-membered aromatic systems (i.e. benzene and pyridine rings), added to which a strong, sharp absorbance at ca.  $750\text{ cm}^{-1}$  is characteristic of  $\nu(\text{C-H})$  out of plane deformations indicative of 1,2-disubstituted benzene and/or 2,6-disubstituted pyridines.<sup>[2]</sup> Carbon, hydrogen and nitrogen analyses (section 7.6) concur with the desired formulation and the mass spectral parent ion  $m/z$  456 corresponds to the molecular weight of  $\text{L}^6$ . Full proton (Table 5.2a) and carbon-13 (Table 5.2b) n.m.r. assignments are also in agreement with the proposed structure of  $\text{L}^6$ .

Table 5.2a  $^1\text{H}$  n.m.r. data<sup>a</sup> for  $\text{L}^6$  in  $\text{CDCl}_3$  and  $\text{CDCl}_3/\text{D}_2\text{O}$  (250.133 MHz) at ambient temperature.



$\text{CDCl}_3$	$\text{CDCl}_3/\text{D}_2\text{O}$		$\text{J}/\text{Hz}$
7.58(t)	7.60(t)	$\text{H}^{14}$	$^3\text{J}(\text{H}^{14}-\text{H}^{13}) = 7.7$
7.47(dd)	7.45(dd)	$\text{H}^6$	$^3\text{J}(\text{H}^6-\text{H}^7) = 7.6$
7.38(t)	7.41(t)	$\text{H}^1$	$^3\text{J}(\text{H}^1-\text{H}^2) = 7.7$
7.20(ddd)	7.20(ddd)	$\text{H}^8$	$^3\text{J}(\text{H}^8-\text{H}^9) = 8.2$
			$^3\text{J}(\text{H}^8-\text{H}^7) = 7.3$
			$^4\text{J}(\text{H}^8-\text{H}^6) = 1.6$
7.18(d)	7.20(d)	$\text{H}^{13}$	$^3\text{J}(\text{H}^{13}-\text{H}^{14}) = 7.7$
6.95(d)	6.97(d)	$\text{H}^2$	$^3\text{J}(\text{H}^2-\text{H}^1) = 7.7$
6.71(dd)	6.71(dd)	$\text{H}^9$	$^3\text{J}(\text{H}^9-\text{H}^8) = 8.2$
6.61(td)	6.61(td)	$\text{H}^7$	$^3\text{J}(\text{H}^7-\text{H}^{6,8}) = 7.4$
6.54(t)	-	NH	$^3\text{J}(\text{NH}-\text{H}^{11}) = 5.7$
4.36(d)	4.38(s)	$\text{H}^{11}$	$^3\text{J}(\text{H}^{11}-\text{NH}) = 5.7$
4.04(s)	4.04(s)	$\text{H}^4$	

<sup>a</sup>In p.p.m., relative to  $\text{SiMe}_4$ .

The proton n.m.r. spectrum (Figure 5.2a) of  $\text{L}^6$  integrates for twenty-four protons with resonance signals representing eleven different chemical environments. The  $\gamma$ -pyridyl protons  $\text{H}^{14}$  and  $\text{H}^1$  are both

assigned to the triplets centered at  $\delta$  7.58 p.p.m. and  $\delta$  7.38 p.p.m. respectively, whilst the  $\beta$ -pyridyl protons  $H^{13}$  and  $H^2$  are both ascribed to the doublet signals at  $\delta$  7.18 p.p.m. and  $\delta$  6.95 p.p.m. respectively.

Attachment of the substituents at the 2- and 6- positions of the pyridyl ring will influence the chemical shifts of the  $\gamma$ - and  $\beta$ -pyridyl protons. Thus, the secondary amine nitrogens are expected to shift the signals for  $H^{16}$  and  $H^{13}$  further downfield relative to the thioether donor atoms and therefore,  $H^1$  and  $H^2$  will resonate at a higher frequency on the basis of electronegativities for these substituent atoms.

The rest of the aromatic protons  $H^5-H^9$ , show the same sequence that was present in the n.m.r. spectrum of the open-chain ligand  $L^1$  (section 2.3). Proton signals for  $H^6$  and  $H^9$  display a doublet of doublets (dd) splitting pattern which arise from three- (ortho-) and four-bond (meta-) couplings to neighbouring phenylene protons. Likewise, the resonance signal due to proton  $H^7$  is a triplet of doublets (td) which is due to two, equal three-bond ortho-couplings to  $H^6$  and  $H^8$  and a four-bond meta-coupling to  $H^9$ . At the same time, the resonance signal for proton  $H^8$  is quite different and displays a doublet of doublets of doublets (ddd) splitting pattern, which is also present in the proton n.m.r. spectrum of  $L^1$ . This type of eight line multiplet has been attributed to slightly different ortho-couplings to protons  $H^7$  and  $H^9$ . From calculation of coupling constants, it appears that the larger value is due to  $^3J(H^8-H^9) = 8.2$  Hz rather than  $^3J(H^8-H^7) = 7.4$  Hz. In addition,  $H^8$  is also meta-coupled to  $H^6$ .

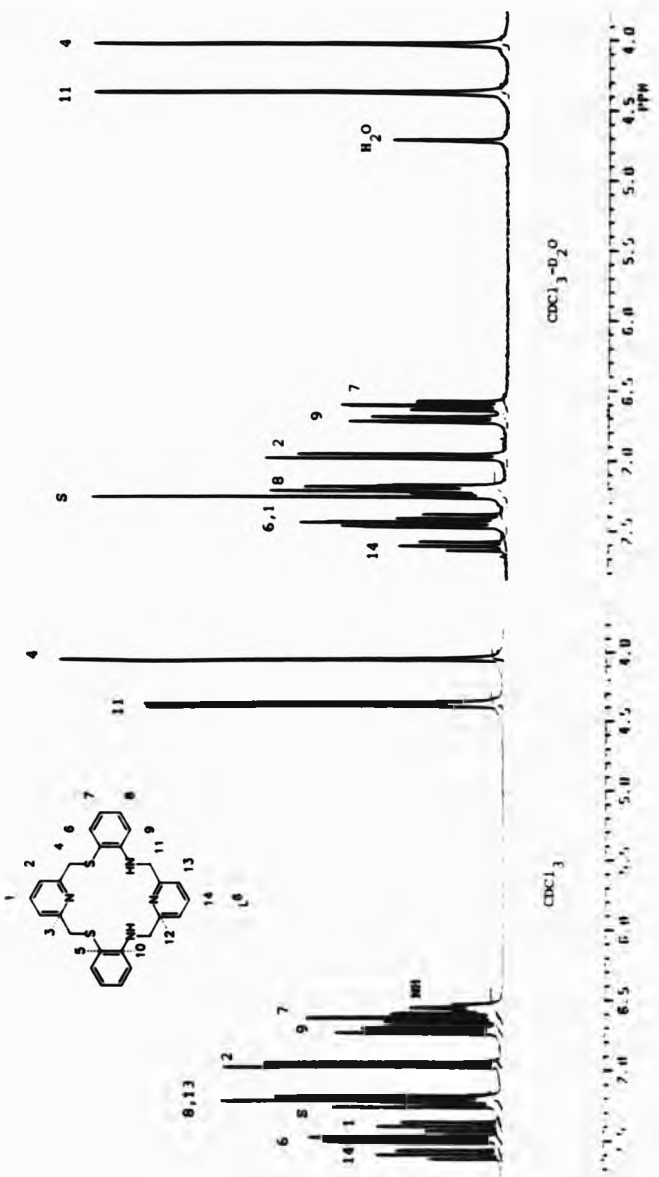


Figure 5.2a  $^1\text{H}$  n.m.r. spectrum of  $\text{L}^6$  in  $d_1$ -chloroform and  $\text{CDCl}_3/\text{D}_2\text{O}$ .

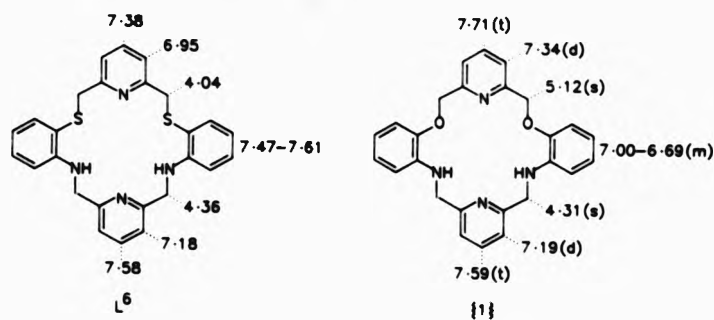
Ideally, each ortho-coupling to protons H<sup>7</sup> and H<sup>8</sup> should be dissimilar since, H<sup>7</sup> and H<sup>8</sup> are not chemically equivalent (H<sup>7</sup> is meta- to sulphur, H<sup>8</sup> is meta- to nitrogen). The methylene protons H<sup>11</sup> and H<sup>4</sup> are assigned according to shielding effects and due to their splitting patterns, namely a doublet and singlet respectively. Free rapid rotation about the C-S bonds in solution makes the methylene protons H<sup>4</sup> magnetically equivalent on the n.m.r. time scale. The same reasoning applies to the methylene protons H<sup>11</sup> as the C-N bonds are also free to rotate in solution. However, these methylene protons H<sup>11</sup> are found to couple to the acidic protons of the secondary amine with <sup>3</sup>J(H<sup>11</sup>-NH) 5.7 Hz. Likewise, the broad singlet expected for acidic protons is in fact a triplet due to methylene proton coupling, <sup>3</sup>J(NH-H<sup>11</sup>) 5.7 Hz.

As a further aid to assignment, the spectrum was re-run with two drops of deuterium oxide (D<sub>2</sub>O shake) in order to identify the acidic (exchangeable) protons. Observation of the d<sub>1</sub>-chloroform/deuterium oxide spectrum of L<sup>6</sup> revealed three significant differences compared to the previous spectrum obtained in d<sub>1</sub>-chloroform alone. Firstly, the broad triplet at δ 6.54 p.p.m. assigned to the NH protons has disappeared completely. Second, the doublet at δ 4.36 p.p.m. labelled as H<sup>11</sup>, collapsed to a singlet (cf. signal for H<sup>4</sup>) and thirdly, slight chemical shifts have occurred for the remaining resonance signals.

Clearly, in d<sub>1</sub>-chloroform the acidic protons couple with the methylene protons to give the resulting multiplets. After a D<sub>2</sub>O shake, the acidic protons exchange with deuterium in the solvent solution, consequently their signal disappears and the methylene signal also becomes decoupled. Generally, the addition of deuterium oxide to a

solvent which is immiscible with water i.e.  $d_1$ -chloroform, through degradation of uniformity can cause magnetic field inhomogeneity. This in turn leads to merging and broadening of all signals in the spectrum since, the nature of the solvent has been altered. Fortunately, in this case, although certain signals have been chemically shifted by the  $D_2O$  shake, the multiplet pattern arising from the resonance of proton  $H^8$  which was previously masked (in  $d_1$ -chloroform) can now be readily observed.

The eighteen-membered  $N_4O_2$  (1)<sup>[1]</sup> analogue of L<sup>6</sup> has also been characterised by proton n.m.r in  $d_1$ -chloroform.

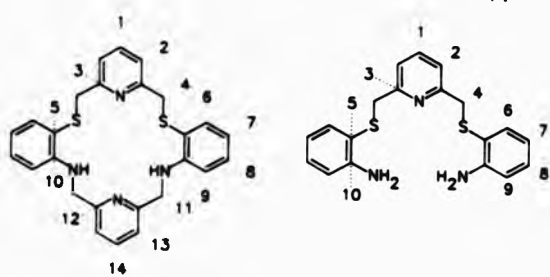


On comparing both sets of n.m.r. data, it becomes apparent that proton signals at the nitrogen-end of the macrocyclic ligands are not affected by the thioether or ether-containing moieties. In terms of heteroatom shielding effects, the pyridyl and methylene signals are chemically shifted further downfield due to oxygen and further upfield due to sulphur relative to those in the vicinity of the nitrogen donor atoms.

The broad band proton decoupled carbon-13 n.m.r. (Table 5.2b) gives rise to resonance signals denoting fourteen unique carbon environments. Assignment of the spectrum was achieved through DEPT 135,

substituent-induced shift parameters<sup>[2]</sup> and comparisons with the carbon-13 n.m.r. spectrum of L<sup>1</sup> (section 2.3). All physical and analytical data obtained has confirmed the integrity of L<sup>6</sup>.

Table 5.2b <sup>13</sup>C n.m.r. data\* for L<sup>6</sup> in CDCl<sub>3</sub> (62.896 MHz) at ambient temperature [cf. <sup>13</sup>C n.m.r. data for L<sup>1</sup> (section 2.3)].



L <sup>6</sup>		L <sup>1</sup>
157.68	c <sup>12</sup>	
157.39	c <sup>3</sup>	157.87
149.42	c <sup>10</sup>	148.83
136.98	c <sup>14</sup>	
136.60	c <sup>6</sup>	136.59
136.50	c <sup>1</sup>	136.65
130.48	c <sup>8</sup>	130.21
121.29	c <sup>13</sup>	
121.17	c <sup>2</sup>	121.48
117.50	c <sup>5</sup>	117.01
116.61	c <sup>7</sup>	118.25
110.51	c <sup>9</sup>	114.93
48.90	c <sup>11</sup>	
41.85	c <sup>4</sup>	41.35

\* In p.p.m., relative to SiMe<sub>4</sub>.

### 5.3 Co-ordination Studies of $[CuL]^{\delta^{2+}}$ and $[NiL]^{\delta^{2+}}$ .

The eighteen-membered, potentially sexidentate  $N_4S_2$  donor macrocyclic ligand  $L^{\delta}$  was found to react with only copper(II) and nickel(II) under the reaction conditions employed. Attempts to complex lead(II), silver(I), mercury(II), cadmium(II) and zinc(II) salts with  $L^{\delta}$  were unsuccessful.

#### 5.3.1 Spectroscopic Studies of $[CuL]^{\delta^{2+}}$ and $[NiL]^{\delta^{2+}}$ .

The reactions of  $L^{\delta}$  with copper(II) and nickel(II) perchlorates afforded two crystalline compounds (Table 5.3a).

Table 5.3a Electronic<sup>a</sup> and magnetic<sup>b</sup> data for  $[ML]^{\delta^{2+}}$ .

COMPLEX	COLOUR	$\lambda_{max}/nm$	$\epsilon/m^2 \text{mol}^{-1}$	$\mu_{eff}/\text{B.M.}^c$
$[CuL]^{\delta} [ClO_4]_2$	Dark green	640.5	21.21	2.01
$[NiL]^{\delta} [ClO_4]_2$	Bright purple	819.0	5.98	3.11
		518.0	3.67	

<sup>a</sup>In methanol. <sup>b</sup>Corrected for diamagnetism of ligand. <sup>c</sup>At 298 K.

The room temperature magnetic moments for both compounds indicates the isolation of paramagnetic complexes with effective magnetic moments equal to 2.01 and 3.11 B.M. for copper(II) and nickel(II) respectively. These values are typical for  $d^9$  and  $d^8$  metal ions with one and two unpaired electrons respectively<sup>[3]</sup>.

The electronic spectra obtained in methanol for the copper(II) and nickel(II) complexes give rise to absorptions at ca. 640.5 nm (copper(II)) and at ca. 819 and 518 nm (nickel(II)). Generally for copper(II) complexes a band between 900-625 nm ( $11000-16000 \text{ cm}^{-1}$ ) is

usually found for octahedral fields, whereas, bands below 500 nm ( $20000 \text{ cm}^{-1}$ ) are attributed to tetrahedral fields.<sup>[4]</sup> Hence, for  $[\text{CuL}^6][\text{ClO}_4]_2$  the absorption band at 640.5 nm has been assigned to a  ${}^2E_g - {}^2T_{2g}$  transition as found for an octahedral environment.<sup>[5]</sup> The  $d^8$  configuration gives rise to three spin-allowed transitions for both tetrahedral and octahedral complexes (section 2.4.1.1).<sup>[6]</sup> Thus, for  $[\text{NiL}^6][\text{ClO}_4]_2$  although only two bands are observed in the electronic spectrum, the band at 819 nm ( $12210 \text{ cm}^{-1}$ ) has been assigned to  ${}^3A_{2g}(F) - {}^3T_{2g}(F)$  which is equal to the crystal-field splitting ( $10Dq$ ) and the band at 518 nm is ascribed to the  ${}^3A_{2g}(F) - {}^3T_{1g}(F)$  transition in accordance with an octahedral co-ordination environment. The high-energy band due to  ${}^3A_{2g}(F) - {}^3T_{1g}(P)$  has been obscured by ligand and charge-transfer bands. The crystal-field splitting for  $L^6$  lies between that observed for 1,2-diaminoethane (en) and 2,2-bipyridyl (bipy) with nickel(II).<sup>[6]</sup>

	$\nu_1$	$\nu_2$	$\nu_3$
	$\text{nm}/(\times 10^3 \text{ cm}^{-1})$		
$[\text{Ni(en)}]^{2+}$	893(11.2)	545(18.3)	345(29.0)
$[\text{NiL}^6]^{2+}$	819(12.2)	518(19.3)	obscured by ligand and CT bands.
$[\text{Ni(bipy)}]^{2+}$	791(12.6)	521(19.2)	
$[\text{Ni(2)}]^{2+}$ <sup>[7]</sup>	785(12.7)	500(20.0)	435(23.0)

As a structural probe, the magnetic and electronic spectral data are in accord with a near octahedral co-ordination geometry for both  $[\text{ML}^6][\text{ClO}_4]_2$  complexes. This is highly probable since,  $L^6$  is potentially sexidentate and flexible enough to assume an octahedral arrangement.

The general features of the infrared spectra (Table 5.3b) were similar for both complexes. In relation to  $L^6$ , both complexes exhibit absorption bands attributed to  $\nu(N-H)$  stretching modes at much lower frequencies. For  $[CuL^6][ClO_4]_2$ , two strong bands are observed at ca. 3280 and  $3240\text{ cm}^{-1}$  which may correspond to chemically different amine nitrogens arising from differences in bonding environment or a result of coupling effects that may occur through the metal ion. In contrast,  $[NiL^6][ClO_4]_2$  has only one medium intensity band at ca.  $3240\text{ cm}^{-1}$ . The  $\nu(N-H)$  stretching frequency for  $L^6$  was at ca.  $3320\text{ cm}^{-1}$ . Clearly, metal-ion co-ordination to the amine nitrogens has caused the  $\nu(N-H)$  stretching mode to shift to lower frequencies.<sup>(8)</sup>

Table 5.3b Infrared data<sup>a</sup> for  $[ML^6]^{2+}$ .

COMPLEX	$\nu(N-H)$	$\nu_3(ClO_4)$	$\nu_4(ClO_4)$
$[CuL^6][ClO_4]_2$	3280s, 3240s	1100s(br)	630s
$[NiL^6][ClO_4]_2$	3240m	1100s(br)	630s

<sup>a</sup>In  $\text{cm}^{-1}$ , as KBr disc.

The three strong bands of equal intensity in the infrared spectrum of  $L^6$  (*vide ante*) at ca. 1600, 1510 and  $1460\text{ cm}^{-1}$  are still present in the infrared spectra of the complexes, but these bands are now of varied intensities and some are even split. Here too, metal-ion co-ordination to the pyridyl nitrogens and the mercaptoamine donor atoms will lead to differences in the vibrational modes of  $L^6$  in the two complexes. The strong, unsplit absorbances at ca. 1100 and  $630\text{ cm}^{-1}$  correspond to the  $\nu_3$  and  $\nu_4$  stretching modes of ionic perchlorate. On this basis, it is concluded that the perchlorate counterions are not co-ordinated to either of the metal centres.<sup>(8)</sup> Thus, it seems  $L^6$  has also been

isolated as its copper(II) and nickel(II) complexes and that major conformational changes have occurred to  $L^6$  on complexation.

Microanalytical data (section 7.6.2) is also consistent with the presence of both  $[ML^6][ClO_4]_2$  complexes.

Fast-atom bombardment mass spectral data (Table 5.3c) for both complexes confirms the existence of  $[ML^6]^{2+}$  with no significant higher mass peaks above a 1:1 metal-to-ligand ratio.

Table 5.3c F.a.b. mass data<sup>a</sup> for  $[ML^6]^{2+}$ .

COMPLEX	FRAGMENTATION ASSIGNMENT	MASS <sup>b</sup>	RELATIVE
			PERCENTAGE
$[CuL^6][ClO_4]_2$	$(CuL^6)ClO_4^+$	618	20
	$[CuL^6]^+$	519	100
$[NiL^6][ClO_4]_2$	$(NiL^6)ClO_4^+$	615	30
	$[NiL^6]^+$	516	100
	$[L^6]^+$	457	6

<sup>a</sup>In NOBA matrix. <sup>b</sup>Positive-ion mode.

### 5.3.2 Single-Crystal X-ray Structure of $[NiL^6][ClO_4]_2$ .

In accordance with magnetic and spectrophotometric data, the crystal structure determination of  $[NiL^6][ClO_4]_2$  has revealed a near octahedral co-ordination environment around the metal atom. The nickel(II) atom is co-ordinated to all six macrocycle donor atoms, with N(2a), N(2b), S(1a) and S(1b) defining the equatorial plane and the pyridyl nitrogens N(1c) and N(3c) occupying the axial sites [N(1c)-Ni-N(3c) 175.6(3) $^\circ$ ] of the octahedral co-ordination sphere (Figure 5.3a).

**Table 5.3d Selected co-ordination sphere bond distances and angles for  $[\text{NiL}^6](\text{ClO}_4)_2$ .**

Bond distances ( $\text{\AA}$ )		Bond angles ( $^\circ$ )	
Ni - N(1c)	1.976(9)	N(1c) - Ni - N(3c)	175.6(3)
Ni - N(2a)	2.122(8)	N(1c) - Ni - N(2a)	81.7(3)
Ni - N(2b)	2.135(8)	N(1c) - Ni - N(2b)	80.9(3)
Ni - N(3c)	2.079(8)	N(2a) - Ni - N(2b)	162.7(3)
Ni - S(1b)	2.407(3)	N(2a) - Ni - N(3c)	97.6(3)
Ni - S(1a)	2.427(3)	N(2b) - Ni - N(3c)	99.7(3)
		N(1c) - Ni - S(1b)	100.4(3)
		N(1c) - Ni - S(1a)	92.4(3)
		N(2a) - Ni - S(1b)	97.6(2)
		N(2a) - Ni - S(1a)	83.8(2)
		N(2b) - Ni - S(1b)	84.6(2)
		N(2b) - Ni - S(1a)	97.9(2)
		N(3c) - Ni - S(1b)	84.0(2)
		N(3c) - Ni - S(1a)	83.2(2)
		S(1a) - Ni - S(1b)	167.2(1)

The nickel(II)-N(anilino) bond distances [Ni-N(2a) 2.122(8); Ni-N(2b) 2.135(8)  $\text{\AA}$ ] are significantly longer than the axial nickel(II)-N(pyridyl) [Ni-N(1c) 1.976(9); Ni-N(3c) 2.079(8)  $\text{\AA}$ ] bond lengths. However, as expected the nickel(II)-sulphur bond lengths are much longer than any nickel(II)-nitrogen distance (Ni-S(1a) 2.427(3); Ni-S(1b) 2.407(3)  $\text{\AA}$ ) (Table 5.3d).

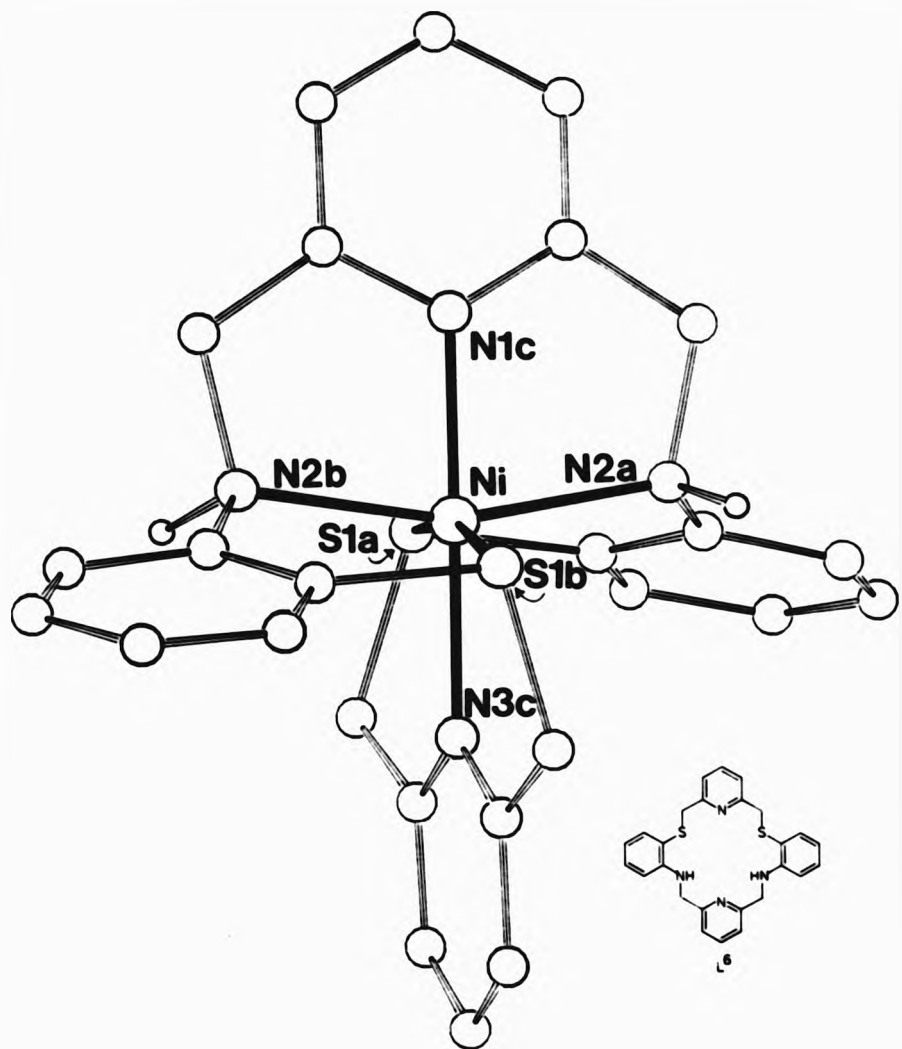


Figure 5.3a Single-crystal X-ray structure of  $[NiL^6][ClO_4]_2$ .

For  $L^6$  to assume an octahedral conformation around the nickel(II) atom, the anilino nitrogens [N(2a) and N(2b)] and the thioether donor atoms [S(1a) and S(1b)] must take up a *trans* arrangement in the equatorial plane, which in turn, cause the pyridyl rings to twist relative to each other by  $84.91^\circ$ . The nickel(II) atom sits  $-0.0260\text{ \AA}$  below a mean plane defined by the atoms N(2a), N(2b), S(1a) and S(1b). Furthermore, the anilino hydrogens are on different sides of this donor atom plane.

In comparison, the open-chain nickel(II) structure of  $L^1$  [ $\text{NiL}^1(\text{Cl})\text{Cl}\cdot\text{MeOH}$  (section 2.4.3)], also contains the anilino nitrogens and thioether donor atoms in a *trans* disposition. But the phenylene rings are coplanar with the 'equatorially defined' plane, whereas, for the present structure the phenylene rings are twisted by  $35.89^\circ$  relative to one another (Figure 5.3b).

Likewise (Figure 5.3c), an eighteen-membered  $N_6$  analogue (2),<sup>[7]</sup> is also found to co-ordinate around a nickel(II) atom in an octahedral fashion. The anilino nitrogens in the equatorial plane have an average Ni-N(anilino) bond length of  $2.041(27)\text{ \AA}$ , whilst the axially positioned pyridyl nitrogens have shorter bonds to the nickel(II) atom [Ni-N(pyridyl)  $1.910(15)\text{ \AA}$ ]. The angle of twist between the pyridyl planes is  $71.4^\circ$ . The  $N_6$  analogue (2), has also been found to complex with lead(II), silver(I), mercury(II), cadmium(II), zinc(II), iron(II), cobalt(III), nickel(II), copper(II) and manganese(II).<sup>[19]</sup> Crystal structure analyses indicate that the complexes of iron(II), cobalt(III) and copper(II) are isomorphous with the structure of  $[\text{Ni}(2)\{\text{ClO}_4\}_2]^{[7]}$ .

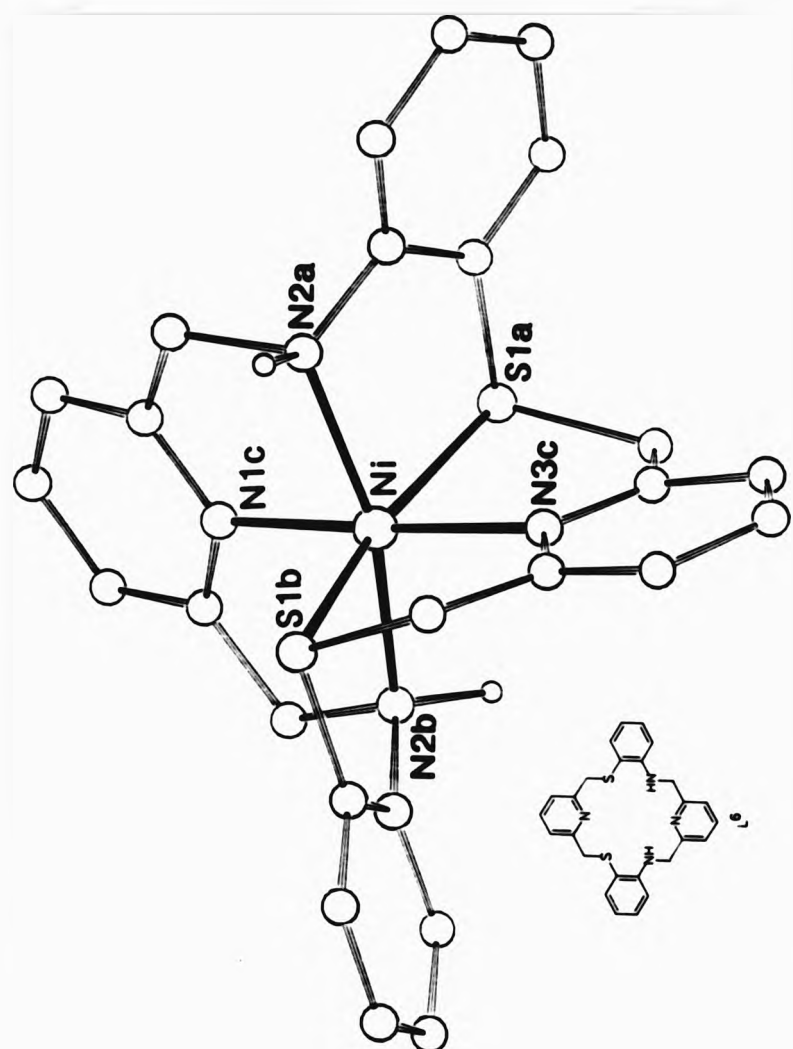


Figure 5.3b Single-crystal X-ray structure of  $[NiL^6][ClO_4]_2$ .

The previously mentioned  $N_4O_2$  analogue (1), can form complexes with the first-row transition metal ions from manganese(II) to zinc(II) with the exception of cobalt(II) and cobalt(III). As for  $L^6$ , the heavy metals lead(II), silver(I) and mercury(II) did not complex with (1), but a single-crystal X-ray analysis of  $[Cd(1)(NO_3)_2]$  denotes a distorted hexagonal bipyramidal geometry about the cadmium(II) ion.<sup>(10)</sup>

In contrast, the eighteen-membered  $N_2O_4$  analogue (3),<sup>(11)</sup> has been designed as a guest molecule for neutral hosts.

The eighteen-membered  $N_2S_4$  analogue  $L^{6x}$ , was also synthesised as part of this project (section 7.6.3), in order to increase the likelihood of toxic heavy metal interactions compared to  $L^6$ . However, no complexing behaviour was observed for this ligand under the reaction conditions employed.

For a series of  $N_2S_2$  macrocyclic ligands (4)-(6),<sup>(12)</sup> where the inner great ring increases from fourteen- to sixteen-membered, distorted octahedral geometries are inferred from the available magnetic and spectrophotometric data for complexes of (5) and (6). In agreement the crystal structure analysis of  $[Ni(5)][ClO_4]_2$  and its nitrogen and oxygen analogues all exhibit octahedral symmetries, with the donor atoms close to planar in the equatorial plane.<sup>(13)</sup> The nickel(II)-sulphur bond lengths are 2.485(1) and 2.438(1) Å and comparable to those for  $[NiL^6][ClO_4]_2$ . The S-Ni-S angle of 'bite' is 80.9°. Additionally, the amine hydrogens are on the same side of the donor atom plane for the  $N_2S_2$  and  $N_2O_2$  analogues, but for the  $N_4$  macrocyclic ligand the amine hydrogens are on opposite sides of the donor atom plane. The same orientations apply for the phenylene rings

in each case. These crystal structures indicate that the fifteen-membered macrocyclic ligands all present a cavity size that is close to ideal for high-spin nickel(II).<sup>[14]</sup>

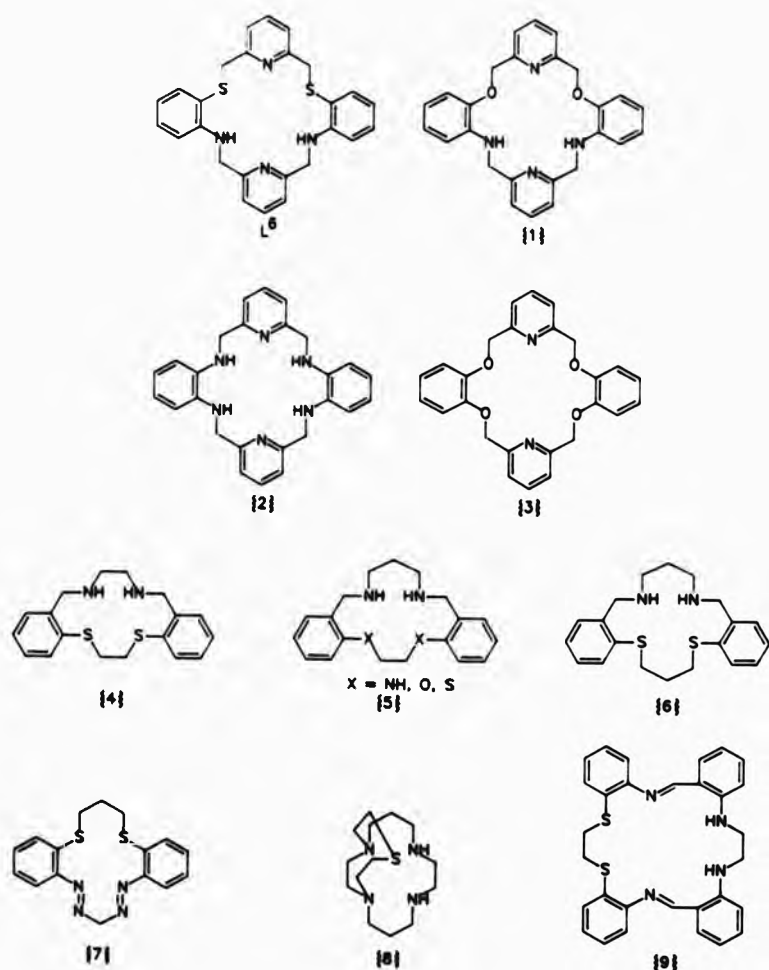


Figure 5.3c Comparable ligands of characterised nickel(II) complexes.

For a fourteen-membered  $N_4S_2$  hydrazine-derivatised macrocyclic ligand (7),<sup>[15]</sup> the nickel(II)-sulphur bond distances are 2.173(3) and 2.177(3) Å which are significantly shorter than those found for  $[\text{NiL}^6][\text{ClO}_4]_2$ . The S-Ni-S angle of 'bite' between the thioether donor atoms is 87.5(1)° which is comparable to that found for  $[\text{Ni}(5)][\text{ClO}_4]_2$ . Although the thioether donor atoms are in a trans-position in  $[\text{NiL}^6][\text{ClO}_4]_2$ , the relative S(1a)-Ni-S(1b) bond angle is found to be 167.2(1)°. Another fourteen-membered  $N_4S$  macrocyclic ligand based on cyclam (8),<sup>[16]</sup> has a pendant thioether donor atom which co-ordinates axially to nickel(II) [Ni-S 2.385(2) Å] with the pseudo octahedral co-ordination sphere being completed by a perchlorate ion. The nickel(II)-nitrogen bond lengths range from 2.055(5)-2.087(5) Å.

#### 5.4 Co-ordination Studies of $[\text{ML}^{6A-D}]^{2+}$ .

In the previous chapter, the template syntheses of  $L^4$  led to the formation of a series of diamagnetic metal-ion complexes,  $[\text{ML}^{4+}]^{m-}$  (section 4.1). In contrast, under the same stoichiometric reaction conditions in the presence of copper(II) and nickel(II) salts, the isolation of green (copper(II)) and pink-to-purple (nickel(II)) crystalline compounds was achieved depending on the reaction solvent employed (A = methanol, B = ethanol, C = propanol, D = butanol (Table 5.4a)).

##### 5.4.1 Spectroscopic Studies of $[\text{ML}^{6A-D}]^{2+}$ .

The magnetic data is consistent with all complexes being paramagnetic with the effective magnetic moments similar to those described for  $[\text{ML}^6]^{2+}$  (section 5.2). Suffice to say, all six complexes isolated are

believed to have distorted octahedral geometries.

Table 5.4a Electronic<sup>a</sup> and magnetic<sup>b</sup> data for  $[ML^{6A-0}]^{2+}$ .

COMPLEX	COLOUR	$\lambda_{\max}$ /nm	$\mu_{eff}^c$ /B.M.
$[\text{CuL}^{6A}][\text{ClO}_4]_2^d$	Dark green	640.5	1.89
$[\text{CuL}^{6B}][\text{ClO}_4]_2^e$	Dark green	640.8	2.01
$[\text{NiL}^{6A}][\text{ClO}_4]_2$	purple	825.8	518.1
$[\text{NiL}^{6B}][\text{ClO}_4]_2$	Dark pink	824.4	511.1
$[\text{NiL}^{6C}][\text{ClO}_4]_2$	Pale pink	827.2	504.1
$[\text{NiL}^{6D}][\text{ClO}_4]_2$	Baby pink	824.4	508.3

<sup>a</sup>In acetonitrile, unless stated otherwise. <sup>b</sup>Corrected for diamagnetism of ligand. <sup>c</sup>At 294 K. <sup>d</sup>In methanol. <sup>e</sup>In ethanol.

Microanalytical data (section 7.6.4-5) for these compounds agrees with the formulation on the addition of two solvent molecules each time. These molecules of alcohol can be associated with the complex in three ways. (i) Co-ordinated to the metal ion, (ii) present as lattice solvent or (iii) as a nucleophile added across a di-imine linkage to yield the carbinolamine derivative.

According to the infrared spectra (Table 5.4b), the absence of  $\nu(\text{C-N})$  bands expected for  $[\text{ML}^4]^{2+}$  complexes and the presence of  $\nu(\text{N-H})$  bands is indicative of nucleophilic addition across the di-imine functions by appropriate solvent molecules to yield the  $[\text{ML}^{6A-0}]^{2+}$  complexes. The actual  $\nu(\text{N-H})$  stretching frequencies are comparable to those found for  $[\text{ML}^6][\text{ClO}_4]_2$  (*vide ante*), such that metal-nitrogen(amine) co-ordination is present in all the complexes. Once again, bands due to benzene and pyridine rings in the region ca.  $1600-1450 \text{ cm}^{-1}$  are split with

different intensities (cf infrared of  $[ML]^{2+}$  section 5.3) but the frequency and pattern are identical for every metal complex. Likewise, the band between ca.  $1121\text{-}1090\text{ cm}^{-1}$  and ca.  $624\text{-}635\text{ cm}^{-1}$  which show no signs of splitting have been attributed to the  $\nu_3$  and  $\nu_4$  modes of ionic perchlorate.

Table 5.4b Infrared data<sup>a</sup> for  $[ML^{6A-D}]^{2+}$ .

COMPLEX	$\nu(\text{N-H})$	$\nu_3(\text{ClO}_4)$	$\nu_4(\text{ClO}_4)$
$[\text{CuL}^{6A}](\text{ClO}_4)_2$	3220m	1100s	630s
$[\text{CuL}^{6B}](\text{ClO}_4)_2$	3202m	1121s(br)	624s
$[\text{NiL}^{6A}](\text{ClO}_4)_2$	3201m	1093s	635s
$[\text{NiL}^{6B}](\text{ClO}_4)_2$	3201m	1093s	625s
$[\text{NiL}^{6C}](\text{ClO}_4)_2$	3234m	1107s	628s
$[\text{NiL}^{6D}](\text{ClO}_4)_2$	3250m	1091s	625s

<sup>a</sup>In  $\text{cm}^{-1}$ , as KBr disc.

Fast-atom bombardment mass spectral data (Table 5.4c) are consistent with the formation of a [1+1] macrocycle condensation product with a 1:1 metal-to-ligand ratio. Additionally, the loss of two R-OH molecules from each complex is evident. Of course, elimination of both alcohol molecules yields the  $[ML]^{2+}$  complexes again which appear to be more prominent in the f.a.b. mass spectra. Furthermore, in each  $[\text{NiL}^{6A-D}]^{2+}$  spectrum obtained, a mass peak at  $m/z$  404 was present which may be attributed to an open-chain nickel(II) complex (Figure 5.4a).

Table 5.4c F.a.b. mass data<sup>a</sup> for  $[ML^{6A-D}]^{2+}$ .

COMPLEX	FRAGMENTATION ASSIGNMENT	MASS <sup>b</sup>	RELATIVE
			PERCENTAGE
$(CuL^{6B})_2(CLO_4)_2$	$[CuL^{6B}]CLO_4^+$	607	86
	$[CuL^{6B}-EtOH]^+$	561	55
	$[CuL^{6B}-(EtOH)_2]^+$	515	35
$(NiL^{6A})_2(CLO_4)_2$	$[NiL^{6A}]CLO_4^+$	673	65
	$[NiL^{6A}]^+$	574	60
	$[NiL^{6A}-MeOH]^+$	541	82
	$[NiL^{6A}-(MeOH)_2]^+$	510	91
		404 <sup>c</sup>	100
$(NiL^{6B})_2(CLO_4)_2$	$[NiL^{6B}]CLO_4^+$	701	85
	$[NiL^{6B}]^+$	601	85
	$[NiL^{6B}-EtOH]^+$	561	65
	$[NiL^{6B}-(EtOH)_2]^+$	511	90
		404 <sup>c</sup>	100
$(NiL^{6C})_2(CLO_4)_2$	$[NiL^{6C}]CLO_4^+$	729	9
	$[NiL^{6C}]^+$	629	10
	$[NiL^{6C}-(Pr'OH)_2]^+$	511	100
		404 <sup>c</sup>	95
$(NiL^{6D})_2(CLO_4)_2$	$[NiL^{6D}]CLO_4^+$	757	5
	$[NiL^{6D}]^+$	658	10
	$[NiL^{6D}-Bu^nOH]^+$	583	25
	$[NiL^{6D}-(Bu^nOH)_2]^+$	510	98
		404 <sup>c</sup>	100

<sup>a</sup>In NOBA matrix. <sup>b</sup>Positive-ion mode. <sup>c</sup>Refer to figure 5.4a.

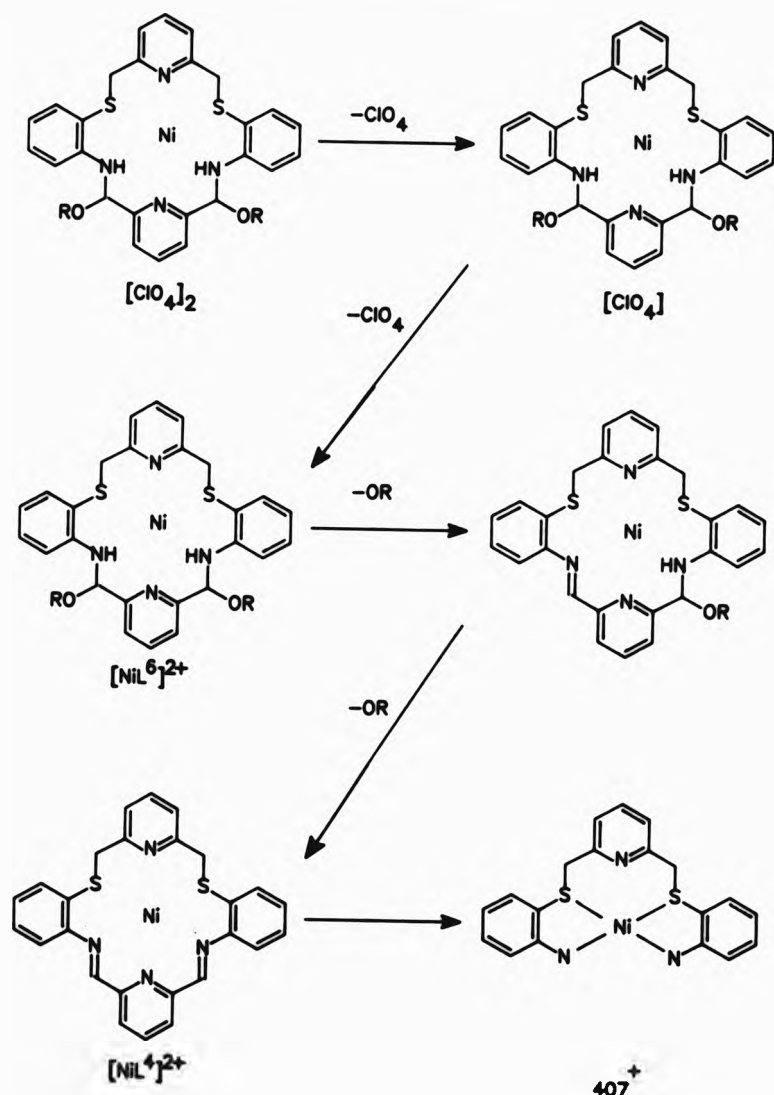


Figure 5.4a. F.a.b. mass fragmentation pattern for the  $[\text{NiL}^{6A-0}]^{2+}$  complexes.

As a representative compound of the carbinolamine derivatives of  $L^6$ , the crystal structure analysis of  $[\text{CuL}^{68}][\text{ClO}_4]_2$  was undertaken.

#### 5.4.2 Single-Crystal X-Ray Structure of $[\text{CuL}^{68}][\text{ClO}_4]_2$ .

The single-crystal X-ray structure analysis revealed the copper(II) atom to be co-ordinated to all six available donor atoms N(1c), N(2a), N(2b), N(3c), S(1a) and S(1b) of the new rearranged ligand,  $L^{68}$  with the generation of two chiral carbon centres (Figure 5.4b). The co-ordination geometry about the copper(II) atom approximates to a very distorted octahedral environment; with the equatorial sites being occupied by N(2a), N(2b), S(1a) and S(1b), and the axial positions taken up by N(1c) and N(3c), [N(1c)-Cu-N(3c) 174.0(1) $^\circ$ ] (Table 5.4d). The copper(II) atom is also closer to the nitrogen-end of the macrocycle, Cu-N(1c) 1.899(25) and Cu-N(3c) 2.034(22) Å (as for  $[\text{PbL}^6(\text{H}_2\text{O})(\text{MeOH})][\text{ClO}_4]_2$  and  $[\text{HgL}^6(\text{SCN})_2]\cdot\text{MeOH}$ ) even though the strong  $\pi$ -acceptor properties of  $L^6$  have been sacrificed, due to ligand solvolysis. In the equatorial plane, the copper(II) atom has shorter bonds to N(2a) [2.188(25) Å] and N(2b) [2.14(3) Å], whilst those to the sulphur donor atoms are much longer [Cu-S(1a) 2.694(10) and Cu-S(1b) 2.693(12) Å]. However, as expected the metal-sulphur bonds are not as long as those found in  $[\text{PbL}^6(\text{H}_2\text{O})(\text{MeOH})][\text{ClO}_4]_2$  or  $[\text{HgL}^6(\text{SCN})_2]\cdot\text{MeOH}$ . Jahn-Teller distortions are also apparent as the axial nitrogen bonds are shorter than the equatorial nitrogen bonds, with Cu-N(1c) significantly shorter than the rest of the copper(II)-nitrogen bond lengths. Co-ordination to all six donor atoms, has led to twisting of the pyridyl rings relative to each other. Thus, the phenylene rings pucker towards the sulphur end of the macrocycle, on different sides of the plane (Figure 5.4c).

Table 5.4d Selected co-ordination sphere bond distances and angles for  $[\text{CuL}^{\text{48}}](\text{ClO}_4)_2$ .

Bond distances ( $\text{\AA}$ )		Bond angles ( $^\circ$ )	
Cu - N(1c)	1.899(25)	N(1c) - Cu - N(2a)	81.0(1)
Cu - N(2a)	2.188(25)	N(1c) - Cu - N(2b)	82.0(1)
Cu - N(2b)	2.14(3)	N(2a) - Cu - S(1a)	76.9(7)
Cu - N(3c)	2.034(22)	N(2b) - Cu - S(1b)	77.2(8)
Cu - S(1a)	2.694(10)	S(1a) - Cu - S(1b)	160.3(4)
Cu - S(1b)	2.693(12)	N(3c) - Cu - S(1a)	82.0(7)
		N(3c) - Cu - S(1b)	78.7(7)
		N(1c) - Cu - N(3c)	174.0(1)

The crystal structure determination of  $[\text{Cu}(2)](\text{ClO}_4)_2$  was also found to contain shorter axial bonds to the pyridyl nitrogens in comparison to the equatorial anilino nitrogen donor atoms (Cu-N(pyridyl) 1.862(19); Cu-N(anilino) 1.977(26)  $\text{\AA}$ ). A distorted octahedral co-ordination environment is displayed by an angle of twist between the pyridyl planes of 69.4  $^\circ$ . [7]

Presumably, the driving force for ligand solvolysis is metal-ion size related. Nickel(II) and Copper(II) are both  $r_{\text{Ni(II)}} = 0.69 \text{ \AA}$ ,  $r_{\text{Cu(II)}} = 0.73 \text{ \AA}$  (hexa-co-ordinate)) relatively small in ionic radii compared to the bonding cavity available in the di-imine macrocyclic ligand L<sup>4</sup>. The intermediate rigidity of L<sup>4</sup> (section 4.1) will not allow the ligand to twist and so prevents all six potential donor atoms from coming into close proximity for effective co-ordination. Thus, solvolysis caused by the alcoholic media disrupts the chain of

conjugation when the imine carbon and nitrogen atoms ( $sp^2$ ) become  $sp^3$  hybridised which leads to free rotation and hence relief of angular strain on complexation. Folding and wrapping of the more flexible ligand  $L^{68}$  (or any other carbinolamine derivative) enables itself to take up a conformation which effectively 'reduces' the bonding cavity available to copper(II) (or nickel(II)) in order to accommodate the smaller metal-ion size.

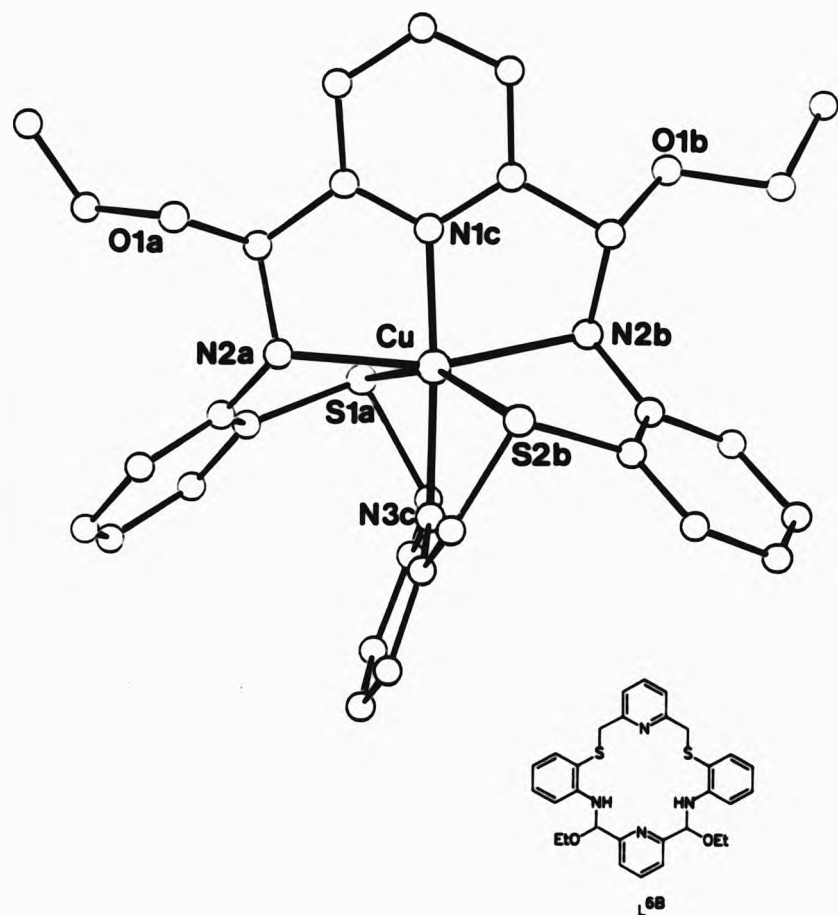


Figure 5.4b Single-crystal X-ray structure of  $[CuL^{68}][ClO_4]_2$ .

As the formation of Schiff-base complexes have been noted to proceed via the formation of carbinolamines,<sup>[17]</sup> it is thought that a combination of metal-ion size and thermodynamically favourable conditions have led to the isolation of these L<sup>6</sup> derivatives. Since, under similar experimental conditions the formation of copper(II)-imine complexes have been widely reported.<sup>[18]</sup> Nevertheless, the addition of alcohol molecules across the di-imine functions was exploited to the extent of employing 1,2-ethanediol as the reaction solvent in order to realise if an interaction could be prompted which would lead to the formation of derivatised pendant arms. However, under these conditions no characterisable products could be isolated from the reaction mixture.

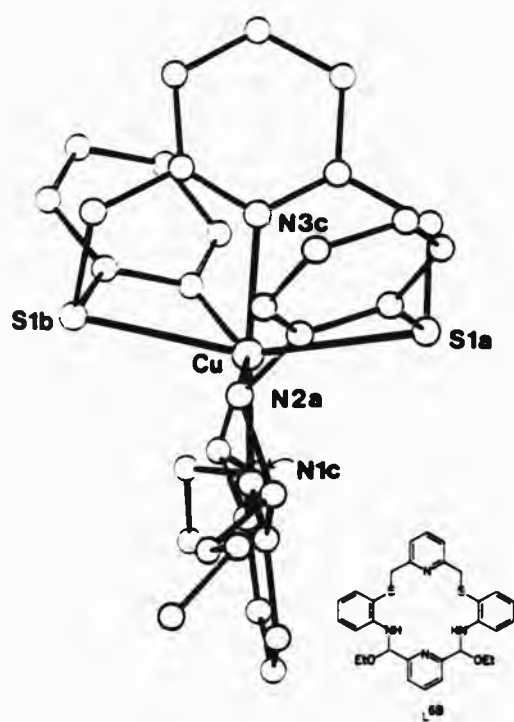


Figure 5.4c Single-crystal X-ray structure of  $[\text{CuL}^{68}](\text{ClO}_4)_2$ .

In an attempt to isolate the di-imine ( $L^4$ ) complexes of copper(II) and nickel(II), acetonitrile was used instead of an alcoholic solvent but this led to degradation of products in the case of copper(II) and intractable tars were obtained for the nickel(II) reactions. Although, on occasions, in the presence of nickel(II) a dark red-yellow solid could be isolated as the initial product from reactions in alcohol or acetonitrile, however, quantities were always minute and conclusive characterisation has not been achieved.

In fact, a twenty-membered  $N_4S_2$  schiff-base macrocyclic ligand (9)<sup>[19]</sup> and its  $N_2S_4$ <sup>[20]</sup> analogue which are also of intermediate rigidity like  $L^4$ , have the ability to take up a pseudo octahedral donor atom arrangement about the central metal ion and consequently, ring hydrolysis does not occur.

*References - Chapter Five.*

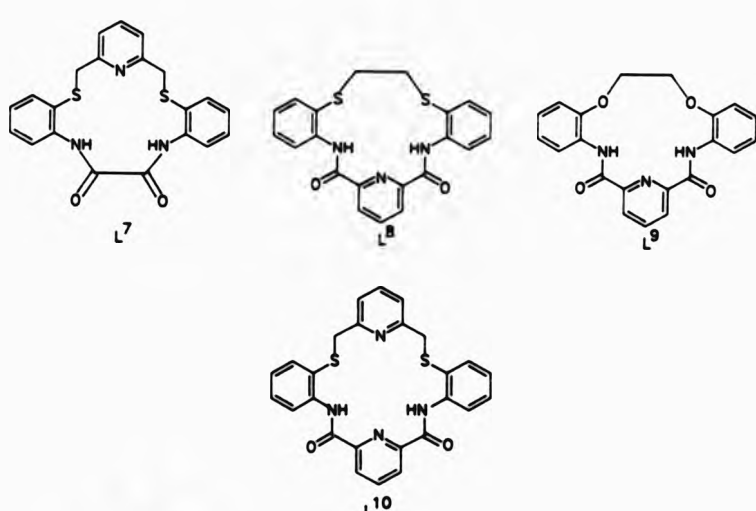
1. D. E. Fenton, B. P. Murphy, A. J. Leong, L. F. Lindoy, A. Bashall and M. McPartlin, *J. Chem. Soc., Dalton Trans.*, 1987, 2543.
2. D. H. Williams and I. Fleming, 'Spectroscopic Methods in Organic Chemistry,' McGraw-Hill, London, (4th edn) 1988.
3. D. Nicholls, 'Complexes and First Row Transition Elements,' Macmillan Press Ltd, London, 1974.
4. B. N. Figgis in 'Comprehensive Coordination Chemistry,' G. Wilkinson (ed), Pergamon Press, Oxford, 1987, vol 1, pp. 213-279.
5. R. W. Hay, N. Govan and M. P. Pujari, *J. Chem. Soc., Dalton Trans.*, 1987, 963.
6. N. N. Greenwood and A. Earnshaw, 'Chemistry of The Elements,' Pergamon Press, Oxford, 1984.
7. S. Chaudhary, Proceedings of the 16th International Symposium on Macroyclic Chemistry, Sheffield, 1991.
8. K. Nakamoto, 'Infrared Spectra of Inorganic and Coordination Compounds,' Wiley-Interscience, New York, (2nd edn) 1970.
9. S. Chaudhary, personal communication.
10. K. R. Adam, S. Donnelly, A. J. Leong, L. F. Lindoy, B. J. McCool, A. Bashall, M. R. Dent, B. P. Murphy, M. McPartlin, D. E. Fenton and P. A. Tasker, *J. Chem. Soc., Dalton Trans.*, 1990, 1635.
11. M. Newcomb, G. W. Gokel and D. J. Cram, *J. Am. Chem. Soc.*, 1974, 96, 6810.
12. L. F. Lindoy and R. J. Smith, *Inorg. Chem.*, 1981, 20, 1314.
13. L. A. Drummond, K. Henrick, M. J. L. Kanagasundaram, L. F. Lindoy, M. McPartlin and P. A. Tasker, *Inorg. Chem.*, 1982, 21, 3923.
14. K. Henrick, L. F. Lindoy, M. McPartlin, P. A. Tasker and M. P. Wood, *J. Am. Chem. Soc.*, 1984, 106, 1641.
15. P. B. Donaldson, P. A. Tasker and N. W. Alcock, *J. Chem. Soc.,*

*Dalton Trans.*, 1976, 2262.

16. D. G. Fortier and A. McAuley, *Inorg. Chem.*, 1989, **28**, 655.
17. L. T. Taylor, F. L. Urbach and D. H. Busch, *J. Am. Chem. Soc.*, 1969, **91**, 1072.
18. (a) J. Hunter, J. Nelson, C. Harding, M. McCann and V. McKee, *J. Chem. Soc., Chem. Commun.*, 1990, 1148. (b) A. Hussein, Y. Sulfab and M. Nasreldin, *Inorg. Chem.*, 1989, **28**, 157. (c) D. E. Fenton and G. Rossi, *Inorg. Chim. Acta.*, 1985, **98**, L29. (d) S. M. Nelson and C. V. Knox, *J. Chem. Soc., Dalton Trans.*, 1983, 2525. (e) M. G. B. Drew, J. Nelson and S. M. Nelson, *J. Chem. Soc., Dalton Trans.*, 1981, 1678; 1685.
19. P. A. Tasker and E. B. Fleischer, *J. Am. Chem. Soc.*, 1970, **92**, 7072.
20. L. F. Lindoy and D. H. Busch, *J. Am. Chem. Soc.*, 1969, **91**, 4690.

CHAPTER SIX

SYNTHESSES, CHARACTERISATION AND CO-ORDINATION STUDIES OF FOUR  
MIXED-DONOR DIOXO MACROCYCLIC LIGANDS  $L^7-L^{10}$ .



$ML^{10}$  should read  $[ML^{10}-2H]$

#### 6.1 General Introduction.

The macrocyclic ligands discussed in this chapter all contain the rigid dioxo (diamide) moiety. The first three ligands L<sup>7</sup>-L<sup>9</sup> are fifteen-membered, with L<sup>7</sup> and L<sup>8</sup> having an N<sub>3</sub>S<sub>2</sub> donor set whilst L<sup>9</sup> contains an N<sub>3</sub>O<sub>2</sub> donor arrangement. Ligand L<sup>10</sup> is eighteen-membered with a potentially sexidentate N<sub>4</sub>S<sub>2</sub> donor atom disposition.

The incorporation of rigid dioxo functional groups has led to diminished ligand reactivity in comparison to the fifteen and eighteen-membered macrocyclic ligands discussed previously (cf. L<sup>3</sup> and L<sup>6</sup> (Chapter 3+4), L<sup>6</sup> (Chapter 5)).

#### 6.2 Syntheses and Characterisation of L<sup>7</sup>-L<sup>10</sup>.

Syntheses of the dioxo macrocyclic ligands have been effected by the reaction of a diamine and a diacid chloride under conditions of high dilution in dichloromethane. The open-chain diamine L<sup>1</sup> (Chapter Two) was employed for the syntheses of L<sup>7</sup> and L<sup>10</sup>, whereas, (1) and (2)<sup>[1]</sup> were the open-chain diamine precursors used in the syntheses of L<sup>8</sup> and L<sup>9</sup> respectively. In each case, the diamine ligands were cyclised with 2,6-pyridinedicarbonyl dichloride with the exception of L<sup>7</sup> where oxaloyl chloride was employed to effect ring closure (Figure 6.2a). Consequently, the isolation and characterisation of the metal-free macrocyclic ligands could be carried out prior to complexation since, the presence of a metal-ion was not required to bring about the final cyclisation step in the formation of the respective products.

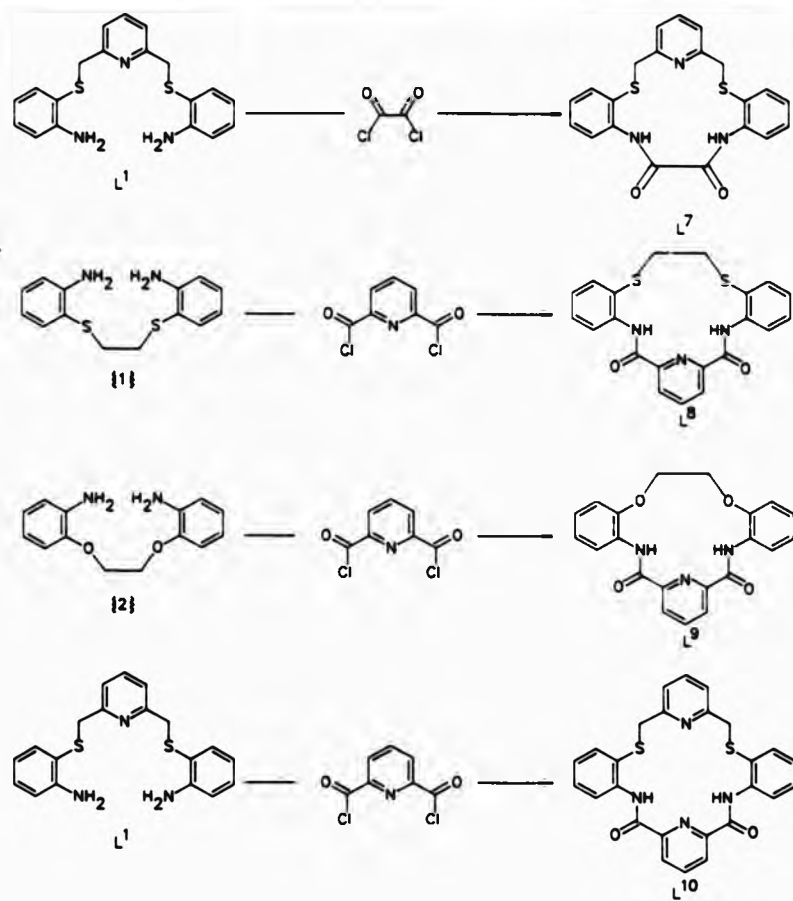


Figure 6.2a Synthetic scheme for syntheses of  $L^7-L^{10}$ .

All four solids isolated were insoluble in alcohol or acetonitrile but soluble in hot dichloromethane and *N,N*-dimethylformamide (DMF). The infrared data (Table 6.2a) for all four macrocyclic ligands  $L^7-L^{10}$  were indicative of amide formation due to the presence of absorption bands between ca.  $3460-3400\text{ cm}^{-1}$  and ca.  $1680-1630\text{ cm}^{-1}$  attributed to  $\nu(\text{N-H})$  and  $\nu(\text{C=O})$  (amide I) stretching vibration modes respectively. In addition, combination bands due to  $\nu(\text{C-N})$  stretching and  $\delta(\text{N-H})$  deformations (amide II) occur between ca.  $1570-1515\text{ cm}^{-1}$ . A further

band (amide V) which is also diagnostic for amides is usually present at ca.  $720\text{ cm}^{-1}$ .<sup>[2]</sup> The mass spectral parent ion ( $m/z$ ) for each compound is also in agreement with that of the desired products.

Table 6.2a Infrared data<sup>a</sup> for  $L^7-L^{10}$ .

COMPOUND	$\nu(\text{N-H})$	$\nu(\text{C=O})$	$\nu(\text{bz/py}), \text{Amide II}$	Amide V	$m/z$
$L^7$	3276s	1686s	1575s, 1513s, 1438s	768s	407
$L^8$	3267s	1686s	1578s, 1535s, 1443s	745s, 730s	407
$L^9$	3360s	1685s	1600s, 1540s, 1445s	740s, 720s	375
$L^{10}$	3320s, 3280s	1680s	1579s, 1528s, 1439s(sp)	749s	484

<sup>a</sup>In  $\text{cm}^{-1}$ , as KBr disc.

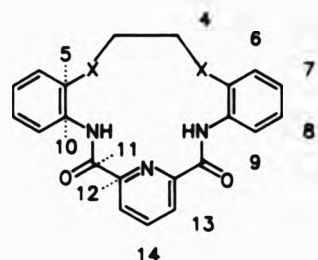
Microanalyses for the ligands  $L^7-L^{10}$  (section 7.7-10) were consistent with the formulation of (1+1) cycloadditions having taken place.

Further characterisation by n.m.r. has also been achieved for  $L^8$  and  $L^9$  (Tables 6.2b-c) and  $L^{10}$  (Tables 6.2d-e). Unfortunately,  $L^7$  was not adequately soluble for proton or carbon-13 n.m.r. analyses. When spectra were obtained in  $d_6$ -chloroform or  $d_7$ -DMF signals were weak and very broad possibly due to ligand-solvent interactions.

For  $L^8$  and  $L^9$ , the proton spectra (Table 6.2b) both integrate for seventeen protons in agreement with the proposed macrocyclic ligands. The gross features of both spectra were quite different, in that,  $L^9$  shows more merging and second-order effects for the aromatic signals compared to  $L^8$ . In the proton spectrum of  $L^8$  (Figure 6.2b), the  $\gamma$ - and  $\beta$ -pyridyl protons  $H^{14}$  and  $H^{13}$  show an eight line multiplet collectively reminiscent of an  $A_2B$  spin system (Appendix A). The remaining aromatic

signals  $H^6-H^9$  appear as either doublet of doublets (dd) or triplet of doublets (td) depending on the extent of ortho- and meta-couplings amongst themselves.

Table 6.2b  $^1H$  n.m.r. data<sup>a</sup> for  $L^8$  and  $L^9$  (250.133 MHz) in  $CDCl_3$  at ambient temperature.<sup>b</sup>



$L^8$	$^3J$	$^4J$	$L^9$
11.66(s) NH			10.83(s) NH
8.52(dd) $H^9$	8.2	1.3	8.73(m) $H^9$
8.46(m) <sup>c</sup> $H^{13}$			8.47(d) <sup>c</sup> $H^{13}$
8.18(t) <sup>c</sup> $H^{14}$			8.14(m) <sup>c</sup> $H^{14}$
7.53(dd) $H^6$	7.8	1.5	7.11(m) $H^{6-8}$
7.40(td) $H^8$	7.8	1.3	
7.15(td) $H^7$	7.6	1.4	
3.20(s) $H^4$			4.50(s) $H^4$

<sup>a</sup>In p.p.m., relative to  $SiMe_4$ . <sup>b</sup>Numbered in an equivalent manner to  $L^6$  (section 5.2) and to  $L^{10}$  (Table 6.2e) i.e.  $H^{1-3}$  do not exist.

<sup>c</sup>Assigned as an  $A_2B$  spin system.

In the proton spectrum of  $L^9$  (Figure 6.2c), the  $\gamma$ - and  $\beta$ -pyridyl protons  $H^{14}$  and  $H^{13}$  appear as a doublet (d) and a four line multiplet respectively. However, the signal for  $H^9$  is a complicated multiplet instead of the usually predicted doublet of doublets (dd) (section 5.2

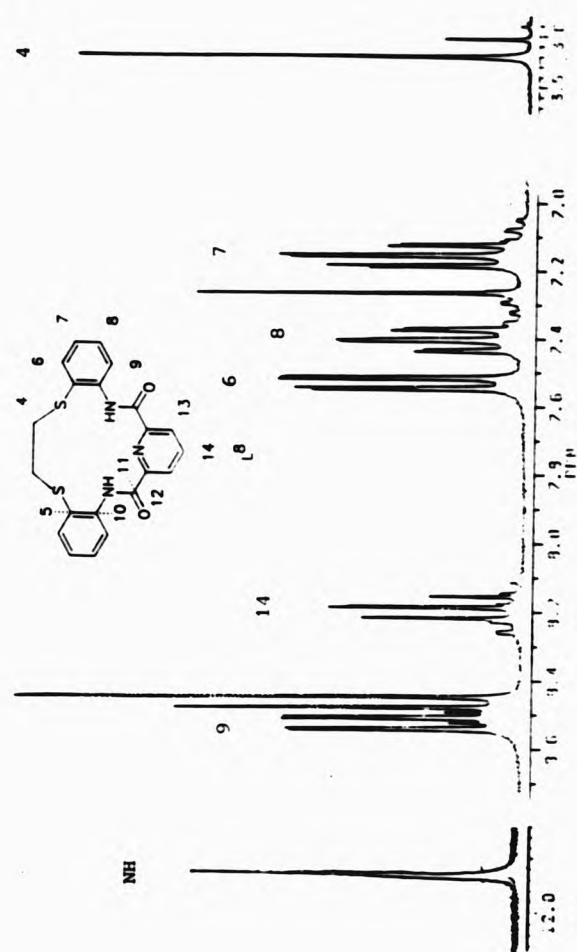


Figure 6.2b  $^1\text{H}$  n.m.r. spectrum of  $\text{L}^8$  in  $d_6$ -chloroform.

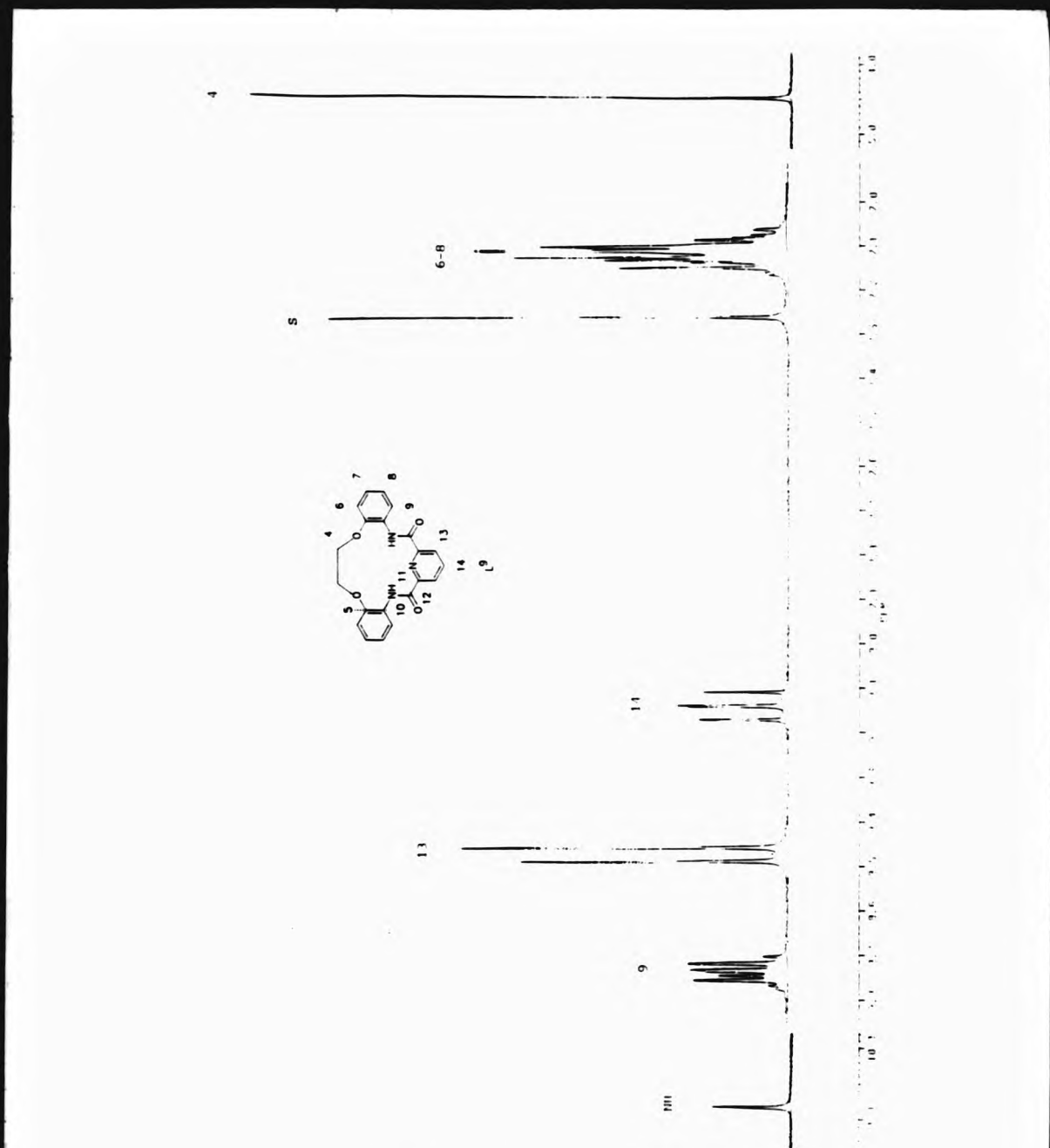


Figure 6.2c  $^1\text{H}$  n.m.r. spectrum of  $\text{L}^9$  in  $d_6$ -chloroform.

or Table 6.2d), which may be due to an overlap with the  $A_2B$  spin system exhibited in part by  $H^{13}$  (which instead is a multiplet rather than the assumed doublet). The rest of the aromatic proton signals  $H^{6-8}$  are clumped together, centered at  $\delta$  7.11 p.p.m. over a wide range ( $\delta$  7.17-7.06 p.p.m.).

For both compounds  $L^8$  and  $L^9$ , the acidic (exchangeable) protons  $NH$  appear as broad singlets at  $\delta$  11.66 and 10.83 p.p.m. respectively. Since, the amine protons ( $NH$ ) are expected to fast exchange in solution with solvent molecules and the fact that the nearest neighbouring proton is four bonds away ( $H^9$ ), coupling with ligand protons is unlikely to occur or be detected - unlike that observed in the proton n.m.r. of  $L^6$  (section 5.2). The methylene proton signal  $H^4$ , is the most upfield singlet in both spectra with the more electronegative ether oxygen drawing electron density away from the methylene protons compared to the thioether donor atoms.

The carbon-13 broad band proton decoupled n.m.r. spectra for both compounds  $L^8$  and  $L^9$  (Table 6.2c) give rise to eleven signals corresponding to eleven unique carbon environments. Full assignment has been achieved through  $^1H, ^{13}C$ -COSY spectra and substituent induced shift parameter calculations. The most downfield and upfield signals are assigned to  $C^{11}$  and  $C^4$  respectively since, the strong electron-withdrawing effects of the carbonyl oxygen will render that carbon site the most electron deficient (i.e.  $\delta+$ ) and the methylene carbons always resonate at lower frequencies compared to aromatic carbon atoms. As a consequence of the differing electronic effects imposed by sulphur and oxygen, the aromatic and quaternary carbon signals resonate at slightly different frequencies with  $C^5, C^6, C^8$  and

$C^{10}$  being chemically shifted the greatest between the two compounds  $L^8$  and  $L^9$ .

Table 6.2c  $^{13}C$  n.m.r. data<sup>a</sup> for  $L^8$  and  $L^9$  (62.896 MHz) in  $CDCl_3$  at ambient temperature.

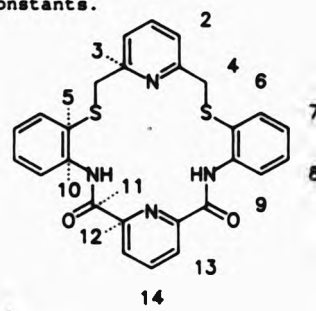
$L^8$		$L^9$	
160.71	$c^{11}$	160.53	$c^{11}$
148.63	$c^{12}$	148.69	$c^{12}$
140.06	$c^{14}$	147.01	$c^5$
138.89	$c^{10}$	139.72	$c^{14}$
133.28	$c^6$	128.64	$c^{10}$
129.31	$c^8$	124.96	$c^{13}$
124.86	$c^{13}$	124.09	$c^7$
124.82	$c^7$	122.85	$c^8$
122.92	$c^5$	119.35	$c^9$
120.45	$c^9$	113.42	$c^6$
34.77	$c^4$	68.24	$c^4$

<sup>a</sup>In p.p.m., relative to  $SiMe_4$ .

For  $L^{10}$ , the proton and carbon-13 n.m.r. spectra (Tables 6.2d-e) were obtained in both  $d_1$ -chloroform and  $d_7$ -DMF. In both cases, the proton n.m.r. (Figures 6.2d-e) integrates for twenty protons. The most downfield singlets are broad and attributed to the acidic amine protons NH. As previously, the  $\gamma$ - and  $\beta$ -pyridyl protons  $H^{14}$  and  $H^{13}$  are assigned as an  $A_2B$  spin system (Appendix A) which is more pronounced in  $d_7$ -DMF rather than in  $d_1$ -chloroform. The  $\gamma$ - and  $\beta$ -pyridyl protons  $H^1$  and  $H^2$  are a triplet and doublet respectively, further upfield relative to the pyridyl protons  $H^{14}$  and  $H^{13}$  contained within the amide moiety of

the ligand. The remaining aromatic protons H<sup>6</sup>-H<sup>9</sup> are both doublet of doublets (dd), whilst the signals for H<sup>7</sup> and H<sup>8</sup> appear as a triplet of triplets (t<sup>2</sup>) in the n.m.r. spectrum.

Table 6.2d <sup>1</sup>H n.m.r. data<sup>a</sup> for L<sup>10</sup> in CDCl<sub>3</sub> (250.133 MHz) and (CD<sub>3</sub>)<sub>2</sub>NDCO (250.134 MHz) at ambient temperature together with three- and four-bond coupling constants.



CDCl <sub>3</sub>	<sup>3</sup> J	<sup>4</sup> J	(CD <sub>3</sub> ) <sub>2</sub> NDCO	<sup>3</sup> J	<sup>4</sup> J
p.p.m.	Hz		p.p.m.	Hz	
10.74(s)	NH		10.86(s)	NH	
8.47(d) <sup>b</sup>	H <sup>13</sup>	7.8	8.46(m) <sup>b</sup>	H <sup>14,13</sup>	
8.14(t) <sup>b</sup>	H <sup>14</sup>				
7.95(dd)	H <sup>9</sup>	8.0 1.4	7.91(dd)	H <sup>9</sup>	8.0 1.5
7.62(dd)	H <sup>6</sup>	7.8 1.6	7.74(dd)	H <sup>6</sup>	7.7 1.5
7.34(td)	H <sup>8</sup>	7.7 1.6	7.52(t)	H <sup>1</sup>	7.7
7.29(t)	H <sup>1</sup>	7.7	7.37(td)	H <sup>8</sup>	7.7 1.6
7.17(td)	H <sup>7</sup>	7.6 1.5	7.25(td)	H <sup>7</sup>	7.6 1.5
6.86(d)	H <sup>2</sup>	7.7	7.14(d)	H <sup>2</sup>	7.7
4.04(s)	H <sup>4</sup>		4.28(s)	H <sup>4</sup>	

<sup>a</sup>Relative to SiMe<sub>4</sub>. <sup>b</sup>Assigned as an A<sub>2</sub>B spin system.

doublets (td) in each case. Finally, the most downfield singlets in both solvents are attributed to the methylene protons H<sup>4</sup>. Clearly, the proton signals have become chemically shifted in the two different

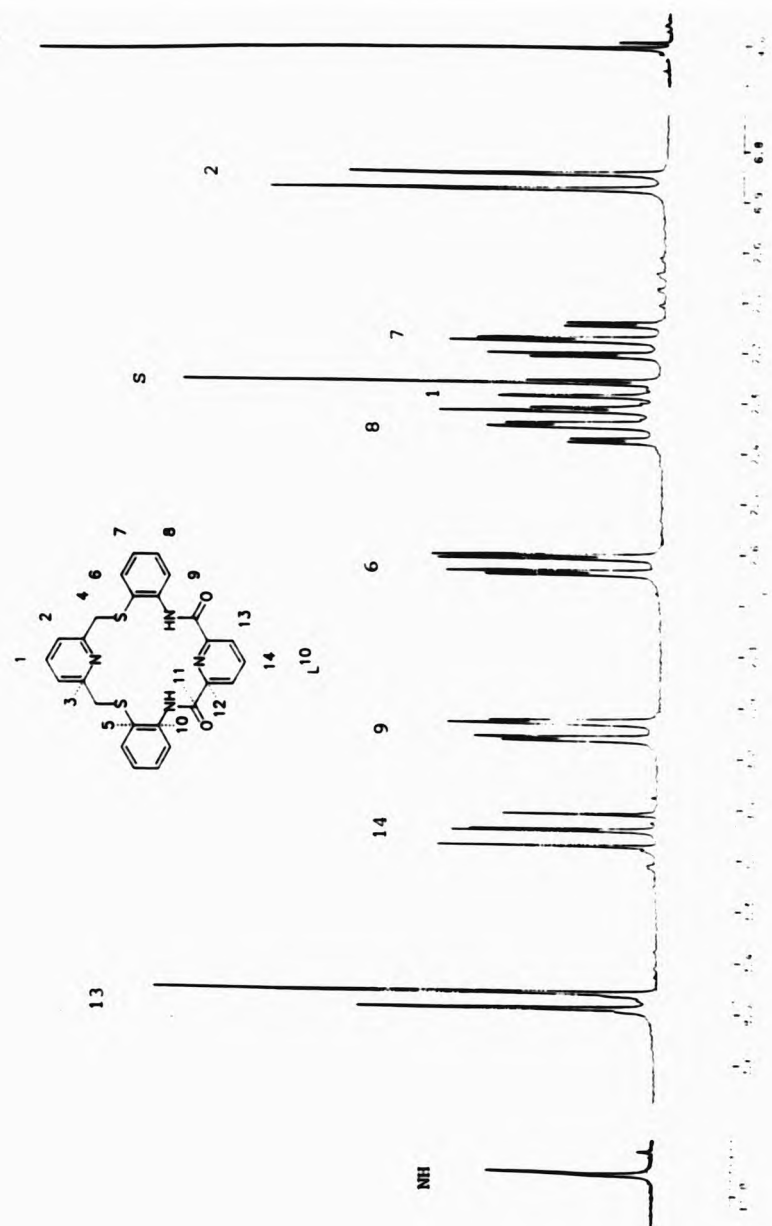


Figure 6.2d  $^1\text{H}$  n.m.r. spectrum of  $\text{L}^{10}$  in  $d_6$ -chloroform.

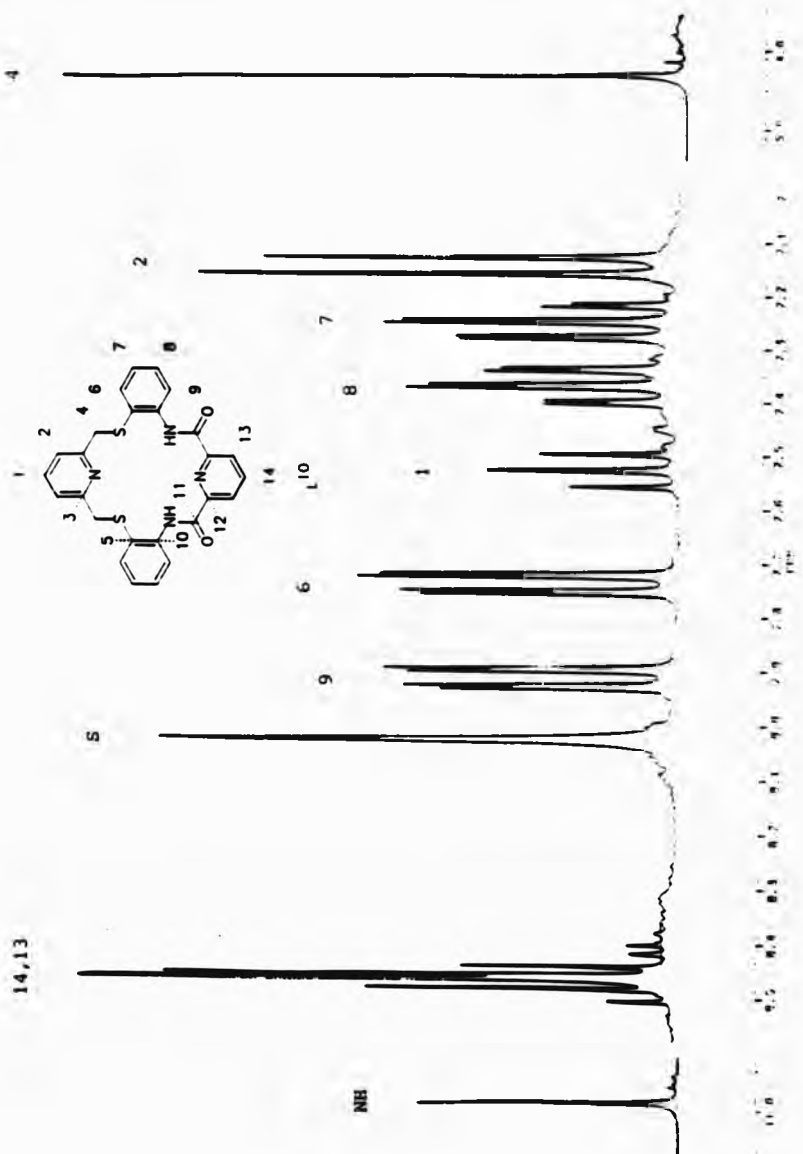


Figure 6.2e  $^1\text{H}$  n.m.r. spectrum of L<sup>10</sup> in d<sub>7</sub>-DMF.

solvents. The proton signals that have been chemically shifted to a greater degree are H<sup>14</sup>, H<sup>1</sup>, H<sup>2</sup> and H<sup>4</sup> by Δδ 0.3, 0.23, 0.28 and 0.24 p.p.m. respectively (Δδ = δ d<sub>7</sub>-DMF - δ d<sub>1</sub>-chloroform).

Table 6.2e <sup>13</sup>C n.m.r. data\* for L<sup>10</sup> in CDCl<sub>3</sub> (62.896 MHz) and (CD<sub>3</sub>)<sub>2</sub>NDCO (62.896 MHz) at ambient temperature.

CDCl <sub>3</sub>		(CD <sub>3</sub> ) <sub>2</sub> NDCO	
161.62	c <sup>11</sup>	162.70	c <sup>11</sup>
156.96	c <sup>12</sup>	157.56	c <sup>12</sup>
148.73	c <sup>3</sup>	149.56	c <sup>3</sup>
139.57	c <sup>14</sup>	141.30	c <sup>14</sup>
138.92	c <sup>1</sup>	139.04	c <sup>10</sup>
137.06	c <sup>10</sup>	137.97	c <sup>1</sup>
134.80	c <sup>6</sup>	134.01	c <sup>6</sup>
129.35	c <sup>8</sup>	129.33	c <sup>8</sup>
127.58	c <sup>5</sup>	128.90	c <sup>5</sup>
126.22	c <sup>7</sup>	126.82	c <sup>7</sup>
125.35	c <sup>13</sup>	125.83	c <sup>13</sup>
124.05	c <sup>9</sup>	124.98	c <sup>9</sup>
121.91	c <sup>2</sup>	122.79	c <sup>2</sup>
42.04	c <sup>4</sup>	40.91	c <sup>4</sup>

\*In p.p.m., relative to SiMe<sub>4</sub>.

The carbon-13 broad band proton decoupled spectra in both solvents are very similar and contain signals denoting fourteen unique carbon environments (Table 6.2e).

### 6.3 Co-ordination Studies of $[ML^{7-10}]$ .

Metal salts of lead(II), silver(I), mercury(II), cadmium(II), zinc(II), copper(II), nickel(II), and platinum(II) were used to determine the complexing behaviour of the macrocyclic dioxo ligands  $L^{7-10}$ . The ligands  $L^7$ ,  $L^8$  and  $L^{10}$  were found to be effective complexing agents for copper(II). In addition,  $L^{10}$  could also be isolated as its platinum(II) complex. In contrast, the  $N_3O_2$  macrocyclic ligand  $L^9$ , could not be complexed with any metal ions under the reaction conditions employed.

#### 6.3.1 Spectroscopic studies of $[ML^{7-10}]$ .

The room temperature magnetic moments (Table 6.3a) are unremarkable for  $d^9$  metal-ion complexes. The Electronic spectra for the copper(II) complexes of  $L^8$  and  $L^{10}$  obtained are not in accord with the existence of octahedral species in solution.<sup>[3]</sup> The absorption maxima are difficult to assign but necessarily arise from transitions of low symmetry complexes.<sup>[4]</sup>

Table 6.3a. Electronic<sup>a</sup> and magnetic<sup>b</sup> data for  $[CuL^8]$  and  $[CuL^{10}]$ .

	COLOUR	$\lambda_{\max}/\text{nm}$	$\epsilon/\text{m}^2 \text{mol}^{-1}$	$\mu_{\text{eff}}/\text{B.M.}$
$[CuL^8]$	Grey	708.5	36.50	1.82 <sup>c</sup>
		540.0	22.55	
$[CuL^{10}]$	Green	700.0	26.01	1.87 <sup>d</sup>
		584.0	32.93	

<sup>a</sup>In DMP. <sup>b</sup>Corrected for diamagnetism of the ligand. <sup>c</sup>At 300 K. <sup>d</sup>At 299 K.

Model studies indicate that the quinquedentate  $N_3S_2$  macrocyclic ligand

$L^8$  cannot conform to a nido-octahedral co-ordination environment and although  $L^{10}$  is potentially sexidentate the dioxo-containing moiety is not flexible enough to assume part of an octahedral arrangement.

Table 6.3b. Infrared data<sup>a</sup> for the complexes  $[ML^{7-10}]$ .

	$\nu(OH)$	$\nu(C=O)$	$\nu(bz/py)$	Amide V
$[CuL^7]$		1610s	1580s, 1480s	770m
$[CuL^8]$		1636s	1617s, 1464s	753m
$[CuL^{10}]$	3512m, 3451m	1609s	1574s, 1466s	756m
$[PtL^{10}]$		1640s	1620s, 1600s, 1590s	750m

<sup>a</sup>In  $\text{cm}^{-1}$ , as KBr disc.

The infrared spectra (Table 6.3b) for each complex isolated did not contain any bands due to  $\nu(N-H)$  stretches attributable to the amide functions [cf. the free ligands (section 6.2)]. Additionally, the amide I band ( $\nu(C=O)$ ) for each complex has lowered in frequency. It is apparent that on co-ordination, deprotonation of the amide nitrogen occurs and consequent delocalisation effectively decreases the carbonyl bond order, hence, shifting  $\nu(C=O)$  to lower frequencies.<sup>[2]</sup> On the other hand, the amide V band has been known to shift to higher frequencies on metal-ion co-ordination.<sup>[5]</sup> For  $[CuL^{10}]$ , the two bands at ca. 3512 and  $3451 \text{ cm}^{-1}$  are in the region where lattice water absorbs ( $\nu(O-H)$  antisymmetric and symmetric stretchings -  $3550-3200 \text{ cm}^{-1}$ ).<sup>[6]</sup> Such an assignment is valid since, the preparation of  $[CuL^{10}]$  does not proceed unless water is present in the reaction mixture, whereupon, the dark green solution begins to yield a dark green crystalline solid leaving behind a pale blue solution with an acetic acid odour when the reaction is complete.

Microanalyses (section 7.7-10) are indicative of the formation of complexes with 1:1 metal-to-ligand ratios in the deprotonated state.

Fast-atom bombardment mass spectral data (Table 6.3c) gives base peaks also corresponding to the presence of deprotonated species.

Table 6.3c. F.a.b. mass spectral data<sup>a</sup> for  $[ML^8]$  and  $[ML^{10}]$ .

COMPLEX	FRAGMENTATION ASSIGNMENT	MASS <sup>b</sup>	RELATIVE
			PERCENTAGE
$[CuL^8]$	$[CuL^8]^+$	469	20
$[CuL^{10}]$	$[CuL^{10}]^+$	546	15
$[PtL^{10}]$	$[PtL^{10}]^+$	678	100

<sup>a</sup>In NOBA matrix. <sup>b</sup>Positive-ion mode.

The e.s.r. spectra recorded (Table 6.3d) for  $[CuL^8]$  and  $[CuL^{10}]$  are typical for mononuclear complexes, exhibiting in each case a four line hyperfine splitting pattern. According to the g components, with  $g_{\parallel}$  being greater than  $g_{\perp}$  the results are consistent with an axially elongated conformation. Thus, the single unpaired electron arising from the d<sup>9</sup> configuration of copper(II) occupies the  $d_{x^2-y^2}$  orbital which leads to the predicted ordering of g values  $g_{\parallel} > g_{\perp} > 2.0$  in the ground state.<sup>[7]</sup> Differences between the g values for each complex vary, with  $[CuL^8]$  having the smallest difference it may be concluded that the complex is distorted in all directions. On the other hand, for  $[CuL^{10}]$  a more pronounced difference in g values is present, stressing that an axially elongated complex exists.

Table 6.3d. E.s.r. data<sup>a</sup> for  $[\text{CuL}^8]$  and  $[\text{CuL}^{10}]$ ;  $[\text{CuL}^{68}]^{2+}$  included for comparison.<sup>b</sup>

COMPLEX	$g_{\perp}$	$g_{\parallel}$	$A \text{   /G}$
$[\text{CuL}^8]$	2.068	2.171	160
$[\text{CuL}^{10}]$	2.058	2.192	168
$[\text{CuL}^{68}]^{2+}$	2.036	2.209	160

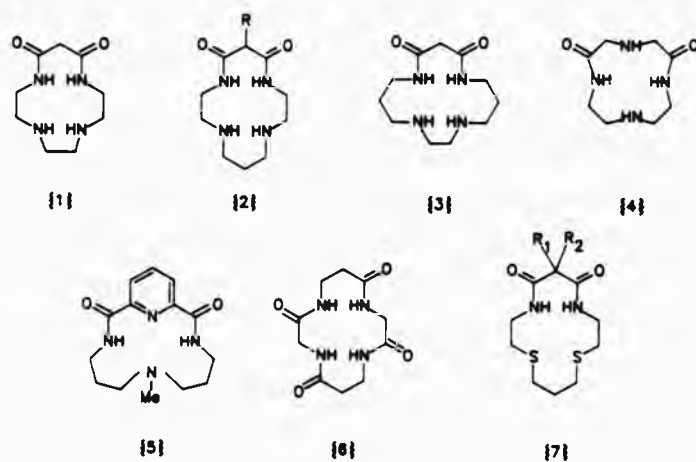
<sup>a</sup>Frozen DMA glass at 113 K. <sup>b</sup>Ligand discussed in Chapter Five.

Several dioxo macrocyclic ligands have been reported but the majority of them contain nitrogen<sup>[8]</sup> and/or oxygen<sup>[9]</sup> donor sets.

For ligands (1)-(5) studies involving thermodynamics and rates of formation and dissociation (kinetics) mainly of their copper(II) and nickel(II) complexes have been undertaken.<sup>[10], [11], [12], [13]</sup> In each case it was indicated that metal-ion promoted ionisation of the amide protons ( $\text{NH}$ ) occurred prior to co-ordination, thus producing doubly deprotonated neutral complexes in solution. Ligand (6)<sup>[14]</sup> becomes quadruply deprotonated in the presence of copper(II) which also yields a neutral complex. Their metal complex rates of formation and dissociation were found to vary according to the pH of the solutions as well as mis-match of cavity size and metal-ion radii, especially in comparison with the more flexible analogous tetra-amine macrocyclic ligands.<sup>[10], [15], [16]</sup>

In addition, the copper(II) and nickel(II) dioxo macrocyclic ligand complexes can be readily converted to give copper(III) and nickel(III) species by anodic or chemical oxidation.<sup>[11], [12], [16], [17]</sup> The

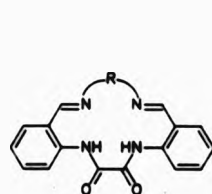
interaction of lead(II), cadmium(II) or zinc(II) did not bring about deprotonation of the ligands {1}-(3) at pH < 7. Under basic conditions, precipitation of the hydrolysed metal ions occurred.<sup>[10]</sup>



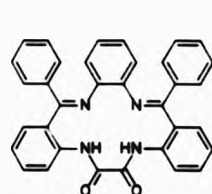
Regulation of pH has also led to the isolation of doubly deprotonated {2} as its copper(II), nickel(II), cobalt(II) and palladium(II) complexes (all square planar) in neutral to alkaline pH, whereas, the platinum(II) complex becomes deprotonated at a much lower pH of < 2.5.<sup>[18]</sup> Furthermore, when R = C<sub>10</sub>H<sub>23</sub> for ligand {2}, both copper(II)<sup>[19]</sup> and platinum(II)<sup>[18]</sup> can be effectively and selectively extracted from an aqueous media into a chloroform phase at pH 7.5 and 3 respectively. The copper(II) extraction is proton driven, whereas, selective extraction of platinum(II) does not occur unless a reductant such as sodium thiosulphate is present in the aqueous phase. In contrast, the tetra-amine analogue cyclam shows no selectivity towards these metal ions.

The crystal structure of [Pt{2}] where R = CH<sub>3</sub>, confirms a square

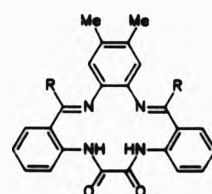
planar geometry for the complex.<sup>[20]</sup> Moreover when R = H, at neutral pH an exocyclic [Pt(2)(Cl)<sub>2</sub>] complex is isolated as a minor product where the platinum(II) has been found to co-ordinate (crystal structure determination) only to the two amino nitrogen donor atoms of the macrocyclic ligand.<sup>[20]</sup> The nitrogen-sulphur analogue {7},<sup>[21]</sup> is highly selective for platinum(II) and palladium(II) over copper(II), nickel(II) and cobalt(II) under the same reaction conditions (no complexes of the latter are formed), producing doubly deprotonated macrocyclic ligand complexes. This difference in selectivity may be relevant to the order of M(II) Lewis acidity to effect deprotonation from the amide ligands; Pt(II) > Pd(II) > Cu(II) > Ni(II) > Co(II). Reduction of the dioxo functions of {7} results in deselectivity, where the newly formed N<sub>2</sub>S<sub>2</sub> ligand complexes with platinum(II) and palladium(II), as well as, copper(II) and nickel(II).<sup>[21]</sup> The macrocyclic ligands {1}-{4} and {6}-{7} are of particular interest since they provide models (i.e. for tripeptides) for biochemical oxidation.



{8}



{9}

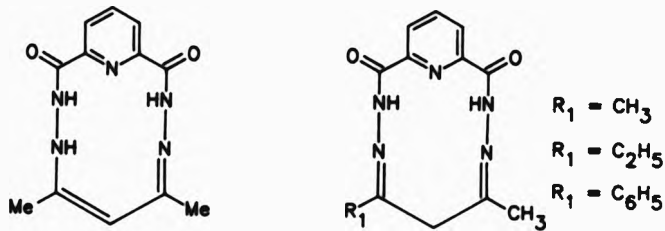


{10}

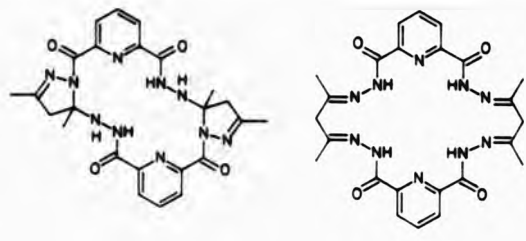
Further, increases in rigidity displayed by the macrocyclic ligands {8}-{10}<sup>[22], [23]</sup> have been investigated with the metal ions copper(II), nickel(II) and cobalt(II). Once again, in each case doubly deprotonated complexes were isolated with co-ordination geometries

ranging from square planar to square pyramidal. Subsequent metallation of the  $[\text{Ni}(10)]$  complex in the presence of  $\text{Cu}(\text{NO}_3)_2$ ,  $\text{ZnCl}_2$  and sodium amalgam with 15-crown-5 has yielded heterobinuclear complexes, whereupon, the second metal ion introduced co-ordinates exocyclically to the dioxo functionalities.

Ligand {11}<sup>[5]</sup> has been isolated as its copper(II), nickel(II) and cobalt(II) complexes which conform to five co-ordinate geometries with two co-ordinating water molecules (i.e. the imino and amino nitrogens are unco-ordinated). A related ligand {12},<sup>[24]</sup> complexes with oxovanadium (IV) where the metal atom is only co-ordinated to the pyridyl nitrogen, both amide nitrogens (deprotonated) and a water molecule, leaving the imino nitrogens unco-ordinated.



The condensation of 2,6-dicarbohydrazidepyridine with pentane-2,4-dione under non-template conditions yields a nucleophilically rearranged product {13}. $5\text{H}_2\text{O}$ . However, in the presence of  $\text{Ni}(\text{OAc})_2$  the ligand rearranges back to the expected imino-containing twenty four-membered  $\text{N}_{10}$  macrocyclic ligand {14}. The complex  $[\text{Ni}_2(14)]$  is quadruply deprotonated where each nickel(II) atom is in a square planar environment.<sup>[25]</sup>



{13}

{14}

### 6.3.2 Single Crystal X-ray Structure of $[\text{CuL}^{10}].\text{H}_2\text{O}$ .

The single-crystal X-ray structure of  $[\text{CuL}^{10}].\text{H}_2\text{O}$  has revealed that the potentially sexidentate macrocyclic ligand  $\text{L}^{10}$  is co-ordinated by only five donor atoms to the copper(II) centre. The co-ordination geometry is very distorted and best described as trigonal bipyramidal to a first approximation (Figure 6.3a). The copper(II) atom is co-ordinated to N(1c), N(2a) and N(2b) in the 'equatorial plane' and 'axially' to N(3c) and S(1b), leaving the other donor atom S(1a) unco-ordinated. Copper(II)-nitrogen bond lengths to the pyridyl [N(1c)] and amido nitrogens [N(2a) and N(2b)] are shorter [1.937(6), 1.976(6) and 2.003(6) Å respectively] than the distance to the fourth nitrogen donor atom [Cu-N(3c) 2.117(6) Å] (Table 6.3e).

However, a 'side-on' view displays a co-ordination geometry that does not conform to any regular polygon (Figure 6.3b). Furthermore, the doubly deprotonated complex generates a near planar ' $\text{N}_3\text{O}_2^{2-}$ ' framework.

**Table 6.3e Selected co-ordination sphere bond distances and angles for  $[\text{CuL}^{10}] \cdot \text{H}_2\text{O}$ .**

Bond distances ( $\text{\AA}$ )		Bond angles ( $^{\circ}$ )	
Cu - N(1c)	1.937(6)	N(1c) - Cu - N(2a)	80.0(3)
Cu - N(2a)	1.976(6)	N(1c) - Cu - N(2b)	79.6(2)
Cu - N(2b)	2.003(6)	N(1c) - Cu - S(1b)	128.8(2)
Cu - N(3c)	2.117(6)	N(2b) - Cu - S(1b)	78.1(2)
Cu - S(1b)	2.552(2)	N(2a) - Cu - S(1b)	115.4(2)
Cu - S(1a)....4.005		N(3c) - Cu - S(1b)	79.6(2)
		N(2a) - Cu - N(2b)	159.7(2)
		N(1c) - Cu - N(3c)	151.2(2)
		N(3c) - Cu - N(2a)	92.0(2)
		N(3c) - Cu - N(2b)	105.9(2)

In the crystal structure of  $[\text{CuL}^{68}] (\text{ClO}_4)_2$  (section 5.4.2), the copper(II) pyridyl bond distances are shorter (axial) whilst those to the amide nitrogens are longer (equatorial) in comparison to those found in the  $[\text{CuL}^{10}] \cdot \text{H}_2\text{O}$  crystal structure.

Bonding interactions between the metal and the sulphur donor atoms are quite different within the complex; copper(II) has a considerably shorter bonding distance to S(1b) [Cu-S(1b) 2.552(2)  $\text{\AA}$ ] (cf. Cu-S(1b) 2.694(10)  $\text{\AA}$  in  $[\text{CuL}^{68}] (\text{ClO}_4)_2$ ) and a non-bonding interaction with S(1a) [Cu....S(1a) 4.005  $\text{\AA}$ ].

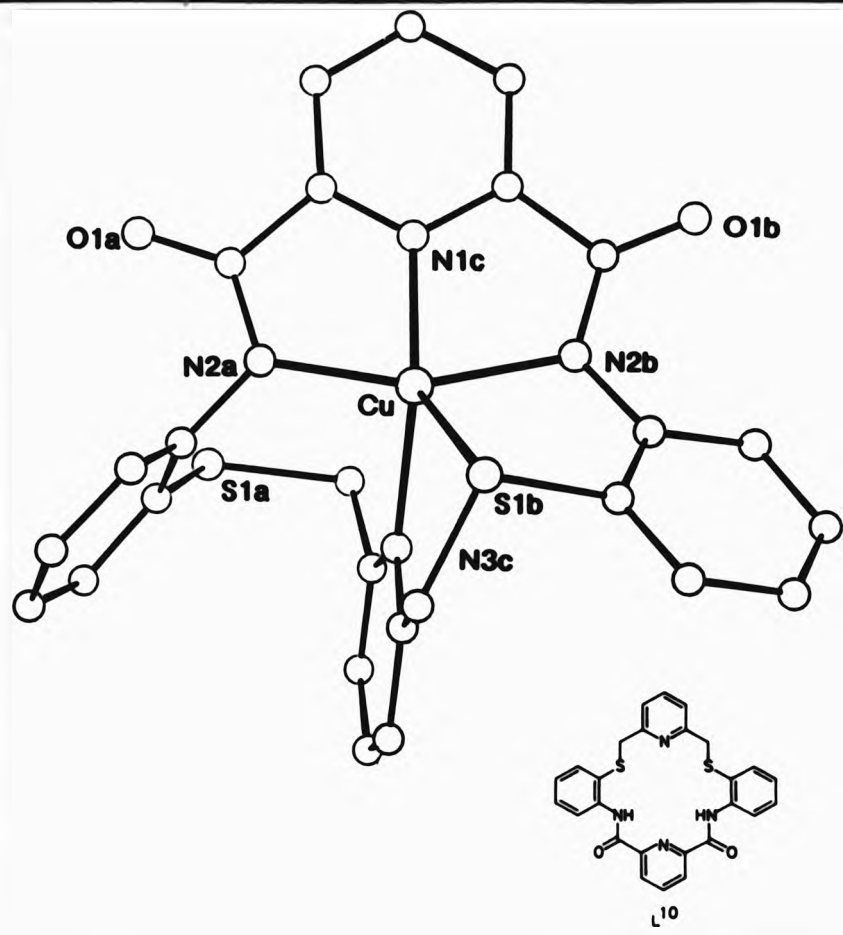


Figure 6.3a Single-crystal X-ray structure of  $[\text{CuL}^{10}] \cdot \text{H}_2\text{O}$ .

Furthermore, unlike  $[\text{CuL}^{68}] (\text{ClO}_4)_2$ , where the trinitrogen unit is flexible enough to permit N(2a) and N(2b) to be slightly staggered (one above and one below the Cu-N(1c) 'plane' (Figure 5.4b)], the metal atom in  $[\text{CuL}^{10}] \cdot \text{H}_2\text{O}$  is coplanar with N(1c), N(2a) and N(2b) [maximum deviation from mean plane Cu, N(1c), N(2a), N(2b) -0.0015 Å (Figure 6.3b)].

Additionally, an atom O(3c) was located in subsequent difference maps

with an intermolecular contact of O(3c)....O(1a) 2.77 Å. Unfortunately, electron densities within oxygen-hydrogen bonding distances which were also found, did not correlate well with the bonding angle expected for a water molecule. Thus, although conclusive evidence is not available from the crystal structure solution of  $(CuL^{10}) \cdot H_2O$ , it is more than likely that the 'stray' atom may be the oxygen atom of a water molecule since, the presence of water is essential for the isolation of this particular complex as previously discussed (*vide ante*).

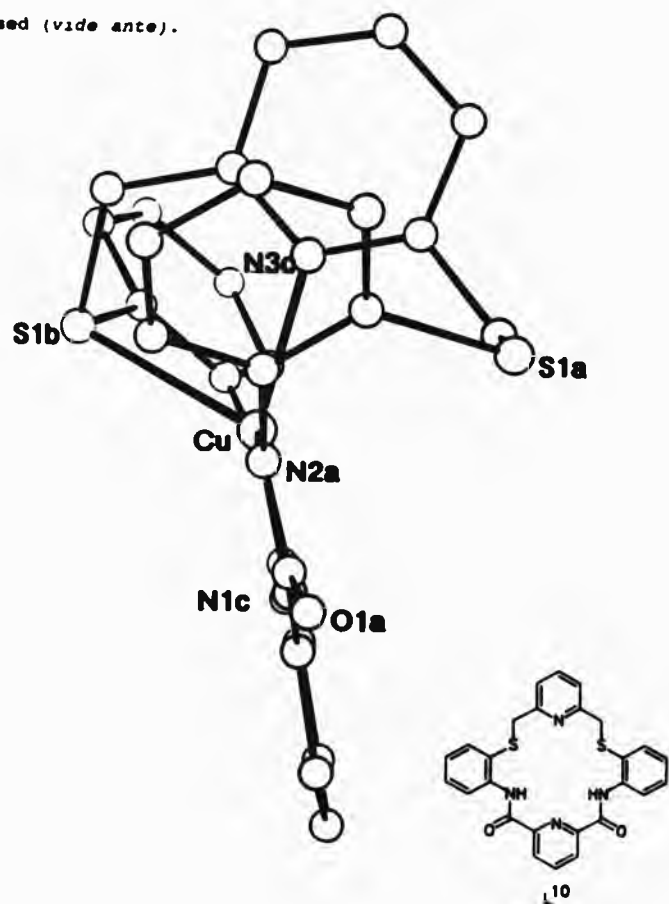


Figure 6.3b Single-crystal X-ray structure of  $(CuL^{10}) \cdot H_2O$ .

Clearly, the copper(II) atom is too small [ $r_{\text{Cu(II)}} = 0.73 \text{ \AA}$  (hexa-co-ordinate)] to co-ordinate to all six donor atoms of the macrocycle L<sup>10</sup> due to its inherent rigidity. The amide (dioxo) moiety is not susceptible to hydrolysis or internal ligand rearrangements under the reaction conditions employed and therefore dictates the co-ordination sphere around the copper(II) atom. This is in contrast to the [CuL<sup>68</sup>][ClO<sub>4</sub>]<sub>2</sub> crystal structure which showed how the copper(II) atom could promote a ligand rearrangement to suit its stereochemical requirements (section 5.4.2).

As a result of planarity the diamide moiety will have a very high in-plane field associated with the 'N<sub>3</sub>O<sub>2</sub><sup>2-</sup>' component and may need a very highly charged Lewis acid to accept such a strong electron density for effective complexation.

*References - Chapter Six.*

1. R. D. Cannon, B. Chiswell and L. M. Venanzi, *J. Chem. Soc.*, 1976, 1277.
2. N. L. Alpert, W. E. Keiser and H. A. Szymanski, 'Infrared Theory and Practice of Infrared Spectroscopy,' Plenum Press, New York, (2nd edn) 1970.
3. (a) N. N. Greenwood and A. Earnshaw, 'Chemistry of the Elements,' Pergamon Press, Oxford, 1984; (b) D. Nicholls, 'Complexes and First-row Transition Elements,' Macmillan Press Ltd, London, 1974.
4. L. F. Lindoy, N. E. Tokel, L. B. Anderson and D. H. Busch, *J. Coord. Chem.*, 1971, 1, 7.
5. V. B. Rana and M. P. Teotia, *Indian J. Chem., Sect. A* 1980, 19A, 267.
6. K. Nakamoto, 'Infrared Spectra of Inorganic and Coordination Compounds,' Wiley-Interscience, New York, (2nd edn) 1970.
7. J. M. Holmes, Ph.D Thesis, Cambridge, 1985.
8. See for example; E. Buhleier, W. Wehner and F. Vögtle, *Liebigs Ann. Chem.*, 1978, 537 and references therein.
9. See for example; R. M. Izatt, D. V. Dearden, P. R. Brown, J. S. Bradshaw, J. D. Lamb and J. J. Christensen, *J. Am. Chem. Soc.*, 1983, 105, 1785 and references therein.
10. M. Kodama and E. Kimura, *J. Chem. Soc., Dalton Trans.*, 1979, 325.
11. M. Kodama and E. Kimura, *J. Chem. Soc., Dalton Trans.*, 1981, 694.
12. L. Fabbrizzi, T. A. Kaden, A. Perotti, B. Seghi and L. Siegfried, *Inorg. Chem.*, 1986, 25, 321.
13. R. W. Hay and P. R. Norman, *Transit. Met. Chem.*, 1980, 5, 232.
14. H. Sigel and R. B. Martin, *Chem. Rev.*, 1982, 82, 385.
15. R. D. Hancock, A. Evers, M. P. Ngwenya and P. W. Wade, *J. Chem. Soc., Chem. Commun.*, 1987, 1129.

16. L. Fabbrizzi, F. Forlini, A. Perotti and B. Seghi, *Inorg. Chem.*, 1984, 807.
17. L. Fabbrizzi and A. Poggi, *J. Chem. Soc., Chem. Commun.*, 1980, 646.
18. E. Kimura, Y. Lin, R. Machida and H. Zenda, *J. Chem. Soc., Chem. Commun.*, 1986, 1020.
19. E. Kimura, C. A. Dalimunte, A. Yamashita and R. Machida, *J. Chem. Soc., Chem. Commun.*, 1985, 1041.
20. E. Kimura, S. Korenari, M. Shionoya and M. Shiro, *J. Chem. Soc., Chem. Commun.*, 1988, 1166.
21. E. Kimura, Y. Kurogi, S. Wada and M. Shionoya, *J. Chem. Soc., Chem. Commun.*, 1989, 781.
22. K. Henrick, P. M. Judd, M. McPartlin, P. A. Tasker and R. W. Turner, *Inorg. Chim. Acta.*, 1981, 53, L265.
23. D. Christodoulou, M. G. Kanatzidis and D. Coucouvanis, *Inorg. Chem.*, 1990, 29, 191.
24. S. Kher, S. K. Sahni, V. Kumari and R. N. Kapoor, *Inorg. Chim. Acta.*, 1979, 37, 121.
25. E. C. Constable, M. J. Doyle, S. M. Elder and P. R. Raithby, *J. Chem. Soc., Chem. Commun.*, 1989, 1376.

**CHAPTER SEVEN**  
**EXPERIMENTAL - SYNTHESES AND CRYSTALLOGRAPHY**

#### PHYSICAL AND ANALYTICAL INSTRUMENTATION EMPLOYED.

Infrared spectra were recorded on a Perkin Elmer 781 spectrophotometer or on a Biorad FT540 as KBr discs. Microanalyses were determined by a Carlo Erba 1106 elemental analyser. Mass spectra were recorded using a Kratos Profile GC-MS. Fast atom bombardment (f.a.b.) source spectra were determined by the Mass Spectrometry Service Centre at the University College of Swansea (funded by the S.E.R.C.). Proton and carbon-13 n.m.r. spectra were obtained using a Bruker AM-250 spectrometer. Room temperature magnetic moments were obtained using a Johnson Matthey Ltd. goudy balance, using  $Hg[Co(SCN)_4]$  to calibrate the instrument. Electronic spectra were recorded on a Shimadzu UV-2100 UV-VIS spectrophotometer in the range 200-900 nm. The e.s.r. spectra were determined at The Open University, Milton Keynes.

#### SYNTHESES

##### 7.1 Synthesis of 2,6-Bis(aminothiophenoxyethyl)pyridine, L<sup>1</sup>.

To a stirred solution of sodium ethoxide (sodium 2.40 g, 0.10 moles; absolute ethanol 150 cm<sup>3</sup>), 2-aminothiophenol (12.80 g, 0.10 moles) in absolute ethanol (150 cm<sup>3</sup>) was added dropwise over a period of 30 min at room temperature, under nitrogen. 2,6-Bis(bromomethyl)pyridine<sup>[1]</sup> (13.60 g, 0.05 moles) in absolute ethanol (100 cm<sup>3</sup>) was added dropwise, and the reaction mixture refluxed for 4 hours. On cooling, the reaction mixture was poured into an equal volume of water (400 cm<sup>3</sup>) where on standing, white flocculent crystals were obtained. The product was collected by filtration, washed with water and dried over phosphorus pentoxide.

Typical analyses gave: Yield 11.23 g, 62 %. (Found: C, 64.63; H, 5.39; N, 11.83. Calc. for  $C_{19}H_{19}N_3S_2$ : C, 64.56; H, 5.42; N, 11.89, %) Mass

spectral parent ion: m/z 353.

#### 7.1.1 Preparation of Metal Complexes of L<sup>1</sup>.

The appropriate metal-ion salt (0.56 mmol) was dissolved or suspended in methanol (50 cm<sup>3</sup>). L<sup>1</sup> (0.56 mmol) in methanol (50 cm<sup>3</sup>) was added dropwise to the methanolic metal-ion solution whilst being stirred and gently heated. Stirring and heating were continued for a further 30 min. The reaction mixture was then placed on a steam bath, where slow evaporation of the solvent produced crystalline complexes. The crystals were collected and washed with ice cold methanol. Metal-ion salts used were those of Ni(ClO<sub>4</sub>)<sub>2</sub>.6H<sub>2</sub>O, NiCl<sub>2</sub>.6H<sub>2</sub>O, HgCl<sub>2</sub>, and Hg(SCN)<sub>2</sub>.

Complex	Yield (%)	Elemental Analyses (%)		
		C	H	N
[HgL <sup>1</sup> (Cl) <sub>2</sub> ]	42	36.59 (36.51)	3.17 (3.06)	6.76 (6.72)
[HgL <sup>1</sup> ](ClO <sub>4</sub> ) <sub>2</sub>	32	30.34 (30.31)	2.62 (2.54)	5.57 (5.58)
[NiL <sup>1</sup> (Cl)]ClMeOH	32	46.49 (46.62)	4.57 (4.50)	8.04 (8.16)
[NiL <sup>1</sup> ](ClO <sub>4</sub> ) <sub>2</sub>	21	37.29 (37.34)	3.16 (3.13)	6.76 (6.88)

#### 7.1.2 Preparation of Metal Complexes of L<sup>1</sup>.

The appropriate metal-ion salt (0.56 mmol) was dissolved or suspended in methanol (50 cm<sup>3</sup>). L<sup>1</sup> (0.56 mmol) in methanol (50 cm<sup>3</sup>) was added dropwise to the methanolic metal-ion solution whilst being stirred at room temperature. Stirring was continued for a further 30 min. The

solvent of the reaction mixture was reduced to half its original volume under a steady stream of nitrogen and then placed in a refrigerator to induce crystallisation. The complexes were collected by filtration and washed with ice cold methanol. Metal-ion salts used were those of  $\text{Cu}(\text{ClO}_4)_2 \cdot 6\text{H}_2\text{O}$ ,  $\text{CuCl}_2 \cdot 6\text{H}_2\text{O}$ ,  $\text{AgClO}_4 \cdot x\text{H}_2\text{O}$ , and  $\text{AgNO}_3$ .

Complex	Yield (%)	Elemental Analyses (%)		
		C	H	N
$(\text{CuL}^1)(\text{ClO}_4)_2$	11	37.85 (37.05)	3.17 (3.11)	6.80 (6.82)
$(\text{AgL}^1)\text{ClO}_4$	47	40.62 (40.69)	3.59 (3.41)	7.50 (7.49)
$(\text{Ag}_2\text{L}^1)(\text{NO}_3)_2$	25	30.02 (32.92)	2.73 (2.76)	9.99 (10.10)

#### 7.1.3 Determination of Protonation Constants for $\text{L}^1$ .<sup>[2]</sup>

A sample of the ligand ( $0.001\text{-}0.0005 \text{ mol dm}^{-3}$ ) was prepared in acid stock, [methanol:water (95 %:5 %);  $0.004 \text{ mol dm}^{-3}$   $\text{HClO}_4$ ,  $I = 0.1 \text{ mol dm}^{-3}$   $\text{Et}_4\text{NClO}_4$ ). The sample solution ( $25.0 \text{ cm}^3$ ) was then titrated against  $\text{CO}_2$  free  $\text{Et}_4\text{NOH}$  ( $0.1 \text{ mol dm}^{-3}$ ) - previously standardised against 1M  $\text{HClO}_4$  (standardised by borax). All dilutions were carried out with doubly distilled water.

#### 7.1.4 Determination of $[\text{CuL}^1]_n^{2+}$ Complex Equilibria.<sup>[2]</sup>

The above procedure was repeated for the ligand and acid stock solutions. After which, small aliquots of the metal stock solution ( $0.25\text{-}0.05 \text{ cm}^3$ ) required to give the desired M:L ratios, 1:1, 1:2, 1:3 etc. were delivered into the titration cell.

### *7.2 Synthesis of 2,6-bis(mercaptoproethylaminomethyl)pyridine, L<sup>2</sup>.*

To a stirred solution of sodium ethoxide (sodium 2.50 g, 0.11 moles; absolute ethanol 150 cm<sup>3</sup>), 2-mercaptoproethylamine hydrochloride (9.05 g, 0.08 moles) in absolute ethanol (150 cm<sup>3</sup>) was added dropwise over a period of 30 min at room temperature, under nitrogen. 2,6-Bis(bromomethyl)pyridine (10.00 g, 0.04 moles) in absolute ethanol (100 cm<sup>3</sup>) was added dropwise, and the reaction mixture refluxed for 4 hours. On refluxing, the sodium chloride deposited was filtered. The filtrate was used to prepare complexes of L<sup>2</sup>. No further work up was undertaken.

#### *7.2.1 Preparation of Metal Complexes of L<sup>2</sup>.*

Since isolation of L<sup>2</sup> was not achieved, complexation reactions were carried out on the reaction mixture filtrate obtained as above (7.2). Gentle warming of the filtrate (20 cm<sup>3</sup>) and the metal-ion salt (0.40 mmol) in methanol or ethanol (20 cm<sup>3</sup>) resulted in metal-ion complexation. Metal-ion salts used were those of Cu(ClO<sub>4</sub>)<sub>2</sub>.6H<sub>2</sub>O, CuCl<sub>2</sub>.6H<sub>2</sub>O, Ni(ClO<sub>4</sub>)<sub>2</sub>.6H<sub>2</sub>O and NiCl<sub>2</sub>.6H<sub>2</sub>O.

Complex	Yield (%)	Elemental Analyses (%)		
		C	H	N
(NiL <sup>2</sup> )[ClO <sub>4</sub> ] <sub>2</sub>	-	26.68 (25.65)	3.89 (3.72)	8.38 (8.16)

### *7.3 Template Synthesis of [AgL<sup>3</sup>]ClO<sub>4</sub>.*

Glyoxal (0.12 g, 0.56 mmol) and AgClO<sub>4</sub> (0.12 g, 0.56 mmol) were refluxed in methanol (100 cm<sup>3</sup>) until all the solid had dissolved. Heating was temporarily stopped, whilst L<sup>1</sup> (0.20 g, 0.56 mmol) in methanol (50 cm<sup>3</sup>) was added dropwise with stirring. The reaction

mixture was refluxed for a further 15 min, and filtered hot. The filtrate was then placed on a steam bath where, on reduction of the solvent by half the original volume, a dark orange solid was obtained.

#### 7.3.1 Template synthesis of $[\text{Cu}_2^{\text{L}}]^{33}[\text{ClO}_4]_2$ .

Glyoxal (0.12 g, 0.56 mmol) and  $\text{Cu}[\text{ClO}_4]_2$  (0.21 g, 0.56 mmol) were refluxed in methanol ( $100 \text{ cm}^3$ ) until all the solid had dissolved. The solution was then allowed to cool to room temperature.  $\text{L}^1$  (0.20 g, 0.56 mmol) in methanol ( $50 \text{ cm}^3$ ) was added dropwise to the cooled solution with stirring. The solvent was removed on a rotary evaporator at room temperature, until a dark greenish brown solid was obtained.

#### 7.3.2 Transmetallation reaction of $(\text{AgL})^{33}\text{ClO}_4$ with $\text{NiCl}_2 \cdot 6\text{H}_2\text{O}$ .

$\text{NiCl}_2 \cdot 6\text{H}_2\text{O}$  (0.16 g, 0.52 mmol) was mixed with  $(\text{AgL})^{33}\text{ClO}_4$  (0.20 g, 0.34 mmol) in acetonitrile ( $50 \text{ cm}^3$ ). The resulting red brown precipitate was filtered off, leaving a pale green filtrate which on standing gave bright purple crystals.

Complex	Yield (%)	Elemental Analyses (%)		
		C	H	N
$(\text{AgL})^{33}\text{ClO}_4$	46	42.39 (43.27)	3.08 (2.94)	6.63 (7.21)
$[\text{Cu}_2^{\text{L}}]^{33}[\text{ClO}_4]_2$	25	46.21 (46.84)	3.23 (3.18)	7.52 (7.80)
$[\text{NiL}^1(\text{Cl})]\text{Cl} \cdot \text{MeOH}$	36	46.46 (46.62)	4.79 (4.50)	8.23 (8.16)

#### 7.4 Non-Template Synthesis of $\text{L}^4$ .

2,6-Diformylpyridine (0.19 g, 1.40 mmol) was refluxed for 5 min in

methanol ( $150 \text{ cm}^3$ ) and filtered hot.  $\text{L}^1$  (0.5 g, 1.40 mmol) in methanol ( $150 \text{ cm}^3$ ) with 2,2-dimethoxypropane (ca.  $5 \text{ cm}^3$ ) was added dropwise with stirring to the filtrate. The pale yellow reaction mixture was refluxed for 2 hours. On refluxing, the solution had intensified in colour. The solvent was reduced under pressure to one quarter of its' original volume. The resultant pale yellow solid was filtered, washed with diethylether and dried over phosphorus pentoxide. Typical analyses gave: Yield 0.15 g, 23 %.

#### 7.4.1 Template Syntheses of $[\text{PbL}^4]^{2+}$ .

The appropriate Pb(II) salt (0.57 mmol) and 2,6-diformylpyridine<sup>(3)</sup> (0.08 g, 0.57 mmol) were dissolved together in methanol ( $50 \text{ cm}^3$ ) with heating, and the solution was filtered.  $\text{L}^1$  (0.20 g, 0.57 mmol) in methanol ( $50 \text{ cm}^3$ ) was added dropwise to the stirred filtrate, giving an immediate colour change from colourless to bright orange. The solution was refluxed for 1 hour and let stand for ca. 24 hours. The orange crystalline or amorphous solid obtained was collected by filtration and washed in cold methanol.

Complex	Yield (%)	Elemental Analyses (%)		
		C	H	N
$[\text{PbL}^4](\text{ClO}_4)_2$	50	36.29 (36.36)	2.44 (2.35)	6.47 (6.52)
$[\text{PbL}^4(\text{NCS})_2]$	45	43.33 (43.34)	2.53 (2.60)	10.75 (10.83)
$[\text{PbL}^4](\text{NO}_3)_2$	23	39.88 (39.84)	2.83 (2.57)	10.60 (10.72)
$[\text{PbL}^4]\text{Cl}_2$	32	42.77 (42.74)	2.74 (2.76)	7.67 (7.67)

#### 7.4.2 Template Syntheses of $(\text{AgL}^4)^+$ .

The appropriate Ag(I) salt (0.57 mmol) and 2,6-diformylpyridine (0.08 g, 0.57 mmol) were dissolved together in methanol ( $50 \text{ cm}^3$ ) and filtered.  $\text{L}^1$  (0.20 g, 0.57 mmol) in methanol ( $50 \text{ cm}^3$ ) was added dropwise to the stirred filtrate and the mixture refluxed for 1 hour. The dark orange solid formed was filtered and recrystallised twice from acetonitrile to give a bright orange or yellow solid. The product was then washed with methanol, followed by diethylether and dried under vacuo.

Complex	Yield (%)	Elemental Analyses (%)		
		C	H	N
$[\text{AgL}^4]\text{ClO}_4$	33	45.93 (46.11)	2.92 (3.27)	8.56 (8.26)
$[\text{AgL}^4\text{SCN}]$	42	51.03 (52.43)	3.98 (3.26)	11.54 (11.32)
$[\text{AgL}^4]\text{NO}_3$	41	50.46 (50.17)	2.61 (3.24)	11.58 (11.25)

#### 7.4.3 Template Synthesis of $[\text{HgL}^4(\text{SCN})_2].\text{MeOH}$ .

To a stirred suspension of  $\text{HgSCN}_2$  (0.18 g, 0.57 mmol) and 2,6-diformylpyridine (0.08 g, 0.57 mmol) in methanol ( $50 \text{ cm}^3$ ),  $\text{L}^1$  (0.20 g, 0.57 mmol) in methanol ( $50 \text{ cm}^3$ ) was added dropwise to give a bright orange solution. The mixture was refluxed for 1 hour and filtered hot. The filtrate was placed in a refridgerator to induce crystallisation. These were collected by filtration and washed in cold methanol followed by diethylether and dried under vacuo.

Complex	Yield (%)	Elemental Analysis (%)		
		C	H	N
$[\text{HgL}^4(\text{SCN})_2] \cdot \text{MeOH}$	52	43.25 (43.72)	2.96 (2.62)	10.79 (10.92)

#### 7.4.4 Template Syntheses of $[\text{CdL}^4]^{2+}$ .

The appropriate Cd(II) salt (0.57 mmol) and 2,6-diformylpyridine (0.08 g, 0.57 mmol) in methanol ( $50 \text{ cm}^3$ ) were gently heated together and then filtered. L<sup>4-</sup> (0.20 g, 0.57 mmol) in methanol ( $50 \text{ cm}^3$ ) was added dropwise to the stirred filtrate and the reaction mixture refluxed for 1 hour. The resulting pale yellow solution was filtered hot and on cooling placed in the refrigerator for 24-72 hours. The solid obtained was recrystallised from a methanol-acetonitrile (1:3) mixture. On filtration, the product was washed with cold methanol followed by diethylether and dried under vacuo.

Complex	Yield (%)	Elemental Analyses (%)		
		C	H	N
$[\text{CdL}^4][\text{ClO}_4]_2$	36	40.67 (40.88)	2.78 (2.64)	7.35 (7.33)
$[\text{CdL}^4(\text{NCS})_2]$	25	49.93 (49.37)	2.92 (2.96)	12.47 (12.34)
$[\text{CdL}^4][\text{NO}_3]_2$	18	46.67 (46.07)	3.19 (4.00)	13.69 (13.43)

#### 7.4.5 Template Syntheses of $[\text{ZnL}^4]^{2+}$ .

The appropriate Zn(II) salt (0.57 mmol) and 2,6-diformylpyridine (0.08 g, 0.57 mmol) in methanol ( $50 \text{ cm}^3$ ) were gently heated together and

filtered.  $L^1$  (0.20 g, 0.57 mmol) in methanol ( $50\text{ cm}^3$ ) was added dropwise to the stirred filtrate and the reaction mixture refluxed for 1 hour. The resulting dark orange solution was filtered hot and the filtrate was left to stand for 48 hours. The product obtained was recrystallised from acetonitrile, washed with diethylether and dried under vacuo.

Complex	Yield (%)	Elemental Analyses (%)		
		C	H	N
$[\text{ZnL}^4](\text{ClO}_4)_2$	25	40.37 (43.56)	2.63 (2.81)	6.61 (7.82)
$[\text{ZnL}^4](\text{NO}_3)_2 \cdot \text{CH}_3\text{CN}$	21	49.56 (49.24)	3.21 (3.39)	13.45 (14.35)

#### 7.5.1 Template Synthesis of $[\text{PbL}^5]\text{Br}_2$ .

$\text{Pb}(\text{ClO}_4)_2 \cdot 3\text{H}_2\text{O}$  (0.20 g, 0.43 mmol) and 2,6-diformylpyridine (0.06 g, 0.43 mmol) in methanol ( $20\text{ cm}^3$ ) were gently heated together and filtered hot. The hot filtrate was added dropwise to a warm stirred solution of  $L^2$  filtrate ( $20\text{ cm}^3$ ), [filtrate of reaction mixture from (7.2)]. Heating was continued for a further 15 min. Gradually, a pale yellow solid began to precipitate. The solid was collected by filtration, washed with ethanol followed by diethylether and dried over phosphorus pentoxide.

#### 7.5.2 Template Synthesis of $[\text{PbL}^5(\text{SCN})_2]$ .

$[\text{PbL}^5]\text{Br}_2$  (0.10 g, 0.14 mmol) was boiled in hot N,N-dimethylformamide ( $40\text{ cm}^3$ ) with excess  $\text{LiSCN}_{(\text{aq})}$ . The pale yellow solid dissolved immediately to give a clear dark yellow solution, this was filtered hot and placed on a steam bath. On standing, dark yellow opaque crystals

were obtained. The crystals were filtered and washed with water and ethanol, followed by diethylether and dried over phosphorus pentoxide.

Complex	Yield (%)	Elemental Analyses (%)		
		C	H	N
$(\text{PbL}^5)\text{Br}_2$	-	30.39 (29.88)	2.77 (2.79)	7.65 (7.74)
$(\text{PbL}^5(\text{SCN})_2$	-	32.50 (35.33)	2.99 (2.97)	12.54 (12.36)

#### 7.6 Synthesis of $\text{L}^6$ .

Sodium tetraborate (0.75 g, 20 mmol) was added portionwise to  $[\text{PbL}^4](\text{ClO}_4)_2$  (1.30 g, 2 mmol) in absolute ethanol ( $200 \text{ cm}^3$ ), at room temperature. The exothermic reaction was cooled on ice whilst being stirred. When the addition was complete, the bright orange solution had turned black. The reaction mixture was then refluxed for 2 hours and filtered hot to remove the solid lead precipitate. The filtrate was then taken to dryness to give a creamy white solid. Soxhlet extraction on the crude solid using acetonitrile gave  $\text{L}^6$  as off-white crystals.

Typical analyses: Yield 11 %. (Found: C, 65.23; H, 5.02; N, 11.20. Calc. for  $\text{C}_{26}\text{H}_{24}\text{N}_4\text{S}_2\cdot\text{H}_2\text{O}$ : C, 65.80; H, 5.52; N, 11.80 %). Mass spectral parent ion: m/z 456.

##### 7.6.1 Synthesis of $[\text{CuL}^6](\text{ClO}_4)_2$ .

$\text{L}^6$  (0.20 g, 0.44 mmol) in methanol ( $25 \text{ cm}^3$ ) was added dropwise to a stirred solution of  $\text{Cu}(\text{ClO}_4)_2\cdot 6\text{H}_2\text{O}$  (0.24 g, 0.66 mmol) in methanol ( $25 \text{ cm}^3$ ) at room temperature. The clear dark green solution was left to

stir overnight with gradual loss of solvent. The resulting dark green crystals were carefully removed from the solvent using a pasteur pipette and washed with cold methanol.

#### 7.6.2 Synthesis of $[NiL^6](ClO_4)_2$ .

$L^6$  (0.20 g, 0.44 mmol) in methanol (25 cm<sup>3</sup>) was added dropwise to a stirred solution of  $Ni(ClO_4)_2 \cdot 6H_2O$  (0.24 g, 0.66 mmol) in methanol (25 cm<sup>3</sup>) and the mixture refluxed for 30 min. The solution was filtered hot and the volume reduced by one third on a steam bath. On cooling, the solution was kept in a refrigerator for ca. 24 hours to give bright purple crystals. These were collected by filtration and washed with cold methanol.

Complex	Yield (%)	Elemental Analyses (%)		
		C	H	N
$[CuL^6](ClO_4)_2$	65	43.26 (43.43)	3.34 (3.36)	7.73 (7.79)
$[NiL^6](ClO_4)_2$	56	43.83 (43.72)	3.42 (3.39)	7.81 (7.84)

#### 7.6.3 Synthesis of $L^{6x}$ .

Under nitrogen, dissolved sodium (0.48 g, 0.021 mol) in absolute ethanol (100 cm<sup>3</sup>) was added dropwise to 1,2-benzenedithiol (1.00 g, 7 mmol) in absolute ethanol (100 cm<sup>3</sup>) at room temperature. 2,6-Bis(bromomethyl)pyridine (1.85 g, 7 mmol) in absolute ethanol (100 cm<sup>3</sup>) was added dropwise to the above reaction mixture over a period of 4 hours. Thereafter, the resulting pale yellow solution was refluxed for 2 hours. Further stirring overnight yielded a cream coloured solid. The product was washed with ice-cold ethanol and air dried.

Typical analyses: Yield 23 %. (Found: C, 63.31; H, 4.45; N, 5.33. Calc. for  $C_{28}H_{24}N_2S$ : C, 63.64; H, 4.52; N, 5.71 %). Mass spectral parent ion: m/z 491.

7.6.4 Template Syntheses of  $[CuL^{6A}]ClO_4$  and  $[CuL^{6B}]ClO_4$ .

$Cu(ClO_4)_2 \cdot 6H_2O$  (0.21 g, 0.57 mmol) and 2,6-diformylpyridine (0.08 g, 0.57 mmol) in methanol or ethanol ( $50\text{ cm}^3$ ) were gently heated to give a pale blue solution. The solution was filtered, and cooled to room temperature. With rapid stirring,  $L^1$  (0.20 g, 0.57 mmol) in methanol or ethanol ( $50\text{ cm}^3$ ) was added dropwise to the cooled filtrate. The solution immediately turned dark green. On standing in the refrigerator for ca. 24 hours, dark green crystals were obtained. These were gently removed from solution using a pasteur pipette and washed with ice cold methanol or ethanol followed by diethylether.

Complex	Yield (%)	Elemental Analyses (%)		
		C	H	N
$[CuL^{6A}]ClO_4$	69	43.00 (43.17)	3.51 (3.62)	7.21 (7.19)
$[CuL^{6B}]ClO_4$	76	44.51 (44.60)	3.85 (4.00)	7.08 (6.90)

7.6.5 Template Syntheses of  $[NiL^{6A-O}]^{2+}$ .

$Ni(ClO_4)_2 \cdot 6H_2O$  (0.21 g, 0.57 mmol) and 2,6-diformylpyridine (0.08 g, 0.57 mmol) were dissolved together in R-OH ( $50\text{ cm}^3$ ) with heating and stirring. The solution was filtered hot.  $L^1$  (0.20 g, 0.57 mmol) in R-OH ( $50\text{ cm}^3$ ) was added dropwise to the warm stirring filtrate, whereupon, the solution turned dark orange and then either pink or

purple depending on R-OH. The reaction solution was gently refluxed for 30 min. Thereafter, the solution was placed on a steam bath to allow evaporation of solvent to yield crystals or a solid. On some occasions, a series of different coloured solids were isolated from the same reaction solvent. These were collected by filtration washed with cold alcohol and diethylether and dried under vacuo. R-OH = methanol, ethanol, i-propanol and n-butanol.

Complex	Yield (%)	Elemental Analyses (%)		
		C	H	N
[NiL <sup>6A</sup> ][ClO <sub>4</sub> ] <sub>2</sub>	20	43.23 (43.43)	3.51 (3.65)	7.21 (7.24)
[NiL <sup>6B</sup> ][ClO <sub>4</sub> ] <sub>2</sub>	12	45.38 (44.80)	3.91 (4.26)	7.17 (6.97)
[NiL <sup>6C</sup> ][ClO <sub>4</sub> ] <sub>2</sub>	32	45.98 (46.29)	4.00 (4.37)	7.01 (6.75)
[NiL <sup>6D</sup> ][ClO <sub>4</sub> ] <sub>2</sub>	15	47.71 (47.57)	4.37 (4.70)	6.93 (6.53)

A = methoxy, B = ethoxy, C = propoxy, D = butoxy, derivatives of L<sup>6</sup>.

#### 7.7 Synthesis of L<sup>7</sup>.

Oxaloyl chloride (0.36 g, 2.80 mmol) in dichloromethane (200 cm<sup>3</sup>) was stirred at room temperature under N<sub>2</sub>. L<sup>1</sup> (1.00 g, 2.80 mmol) in dichloromethane (200 cm<sup>3</sup>) was added dropwise over a period of 1 hour. The reaction mixture was then refluxed for 2 hours and subsequently taken to dryness to give a greenish white solid. This was stirred in refluxing methanol (100 cm<sup>3</sup>) and the resulting solution filtered hot. The bottle green filtrate was discarded, leaving a clean white solid as the desired product.

Typical analyses gave: Yield 0.70 g, 58 %. (Found: C, 61.42; H, 4.11; N, 10.05. Calc. for  $C_{21}H_{17}N_3S_2O$ : C, 61.85; H, 4.21; N, 10.31 %). Mass spectral parent ion: m/z 407.

#### 7.7.1 Synthesis of $CuL^7$ .

$Cu(OAc)_2 \cdot H_2O$  (0.05 g, 0.25 mmol) in methanol ( $25\text{ cm}^3$ ) was added dropwise to a stirred solution of  $L^7$  (0.10 g, 0.25 mmol) in dichloromethane ( $25\text{ cm}^3$ ) and the mixture refluxed for 30 min. The resulting dark green solution was filtered hot, and the filtrate solvent evaporated to give a dark green solid. Attempted recrystallisations to give a crystalline solid were unsuccessful.

Complex	Yield (%)	Elemental Analysis (%)		
		C	H	N
$[CuL^7] \cdot CH_2Cl_2$	35	49.98 (47.70)	3.69 (3.09)	7.28 (7.59)

#### 7.8 Synthesis of $L^8$ .

1,2-Bis(o-aminothiophenoxy)ethane<sup>[4]</sup> (1.00 g, 3.60 mmol) in dichloromethane ( $100\text{ cm}^3$ ) was added dropwise with stirring to 2,6-pyridinedicarbonyl dichloride (0.74 g, 3.60 mmol) in dichloromethane ( $100\text{ cm}^3$ ) and the mixture refluxed for 2 hours. The reaction mixture was taken to dryness and redissolved in hot methanol ( $100\text{ cm}^3$ ). The resulting white solid which was insoluble in methanol was the desired product and was subsequently filtered and dried under vacuo.

Typical analyses gave: Yield 0.67 g, 45 %. (Found: C, 61.62; H, 4.20; N, 10.26. Calc. for  $C_{21}H_{17}N_3S_2O$ : C, 61.85; H, 4.21; N, 10.31 %). Mass spectral parent ion: m/z 407.

#### 7.8.1 Synthesis of $CuL^8$ .

$Cu(OAc)_2 \cdot H_2O$  (0.10 g, 0.50 mmol) in methanol ( $50 \text{ cm}^3$ ) was added dropwise to a suspension of  $L^8$  (0.20 g, 0.50 mmol) in methanol ( $50 \text{ cm}^3$ ) and the mixture refluxed for 1 hour until the dark green solution turned almost blue black. On standing, fine blue black crystals appeared which were collected by filtration and washed with ice cold methanol and dried under vacuo.

Complex	Yield (%)	Elemental Analysis (%)		
		C	H	N
$CuL^8$	58	53.98 (53.77)	3.29 (3.22)	8.93 (8.96)

#### 7.9 Synthesis of $L^9$ .

1,2-Bis(*o*-aminophenoxy)ethane<sup>[4]</sup> (2.00 g, 8.00 mmol) in dichloromethane ( $100 \text{ cm}^3$ ) was added dropwise with stirring to 2,6-pyridinedicarbonyl dichloride (1.70 g, 8.00 mmol) in dichloromethane ( $100 \text{ cm}^3$ ), and the mixture refluxed for 2 hours. The reaction mixture was taken to dryness and redissolved in hot methanol ( $100 \text{ cm}^3$ ). The resulting insoluble white solid was recrystallised from dichloromethane/ methanol (1:1) to give long white fibrous crystals. These were collected by filtration and dried under vacuo.

Typical analyses gave: Yield 2.18 g, 71 %. (Found: C, 67.53; H, 4.63; N, 11.32. Calc. for  $C_{21}H_{17}N_3O_4$ : C, 67.19; H, 4.56; N, 11.19 %). Mass

Spectral parent ion: m/z 375.

7.10 Synthesis of  $L^{10}$ .

$L^1$  (1.00 g, 2.80 mmol) in dichloromethane (100 cm<sup>3</sup>) was added dropwise to a stirred solution of 2,6-pyridinedicarbonyl dichloride (1.37 g, 2.80 mmol) in dichloromethane (100 cm<sup>3</sup>), at room temperature. The resultant solution was taken to dryness and the crude solid refluxed in hot methanol (150 cm<sup>3</sup>) for half an hour. On filtration, a pale grey solid was collected which was dried under vacuo.

Typical analyses gave: Yield 0.075 g, 54 %. (Found: C, 64.09; H, 4.15; N, 11.56. Calc. for  $C_{26}H_{20}N_4S_2O_2$ : C, 64.52; H, 4.17; N, 11.58 %). Mass spectral parent ion: m/z 484.

7.10.1 Synthesis of  $[CuL^{10}] \cdot H_2O$ .

To a stirred suspension of  $L^{10}$  (0.20 g, 0.36 mmol) in methanol (40 cm<sup>3</sup>),  $Cu(OAc)_2 \cdot H_2O$  (0.08 g, 0.36 mmol) in methanol (40 cm<sup>3</sup>) was added dropwise and the reaction mixture refluxed for 1 hour. After hot filtration, the dark green solution was cooled to room temperature. A few drops of water (ca. 5 cm<sup>3</sup>) were added to the filtrate and placed in the refrigerator. On standing, for ca. 24 hours, the solution gave dark green crystals from a pale blue solution with a characteristic acetic acid odour. The crystals were collected by filtration and washed with ice cold methanol and dried over phosphorus pentoxide.

7.10.2 Synthesis of  $PtL^{10}$

$L^{10}$  (0.20 g, 0.41 mmol) was refluxed in *N,N*-dimethylformamide (75 cm<sup>3</sup>) until all the solid dissolved.  $K_2PtCl_4$  (0.17 g, 0.41 mmol) in water (25 cm<sup>3</sup>) was added dropwise to the refluxing solution. The resulting

cloudy solution was filtered hot. The clear yellow solution was placed in the refrigerator to give a dark orange solid. The solid was collected by filtration, washed with water, and ethanol followed by diethylether, and dried over phosphorus pentoxide.

Complex	Yield (%)	Elemental Analyses (%)		
		C	H	N
$[\text{CuL}^{10}] \cdot \text{H}_2\text{O}$	78	56.36 (55.35)	3.65 (3.57)	10.21 (9.93)
$\text{PtL}^{10}$	40	46.05 (46.08)	2.68 (2.68)	8.23 (8.27)

*References - Syntheses.*

1. W. Baker, K. M. Buggle, J. F. W. McCormie and D. A. M. Watkins, *J. Chem. Soc.*, 1958, 3595.
2. T. Lac, B.Sc Project, University of North London, 1991.
3. D. Jerchel, J. Heider and H. Wagner, *Leibigs Ann. Chem.*, 1958, 613, 153.
4. R. D. Cannon, B. Chiswell and L. M. Venanzi, *J. Chem. Soc.*, 1976, 1277.

#### CRYSTALLOGRAPHY.

A Philips PW 1100 four-circle diffractometer was used for X-ray data collection with Mo- $K_{\alpha}$  radiation from a graphite-crystal monochromator. All computing was carried out on a DEC VAX11-780 mainframe computer (VMS version 5.4-3).

This section outlines the experimental X-ray structural solution of  $[\text{CuL}^{10}].\text{H}_2\text{O}$ . The structure is discussed in detail in Chapter Six, where fully labelled diagrams and principal bond lengths and angles are tabulated. Full X-ray data is listed in Appendix C.

#### Crystal Data for $[\text{CuL}^{10}].\text{H}_2\text{O}$ .

$\text{C}_{26}\text{H}_{20}\text{CuN}_4\text{S}_2\text{O}_3$ ,  $M = 566.15$ , monoclinic, space group  $P2_1/n$ ,  $a = 16.338(4)$ ,  $b = 16.679(4)$ ,  $c = 8.929(2) \text{ \AA}$ ,  $\beta = 97.96(3)^\circ$ ,  $Z = 4$ ,  $U = 2409.72 \text{ \AA}^3$ ,  $D_c = 1.555 \text{ g cm}^{-3}$ ,  $F(000) = 1156$ ,  $\mu(\text{Mo-}K_{\alpha}) = 10.52 \text{ cm}^{-1}$ .

#### Data Collection.

The methods of data collection and data processing used for  $[\text{CuL}^{10}].\text{H}_2\text{O}$  were similar to those described previously.<sup>[1]</sup> The crystal selected for data collection had dimensions of  $0.27 \times 0.34 \times 0.10 \text{ mm}$ . A scan width of  $0.90^\circ$  in  $\theta$  was used to collect data in the  $\theta$ -range  $3-25^\circ$  by the  $w/2\theta$  technique. Equivalent reflections were merged to give 2855 unique data with  $I > 3\sigma(I)$ .

#### Structure Solution and Refinement.

The following steps outline the procedure involved in solving the Patterson map. Systematic absences in the data of the type :  $OK0$ ,  $K = 2n + 1$  is consistent with the presence of a  $2_1$  screw axis. In

addition, systematic absences of the type  $h0l$ ,  $h+1 = 2n + 1$  denotes the presence of an  $n$ -glide plane perpendicular to the  $z_1$  screw axis. From this data the space group was determined to be  $P2_1/n$ .

a) Patterson Solution.

The equivalent positions for the space group  $P2_1/n$  were obtained from International Tables (Vol 1) and are as follows:

$x,$	$y,$	$z$
$\bar{x},$	$\bar{y},$	$\bar{z}$
$0.5 + x, 0.5 - y, 0.5 + z$		
$0.5 - x, 0.5 + y, 0.5 - z$		

The series of unique vectors between two atoms (1) and (2) are given by:

$$\begin{array}{lll} x_1 - x_2' & y_1 - y_2' & z_1 - z_2 \\ x_1 + x_2' & y_1 + y_2' & z_1 + z_2 \\ 0.5 + (x_1 - x_2), \quad 0.5 + (y_1 + y_2), \quad 0.5 + (z_1 - z_2) \\ 0.5 + (x_1 + x_2), \quad 0.5 + (y_1 - y_2), \quad 0.5 + (z_1 + z_2) \end{array}$$

Since the structure of  $[CuL^{10}].H_2O$  contains one heavy metal atom per molecule, the Patterson synthesis could be best resolved by identifying the appropriate Harker vectors in this space group:

$$\begin{array}{lll} 2x, & 2y, & 2z \\ 0.5, & 0.5 + 2y, & 0.5 \\ 0.5 + 2x, & 0.5, & 0.5 + 2z \end{array}$$

The Patterson map was searched for the highest peaks corresponding to these vectors.

The following type of u, v, w vector was searched for:

0.5, 0.5 + 2y, 0.5

0.5, ? 0.5

A possible maximum was found at peak height 488:

0.500, 0.493, 0.500

A vector of the following type was searched for and a possible maximum was found at peak height 233:

0.5 + 2x, 0.5, 0.5 + 2z

? 0.500 ?

0.071, 0.500, 0.458

Hence, for 2x, 2y, 2z the following vector was searched for:

-0.429, 0.007, -0.042

The closest observed vector was found at peak height 223:

2x, 2y, 2z

0.426, -0.007, 0.044

From the solution of the appropriate u, v, w peaks, the following fractional co-ordinates for the copper(II) atom were deduced:

x, y, z

-0.213, -0.0035, -0.022

In this way the co-ordinates of the copper(II) atom were deduced from the Patterson synthesis.

*b) Location of Hetero, Carbon and Hydrogen Atoms.*

The fractional co-ordinates of the copper(II) atom were subsequently used in a series of difference-Fourier maps to generate the fractional atomic co-ordinates of the entire ligand framework.

The hydrogen atoms attached to the macrocycle carbon atoms were carefully located using the  $\sin\theta < 0.35$  technique. Maxima corresponding to atoms H11A, H14A, H11B, H12B, H14B and H1C, were located from suitable electron density maps. These were included in the structure factor calculations with fixed thermal factors of 0.08  $\text{\AA}^2$ , but their parameters were not refined. The remaining hydrogen atoms could not be found and were included in geometrical idealised calculated positions (C-H 1.08  $\text{\AA}$ ) with a common isotropic thermal parameter of 0.08  $\text{\AA}^2$  which were not refined. The carbon atoms of the two phenylene rings were constrained to regular hexagonal geometry (C-C 1.395  $\text{\AA}$ ).

c) Refinement.

Absorption corrections were then applied to the data after initial refinement with isotropic thermal parameters for all atoms. In the final cycles of the full matrix refinement, the copper, nitrogen, sulphur and oxygen atoms were assigned anisotropic thermal parameters. Refinement converged at  $R = 0.0533$  and  $R_w = 0.0530$  with weights of  $w = 1/\sigma^2(I)$  assigned to the individual reflections.

*Crystal Data for New Structures Described in this Report.*

The remaining seven crystal structures synthesized and discussed in this report were solved by co-workers at the University of North London: W.S. Li and N. Choi - 7.1, 7.2 and 7.6; Dr. H. R. Powell - 7.3, 7.4, 7.7; A. Bashall - 7.5. The structures [7.1 - 7.7] were solved in an analogous manner to that of  $[\text{CuL}]^{10}\text{H}_2\text{O}$ , with the exception of structure [7.5] which was solved using direct methods.

7.1  $[\text{HgL}^1(\text{Cl})_2]$  - Chapter Two.

$\text{C}_{19}\text{H}_{19}\text{Cl}_2\text{N}_3\text{S}_2\text{Hg}$ , M = 625.02, monoclinic, space group = P2<sub>1</sub>/n,  $a = 12.111$ ,  $b = 7.925$ ,  $c = 21.676 \text{ \AA}$ ,  $\alpha = 90.0^\circ$ ,  $\beta = 92.92^\circ$ ,  $\gamma = 90.0^\circ$ ,  $z = 4$ ,  $U = 2077.75 \text{ \AA}^3$ ,  $D_c = 1.998 \text{ g cm}^{-3}$ ,  $F(000) = 1200$ . A dark blue crystal of size  $0.32 \times 0.20 \times 0.04 \text{ mm}$ ,  $\mu(\text{Mo-}K_\alpha) = 75.64 \text{ cm}^{-1}$ . Equivalent reflections were merged to give a total of 2174 unique data with  $I > 3\sigma(I)$ . Individual weights of  $1/\sigma^2(I)$  were assigned to each reflection and refinement converged at  $R = 0.0488$  and  $R_w = 0.0493$ .

7.2  $[\text{NiL}^1(\text{Cl})]\text{Cl} \cdot \text{MeOH}$  - Chapter Two.

$\text{C}_{20}\text{H}_{23}\text{Cl}_2\text{N}_3\text{S}_2\text{ONi}$ , M = 515.16, orthorhombic, space group = Pna2<sub>1</sub>,  $a = 14.672(3)$ ,  $b = 9.652(2)$ ,  $c = 15.326(3) \text{ \AA}$ ,  $z = 4$ ,  $U = 2170.38 \text{ \AA}^3$ ,  $D_c = 1.998 \text{ g cm}^{-3}$ ,  $F(000) = 1064$ . A violet crystal of size  $0.30 \times 0.20 \times 0.25 \text{ mm}$ ,  $\mu(\text{Mo-}K_\alpha) = 13.20 \text{ cm}^{-1}$ . Equivalent reflections were merged to give a total of 1156 unique data with  $I > 3\sigma(I)$ . Individual weights of  $1/\sigma^2(I)$  were assigned to each reflection and refinement converged at  $R = 0.0442$  and  $R_w = 0.0425$ .

7.3  $[\text{PbL}^4(\text{H}_2\text{O})(\text{MeOH})](\text{ClO}_4)_2$  - Chapter Four.

$\text{C}_{27}\text{H}_{26}\text{Cl}_2\text{N}_4\text{O}_10\text{S}_2\text{Pb}$ , M = 908.92, triclinic, space group = P1 (no. 2),  $a = 13.037(4) \text{ \AA}$ ,  $b = 11.673(3) \text{ \AA}$ ,  $c = 10.844(3) \text{ \AA}$ ,  $\alpha = 93.93(2)^\circ$ ,  $\beta = 11.673(3)^\circ$ ,  $\gamma = 94.82(2)^\circ$ ,  $z = 2$ ,  $U = 1607.41 \text{ \AA}^3$ ,  $D_c = 1.87 \text{ g cm}^{-3}$ ,  $F(000) = 884$ . A pale orange crystal of size  $0.35 \times 0.24 \times 0.34 \text{ mm}$ ,  $\mu(\text{Mo-}K_\alpha) = 55.48 \text{ cm}^{-1}$ . Equivalent reflections were merged to give a total of 3713 unique data with  $I > 3\sigma(I)$ . Individual weights of  $1/\sigma^2(I)$  were assigned to each reflection and refinement converged at  $R = 0.0569$  and  $R_w = 0.0545$ .

7.4  $[\text{HgL}^6(\text{SCN})_2] \cdot \text{MeOH}$  - Chapter Four.

$\text{C}_{29}\text{H}_{24}\text{N}_6\text{OS}_4\text{Hg}$ ,  $M = 801.38$ , triclinic, space group = P1 (no. 2),  $a = 13.657(4)$  Å,  $b = 12.085(4)$  Å,  $c = 9.393(3)$  Å,  $\alpha = 89.64(2)^\circ$ ,  $\beta = 97.17(3)^\circ$ ,  $\gamma = 102.96(3)^\circ$ ,  $z = 2$ ,  $U = 1498.58$  Å<sup>3</sup>,  $D_c = 1.52$  g cm<sup>-3</sup>,  $F(000) = 668$ . An orange crystal of size  $0.26 \times 0.08 \times 0.16$  mm,  $\mu(\text{Mo-}K_\alpha) = 52.23$  cm<sup>-1</sup>. Equivalent reflections were merged to give a total of 2839 unique data with  $I > 3\sigma(I)$ . Individual weights of  $1/\sigma^2(I)$  were assigned to each reflection and refinement converged at  $R = 0.0439$  and  $R_w = 0.0405$ .

7.5  $\text{L}^{48}$  - Chapter Four.

$\text{C}_{26}\text{H}_{20}\text{N}_4\text{OS}_2$ ,  $M = 468.60$ , triclinic, space group = P1,  $a = 9.782(3)$ ,  $b = 13.170(4)$ ,  $c = 8.888(3)$  Å,  $\alpha = 102.58$ ,  $\beta = 97.73(3)^\circ$ ,  $\gamma = 85.39(2)^\circ$ ,  $z = 2$ ,  $U = 1105.85$  Å<sup>3</sup>,  $D_c = 1.41$  g cm<sup>-3</sup>,  $F(000) = 488$ , A colourless crystal of size  $0.35 \times 0.28 \times 0.15$  mm,  $\mu(\text{Mo-}K_\alpha) = 2.22$  cm<sup>-1</sup>. Equivalent reflections were merged to give a total of 2001 unique data with  $I > 3\sigma(I)$ . Individual weights of  $1/\sigma^2(I)$  were assigned to each reflection and refinement converged at  $R = 0.0567$  and  $R_w = 0.0590$ .

7.6  $[\text{NiL}^6][\text{ClO}_4]_2$  - Chapter Five.

$\text{C}_{26}\text{H}_{24}\text{Cl}_2\text{N}_4\text{S}_2\text{O}_4\text{Ni}$ ,  $M = 714.23$ , orthorhombic, space group = Pca2<sub>1</sub>,  $a = 16.787(2)$ ,  $b = 12.790(2)$ ,  $c = 13.443(3)$  Å,  $z = 4$ ,  $U = 2886.29$  Å<sup>3</sup>,  $D_c = 1.644$  g cm<sup>-3</sup>,  $F(000) = 1464$ . A violet crystal of size  $0.44 \times 0.28 \times 0.22$  mm,  $\mu(\text{Mo-}K_\alpha) = 10.30$  cm<sup>-1</sup>. Equivalent reflections were merged to give a total of 1738 unique data with  $I > 3\sigma(I)$ . Individual weights of  $1/\sigma^2(I)$  were assigned to each reflection and refinement converged at  $R = 0.0453$  and  $R_w = 0.0472$ .

7.7  $[\text{CuL}^{68}][\text{ClO}_4]_2$  - Chapter Five.

$\text{C}_{30}\text{H}_{32}\text{Cl}_2\text{N}_2\text{O}_{10}\text{S}_2\text{Cu}$ ,  $M = 801.38$ , monoclinic, space group  $P2_1/n$ ,  $a = 16.763(5)$  Å,  $b = 23.255(6)$  Å,  $c = 9.131(3)$  Å,  $\beta = 102.38(3)^\circ$ ,  $z = 4$ ,  $v = 3476.71$ ,  $D_c = 1.51 \text{ g cm}^{-3}$ ,  $F(000) = 1620$ . A dark green crystal of size  $0.19 \times 0.40 \times 0.14$  mm,  $\mu(\text{Mo}-K_\alpha) = 8.97 \text{ cm}^{-1}$ . Equivalent reflections were merged to give a total of 1196 unique data with  $I > 3\sigma(I)$ . Individual weights of  $1/\sigma^2(I)$  were assigned to each reflection and refinement converged at  $R = 0.1220$  and  $R_w = 0.1167$ .

References - Crystallography.

1. (a) P. F. Jackson, B. F. G. Johnson, J. Lewis, W. J. H. Nelson and M. McPartlin, *J. Chem. Soc., Dalton Trans.*, 1982, 2099; (b) N. F. M. Henry and K. Lonsdale (eds), 'International Tables for X-ray Crystallography,' Kynoch Press, Birmingham, 1952, Vol 1; (c) G. M. Sheldrick, 'SHELX76 programme for crystal structure determination,' University of Cambridge, 1976; (d) C. K. Johnson, 'ORTEP-II programme for plotting crystal structures,' Oak Ridge National Laboratory, 1976; (e) E. Keller, 'SCHAKAL programme for space filling diagrams,' University of Frieberg, 1982.

**APPENDIX A**

**N.M.R. -  $AB_2$  SPIN SYSTEM.**

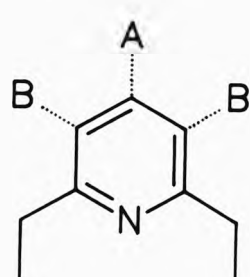
COUPLING OF NUCLEAR SPINS: DESCRIPTION OF  $\text{AB}_2$  ( $\text{A}_2\text{B}$ )<sup>[1]</sup> SPIN SYSTEM AND  
CALCULATION OF SIGNAL FREQUENCY.

When coupled multiplets conform to the condition:

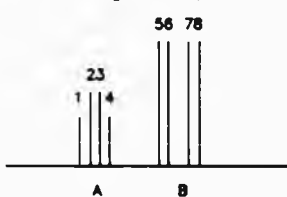
$$\nu_0 \delta/J \geq 10$$

where  $\nu_0$  is the operating frequency, the multiplets are considered to be first-order and the n.m.r. spectra can then be analysed according to  $(n+1)$  selection rules. As  $\delta/J$  becomes less than ca. 10, spectra often show extra lines where spacings exhibit no obvious regularity and their intensities no longer approximate to Pascal's Triangle. In these cases, second-order effects are displayed and assignment of lines by inspection alone is not possible.<sup>[2]</sup>

Two magnetically equivalent nuclei coupled to a third constitute an  $\text{AB}_2$  spin system. For instance, the  $\gamma$  and  $\beta$  protons of a 2,6-disubstituted pyridyl ring can often give a complicated multiplet splitting pattern as opposed to the simple first-order triplet (A) and doublet (B) normally expected.



In all, a total of eight lines can be observed in the second-order  $AB_2$  sub-spectrum, where the central line of the triplet is split and each line of the doublet splits into two (a ninth combination line also exists on the  $B_2$  side of the spectrum, but is rarely detected).



Additionally, it should be noted that not all eight lines are necessarily always resolved and that second-order effects can be reduced by increasing the operating frequency of the spectrometer.

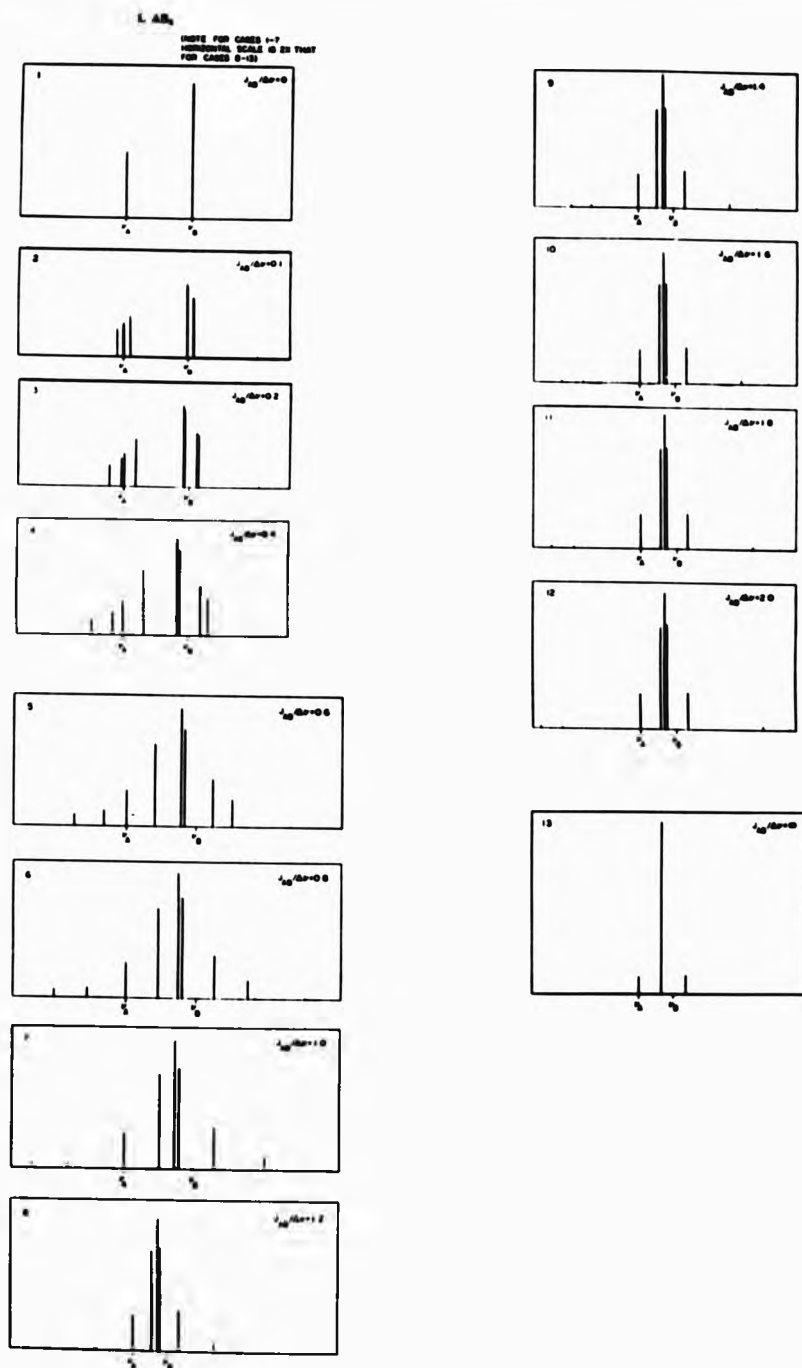
For these type of spectra, the chemical shift  $\delta$  in Hertz ( $\nu$ ) is given by line 3 for  $\nu_A$  and from the mean of lines 5 and 7  $\nu_B$  can be found. The coupling constant  $J_{AB}$  can then be obtained from the calculation:

$$J_{AB} = 1/3[(\nu_5 - \nu_6) + (\nu_7 - \nu_1)]$$

As  $J_{AB}$  becomes infinitely larger, the  $AB_2$  spectrum is reduced to a triplet.

#### References.

1. An  $A_2B$  spectrum will be the mirror image of an  $AB_2$  system.
2. F. A. Bovey, 'Nuclear Magnetic Resonance Spectroscopy,' Academic Press, New York, 1969.



**APPENDIX B.**

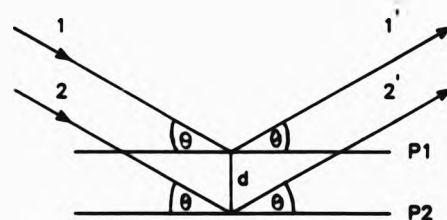
**A BRIEF RESUME OF CRYSTALLOGRAPHIC BACKGROUND.**

#### *Crystal Dimensions.*

Crystals are composed of a regularly repeating array of atoms, ions or molecules in three-dimensions. A crystal lattice is an array of points (each of identical environment) separated by unit cell translations. The unit cell is the defined repeat unit (continuous replication, generates the entire crystal) and is characterised by six parameters; the edge lengths  $a$ ,  $b$ , and  $c$ , and the angles  $\alpha$ ,  $\beta$ , and  $\gamma$ , between pairs of sides ( $\alpha$  is between  $bc$ ,  $\beta$  is between  $ac$  and  $\gamma$  is between  $ab$ ). Any point or atom within the unit cell is defined by fractional co-ordinates  $x$ ,  $y$ , and  $z$ , where  $x = X/a$ ,  $y = Y/b$ , and  $z = Z/c$ . The co-ordinates are defined parallel to the corresponding unit cell axis and  $X$ ,  $Y$ , and  $Z$  are in Å.

#### *X-Ray Diffraction Conditions.*

With the discovery of X-rays at the end of the last century there was evidence to indicate that their wavelengths were comparable to atomic spacings in crystals. Laue (in 1912) suggested and demonstrated that their wave-like nature could cause X-rays to be diffracted when passed through a crystal. The conditions for diffraction in three dimension are complex but were simplified by Bragg who noticed that diffraction of X-rays by crystals was geometrically similar to ordinary 'reflection' from sets of mathematically defined planes.



The condition for constructive interference (i.e. diffraction) occurs only if the path-length difference ( $AB + BC$ ) =  $n\lambda = 2d \sin\theta$ . Where  $n$  is an integer,  $\lambda$  is the wavelength of the radiation incident at an angle  $\theta$  (as well as reflected at an angle  $\theta$ ), from a set of planes separated by a distance  $d$ .

Each set of planes is denoted by the indices  $h$ ,  $k$ , and  $l$ , which cut the unit cell axes with intercepts  $a/h$ ,  $b/k$ , and  $c/l$ . More specifically, the equation becomes:

$$\lambda = 2d_{hkl} \sin\theta_{hkl}$$

where  $\lambda$  is the wavelength of the X-radiation,  $\theta_{hkl}$  is the Bragg angle, and  $d_{hkl}$  is the perpendicular spacing between adjacent planes in the  $hkl$  set. Measurement of the angle and the direction of the diffracted beam allows unit cell dimensions to be deduced.

#### Crystal Symmetry.

Almost all crystals have some symmetry, since this is dependent on the way in which atoms are arranged in the crystal lattice, a knowledge of the symmetry of atomic arrangement is very useful for structure determination.

The symmetry present in any crystal causes it to conform to one of seven crystal systems, which impose special restrictions on the unit cell dimensions. These restrictions range from none ( $a \neq b \neq c$  and  $\alpha \neq \beta \neq \gamma \neq 90^\circ$ ) for triclinic crystals to  $a = b = c$  and  $\alpha = \beta = \gamma = 90^\circ$  for cubic crystals. The notation used in crystallography for the symmetry elements are those of Hermann-Mauguin as opposed to the

Schoenflies notation used in spectroscopy.

Two simple types of symmetry can exist in the internal structure of a crystal; rotation and reflection. Rotation is necessarily about an axis, and designated as n-fold (where  $n = 1, 2, 3, 4$  or  $6$ ) if on rotating  $360^\circ/n$ , the resulting arrangement is in a position indistinguishable from the initial position. Reflection arises when two points are related by a plane of symmetry or mirror plane, and is given the symbol m.

Combinations of simple symmetry elements produce more complex symmetry: Centrosymmetry occurs by a single operation called inversion, amounting to a reflection on a point called the centre of symmetry or the inversion centre midway between them, and a rotation axis combined with an inversion centre produces a rotary inversion axis which is designated by a bar over an integer.

Every lattice is inherently centrosymmetric since lattice points and points midway between them are centres of symmetry. An inversion centre is the only symmetry possessed by the triclinic lattice, and it is indicated as a one-fold axis  $\bar{1}$ ; that is rotation of  $360^\circ/1$  followed by inversion through the origin. All other lattices display additional symmetry. For the monoclinic lattice the symbol  $2/m$ , indicates a two-fold axis with a mirror plane perpendicular to it. Convention dictates b to be the unique axis, perpendicular to ac.

Furthermore, combinations of either rotation or reflection with translations give additional symmetry elements. A rotational axis and a translation parallel to the axis produces a screw axis, which is

designated by an integer  $n$  and a subscript  $m$ , where  $n = 1, 2, 3, 4$  or  $6$  is the order of the axis and  $m$  is an integer factor of  $n$ . A mirror plane and a translation parallel to the reflecting plane produces a glide plane. A glide plane is designated by  $a$ ,  $b$  or  $c$  if the translation is  $a/2$ ,  $b/2$  or  $c/2$ , and by  $n$  if the translation is  $(a+b)/2$ ,  $(a+c)/2$  or  $(b+c)/2$ .

#### Lattice Types.

When a unit cell is selected so that the lattice points occur only at the corners of the unit cell, the lattice is termed primitive and given the symbol  $P$ . Combination of a primitive lattice with one or more offset identical copies of itself gives rise to non-primitive lattices. The non-primitive lattices are essential in order to describe the maximum symmetry of some monoclinic crystals. Centered lattices, have unit cells specially selected to give lattice points not only at the corners of the unit cell, but also either in the centre of the unit cell or in the centre of its faces. There are seven primitive and seven non-primitive lattices arising from the seven crystal systems known as the fourteen Bravais lattices. For each crystal system, the lattice symmetry represents the highest point group symmetry that is possible.

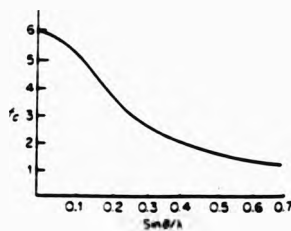
Crystal System.	Point Group Notations. Hermann-Mauguin      Schoenflies		Lattice Symmetry.
Triclinic	$l, \bar{l}$	$C_1, C_i$	$\bar{1}$
Monoclinic	$m, 2, 2/m$	$C_s, C_{2v}, C_{2h}$	$2/m$

There are 32 unique point groups classified under seven crystal systems. These together with the fourteen Bravais lattices result in

230 unique space groups. A space group is identified by a lattice type followed by point groups.

#### The Atomic Scattering Factor.

Since it is the electrons of an atom that diffract the X-rays, the degree of diffraction depends on the number of electrons, and therefore on the atomic number of the element. The expression for the scattering power of an atom is known as the atomic scattering factor ( $f$ ). The atomic scattering factor ( $f$ ) is a function of  $\sin\theta/\lambda$  and decreases with increasing angle of diffraction.



#### The Structure Factor.

The intensities  $I_{hkl}$  of all the diffracted beams, known as 'reflections' are related to the structure factor  $F_{hkl}$ , where  $I_{hkl} = |F_{hkl}|^2$ . The structure factor is the resultant of  $N$  waves scattered in the direction of the reflection  $hkl$  by the  $N$  atoms in the unit cell and may be expressed:

$$F_{hkl} = \sum_{n=1}^{N=N} f_n e^{2\pi i(hx_n + ky_n + lz_n)}$$

The scattering factor of the  $n^{\text{th}}$  atom is  $f_n$ , where  $x_n$ ,  $y_n$ , and  $z_n$  are the fractional co-ordinates of the  $n^{\text{th}}$  atom.

Conversion of measured intensities  $I_{hkl}$  to structure factor amplitudes  $F_o$ , is known as data reduction. This involves the application of a number of correction factors to the values of  $F_o$  and to their estimated standard deviations (e.s.d.s)  $\sigma(F_o)$ . In addition Lorentz and polarisation errors are also corrected for the raw data.

#### The Phase Problem.

The target of X-ray structure determination is to define the position of all the atoms in the crystal and hence the complete geometry of the molecules. In theory, the fractional co-ordinates  $x_n$ ,  $y_n$ ,  $z_n$  for each of the  $N$  atoms in the unit cell may be obtained by calculating the electron density,  $\rho_{xyz}$  at a grid of points  $x$ ,  $y$ ,  $z$  calculated from the Fourier synthesis:

$$\rho_{xyz} = 1/V \sum_{hkl} F_{hkl} e^{-2\pi i(hx+ky+lz)}$$

where  $V$  is the unit cell volume. Although the magnitude of the structure factor  $F_{hkl}$  may be obtained from the corrected intensity data  $I_{hkl}$ , because  $I_{hkl}$  is proportional to the square modulus  $|F_{hkl}|^2$ , the phase angle is unknown. This is known as the phase problem. However, in this work all the crystals discussed were centrosymmetric and so the expression for the structure factor simplifies to:

$$F_{hkl} = 2 \sum_n f_n \cos 2\pi(hx_n + ky_n + lz_n)$$

Thus the phase problem is reduced to a 'sign' problem (+ or -), and it is the sign of  $F_{hkl}$  that has to be determined before an electron density map can be calculated.

Nearly all methods for solving the phase problem rely on initially deducing the co-ordinates for one or more atoms of relatively high scattering power. These atomic co-ordinates can be used to calculate approximate values of the structure factor,  $F_c$ , for each reflection. If the atoms of the 'partial structure' contribute significantly to the diffraction many of the calculated signs will be correct. The strategy then employed is to assign these calculated signs (+ or -) to the corresponding observed structure factors  $F_o$  and use them in the Fourier series for the calculation of electron density:

$$\rho_{xyz} = 1/V \sum_{hkl} S_c F_o \cos 2\pi(hx + ky + lz)$$

This iterative process is repeated until all the non-hydrogen atoms have been found. In some instances, even hydrogen atoms may be located. The X-ray scattering ability of hydrogen is relatively higher at low angle reflections ( $\sin\theta < 0.35$ ) compared to other atoms, and therefore the hydrogen peaks may be resolved more easily from a difference-Fourier synthesis based on data with high angle reflections excluded. This has the advantage of minimising termination of series errors:

$$\rho_{xyz} = 1/V \sum S_c (|F_o| - |F_c|) \cos 2\pi(hx + ky + lz)$$

#### The Patterson Synthesis.

For metal co-ordination compounds the Patterson synthesis provides a method of deducing the position of the metal atom and this, having a relatively high number of electrons, provides a suitable starting place for a 'partial structure'. The Patterson synthesis involves the

insertion of  $I_{hkl}$  in place of  $F_{hkl}$  in a Fourier synthesis:

$$\rho_{uvw} = 1/V \sum |F_{hkl}|^2 e^{-2\pi i(hu+kv+lw)}$$

where  $\rho_{uvw}$  is the Patterson density at a point of fractional co-ordinate  $uvw$ . This function represents interatomic vectors rather than fractional atomic co-ordinates. That is  $u$ ,  $v$ ,  $w$ , gives the vector between two atoms of fractional co-ordinates  $x_1$ ,  $y_1$ ,  $z_1$  and  $x_2$ ,  $y_2$ ,  $z_2$ , where,

$$u = x_1 - x_2$$

$$v = y_1 - y_2$$

$$w = z_1 - z_2$$

The Patterson summation will always involve a large peak at the origin  $(0,0,0)$ , and all corners of the unit cell, due to superposition of all vectors which arise from every atom to the identical atom in the adjacent unit cell. In general, if an atom  $i$  contains  $Z_i$  electrons and an atom  $j$  contains  $Z_j$  electrons, the peak in the Patterson summation which represents the vector between atoms  $i$  and  $j$ , will have a height proportional to  $Z_i Z_j$ . Thus the heavier atoms will give rise to higher peaks in the Patterson map which can be readily distinguished. This accounts for the use of the Patterson synthesis as a method for determining the positions of metal atoms.

#### Refinement.

Once all the atoms in the crystal have been located the model is systematically adjusted to obtain the best fit between the observed data and the calculated structure factors. The latter depend on a

large number of parameters made up of the fractional co-ordinates of the atoms and their thermal parameters. Additionally an overall scale factor, K is applied to all the observed structure factors to bring them onto the same scale as the calculated values. The method of least-squares refinement involves systematically altering the parameters to minimise the function,

$$\sum w_{hkl} (F_o - F_c)^2$$

The weighting factor is assigned to each individual reflection to take into account the different precision of the observed structure amplitudes  $(F_o)_{hkl}$ . In this work the standard weight,

$$1/\sigma^2 (F_o)_{hkl}$$

was used.

#### Absorption Corrections.

In addition to being scattered, the incident and diffracted X-rays are also absorbed by crystals. The intensity I of a beam after passing through a thickness t of crystal is given by,

$$I = I_0 e^{-\mu t}$$

Where  $I_0$  is the intensity of the incident beam and  $\mu$  the linear absorption coefficient. The value of the linear absorption coefficient is dependent on the wavelength of the X-rays used, the type of atoms

present, and the density of the crystal.

This may be corrected by the method of Stuart and Walker. It involves use of a Fourier series to model the discrepancy between the calculated and observed structure factor amplitudes. The correction is evaluated using observed structure factors of the full data set without averaging symmetry-equivalent or Friedel-pair reflections. The calculated structure factors are based on the best model obtained with isotropic thermal parameters for all the atoms.

*References.*

1. N. Walker and D. Stuart, *Acta Crystallogr., Sect. A* 1983, **A39**, 158.
2. G. H. Stout and L. H. Jensen, 'X-Ray Structure Determination - A practical Guide,' Wiley-Interscience, New York, (2nd edn) 1989.
3. P. W. Atkins, 'Physical Chemistry,' Oxford University Press, Oxford, (2nd edn) 1984.

**APPENDIX C**  
**FULL CRYSTAL DATA FOR  $[\text{CuL}^{10}] \cdot \text{H}_2\text{O}$**

TABLE C.1 FRACTIONAL ATOMIC CO-ORDINATES AND THERMAL PARAMETERS ( $\text{\AA}^2$ )  
FOR  $[\text{CuL}^{10}]\cdot\text{H}_2\text{O}$ .

Atom	x	y	z	$U_{\text{iso}}$ or $U_{\text{eq}}$
Cu	0.21422(5)	-0.00347(6)	0.02237(10)	0.0284(5)
S(1a)	0.3040(1)	-0.2213(1)	0.1412(3)	0.049(1)
S(1b)	0.2495(1)	0.1386(1)	0.1159(2)	0.039(1)
O(1a)	0.0906(3)	-0.1766(3)	0.2183(7)	0.053(4)
O(1b)	0.1158(3)	0.0784(3)	-0.3975(6)	0.041(3)
N(2a)	0.1863(4)	-0.0793(4)	0.1776(7)	0.034(4)
N(2b)	0.2046(4)	0.0582(3)	-0.1718(7)	0.029(3)
N(1c)	0.1103(3)	-0.0447(4)	-0.0788(7)	0.030(4)
N(3c)	0.3425(4)	-0.0158(3)	0.0957(7)	0.031(4)
C(1c)	-0.0378(5)	-0.0973(5)	-0.2141(10)	0.043(2)
C(2a)	-0.0077(5)	-0.1264(5)	-0.0677(10)	0.043(2)
C(3a)	0.0696(5)	-0.0973(5)	-0.0055(9)	0.033(2)
C(4a)	0.1161(5)	-0.1223(5)	0.1443(9)	0.037(2)
C(5a)	0.2405(4)	-0.1014(4)	0.3099(9)	0.031(2)
C(11a)	0.2371(5)	-0.0604(5)	0.4429(10)	0.042(2)
C(12a)	0.2898(6)	-0.0791(5)	0.5757(11)	0.053(2)
C(13a)	0.3491(5)	-0.1393(5)	0.5692(10)	0.050(2)
C(14a)	0.3537(5)	-0.1781(5)	0.4341(10)	0.043(2)
C(6a)	0.2990(5)	-0.1606(5)	0.3043(9)	0.035(2)
C(7a)	0.3249(5)	-0.1506(5)	-0.0083(10)	0.047(2)
C(8a)	0.3787(5)	-0.0858(5)	0.0628(10)	0.044(2)
C(9a)	0.4638(7)	-0.1009(7)	0.1039(13)	0.070(3)
C(10c)	0.5078(7)	-0.0442(8)	0.1860(14)	0.086(4)
C(2b)	0.0047(5)	-0.0421(5)	-0.2911(9)	0.038(2)
C(3b)	0.0812(4)	-0.0166(4)	-0.2167(8)	0.029(2)

Table C.1 continued

C(4b)	0.1365(5)	0.0450(5)	-0.2736(9)	0.034(2)
C(5b)	0.2576(4)	0.1237(4)	-0.1857(8)	0.028(2)
C(11b)	0.2835(5)	0.1470(5)	-0.3245(10)	0.043(2)
C(12b)	0.3380(5)	0.2104(5)	-0.3268(11)	0.049(2)
C(13b)	0.3678(5)	0.2529(5)	-0.1944(10)	0.047(2)
C(14b)	0.3399(5)	0.2302(5)	-0.0580(10)	0.042(2)
C(6b)	0.2867(4)	0.1654(4)	-0.0549(8)	0.029(2)
C(7b)	0.3453(5)	0.1121(5)	0.2346(10)	0.051(2)
C(8b)	0.3860(5)	0.0406(5)	0.1819(10)	0.047(2)
C(9b)	0.4736(7)	0.0288(7)	0.2309(13)	0.077(3)
O(3c)	0.5452(5)	0.2684(5)	0.1579(9)	0.088(2)

TABLE C.2 Fractional atomic co-ordinates for the hydrogen atoms of  
 $[\text{CuL}^{10}].\text{H}_2\text{O}$ .

Atom	x	y	z
H(2a)	-0.0416	-0.1685	-0.0080
H(12a)	0.2851	-0.0483	0.6806
H(13a)	0.3905	-0.1550	0.6700
H(7a1)	0.2676	-0.1258	-0.0641
H(7a2)	0.3563	-0.1815	-0.0902
H(9a)	0.4917	-0.1559	0.0720
H(10c)	0.5731	-0.0545	0.2187
H(2b)	-0.0192	-0.0208	-0.4028
H(13b)	0.4109	0.3018	-0.1976
H(7b1)	0.3316	0.1005	0.3475
H(7b2)	0.3874	0.1621	0.2371
H(9b)	0.5108	0.0731	0.2971
H(11a)	0.1978	-0.0054	0.4376
H(14a)	0.3976	-0.2198	0.4229
H(11b)	0.2627	0.1116	-0.4180
H(12b)	0.3595	0.2344	-0.4419
H(14b)	0.3580	0.2671	0.0550
H(1c)	-0.0856	-0.1285	-0.2659

TABLE C.3 Anisotropic thermal parameters ( $\text{\AA}^2$ ) for  $(\text{CuL}^{10}) \cdot \text{H}_2\text{O}$ .

Atom	$U_{11}$	$U_{22}$	$U_{33}$	$U_{23}$	$U_{13}$	$U_{12}$
Cu	0.026(1)	0.033(1)	0.027(1)	0.004(1)	0.000(1)	-0.003(1)
S(1a)	0.076(2)	0.032(1)	0.038(1)	0.002(1)	0.016(1)	0.008(1)
S(1b)	0.013(1)	0.037(1)	0.036(1)	-0.009(1)	0.013(1)	-0.003(1)
O(1a)	0.044(3)	0.053(4)	0.06(4)	0.023(3)	0.009(3)	-0.014(3)
O(1b)	0.013(3)	0.052(4)	0.029(3)	0.008(3)	-0.005(3)	-0.003(3)
N(2a)	0.035(4)	0.037(4)	0.029(4)	0.012(3)	0.003(3)	0.000(3)
N(2b)	0.031(3)	0.026(3)	0.030(3)	0.004(3)	-0.002(3)	-0.006(3)
N(1c)	0.023(3)	0.034(4)	0.032(4)	-0.001(3)	0.000(3)	-0.002(3)
N(3c)	0.031(3)	0.034(4)	0.030(3)	0.010(3)	0.003(3)	-0.001(3)

TABLE C.4 Bond lengths (Å) for  $(\text{CuL}^{10}) \cdot \text{H}_2\text{O}$ .

Cu	-S(1b)	2.552(2)	Cu	-N(2a)	1.976(6)
Cu	-N(2b)	2.003(6)	Cu	-N(1c)	1.937(6)
Cu	-N(3c)	2.117(6)	S(1a) -C(6a)	1.785(8)	
S(1a) -C(7a)	1.848(9)	S(1b) -C(6b)	1.774(8)		
S(1b) -C(7b)	1.819(9)	O(1a) -C(4a)	1.228(10)		
O(1b) -C(4b)	1.242(9)	N(2a) -C(4a)	1.350(10)		
N(2a) -C(5a)	1.424(9)	N(2b) -C(4b)	1.354(9)		
N(2b) -C(5b)	1.411(9)	N(1c) -C(3a)	1.327(10)		
N(1c) -C(3b)	1.341(9)	N(3c) -C(8a)	1.359(11)		
N(3c) -C(8b)	1.354(10)	C(1c) -C(2a)	1.417(12)		
C(1c) -C(2b)	1.390(12)	C(2a) -C(3a)	1.394(11)		
C(3a) -C(4a)	1.503(11)	C(5a) -C(11a)	1.379(12)		
C(5a) -C(6a)	1.380(11)	C(11a) -C(12a)	1.401(12)		
C(12a) -C(13a)	1.402(13)	C(13a) -C(14a)	1.380(13)		
C(14a) -C(6a)	1.393(11)	C(7a) -C(8a)	1.480(12)		
C(8a) -C(9a)	1.411(13)	C(9a) -C(10c)	1.344(16)		
C(10c) -C(9b)	1.421(17)	C(2b) -C(3b)	1.398(10)		
C(3b) -C(4b)	1.502(11)	C(5b) -C(11b)	1.418(12)		
C(5b) -C(6b)	1.385(10)	C(11b) -C(12b)	1.384(12)		
C(12b) -C(13b)	1.407(12)	C(13b) -C(14b)	1.410(13)		
C(14b) -C(6b)	1.390(11)	C(7b) -C(8b)	1.473(13)		
C(8b) -C(9b)	1.451(14)				

TABLE C.5 Bond angles ( $^{\circ}$ ) for  $[\text{CuL}^{10}] \cdot \text{H}_2\text{O}$ .

N(2a) - Cu	-S(1b)	115.4(2)	N(2b) - Cu	-S(1b)	78.1(2)
N(2b) - Cu	-N(2a)	159.7(2)	N(1c) - Cu	-S(1b)	128.8(2)
N(1c) - Cu	-N(2a)	80.0(3)	N(1c) - Cu	-N(2b)	79.6(2)
N(3c) - Cu	-S(1b)	79.6(2)	N(3c) - Cu	-N(2a)	92.0(2)
N(3c) - Cu	-N(2b)	105.9(2)	N(3c) - Cu	-N(1c)	151.2(2)
C(7a) - S(1a) - C(6a)		105.2(4)	C(6b) - S(1b) - Cu		92.4(2)
C(7b) - S(1b) - Cu		95.8(3)	C(7b) - S(1b) - C(6b)		101.2(4)
C(4a) - N(2a) - Cu		117.2(5)	C(5a) - N(2a) - Cu		124.8(5)
C(5a) - N(2a) - C(4a)		117.2(6)	C(4b) - N(2b) - Cu		117.2(5)
C(5b) - N(2b) - Cu		119.9(4)	C(5b) - N(2b) - C(4b)		121.6(6)
C(3a) - N(1c) - Cu		118.1(5)	C(3b) - N(1c) - Cu		118.7(5)
C(3b) - N(1c) - C(3a)		123.1(6)	C(8a) - N(3c) - Cu		117.3(5)
C(8b) - N(3c) - Cu		121.9(5)	C(8b) - N(3c) - C(8a)		120.6(7)
C(2b) - C(1c) - C(2a)		123.3(7)	C(3a) - C(2a) - C(1c)		115.4(8)
C(2a) - C(3a) - N(1c)		121.4(7)	C(4a) - C(3a) - N(1c)		113.4(6)
C(4a) - C(3a) - C(2a)		125.2(7)	N(2a) - C(4a) - O(1a)		127.9(7)
C(3a) - C(4a) - O(1a)		121.1(7)	C(3a) - C(4a) - N(2a)		111.0(7)
C(11a) - C(5a) - N(2a)		119.4(7)	C(6a) - C(5a) - N(2a)		120.6(7)
C(6a) - C(5a) - C(11a)		119.9(7)	C(12a) - C(11a) - C(5a)		121.6(8)
C(13a) - C(12a) - C(11a)		118.2(9)	C(14a) - C(13a) - C(12a)		119.6(8)
C(6a) - C(14a) - C(13a)		121.5(8)	C(5a) - C(6a) - S(1a)		123.1(6)
C(14a) - C(6a) - S(1a)		117.6(6)	C(14a) - C(6a) - C(5a)		119.2(7)
C(8a) - C(7a) - S(1a)		108.3(6)	C(7a) - C(8a) - N(3c)		118.0(7)
C(9a) - C(8a) - N(3c)		122.7(8)	C(9a) - C(8a) - C(7a)		119.1(8)
C(10a) - C(9a) - C(8a)		117(1)	C(9b) - C(10c) - C(9a)		124(1)

**Table C.5 continued**

C(3b) -C(2b) -C(1c)	116.2(7)	C(2b) -C(3b) -N(1c)	120.6(7)
C(4b) -C(3b) -N(1c)	113.4(6)	C(4b) -C(3b) -C(2b)	126.0(7)
N(2b) -C(4b) -O(1b)	128.5(7)	C(3b) -C(4b) -O(1b)	120.3(6)
C(3b) -C(4b) -N(2b)	111.1(6)	C(11b)-C(5b) -N(2b)	123.4(6)
C(6b) -C(5b) -N(2b)	117.2(7)	C(6b) -C(5b) -C(11b)	119.4(7)
C(12b)-C(11b)-C(5b)	119.5(8)	C(13b)-C(12b)-C(11b)	121.4(9)
C(14b)-C(13b)-C(12b)	118.3(8)	C(6b) -C(14b)-C(13b)	120.3(7)
C(5b) -C(6b) -S(1b)	118.7(6)	C(14b)-C(6b) -S(1b)	120.1(6)
C(14b)-C(6b) -C(5b)	121.0(7)	C(8b) -C(7b) -S(1b)	113.6(6)
C(7b) -C(8b) -N(3c)	121.3(7)	C(9b) -C(8b) -N(3c)	119.7(8)
C(9b) -C(8b) -C(7b)	118.9(8)	C(8b) -C(9b) -C(10c)	116(1)

TABLE C.6 Intermolecular distances ( $\text{\AA}$ ) for  $[\text{CuL}^{10}]\cdot\text{H}_2\text{O}$ .

atom1	atom2	dist	S	a	b	c
H(12a)...	Cu	3.49	1	0.0	0.0	1.0
C(1c) ...Cu		3.93	-1	0.0	0.0	0.0
C(2a) ...Cu		4.08	-1	0.0	0.0	0.0
S(1b) ...S(1a)		3.38	2	0.0	0.0	0.0
C(11b) ...S(1a)		3.71	2	0.0	0.0	-1.0
C(12b) ...S(1a)		3.57	2	0.0	0.0	-1.0
H(12b) ...S(1a)		3.09	2	0.0	0.0	-1.0
H(1c) ...S(1a)		3.13	-2	0.0	0.0	0.0
C(1c) ...S(1b)		3.75	-1	0.0	0.0	0.0
H(1c) ...S(1b)		3.16	-1	0.0	0.0	0.0
C(14a) ...S(1b)		3.49	2	0.0	-1.0	0.0
C(6a) ...S(1b)		3.54	2	0.0	-1.0	0.0
H(14a) ...S(1b)		3.35	2	0.0	-1.0	0.0
H(72b) ...O(1a)		2.74	2	0.0	0.0	0.0
O(3c) ...O(1a)		2.77	2	0.0	0.0	0.0
H(14b) ...O(1a)		2.28	2	0.0	0.0	0.0
H(11a) ...O(1b)		2.54	1	0.0	0.0	1.0
C(2b) ...O(1b)		3.23	-1	0.0	0.0	-1.0
H(2b) ...O(1b)		2.41	-1	0.0	0.0	-1.0
O(3c) ...O(1b)		2.88	-2	1.0	1.0	1.0
H(12a) ...N(2b)		2.66	1	0.0	0.0	1.0
H(13b) ...C(1c)		2.87	2	0.0	0.0	-1.0
H(13b) ...C(2a)		3.04	2	0.0	0.0	-1.0
H(14a) ...C(2a)		2.99	-2	1.0	0.0	1.0
H(12b) ...C(4a)		3.06	2	0.0	0.0	-1.0

Table C.6 continued

H(14b) ... C(5a)	3.06	2	0.0	0.0	0.0
C(4b) ... H(12a)	2.96	1	0.0	0.0	-1.0
H(9b) ... C(13a)	2.67	-1	1.0	0.0	1.0
O(3c) ... H(13a)	2.57	-1	1.0	0.0	1.0
O(3c) ... C(7a)	3.31	-1	1.0	0.0	0.0
O(3c) ... H(7a2)	2.31	-1	1.0	0.0	0.0
C(13b) ... H(9a)	2.90	-1	1.0	0.0	0.0
C(14b) ... H(9a)	3.03	-1	1.0	0.0	0.0
O(3c) ... H(9a)	2.79	-1	1.0	0.0	0.0
C(5b) ... H(10c)	3.05	-1	1.0	0.0	0.0
C(11b) ... H(10c)	2.86	-1	1.0	0.0	0.0
C(12b) ... H(10c)	3.07	-1	1.0	0.0	0.0
H(2b) ... C(2b)	2.97	-1	0.0	0.0	-1.0
H(13b) ... C(2b)	2.95	2	0.0	0.0	-1.0
H(11a) ... C(4b)	3.01	1	0.0	0.0	1.0

Symmetry Transformations:

The second atom is related to  
the first atom, at  $(x,y,z)$ , by the  
symmetry operation  $S$  with  $(a,b,c)$   
added to the  $(x',y',z')$  of  $S$ .

Where  $S =$ 

$$\begin{array}{lll} 1 & x, & y, \\ 2 & 0.5+x, & 0.5-y, \end{array} \quad z$$

TABLE C.7 Intramolecular distances ( $\text{\AA}$ ) for  $[\text{CuL}^{10}]\cdot\text{H}_2\text{O}$ .

S(1a) ... Cu	4.01	O(1a) ... Cu	4.06
C(2a) ... Cu	4.14	C(3a) ... Cu	2.82
C(4a) ... Cu	2.86	C(5a) ... Cu	3.02
C(11a) ... Cu	3.84	C(6a) ... Cu	3.76
C(7a) ... Cu	3.08	H(7a1) ... Cu	2.39
C(8a) ... Cu	2.99	C(3b) ... Cu	2.84
C(4b) ... Cu	2.88	C(5b) ... Cu	2.97
C(6b) ... Cu	3.17	C(7b) ... Cu	3.28
H(7b1) ... Cu	3.68	C(8b) ... Cu	3.06
O(1a) ... S(1a)	3.72	N(2a) ... S(1a)	3.10
N(3c) ... S(1a)	3.52	C(4a) ... S(1a)	3.49
C(5a) ... S(1a)	2.79	C(14a) ... S(1a)	2.73
H(7a1) ... S(1a)	2.44	H(7a2) ... S(1a)	2.43
C(8a) ... S(1a)	2.71	C(9a) ... S(1a)	3.35
H(9a) ... S(1a)	3.39	H(14a) ... S(1a)	2.76
N(2b) ... S(1b)	2.90	N(3c) ... S(1b)	3.01
C(5b) ... S(1b)	2.73	C(14b) ... S(1b)	2.75
H(7b1) ... S(1b)	2.39	H(72b) ... S(1b)	2.39
C(8b) ... S(1b)	2.76	H(14b) ... S(1b)	2.88
N(2a) ... O(1a)	2.32	C(2a) ... O(1a)	2.94
H(2a) ... O(1a)	2.75	C(3a) ... O(1a)	2.38
C(5a) ... O(1a)	2.77	C(6a) ... O(1a)	3.39
N(2b) ... O(1b)	2.34	C(2b) ... O(1b)	2.95
H(2b) ... O(1b)	2.75	C(3b) ... O(1b)	2.38
C(5b) ... O(1b)	2.88	C(11b) ... O(1b)	2.96

Table C.7 continued

H(11b) ... O(1b)	2.49	N(1c) ... N(2a)	2.52
N(3c) ... N(2a)	2.95	C(3a) ... N(2a)	2.35
C(11a) ... N(2a)	2.42	C(6a) ... N(2a)	2.44
C(7a) ... N(2a)	3.21	H(7a1) ... N(2a)	2.80
C(8a) ... N(2a)	3.44	H(11a) ... N(2a)	2.61
N(1c) ... N(2b)	2.52	N(3c) ... N(2b)	3.29
C(3b) ... N(2b)	2.36	C(11b) ... N(2b)	2.49
C(6b) ... N(2b)	2.39	H(11b) ... N(2b)	2.66
C(1c) ... N(1c)	2.70	C(2a) ... N(1c)	2.37
C(4a) ... N(1c)	2.37	H(7a1) ... N(1c)	2.89
C(2b) ... N(1c)	2.38	C(4b) ... N(1c)	2.38
C(5a) ... N(3c)	3.06	C(6a) ... N(3c)	3.19
C(7a) ... N(3c)	2.43	H(7a1) ... N(3c)	2.53
C(9a) ... N(3c)	2.43	C(10c) ... N(3c)	2.75
C(6b) ... N(3c)	3.38	C(7b) ... N(3c)	2.46
H(7b1) ... N(3c)	2.99	C(9b) ... N(3c)	2.43
H(2a) ... C(1c)	2.20	C(3a) ... C(1c)	2.38
H(2b) ... C(1c)	2.17	C(3b) ... C(1c)	2.37
C(4a) ... C(2a)	2.57	C(2b) ... C(2a)	2.47
C(3b) ... C(2a)	2.79	H(1c) ... C(2a)	2.03
C(3a) ... H(2a)	2.17	C(4a) ... H(2a)	2.85
C(2b) ... C(3a)	2.78	C(3b) ... C(3a)	2.35
C(5a) ... C(4a)	2.37	C(11a) ... C(4a)	3.26
C(6a) ... C(4a)	3.19	C(12a) ... C(5a)	2.43
C(13a) ... C(5a)	2.79	C(14a) ... C(5a)	2.39
C(7a) ... C(5a)	3.42	C(8a) ... C(5a)	3.38
H(11a) ... C(5a)	2.14	H(12a) ... C(11a)	2.17
C(13a) ... C(11a)	2.40	C(14a) ... C(11a)	2.75

Table C.7 continued

C(6a) ...C(11a)	2.39	H(13a)...C(12a)	2.15
C(14a)...C(12a)	2.40	C(6a) ...C(12a)	2.80
H(11a)...C(12a)	2.19	C(13a)...H(12a)	2.16
C(6a) ...C(13a)	2.42	H(14a)...C(13a)	2.10
C(14a)...H(13a)	2.14	C(7a) ...C(6a)	2.89
C(8a) ...C(6a)	2.95	H(14a)...C(6a)	2.05
C(9a) ...C(7a)	2.49	H(9a) ...C(7a)	2.72
C(8a) ...H(7a1)	2.11	C(8a) ...H(7a2)	2.10
C(9a) ...H(7a2)	2.65	H(9a) ...C(8a)	2.18
C(10c)...C(8a)	2.35	C(8b) ...C(8a)	2.36
C(9b) ...C(8a)	2.77	H(10c)...C(9a)	2.08
C(8b) ...C(9a)	2.82	C(9b) ...C(9a)	2.44
C(10c)...H(9a)	2.12	C(8b) ...C(10c)	2.44
H(9b) ...C(10c)	2.19	C(9b) ...H(10c)	2.15
C(4b) ...C(2b)	2.59	H(1c) ...C(2b)	2.10
C(3b) ...H(2b)	2.17	C(4b) ...H(2b)	2.86
C(5b) ...C(4b)	2.41	C(11b)...C(4b)	3.03
H(11b)...C(4b)	2.81	C(12b)...C(5b)	2.42
C(13b)...C(5b)	2.82	C(14b)...C(5b)	2.42
H(11b)...C(5b)	2.10	C(13b)...C(11b)	2.43
C(14b)...C(11b)	2.80	C(6b) ...C(11b)	2.42
H(12b)...C(11b)	2.26	H(13b)...C(12b)	2.17
C(14b)...C(12b)	2.42	C(6b) ...C(12b)	2.78
H(11b)...C(12b)	2.15	C(6b) ...C(13b)	2.43
H(12b)...C(13b)	2.22	H(14b)...C(13b)	2.27
C(14b)...H(13b)	2.17	C(7b) ...C(14b)	3.26
H(72b)...C(14b)	2.88	C(7b) ...C(6b)	2.78
H(72b)...C(6b)	2.89	C(8b) ...C(6b)	3.24

**Table C.7 continued**

H(14b) ... C(6b)	2.21	C(9b) ... C(7b)	2.52
H(9b) ... C(7b)	2.76	H(14b) ... C(7b)	3.07
C(8b) ... H(7b1)	2.08	C(9b) ... H(7b1)	2.93
C(8b) ... H(72b)	2.08	C(9b) ... H(72b)	2.64
H(9b) ... C(8b)	2.22		

**THE BRITISH LIBRARY**  
**BRITISH THESIS SERVICE**

METAL COMPLEXES OF OXYGEN-, NITROGEN-, AND SULPHUR-CONTAINING

**TITLE.** MACROCYCLIC LIGANDS; SYNTHETIC AND STRUCTURAL STUDIES.

**AUTHOR** ..... SHRUTI WAIKAR .....

**DEGREE** .....

**AWARDING BODY** (ENAA)  
University of North London.  
**DATE** (1992) .....

**THESIS**  
**NUMBER** .....

**THIS THESIS HAS BEEN MICROFILMED EXACTLY AS RECEIVED**

The quality of this reproduction is dependent upon the quality of the original thesis submitted for microfilming. Every effort has been made to ensure the highest quality of reproduction.

Some pages may have indistinct print, especially if the original papers were poorly produced or if the awarding body sent an inferior copy.

If pages are missing, please contact the awarding body which granted the degree.

Previously copyrighted materials (journal articles, published texts, etc.) are not filmed.

This copy of the thesis has been supplied on condition that anyone who consults it is understood to recognise that its copyright rests with its author and that no information derived from it may be published without the author's prior written consent.

Reproduction of this thesis, other than as permitted under the United Kingdom Copyright Designs and Patents Act 1988, or under specific agreement with the copyright holder, is prohibited.

1	2	3	4	5	6	REDUCTION X <b>20</b>
				CAMERA	<b>5</b>	
				No. of pages		

**DX**

**172231**